

INMATEH -

**AGRICULTURAL
ENGINEERING**

SEPTEMBER - DECEMBER

No liability is assumed by the editorial staff for the content of scientific papers and opinions published in this volume. They represent the author's point of views

Editorial

The National Institute of Research-Development for Machines and Installations designed to Agriculture and Food Industry - INMA Bucharest has the oldest and most prestigious research activity in the field of agricultural machinery and mechanizing technologies in Romania.

Short History

- ✓ In 1927, the first research Center for Agricultural Machinery in Agricultural Research Institute of Romania - ICAR (Establishing Law was published in O. D. no. 97/05.05.1927) was established;
- ✓ In 1930, was founded The Testing Department of Agricultural Machinery and Tools by transforming Agricultural Research Centre of ICAR - that founded the science of methodologies and experimental techniques in the field (Decision no. 2000/1930 of ICAR Manager - GHEORGHE IONESCU ȘIȘEȘTI);
- ✓ In 1952, was established the Research Institute for Mechanization and Electrification of Agriculture - ICMA Băneasa, by transforming the Department of Agricultural Machines and Tools Testing;
- ✓ In 1979, the Research Institute of Scientific and Technological Engineering for Agricultural Machinery and Tools - ICSITMUA was founded - subordinated to Ministry of Machine Building Industry - MICM, by unifying ICMA subordinated to MAA with ICPMA subordinated to MICM;
- ✓ In 1996 the National Institute of Research-Development for Machines and Installations designed to Agriculture and Food Industry - INMA was founded - according to G.D. no. 1308/25.11.1996, by reorganizing ICSITMUA, G.D. no. 1308/1996 coordinated by the Ministry of Education and Research G.D. no. 823/2004;
- ✓ In 2008 INMA has been accredited to carry out research and developing activities financed from public funds under G.D. no. 551/2007, Decision of the National Authority for Scientific Research - ANCSno. 9634/2008.

As a result of widening the spectrum of communication, dissemination and implementation of scientific research results, in 2000 was founded the institute magazine, issued under the name of SCIENTIFIC PAPERS (INMATEH), ISSN 1583 – 1019.

Starting with volume 30, no. 1/2010, the magazine changed its name to INMATEH - *Agricultural Engineering*, appearing both in print format (ISSN 2068 - 4215), and online (ISSN online: 2068 - 2239). The magazine is bilingual,

being published in Romanian and English, with a rhythm of three issues / year: January-April, May-August, September-December and is recognized by CNCSIS - with B⁺ category. Published articles are from the field of AGRICULTURAL ENGINEERING: technologies and technical equipment for agriculture and food industry, ecological agriculture, renewable energy, machinery testing, environment, transport in agriculture etc. and are evaluated by specialists inside the country and abroad, in mentioned domains.

Technical level and performance processes, technology and machinery for agriculture and food industry increasing, according to national requirements and European and international regulations, as well as exploitation of renewable resources in terms of efficiency, life, health and environment protection represent referential elements for the magazine „INMATEH - *Agricultural Engineering*”.

We are thankful to all readers, publishers and assessors.

Editor in chief,
Ph. D. Eng. Vladut Nicolae - Valentin

Managing Editorial Board - INMA Bucharest

<u>Editor in Chief</u> VLĂDUȚ NICOLAE - VALENTIN Ph.D.Eng, SR I	
<u>Executive Editor</u> POPA LUCREȚIA Ph.D.Eng, SR I	<u>Logistic support, database</u> MURARU VERGIL , Ph.D.Eng, SR I ȚICU TANIA , techn.
<u>Scientific Secretary</u> CÂRDEI PETRE , math.	<u>Official translators</u> RADU DANIELA-CRISTINA Prof.English, French

E-mail: inmatehjournal@gmail.com**Editorial Board**

- Acad. HERA Cristian - Romania, Honorary President of ASAS - Academy of Agricultural and Forestry Sciences "Gheorghe Ionescu Șişești", member of Romanian Academy;
- Acad. Prof. Ph.D. SIN Gheorghe - Romania, President of ASAS - Academy of Agricultural and Forestry Sciences "Gheorghe Ionescu Șişești";
- Prof.Ph.D. NICOLESCU I. Mihai - Romania, Vicepresident of ASAS - Academy of Agricultural and Forestry Sciences "Gheorghe Ionescu Șişești";
- Hon.Prof.Ph.D.Eng. GĂNGU Vergil - Romania, President of the Department of Agricultural Mechanization of ASAS - Academy of Agricultural and Forestry Sciences "Gheorghe Ionescu Șişești";
- Ph.D. Eng. NICOLESCU C. Mihai - Romania, Scientific General Secretary of the ASAS-Academy of Agricultural and Forestry Sciences "Gheorghe Ionescu Șişești";
- Assoc.Prof. Ph.D. Eng. BELC Nastasia - Romania, IBA Bucharest;
- Ph.D. Eng. BUȚU Alina - Romania, INSB Bucharest;
- Prof. Ph.D. Eng. PARASCHIV Gigel - Romania, P.U. Bucharest;
- Prof. Ph.D.Eng. BIRIȘ Sorin - Romania, P.U. Bucharest;
- Prof. Ph.D. Eng. NICULIȚĂ Petru - Romania, USAMV Bucharest;
- Prof. Ph.D. Eng. VLASE Sorin - Romania, "Transilvania" University Brașov;
- Prof. Ph.D. Eng. ROȘ Victor - Romania, Technical University Cluj Napoca;
- Prof. Ph.D. Eng. FILIP Nicolae - Romania, Technical University Cluj Napoca;
- Prof. Ph.D. Eng. VOICU Gheorghe - Romania, P.U. Bucharest;
- Prof. Ph.D. Eng. GERGEN Iosif - Romania, USAMVB Timișoara;
- Prof. Ph.D. Eng. ȚENU Ioan - Romania, USAMV Iași;
- Assoc.Prof.Ph.D.Eng. BUNGESCU Sorin - Romania, USAMVB Timișoara;
- Prof. Ph.D.Eng. FENYVESILászló - Hungary, Hungarian Institute of Agricultural Engineering Godolo;
- Prof.Ph.D.Eng. KOSUTIC Silvio - Croatia, University of Zagreb;
- Ph.D. BIOCCA Marcello - Italy Agricultural Research Council, Agricultural Engineering Research Unit;
- Prof.Ph.D.Eng. MIHAILOV Nikolay - Bulgaria, University of Rousse;
- Assoc.Prof. Ph.D.Eng. ATANASOV At. - Bulgaria, University of Rousse;
- Assoc.Prof. Ph.D. ERTEKINCan - Turkey, Akdeniz University Antalya;
- Prof. Ph.D.Sc. Eng. VARTUKAPTEINIS Kaspars - Latvia, Latvia University of Agriculture, Institute of Agricultural Machinery;
- ir. HUYGHEBAERT Bruno - Belgium, Walloon Agricultural Research Center CRA-W;
- Prof. Ph.D. Eng. FABRO Dal Inacio Maria - Brazil, Campinas State University;
- Prof. Ph.D. Eng. DE WRACHIEN Daniele - Italy, State University of Milan;
- Prof. Ph.D. Guanxin YAO - P.R.China, Along Agriculture R&D Technology and Management Consulting Co., Ltd;
- Prof. Ph.D. Eng. GONZÁLEZ Omar - Republic of Cuba, Central University "Marta Abreu" de las Villas;
- Assist.Prof.Dr. KABAŞ Önder - Turkey, Akdeniz University;
- Asist.Prof.Dr. SELVÍ Kemal Çağatay - Turkey, Ondokuz Mayıs University.

In the present, *INMATEH - Agricultural Engineering* journal is indexed in the next international databases: **Emerging Sources Citation Index, ULRICHWeb: Global Serials Directory, CABI, SCIPRO, ELSEVIER /SciVerse SCOPUS, Index COPERNICUS International, EBSCO Publishing, Elektronische Zeitschriftenbibliothek**

INMATEH - Agricultural Engineering vol. 53, no.3 / 2017 NATIONAL INSTITUTE OF RESEARCH-DEVELOPMENT FOR MACHINES AND INSTALLATIONS DESIGNED TO AGRICULTURE AND FOOD INDUSTRY - INMA Bucharest 6 Ion Ionescu de la Brad Blvd., sector 1, Bucharest Three issues per year, eISSN: 2068 – 2239 pISSN: 2068 – 4215 Edited by: INMA Bucharest Copyright: INMA Bucharest / Romania
--

CONTENT

		Pag.
1.	<p>CFD ANALYSIS OF AN IMPROVED TLUD BASED EQUIPMENT FOR HEATING SMALL GREENHOUSES AND HOTHOUSES / ANALIZA CFD A UNUI ECHIPAMENT TLUD PENTRU ÎNCĂLZIREA SERELOR ȘI SOLARIILOR DE MICI DIMENSIUNI Prof. Ph.D. Eng. Maican E.¹⁾, Lect. Ph.D. Eng. Duțu I.C.¹⁾, Ph.D. Eng. Matache G.²⁾, Ph.D. Eng. Dumitrescu C.²⁾, Ph.D. Stud. Pavel I.²⁾ ¹⁾“Politehnica” University of Bucharest, Faculty of Biotechnical Systems Engineering / Romania ²⁾Hydraulics and Pneumatics Research Institute INOE 2000 - IHP / Romania</p>	5
2.	<p>DESIGN SUBSTANTIATION OF THE THREE-TIER CENTRIFUGAL TYPE MINERAL FERTILIZERS SPREADER / ОБГРУНТУВАННЯ ДИЗАЙНУ ТРИ РІВНЕВОГО ВІДЦЕНТРОВОГО РОЗКИДАЧА МІНЕРАЛЬНИХ ДОБРИВ Prof. Ph.D. Eng. Kobets A.S.¹⁾, Lect. Ph.D. Eng. Naumenko M.M.¹⁾, Lect. Ph.D. Eng. Ponomarenko N.O.¹⁾, Prof. Ph.D. Agri. Kharytonov M.M.^{1)*}, Lect. Ph.D. Econ. Velychko O.P.¹⁾, Lect. Ph.D. Eng. Yaropud V.M.²⁾ ¹⁾Dnipropetrovsk State Agrarian and Economic University, Faculty of Agrarian Engineering / Ukraine; ²⁾Vinitsky National Agrarian University, Faculty of Agrarian Engineering / Ukraine</p>	13
3.	<p>SOWING MACHINES AND SYSTEMS BASED ON THE ELEMENTS OF FLUIDICS / ВИСІВНІ МАШИНИ ТА СИСТЕМИ НА ОСНОВІ ЕЛЕМЕНТІВ ПНЕВМОНИКИ Prof. D.Sc. Eng. Aulin V.V., Prof. D.Sc. Eng. Chernovol M.I., Ph.D. Eng. Pankov A.O., Ph.D. Eng. Zamota T.M., Ph.D. Eng. Panayotov K.K. Kirovograd National Technical University / Ukraine</p>	21
4.	<p>A NEW BLADE DESIGN OF ROTARY TILLER AND STATIC ANALYSIS USING COMPUTER-AIDED TOOL / БІЛГІСАЙАР ДЕСТЕКЛІ ТАСАРИМ İLE ROTOTİLLER İÇİN YENİ BİR BIÇAK TASARIMI VE STATİK ANALİZİ Assist. Prof. Dr. Selvi K.Ç.¹⁾ ¹⁾Faculty of Agriculture, Ondokuz Mayıs University, Atakum / Turkey</p>	29
5.	<p>MODERN ASPECTS OF TILLED CROPS PRODUCTIVITY FORECASTING / СУЧАСНІ АСПЕКТИ ПРОГРАМУВАННЯ ВРОЖАЙНОСТІ ПРОСАПНИХ КУЛЬТУР Lect. Ph.D. Biol. Mostypan M.I., Lect. Ph.D. Eng. Vasytkovska K.V., Lect. Ph.D. Agric. Andriyenko O.O., Lect. Ph.D. Agric. Reznichenko V.P. Central Ukrainian National Technical University / Ukraine</p>	35
6.	<p>CHICORY ROOT CROPS COMBINED HARVESTER / КОМБІНОВАНИЙ КОПАЧ КОРЕНЕПЛОДІВ ЦИКОРІЮ Prof. Ph.D. Eng. Baranovsky V.M.¹⁾, P.G. Skalsky O.Ju.¹⁾, Assoc. Prof. Ph. D. Pankiv M.R.¹⁾, Ph.D. Eng. Pastushenko A.S.²⁾ ¹⁾Ternopil Ivan Puluj National Technical University, Ternopil / Ukraine; ²⁾Mykolayiv National Agrarian University, Mykolaiv / Ukraine</p>	41
7.	<p>RESEARCH OF THE DYNAMIC MODEL OF THE FLAX STEMS LINE ARRANGING MECHANISM / ДОСЛІДЖЕННЯ ДИНАМІЧНОЇ МОДЕЛІ МЕХАНІЗМУ ПІДБИВАННЯ СТРИЧКИ СТЕБЕЛ ЛЬОНУ-ДОВГУНЦЯ Prof. Ph.D. Eng. Nalobina O.O.¹⁾, Ph.D. Eng. Gerasymchuk O.P.¹⁾, Ph.D. Eng. Puts V.S.¹⁾, Prof. Ph.D. Eng. Marchuk M.M.²⁾ ¹⁾ Lutsk National Technical University / Lvivska str., 75, Lutsk / Ukraine; ²⁾ National University of Water Management and Nature Resources Use, Rivne / Ukraine</p>	51
8.	<p>SIMULATION OF BULK MATERIALS SEPARATION PROCESS IN SPIRAL SEPARATOR / МОДЕЛЮВАННЯ ПРОЦЕСУ СЕПАРАЦІЇ СИПКИХ МАТЕРІАЛІВ НА СПІРАЛЬНОМУ СЕПАРАТОРІ Lect. Ph.D. Eng. Dudarev I., Lect. Ph.D. Eng. Kirchuk R. Lutsk National Technical University / Ukraine</p>	57
9.	<p>ANALYTICAL ASSESSMENT OF THE PNEUMATIC SEPARATION QUALITY IN THE PROCESS OF GRAIN MULTILAYER FEEDING / АНАЛІТИЧНА ОЦІНКА ЯКОСТІ ПНЕВМОСЕПАРАЦІЇ ПРИ БАГАТОРІВНЕВОМУ ВВЕДЕННІ ЗЕРНА As. Nesterenko A.V., Lect. Ph.D. Eng. Leshchenko S.M., Lect. Ph.D. Eng. Vasytkovskyi O.M., Lect. Ph.D. Eng. Petrenko D.I. Central Ukrainian National Technical University / Ukraine</p>	65
10.	<p>DEVELOPMENT AND EXPERIMENTAL STUDY OF INFRARED BELT DRYER FOR RAPESEED / 用于油菜籽干燥的红外带式干燥机研制和实验 Prof. Ph.D. Eng. Yang M.J.¹⁾, Ms. Stud. Eng. Liu B.¹⁾, Ms. Stud. Eng. Yang Z.R.¹⁾, Ms. Eng. Ding Z.Y.¹⁾, Prof. Ph.D. Eng. Yang L.¹⁾, Prof. Ph.D. Eng. Xie S.Y.¹⁾, Prof. Eng. Chen X.B.²⁾ ¹⁾ Southwest University, College of Engineering and Technology, Chongqing Key Laboratory of Agricultural Equipment for Hilly and Mountainous Regions / P. R. China; ²⁾ Agricultural Machinery Quality Control and Inspection Technology Centre, Nanjing Research Institute for Agricultural Mechanization Ministry of Agriculture / P. R. China</p>	71

		Pag.
11.	<p>DETERMINATION OF PERFORMANCE CHARACTERISTICS OF HORIZONTAL WIND TUNNEL IN THE CLEANING OF CORN-COB MIX / MISIR-KOÇAN KARIŞIMININ TEMİZLENMESİNDE YATAY HAVA TÜNELİNİN PERFORMANS KARAKTERİSTİKLERİNİN BELİRLENMESİ Ress.Assist. Karaköse T. ^{*1)}, Assist.Prof.Dr. Tekgüler A. ²⁾ ¹⁾Ondokuz Mayıs University, Faculty of Agriculture, Atakum / Turkey ²⁾Ondokuz Mayıs University, Samsun Vocational School, İlkadım / Turkey</p>	81
12.	<p>GRAIN CROPS INJURIES AND DRYING MODES DURING SEEDS PREPARATION / ТРАВМУВАННЯ ЗЕРНІВОК ТА РЕЖИМИ ПІДСУШУВАННЯ ПРИ ПІДГОТОВЛЕННІ НАСІННЯ Ph.D. Eng. Derevjnko D., Ph.D. Eng. Sukmaniuk E, Stud. Derevjnko O. Zhytomyr National Agroecological University / Ukraine</p>	89
13.	<p>MICROWAVE DEHYDRATION OF SUGAR CUBE: THERMOPHYSICAL INVESTIGATION AND FINITE ELEMENT SOLUTION / آبزدایی از حبه قند با مایکروویو: بررسی ترموفیزیکی و حل المان محدود Ph.D. Stud. Eng. Hazervazifeh A. ¹⁾, Assoc.Prof. Ph.D. Eng. Nikbakht A.M. ^{*1)}, Assoc.Prof. Ph.D. Eng. Moghaddam P.A. ¹⁾, Assist.Prof. Ph.D. Eng. Sharifian F. ¹⁾ ¹⁾Department of Mechanical Engineering of Biosystems, Urmia University / Iran</p>	95
14.	<p>EXPERIMENTAL SETUP OF SOLAR DISH COLLECTOR WITH CHANGEABLE STRUCTURE واحد آزمایشی کلکتور بشقابی خورشیدی با ساختار متغیر Ph.D. Stud. Eng. Feizolahzadeh M. ^{*1)}, Lect. Ph.D. Eng. Modarres Motlagh A. ¹⁾, Lect. Ph.D. Eng. Banakar A. ²⁾ ¹⁾Urmia University, Department of Mechanical Engineering of Biosystems / Iran; ²⁾Tarbiat Modarres University, Department of Mechanical Engineering of Biosystems / Tehran</p>	103
15.	<p>MACHINING METHOD WITH EVENLY DISTRIBUTED ALLOWANCE BASED ON THE NORMAL LINKAGE MODEL OF NON-CIRCULAR GEAR SHAPING / 基于法向插削联动模型的非圆齿轮齿面余量匀化加工方法 As. Ph.D. Stud. Eng. Gao T. ¹⁾, Prof. Ph.D. Eng. Han J. ¹⁾, Ph.D. Eng. Tian X.Q. ^{1,2)}, Prof. Ph.D. Eng. Xia L. ^{*1)} ¹⁾School of Mechanical Engineering, Hefei University of Technology, Hefei / China; ²⁾S. M. Wu Manufacturing Research Centre, University of Michigan, Ann Arbor / United States</p>	113
16.	<p>KINEMATICS AND PERFORMANCE INDEX ANALYSIS OF A NOVEL 5-DOF PARALLEL MECHANISM / 新型五自由度并联机构运动学及其性能指标分析 Ph.D. Huang Jie, Ph.D. Wang Xuelei ¹⁾, Ph.D. Zhao Dongjie ²⁾, Ph.D. San Yunlong ¹⁾, Prof. Hou Shulin ^{*1)} ¹⁾College of Engineering, China Agricultural University, Beijing/China; ²⁾School of Mechanical and Automobile Engineering, Liaocheng University, Liaocheng/China</p>	123
17.	<p>THEORETICAL GROUNDING OF RATIONAL DESIGN FOR STRAW DISPERSER WORKING ELEMENTS OF GRAIN COMBINE HARVESTER / ТЕОРЕТИЧЕСКОЕ ОБОСНОВАНИЕ РАЦИОНАЛЬНОЙ КОНСТРУКЦИИ РАБОЧИХ ОРГАНОВ ИЗМЕЛЬЧИТЕЛЯ-РАЗБРАСЫВАТЕЛЯ ЗЕРНОУБОРОЧНОГО КОМБАЙНА Prof. Ph.D. Eng.Sc. Rodimtsev S.A. ¹⁾, Prof. Ph.D. Eng.Sc. Kuznetsov Y.A. ¹⁾, Prof. Ph.D. Eng.Sc. Kolomeichenko A.V. ¹⁾, Assoc. Prof. D.Eng.Sc. Goncharenko V.V. ¹⁾, Post Grad. Stud. Yagelsky M.Y. ¹⁾, Senior Lecturer Ivanushkina N.M. ¹⁾, Prof. Ph.D. Phil.Sc. Kalashnikova L.V. ²⁾ ¹⁾Orel State Agrarian University named after N.V. Parakhin / Russia ²⁾Orel State University named after I.S. Turgenev / Russia</p>	133
18.	<p>TROPICAL WOOD CLASSIFICATION BASED ON LBP-LIKE DESCRIPTOR AND NEAREST NEIGHBOR CLASSIFIER / 基于纹理特征及最近邻分类器的木材分类识别 Chao Xiaofei, Cai Cheng, Zhang Zhiyong, Nie Liangbing, Li Shuqin College of Information Engineering, Northwest A&F University, Yangling, Shaanxi 712100, P.R. China</p>	141
19.	<p>COMPARATIVE ANALYSIS OF SOME TIRE DEFORMATION MODELS USED FOR THE PREDICTION OF TRACTION CHARACTERISTICS / ANALIZA COMPARATIVĂ A UNOR MODELE DE DEFORMARE A PNEULUI ÎN SCOPUL OBȚINERII CARACTERISTICILOR DE TRACȚIUNE Prof. Ph.D. Stud. Eng. Roșca R. ^{*1)}, Assoc. Prof. Ph.D. Eng. Cârlescu P. ¹⁾, Prof. Ph.D. Eng. Țenu I. ¹⁾ ¹⁾University of Agricultural Sciences and Veterinary Medicine "Ion Ionescu de la Brad" Iași / Romania</p>	151
20.	<p>THEORETICAL JUSTIFICATION OF THE TURN OF A WIDE SPAN TRACTOR (VEHICLE) FOR CONTROLLED TRAFFIC FARMING / ТЕОРЕТИЧНЕ ОБҐРУНТУВАННЯ ПОВОРОТУ ШИРОКОКОЛІЙНИХ ТРАКТОРІВ (ТРАНСПОРТНИХ ЗАСОБІВ) ДЛЯ КОЛІЙНОЇ СИСТЕМИ ЗЕМЛЕРОБСТВА Prof. Ph.D.Eng. Bulgakov V. ¹⁾, Prof. Ph.D. Eng. Adamchuk V. ²⁾, Ph.D. Eng. Kuvachov V. ³⁾, Prof. Ph.D.Eng. Ivanovs S. ⁴⁾ ¹⁾National University of Life and Environmental Sciences / Ukraine, ²⁾National Scientific Centre "Institute for Agricultural Engineering and Electrification" / Ukraine, ³⁾Tavria State Agrotechnological University / Ukraine, ⁴⁾Latvia University of Agriculture / Latvia</p>	159

**CFD ANALYSIS OF AN IMPROVED TLUD BASED EQUIPMENT
FOR HEATING SMALL GREENHOUSES AND HOTHOUSES**
/
**ANALIZA CFD A UNUI ECHIPAMENT TLUD PENTRU ÎNCĂLZIREA
SERELOR ȘI SOLARIILOR DE MICI DIMENSIUNI**

Prof. Ph.D. Eng. Maican E. ¹⁾, Lect. Ph.D. Eng. Duțu I.C. ¹⁾,
Ph.D. Eng. Matache G. ²⁾, Ph.D. Eng. Dumitrescu C. ²⁾, Ph.D. Stud. Pavel I. ²⁾
¹⁾“Politehnica” University of Bucharest, Faculty of Biotechnical Systems Engineering / Romania
²⁾Hydraulics and Pneumatics Research Institute INOE 2000 - IHP / Romania
E-mail: edmond.maican@upb.ro

Keywords: TLUD, pyrolysis, greenhouse, hothouse, CFD, agricultural residues.

ABSTRACT

The paper investigates the performance of an optimized version of a novel heating equipment that is based on a top lit updraft (TLUD) gasifier. The system uses the bioenergy potential of residues from agriculture, in order to increase the energy independence of greenhouses and hothouses. It also produces 10 to 15% biochar that can be subsequently used as fertilizer in the same greenhouse or hothouse. A Computational Fluid Dynamics analysis on an improved model of a previous design was performed, in order to evaluate the flow and temperature of the heated air to the outlet of the system. Also, the total mass flow of air to be used for greenhouse heating is calculated.

REZUMAT

Lucrarea analizează performanțele unei versiuni optimizate a unui model de echipament de încălzire care are la bază un gazeificator TLUD. Echipamentul utilizează potențialul energetic al reziduurilor agricole, pentru creșterea independenței energetice a serelor și solarilor de mici dimensiuni. Ca produs secundar, se obține 10-15% biochar, care poate fi utilizat ca fertilizator în aceeași seră sau solar. Procesele termodinamice și performanțele sistemului sunt determinate cu ajutorul analizei CFD, iar în baza rezultatelor obținute se propune o soluție optimă. De asemenea, este calculat debitul total maxim de aer cald care poate fi furnizat de echipament pentru încălzirea serei.

INTRODUCTION

Exploitation of the full potential of biomass is a strategic aspect of the EU renewable energy policy, as stated in Directive 2009/28/EC on the promotion of renewable energy sources (*EUParliament, 2009*). In the framework of the EU Directive, 20% improvement in energy production and 20% greenhouse gas emissions (GHG) savings should be achieved. These targets can be reached by means of a strategy that, among others, should establish efficient supply chains and technology paths.

In this respect, the lignocellulosic residual biomass generated by agricultural and forestry related activities represent an economically and environmentally convenient bioenergy resource. Critical aspects such as abundancy, land competition with food crops, or GHG emissions, render residual biomass as being advantageous when compared with dedicated energy crops (*Ayhan, 2008*) (*Paiano & Lagioia, 2016*). Moreover, unlike wind or solar energy, biomass can be easily stored and constantly supplied when required.

In the framework of this legislative context, scientific research aims to achieve these objectives towards a strategical implementation of efficient biomass based energy solutions. It is therefore mandatory to overcome the current specific technical and economical impediments. Disadvantages like biomass low bulk density, its dispersion over territory, water content, and its low energy density versus fossil fuels, significantly increase the collection and transportation costs per unit of energy produced from residual biomass. From this point of view, a viable solution for rural areas consists of using small scale solutions for heat generation. It is therefore possible to use the locally available biomass resources, and thus to reduce or eliminate transportation costs.

Heat production through biomass burning has however low efficiency and generates problems related to air quality, due to emissions of N₂O, CH₄, particulate matter (PM) and polycyclic aromatic hydrocarbons (PAH) (*Devesa-Rey, et al., 2011*). Thermo-chemical biomass conversion through gasification is an alternative of higher efficiency. Gasification reactors demonstrated many benefits depending on their type,

such as high carbon conversion, ability to scale-up, or low tar production. Apart from these advantages, they also pose disadvantages like sensitivity to biofuel moisture, complexity, low production of H_2 and CO , resilience, ash deposition on the reactor walls that lead to bed sintering, or maintenance costs (Molino, et al., 2016), (Iovane, et al., 2013), (Wang, et al., 2008).

To improve the gasification sustainability, researchers oriented towards the use of biochar product from gasification mainly as soil amendment. Up to 80% of biochar composition is unreacted carbon. It has increased capacity to hold water, and demonstrated the capacity to improve soil fertility, to reduce its acidity, and to mitigate the process of pesticides leaching to groundwater (Patuzzi, et al., 2016), (Fowles, 2008). Negative aspects related to gasification char are also encountered in terms of potential contaminant content, such as furans, heavy metals, dioxins, or PAH. Yet it has been demonstrated that higher pyrolysis time and temperature decrease PAH concentrations below the existing environmental quality standards (Hale, et al., 2012). Having a highly porous structure, biochar can also be used to adsorb heavy metals or organic pollutants in filtering processes, such as for water and air filtration (Shen, 2015), (Acharya, et al., 2013).

The TLUD gasification process is more convenient when compared to regular gasification types. TLUD reactors are also known as inverted downdraft gasifiers. They have durable and simple designs, an aspect that positively contributes to the initial investment cost and to the maintenance costs. The gasification process is tolerant to biomass moisture and size, and auto-adaptive. It demonstrated good operation when fuels with up to 30% moisture content were used (Reed, et al., 2000). If both streams of air involved in the process (called primary and secondary air) are properly adjusted, very low emissions of CO and PM are recorded. Efficiencies of up to 93% were demonstrated on a forced draft equipment, depending on the used fuel (Mukunda, et al., 2010). The biochar produced by TLUD reactors has a microporous structure with high adsorption capacity. It proved fine emissions to be an efficient soil amendment, and showed very good performance when used for wastewater treatment and nutrient recovery (Huggins, et al., 2016).

MATERIALS AND METHODS

A TLUD reactor (Fig.1) can use pellets or biomass chopped at 10 – 50 mm, usually dried naturally at 20% or less. The process starts with the ignition of the top layer of biomass. Primary air flows upward, through the biomass bed. Partial oxidation of biomass takes place in the presence of oxygen from the primary air.

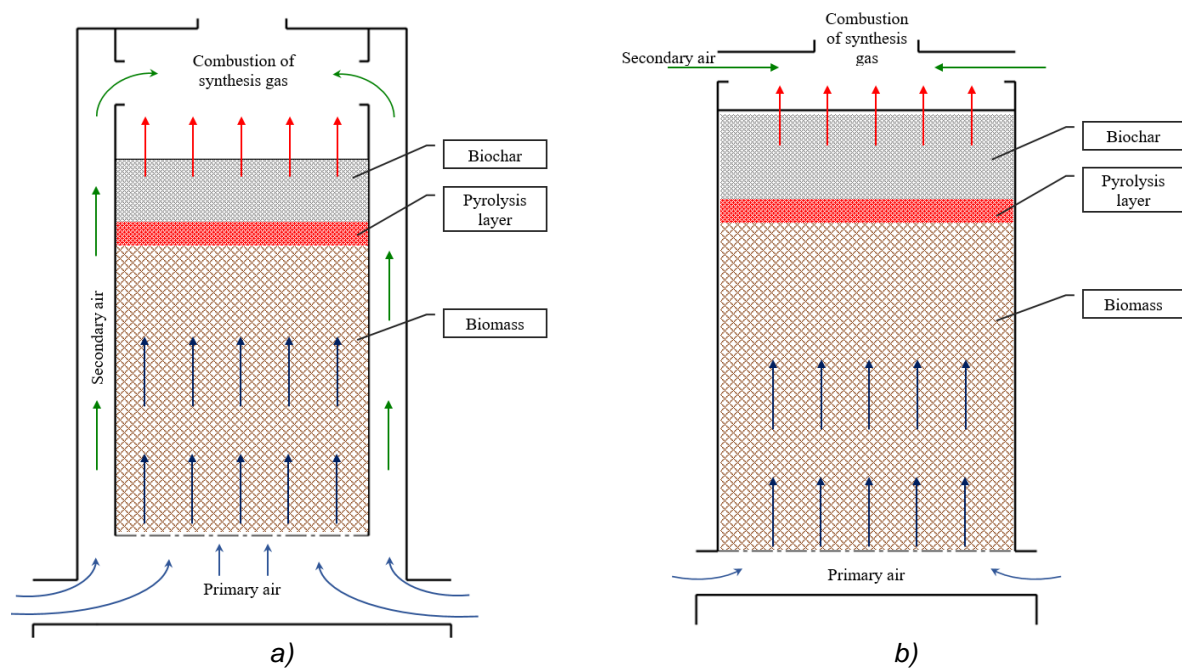


Fig. 1 - Diagram of a TLUD reactor

(a) with secondary air preheated from the reactor walls; (b) without preheating the secondary air

Due to the heat generated by the oxidation process, the biomass in the proximity will decompose through pyrolysis, thus generating synthesis gas with a lower heating value (LHV) of $3.5 - 4.5 \text{ MJ/Nm}^3$. Adding the enthalpy of the hot gas at 500°C , the total energy will be $1.2 - 1.5 \text{ kWh}_{\text{th}}/\text{Nm}^3$ (Mukunda, et al.,

2010), (Murad, et al., 2015). The secondary air flow is mixed with synthesis gas and burned at approximately 900°C. When passing through the incandescent layer, tars are cracked and reduced, and the pyrolysis layer progressively moves downward. At the end of the process, up to 15% char with some incorporated ash will remain. As previously calculated (Murad, et al., 2015), a TLUD reactor that uses 13.44 t/year biomass as fuel, generates 1.78 t of biochar, which corresponds to a negative CO₂ balance of -6.2 t/year if it is incorporated into the soil. To reduce the PM_{2.5} concentration in the exhaust gas below 2.4 mg/MJ (the limit established by the current EU legislation), the superficial velocity of the syngas should be less than 0.1 m/s (Burkhard & Albrecht, 2008).

Based on these principles, as well as considering the affordability, the minimalistic design, and maintenance simplicity, an equipment using a TLUD reactor was proposed by the authors in a previous paper (Maican, et al., 2016), to heat small greenhouses during cold weather, using as fuel the residual biomass obtained from local agricultural activities (branches, vines, other lignocellulosic debris). Figure 2 presents the TLUD module, while Figure 3 shows the heating system which includes the TLUD module.

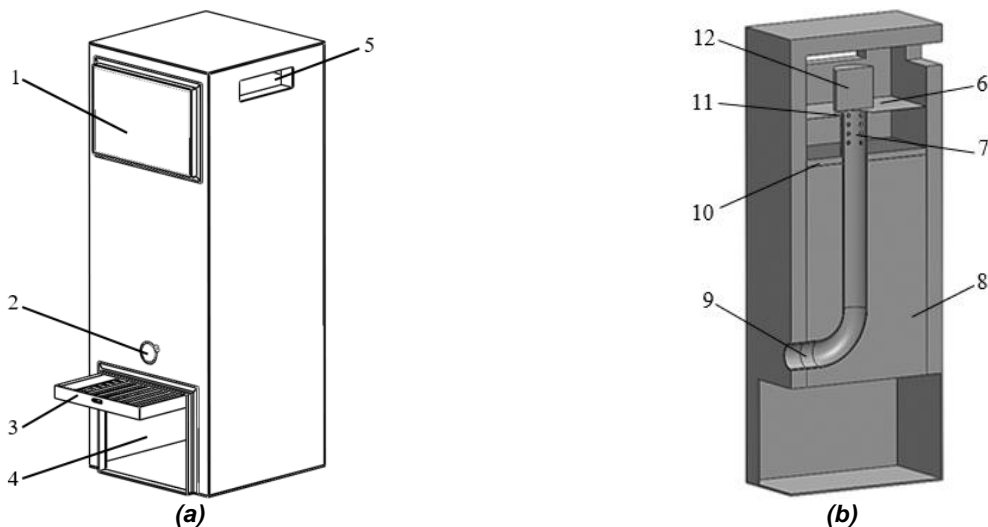


Fig. 2 - TLUD module: (a) isometric view; (b) section view (simplified model for CFD analysis)

1 – biomass feeding door; 2 – cover for adjusting secondary air flow; 3 – grate; 4 – primary air inlet and biochar evacuation chamber; 5 – lateral exhaust outlet; 6 – removable plate; 7, 11 – mixing system for primary and secondary air (7 – holes; 11 – annular gap); 8 – biomass bed; 9 – pipe for secondary air; 10 – layer of biochar and pyrolysis front; 12 – approximation of the initial combustion volume.



Fig.3 - Greenhouse heating equipment (lateral wall hidden): (a) original design; (b) simplified design, for CFD simulation;

1 – steel frame; 2 – TLUD module; 3 – heat exchanger; 4 – insulated exterior wall; 5 – flue gas evacuation; 6 – pipe for hot fresh air evacuation

In operation, hot flue gases are evacuated through the TLUD module's exhaust outlets 5. Due to a fan mounted inside pipe 5, gases flow from the upper part of the equipment towards the pipe. Heat is transferred from hot gases to the fresh air from inside the heat exchanger 3. Hot fresh air evacuated through pipe 6 will be mixed with cold air until the mixture reaches 22°C ... 28°C, and then will be used to heat the greenhouse

or hothouse. Because the target of the subsequent CFD analysis is to assess the flow and temperature of the fresh air to the heat exchanger outlet, the mixing system is not represented here.

The results that were obtained in previous research after performing a preliminary CFD analysis to test the functionality of the system, showed the following performance parameters:

- The optimum flowrate ratio was $Q_{sa}/Q_{pa} = 2.62$, where Q_{sa} is the volumetric flow of secondary air, and Q_{pa} is the volumetric flow of primary air. Scientific data (Sundblad, 2014), (Supramono & Inayati, 25-28 June 2013) show that flowrate ratio should be in the interval 2.44 ... 3.3 for best results.
- The superficial velocities of synthesis gas range between 0.03 m/s and 0.04 m/s, below the upper threshold of 0.1 m/s where the specific concentration of $PM_{2.5}$ increases above 2.4 mg/MJ.
- At the outlet of the reactor, flue gas has a flow of 0.007 m³/s and an average temperature of 694°C.
- Temperature of flue gas at the outlet of the equipment varied between 130°C and 244°C, depending on the flow of fresh air that receives heat from flue gas.
- Temperature of fresh air at the outlet of the heat exchanger varied between 78°C and 243°C, also depending on fresh air flow.

The major target is to obtain the highest flow of warm air to be sent inside the greenhouse or hothouse. Therefore, in this paper the following improvements on the design of the TLUD module are made in order increase the performance of the system:

- An array of 49 small-size outlets were drilled into the TLUD's top wall, in order to allow hot flue gas to reach the horizontal section of the exchanger.
- Thickness of the upper section of heat exchanger was increased to 2 mm, for better resistance to flame action.
- The top refractory wall thickness was thinned out, from 35 mm to 15 mm.
- The lateral and rear walls of the TLUD module were also thinned out from 35 mm to 15 mm. Thinning of top, lateral and rear walls reduced the total weight by 28 kg. Inside the heating equipment, flue gas flows at the exterior of the TLUD module. Therefore, thinning the walls positively improves heat transfer from the exterior of the TLUD module towards the biomass bed and primary air. It is expected that a hotter primary air will and a drier and hotter biomass bed will improve pyrolysis, further reducing emissions of GHG and $PM_{2.5}$.

The simplified CAD model (Figure 3 b) is equipped with the improved TLUD module. To evaluate the performance of the new system, a CFD analysis is made by means of SolidWorks Flow Simulation, in the same conditions as described earlier for non-improved equipment (Maican & Duțu, 2017), namely:

- The options for buoyancy effects and heat conduction in solids were activated.
- Turbulence intensity at the inlets was considered to be 5%. This is a medium turbulence and is found in ventilation flows, flows at low speeds, or in large pipes. Because it is difficult to provide a value for the inlet turbulence length L_t , the default $L_t=0.01$ m (as predetermined by the analysis software) was used.
- Ambient temperature was set to 5□°C.
- The Reynolds number, the effective wall length, as well as the equivalent hydraulic diameter, are automatically calculated by the simulation software and then used to find the thickness of the default boundary layer.
- The 70% porosity of the isotropic biomass bed corresponds to biomass chips of 40-50 mm (Karaj, et al., 2011).
- In a previous research (Maican, et al., 2016), the pressure gradient variation of the biomass bed was calculated as a function of air speed:

$$\nabla P = 2495.9v^2 + 159.43v \quad (1)$$

- Mesh refinement was performed in areas prone to high temperature and flow gradients. The global mesh size was adjusted after three runs that provided grid independent results.

RESULTS

Best results in terms of emissions from the pyrolysis process, and of operating time with a charge of biomass, were previously obtained (Maican, et al., 2016) when the total gas flow at the outlet of the TLUD module was $Q_{tg} = 0.007$ m³/s. Thus, four CFD simulations were performed, for each of them keeping a constant flow of gasses (0.007 m³/s), and changing the flow of fresh air Q_{fa} through the heat exchanger:

$$Q_{fa} = \{0.007; 0.014; 0.021; 0.028\} \left(\frac{m^3}{s}\right)$$

Figure 4 shows temperature distribution for $Q_{fa} = 0.028 \text{ m}^3/\text{s}$, on two vertical planes: one that cuts through the middle of the hot air outlet pipe, and the other through flue gas outlet pipe.

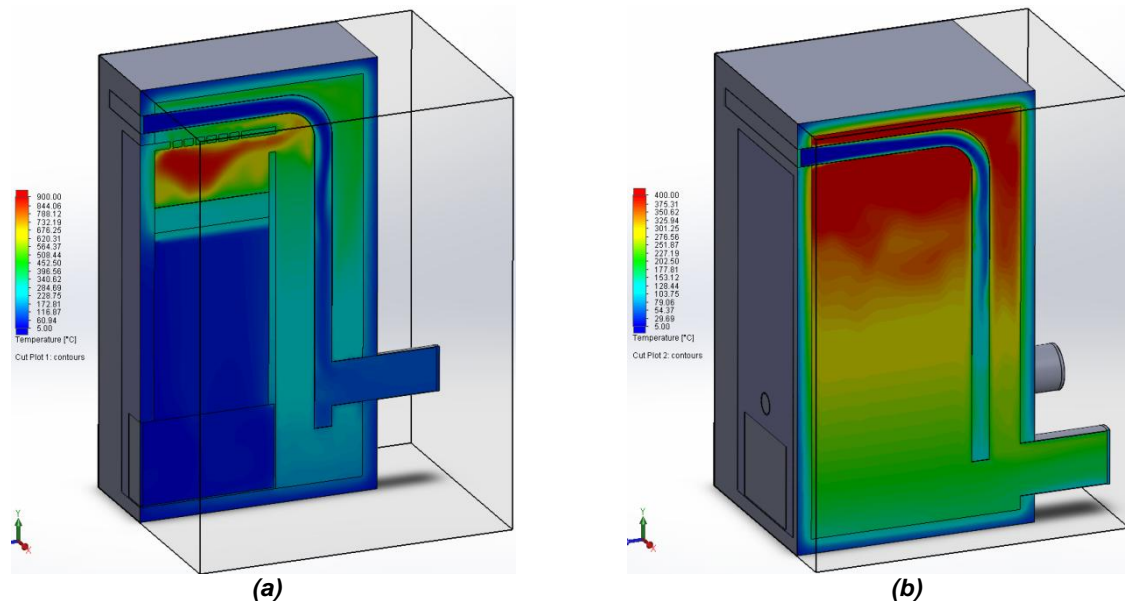


Fig. 4 - Temperature distribution on two vertical planes cutting through both system outlets; Fresh air flow through heat exchanger: $0.028 \text{ m}^3/\text{s}$.

Average flows and temperatures of hot air from heat exchanger and flue gas at the outlet pipes were recorded. The hot air from the heat exchanger outlet will be mixed with fresh cold air until the temperature of the mixture drops to 28°C . The warm air is then used to heat the greenhouse or hothouse. In order to achieve the maximum efficiency of the system, it is necessary to find the maximum flow of warm air that can be delivered considering the four simulation cases. Also, results will be compared with those from previous research, where the non-optimized TLUD module was used.

The required mass flow of cold air to be mixed with the hot air provided by heat exchanger can be calculated with the following equation:

$$\dot{m}_{ca} = \dot{m}_{ha} \frac{T_{ha} - T_{mix}}{T_{mix} - T_{ca}} \quad (2)$$

where: \dot{m}_{ca} – mass flow of fresh cold air;
 \dot{m}_{ha} – mass flow of hot air from the heat exchanger outlet;
 T_{ha} – hot air temperature;
 T_{ca} – temperature of fresh cold air (in this case, 5°C);
 T_{mix} – air temperature after mixing hot air with cold air.

Both mass flow rates, as well as the temperature of hot air are provided by the simulation software. The total mass flow \dot{m}_{mix} to be delivered for greenhouse heating will be:

$$\dot{m}_{mix} = \dot{m}_{ca} + \dot{m}_{ha} = \dot{m}_{ha} \frac{T_{ha} - T_{ca}}{T_{mix} - T_{ca}} \quad (3)$$

These values as well as equations (2) and (3) are used in an Excel spreadsheet to calculate the total mass flow for each of the four simulations, both in case of the improved TLUD module and for the former, non-improved model (Table 1).

One can notice that the highest flow of warm air at 28°C is $\dot{m}_{mix} = 0.109 \text{ kg/s}$, and it resulted for the improved version of the TLUD module. It corresponds to a volumetric flow of $0.028 \text{ m}^3/\text{s}$ of hot air exiting the heat exchanger at a temperature of 98°C . Compared with the calculated flow of 0.086 kg/s warm air for the non-improved TLUD module, an increase of about 27% of total mass flow delivered to the small hothouse or greenhouse was achieved by means of simple changes to the initial design.

Table 1

The main parameters of fresh air and flue gas at the outlets, and calculated mass flow of warm air for greenhouse heating, for improved and non-improved TLUD module

Type of TLUD module	Air flow through heat exchanger (m ³ /s)	Hot air temperature at the heat exchanger outlet (°C)	Flue gas temperature at the outlet (°C)	Air flows to be mixed for greenhouse heating		Total flow of warm air for greenhouse heating (kg/s)
				Mass flow at the outlet of heat exchanger (kg/s)	Mass flow of fresh cold air (kg/s)	
Improved	0.007	249	246	0.0047	0.045	0.050
	0.014	138	142	0.012	0.057	0.069
	0.021	101	133	0.02	0.063	0.083
	0.028	98	129	0.027	0.082	0.109
Not improved	0.007	243	249	0.0048	0.045	0.050
	0.014	172	208	0.011	0.069	0.080
	0.021	99	141	0.02	0.062	0.082
	0.028	78	130	0.028	0.061	0.089

In figure 5, the variation of air temperature at the heat exchanger outlet is plotted against the volumetric flow of fresh air at the heat exchanger inlet, and a reciprocal logarithmic trendline is added. As expected, one can notice that a further increase of volumetric flow will continue to reduce the temperature of the air at the heat exchanger outlet, but at a progressively slower rate. Thus, in a further research it would be interesting to evaluate the performance of the heating system at an air flow through the exchanger above the value of 0.028 m³/s, and to recalculate and maximize the total flow of warm air to be used for greenhouse or hothouse.

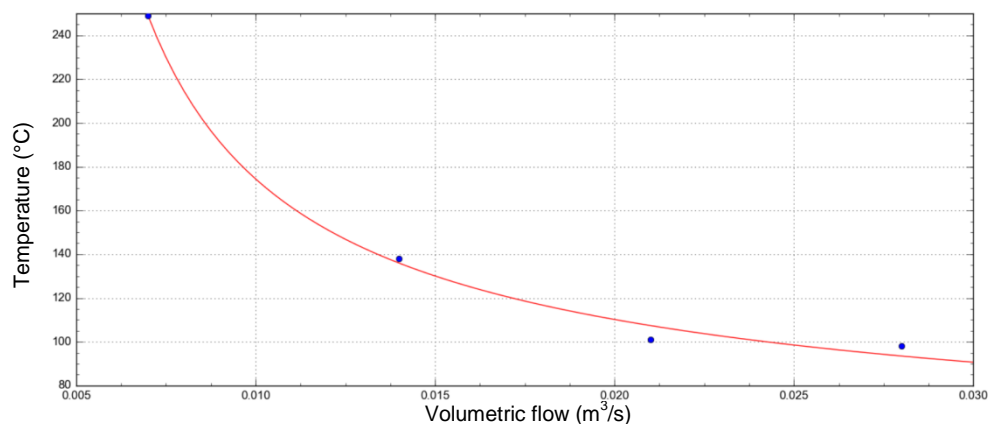


Fig. 5 - Variation of air temperature at the outlet of heat exchanger, with volumetric flow at the inlet of heat exchanger

CONCLUSIONS

CFD simulations were performed on a system for heating small greenhouses or hothouses with an improved design of a TLUD module. Four cases were considered, each of them with a different flow of air through the heat exchanger (from 0.007 to 0.028 m³/s), while the primary and secondary air flows through the TLUD module were kept constant, at 0.007 m³/s. In a previous research (Maican, et al., 2016) it was demonstrated that this value produces the lowest emissions in terms of GHG and PM_{2.5}, for the proposed TLUD design.

Results were compared with those from a previous research (Maican & Duțu, 2017), where an initial, non-improved TLUD design was used. Also, the total mass flow of warm air to be used for greenhouse heating was calculated.

It was found that the highest flow of warm air was delivered when the air flow through the heat exchanger was 0.028 m³/s, for the improved TLUD design. This represents an increase of 27% when compared to the previous one.

The plot representing the variation of air temperature at the outlet against its flow suggests that there is further room for improvement, by means of slightly increasing the air flow through the heat exchanger above 0.028 m³/s. This aspect will be the subject of further research. A secondary effect of the design improvement was that the total weight of the equipment was reduced by 28 kg.

REFERENCES

- [1] Acharya C., Jiang F., Liao C., Cattolica R., (2013), Tar and CO₂ removal from simulated producer gas with activated carbon and charcoal. *Fuel Processing Technology*, 106, pp.201-208;
- [2] Ayhan D., (2008), Importance of biomass as energy sources for Turkey. *Energy Policy*, 36, pp.834-842;
- [3] Burkhard E., Albrecht R., (2008), *Biomass Combustion in Europe - Overview on Technologies and Regulations*. Verenum Switzerland: Thomas Nussbaumer;
- [4] Devesa-Rey R., Vecino X., Varela-Alende J., Barral M., Cruz J., A.B. M., (2011), Valorization of winery waste vs. the costs of not recycling, *Waste Management* (31), pp.2327-2335;
- [5] EU Parliament, (2009), Directive 2009/28/EC of the European Parliament and of the Council on the promotion of the use of energy from renewable sources, *Official Journal of the European Union*. Brussels;
- [6] Fowles M., (2008), Black carbon sequestration as an alternative to bioenergy. *Energy Policy*, 36, pp.426-432;
- [7] Hale S., Lehmann J., Rutherford D., Zimmerman A., Bachmann R., Shitumbanuma V., Cornelissen G., (2012), Quantifying the total and bioavailable polycyclic aromatic hydrocarbons and dioxins in biochars, *Environmental Science and Technology*, 46, pp.2830-2838;
- [8] Huggins T., Haeger A., Biffinger J., Ren Z., (2016), Granular biochar compared with activated carbon for wastewater treatment and resource recovery, *Water Research*, 94, pp.225-232;
- [9] Iovane P., Donatelli A., Molino A., (2013), Influence of feeding ratio on steam gasification of palm shells in a rotary kiln pilot plant. Experimental and numerical investigations. *Biomass and Bioenergy*, 56, pp.423–431;
- [10] Karaj S., Barfuss I., Schalk J., Reisinger G., Pude R., Müller J., (2011), Modelling of air resistance during drying of wood-chips. *Proceedings of the CIGR International Symposium on Sustainable Bioproduction - Water, Energy and Food*, Tokyo, Japan;
- [11] Maican E., Duțu I., (2017), CFD validation of a novel heat generation equipment for greenhouses and hothouses. *Proceedings of the 45-th International Symposium "Actual Tasks on Agricultural Engineering"*, pp. 481-490, Opatija, Croatia;
- [12] Maican E., Murad E., Cican G., Duțu I., (2016), Analysis of a Top Lit Updraft Gasification System Designed for Greenhouses and Hothouses. *Proceedings of the 16-th International Multidisciplinary Scientific Geoconferences (SGEM), vol. Renewable Energy Sources and Clean Technologies*, pp. 107-114, Albena, Bulgaria;
- [13] Molino A., Chianese S., Musmarra D., (2016), Biomass gasification technology: The state of the art overview. *Journal of Energy Chemistry*, 25, pp.10-25;
- [14] Mukunda H., Dasappa S., Paul P., Rajan N., Yagnaraman M., Ravi Kumar D., Deogaonkar M., (2010), Gasifier stoves - Science, technology and field outreach. *Current Science*, 98(5), pp.627-638;
- [15] Murad E., Maican E., Dumitrescu C., Biris S., (2015), Extending the Use of Hothouses through Heating with Residual Agricultural Biomass. *Journal of Energy and Power Engineering*, 9(9), pp.769-774;
- [16] Paiano A., Lagioia G., (2016), Energy potential from residual biomass towards meeting the EU renewable energy and climate targets. The Italian case. *Energy Policy*, 91, pp.161–173;
- [17] Patuzzi F., Prando D., Vakalis S., Rizzo A., Chiaramonti D., Tirlor W., Baratieri M., (2016), Small-scale biomass gasification CHP systems: Comparative performance assessment and monitoring experiences in South Tyrol (Italy). *Energy*, 112, pp.285–293;
- [18] Reed T., Anselmo E., Kirker K., (2000), Testing and modeling the wood-gas turbo stove. *Proceedings of the Progress in Thermochemical Biomass Conversion Conference*. Tayrol, Austria;
- [19] Shen Y., (2015), Chars as carbonaceous adsorbents/catalysts for tar elimination during biomass pyrolysis or gasification. *Renewable & Sustainable Energy Reviews*, 43, pp.281–295;

- [20] Sundblad F., (2014), An improved cooking stove for the urban and peri-urban areas in Zambia (Master of Science Thesis in Industrial Design Engineering). Gothenburg, Sweden: Chalmers University of Technology;
- [21] Supramono D., Inayati F., (2013), Performance of a Biomass-Gas Stove using Fuel of Rubber Wood Pellets. *Proceeding of the 13th International Conference on QIR (Quality in Research)*. Yogyakarta, Indonesia;
- [22] Wang L., Weller C., Jones D., Hanna M., (2008), Contemporary issues in thermal gasification of biomass and its application to electricity and fuel production. *Biomass Bioenergy*, 32, pp.573-581.

DESIGN SUBSTANTIATION OF THE THREE-TIER CENTRIFUGAL TYPE MINERAL FERTILIZERS SPREADER

ОБГРУНТУВАННЯ ДИЗАЙНУ ТРИ РІВНЕВОГО ВІДЦЕНТРОВОГО РОЗКИДАЧА МІНЕРАЛЬНИХ ДОБРИВ

Prof. Ph.D. Eng. Kobets A.S.¹⁾, Lect. Ph.D. Eng. Naumenko M.M.¹⁾, Lect. Ph.D. Eng. Ponomarenko N.O.¹⁾, Prof. Ph.D. Agri. Kharytonov M.M.^{1)*}, Lect. Ph.D. Econ. Velychko O.P.¹⁾, Lect. Ph.D. Eng. Yaropud V.M.²⁾

¹⁾Dnipropetrovsk State Agrarian and Economic University, Faculty of Agrarian Engineering / Ukraine

²⁾Vinitsky National Agrarian University, Faculty of Agrarian Engineering / Ukraine

Tel: 0973456227; E-mail: envteam@ukr.net, Dnipro, Ukraine

Keywords: fertilizer, centrifugal spreader, disk distribution quality, movement analysis, spreading features.

ABSTRACT

The mathematical model for substantiation of engineering factors of machineries for centrifugal type mineral fertilization is developed.

It is proposed the design of the disk application for which one could improve evenness of mineral fertilizers spreading by centrifugal type spreaders. Simplified formulas for agricultural engineering usage, giving the opportunity to explain the construction of the fertilizer spreader which provides qualitative spreading for the given bandwidth, are also presented.

РЕЗЮМЕ

Розроблено математичну модель для обґрунтування технологічних параметрів машин для внесення мінеральних добрив відцентрового типу.

Запропонована конструкція диска, застосування якого може покращити рівномірність розсівання добрив розкидачами відцентрового типу. Виведені спрощені для інженерного застосування формули, що дають можливість обґрунтовувати конструкцію дискового розкидача добрив, який забезпечує якісне розсівання на смугу заданої ширини.

INTRODUCTION

The uneven distribution of fertilizers on the surface of the field determines the variability of crops management, yields, the different periods of maturation of crops, debris, deterioration of product quality (Kravchuk et al., 2004; Ning et al, 2015, Velychko, 2015; Vasylieva and Pugach, 2017). More than 90% of modern machinery for fertilizer application equips centrifugal spreaders that successfully transfer granular and crystalline fertilizers to the soil (Petcu et al., 2014; 2015; Tijskens et al., 2008).

Consequently substantiation of design and options of fertilizer distributor's centrifugal tool is very relevant (Allaire and Parent, 2004; Biocca et al., 2015; Nukesheva et al, 2016). The composition of the spreaders includes a disk with blades. This disk is placed under the spout and is rotationally driven around the vertical axis. In this case the fertilizer, which is uniformly distributed by the spout from the hopper, is received on the working surface of the rotating disc. Here it is captured by the vanes and forced into a rotary motion. Under the action of centrifugal forces particles of fertilizer are moving with acceleration on the working surface of the disc along the blades (from the disk centre to the periphery). The fertilizer particles are much faster after the disappearance of the disk (Antille et al., 2013; Šimaet al., 2013). The velocity vector is directed horizontally or at a certain angle to the horizon upwards.

The theory of single part movement on horizontal disk which turns around vertical axis as well as on disk with straight or curve blade was developed in numerous studies (Petcu et al., 2015; Vilette et al., 2005). However, despite the fundamental surveys in the theory of granule and disk interaction and numerous improvements of the working body design, evenness of mineral fertilizer spreading is far from perfect (Reumers et al, 2003).

Centrifugal machines are characterized by a significant separation of unilateral fertilizer to fractions and mixed components (Hofstee, 1992). Significant uneven distribution of fertilizers in width of the spreaders centrifugal type is due to the ballistic properties of the fertilizer particles. The list of ways to improve centrifugal devices include the following: a) the use of conical disks (Ancza et al., 2009; Dong et al., 2013),

b) blades with different length and tapered pointed shape, c) the discs installed in several tiers with inclination to the horizontal and at a considerable height above the ground (Hijazi et al., 2014); d) create a windproof device-specific profile (Fulton, et al., 2001).

MATERIALS AND METHODS

The process of granules distribution on the field surface is multivariate probabilistic in nature. In the general case this process cannot be normal. Meanwhile, the distribution of the granules may be close to normal if we can provide a sufficient number of variants of the granules original climbing from the disk surface. Graphical interpretation of this situation is shown in Fig.1.

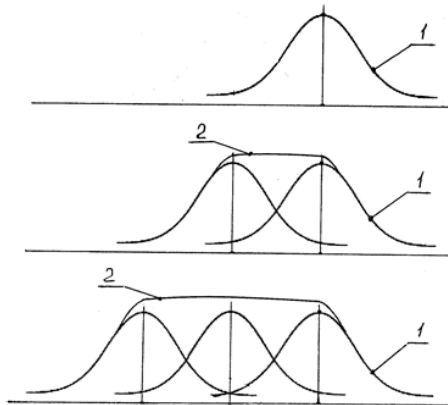


Fig. 1 - Graphical interpretation of fertilizer granules distribution on the field surface in the presence of other (a) two (b) three and (c) vanishing points from a disk surface:
1 – single distribution law; 2 – a plot of the normal distribution

The amount of distributions on the type 1 allows obtaining plots of the type 2, which are close to a normal distribution. Thus, it is necessary to provide the gathering from disk multiple streams of pellets with different initial speeds. It is necessary also to avoid overlapping of flows during the flight.

One of the significant reasons of spreading unevenness is explained in fig.2, where is shown the possible distribution of granules which are thrown by disk in ideal conditions: all granules are thrown with equal speed and evenly (the same amount thrown in a sequence of time), the granules have equal size and as a consequence drop out at the same distance B from the centre, in the case when the machine-tractor aggregate doesn't move.

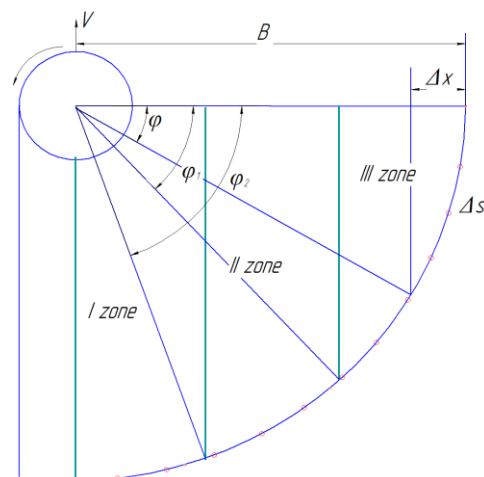


Fig. 2 - Scheme for analysing the uneven fertilizer spreading along the working width if centrifugal working body rotates evenly

If all granules, while disk unloads, are thrown at the equal distance B from the centre, in case the aggregate doesn't move, then while the aggregate is moving the compaction spreading on the periphery of working width becomes more obvious. Based on accepted idealized schematic layout of spreading, it may be concluded that granules amount is attributable to Δx by working width, proportional to appropriate length of semi-circular arc Δs . It gives an opportunity to define intensity of spreading area, which is being processed, in ratio $\Delta s/\Delta x = \omega$. In other words, the ratio of arc length to the working width is corresponding to it. This

gives the opportunity to characterize the intensity of the sowing area, which is being processed, the ratio $\Delta S/\Delta X$.

During the work of the spreader, the upper disk will sow three lanes, the second two and the third - one. It was established that for providing spreading uniformity, it is necessary that materials amount which will drop out from the middle disk additionally on second and third lane be 53.56% of the amount spread by the upper disk. On the first lane from the bottom disk will drop 11.24% fertilizers from the same amount. That way, spreading materials between bands can be evaluated by equation:

$$V=X+0.5366X+0.1124X \quad (1)$$

V – Total fertilizers outlay, X - delivery, provided by the upper disk.

Eq.1 gives an opportunity to estimate that the upper disk should provide delivery 0.61 V ; middle – 0.325 V ; nether – 0.065 V .

The spreader three-tier design was proposed for spreading evenness improving (fig.3).

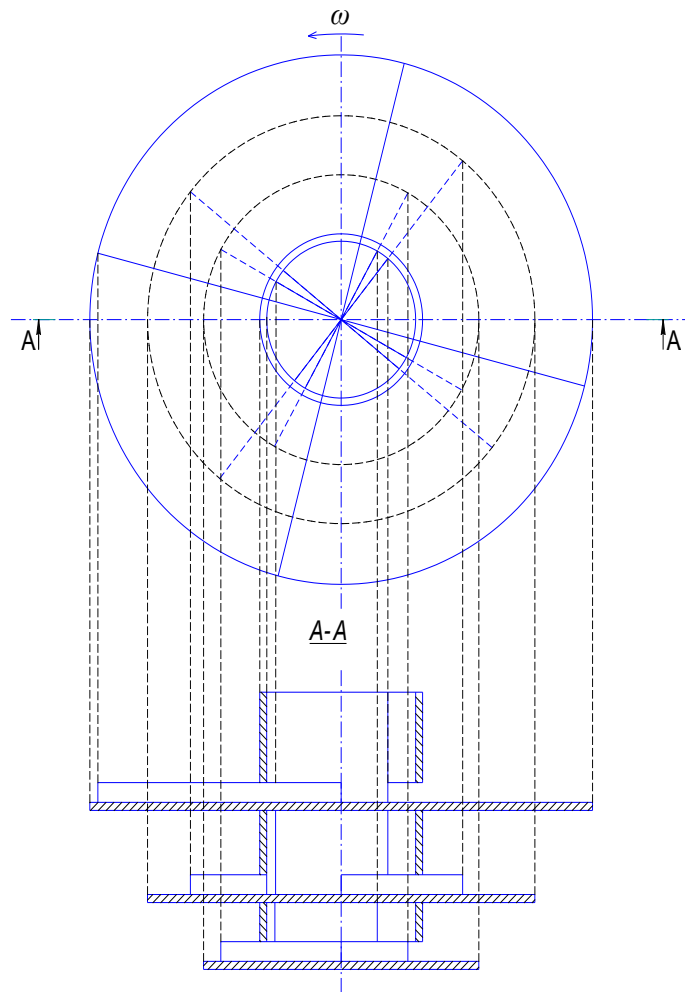


Fig. 3 – Design of spreader's construction

RESULTS

According to the proposed spreader design, it was estimated the distribution of materials flow provided by conical feeder with disks which turns around. The cross section of the feeder is divided by vertical partitions into separate sectors, the area of which is correlated in accordance with the weight of material to prepare separate discs. To ensure the desired distribution of fertilizer flow, it is necessary to determine diameters of three disks of the spreader.

The dependence between disk diameter and flying distance with assigned angular velocity is established. For estimation of escaping velocity of separate granule from a disk, its relative motion is considered.

The design model for movement analyse is shown in fig.4.

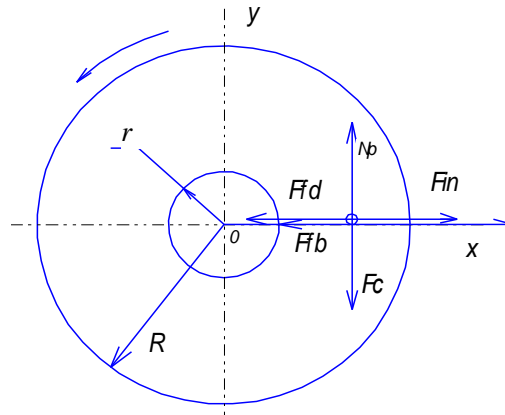


Fig. 4 - Scheme of forces distribution that influences the granule during disk rotation

Vector equation of the granule relative motion has the following form:

$$m\overline{W}_r = \overline{F}_e^{in} + \overline{F}_{fb} + \overline{F}_{fd} + \overline{F}_c^{in} + \overline{N}_p + \overline{N}_d + \overline{P} \quad (2)$$

According to the known granules weight $-m$, angular velocity of the disk ω and friction coefficient f , forces that influence the granule in relative motion along the axis OX (fig. 2) are defined as:

\overline{F}_e^{in} - inertia transfer, $\overline{F}_e^{in} = m\omega^2 x$;

\overline{F}_c^{in} - Coriolis' inertial force, $\overline{F}_c^{in} = 2m\omega\dot{x}$;

F_{fb} – frictional force during interaction with edge; $F_{fb} = 2fm\omega\dot{x}$;

N_p – edge pressure; $N_p = \overline{F}_c^{in}$;

\overline{N}_d – disk reaction; $\overline{N}_d = P$;

P – weight; $P = mg$;

F_{fd} – frictional force when granule is interacting with disk, $F_{fd} = fmg$;

W_r – relative acceleration $W_r = \ddot{x}$; \dot{x} - relative velocity.

According to the above written, the differential equation of granule relative motion can be written in the form:

$$m\ddot{x} = m\omega^2 x - 2fm\omega\dot{x} - fmg,$$

$$\text{or} \quad \ddot{x} + 2n\dot{x} - \omega^2 x = fg \quad (3)$$

where $n = f\omega$

Solving of the differential equation (3) looks like:

$$x = c_1 e^{\omega\sqrt{(1+f^2-f)}t} + c_2 e^{-\omega\sqrt{(1+f^2+f)}t} - \frac{fg}{\omega^2} \quad (4)$$

Whence

$$\dot{x} = c_1 \omega \sqrt{(1+f^2)} e^{\omega\sqrt{(1+f^2-f)}t} - c_2 (\omega\sqrt{(1+f^2+f)} + f) e^{-\omega\sqrt{(1+f^2+f)}t} \quad (5)$$

Given that the initial relative velocity is zero from the equation (5) we get: $c_1 = c_2 (\sqrt{1+f^2} + f)^2$

Taking that at the time $t=0$, $x = r$ equation (4) we have:

$$r = c_2 (\sqrt{1+f^2} + f)^2 + c_2 - \frac{fg}{\omega^2},$$

than

$$c_2 = \frac{r\omega^2 + fg}{((\sqrt{1+f^2} + f)^2 + 1)\omega^2}, \quad \text{and} \quad c_1 = \frac{(r\omega^2 + fg)(\sqrt{1+f^2} + f)^2}{\sqrt{1+f^2} + f}.$$

Thus, formulas (4) and (5) make it possible to determine at any time not only the position of a granule, which moves along the edge, but also its relative velocity. Absolute velocity of the granule can be found as a

vector sum of relative (5) and portable velocity. The vector sum of velocities is determined for the current value of coordinate x by the formula (4), as $V_e = wx$.

The graphical dependence between the current coordinate of the granule on the disk and the absolute speed is made using a table processor *Excel* (fig.5).

In the example above, it was assumed that the relative motion begins at the time when $x=r$, where r – feeder radius ($r = 0.05$ m); angular velocity $w = 56.7$ rad/s; the friction coefficient during granule sliding by disk $f = 0.1$.

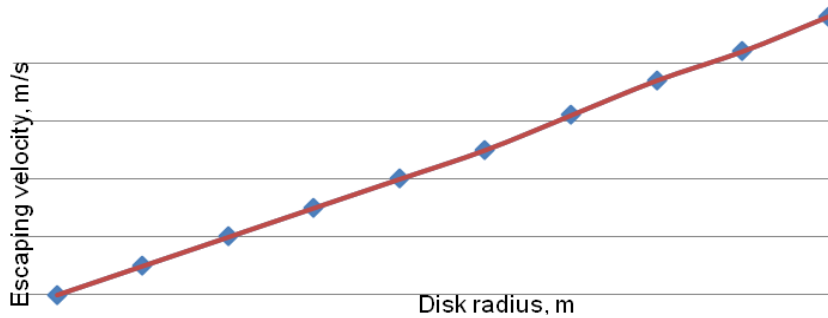


Fig. 5 - The dependence of granule escaping velocity on the disk radius

As shown in Fig. 5, for real values, the length of the edge is within range: $0.05 \leq x \leq 0.4$. Under these conditions, dependence of the absolute velocity on granule coordinate on the disk is close to the linear one. It is clear that the given dependence (for given output values) can be used when assigning the diameter of the disk to provide the required granule escaping velocity from the disk.

To determine the range of flight it is necessary to investigate the movement of a granule that will fly from a spreader with a horizontal initial velocity V_0 .

In the coordinate system XOY differential equations of flight have the form (Fig.6).

$$m\ddot{x} = -Q \cos\alpha; \quad m\ddot{y} = P - Q \sin\alpha,$$

where

Q - air resistance, which we consider like proportional to the flight velocity, i.e. $Q = \mu V$;

P – granule weight; α – angle that formed by velocity vector and axis x .

Taking into account that $V = \sqrt{\dot{x}^2 + \dot{y}^2}$, $\cos\alpha = \frac{\dot{x}}{\sqrt{\dot{x}^2 + \dot{y}^2}}$ and $\sin\alpha = \frac{\dot{y}}{\sqrt{\dot{x}^2 + \dot{y}^2}}$ instead of equations (6)

and (7) we will get

$$m\ddot{x} = -\mu\dot{x}; \tag{8}$$

$$m\ddot{y} = mg - \mu\dot{y} \tag{9}$$

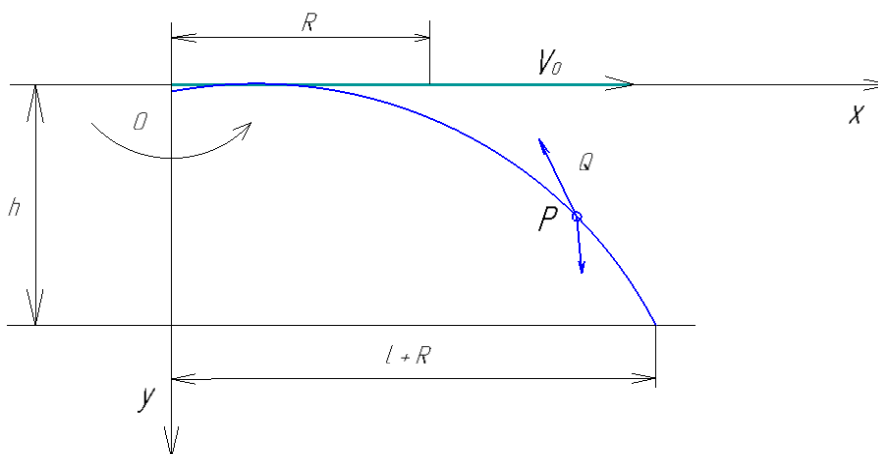


Fig. 6 - Diagram of granules flight analysis

From the differential equation (8) we will get $\frac{d\dot{x}}{\dot{x}} = -\frac{\mu}{m} dt$, i. e. $\ln \dot{x} = -\frac{\mu}{m} t + c$

Given that the escaping velocity is known V_0 we will get:

$$\ln \dot{x} = -\frac{\mu}{m} t + \ln V_0$$

Than $\ln \frac{\dot{x}}{V_0} = -\frac{\mu}{m} t$ from here $\dot{x} = V_0 e^{-\frac{\mu}{m} t}$

Than $x = -V_0 \frac{m}{\mu} e^{-\frac{\mu}{m} t} + C_1$, or taking into account, that the flight began at the edge of disk, where $x_0 = R$

$$x = V_0 \frac{m}{\mu} \left(1 - e^{-\frac{\mu}{m} t} \right) \tag{10}$$

While integrating the differential equation (9) we will get:

$$\frac{dy}{q - \frac{\mu}{m} y} = dt$$

Whence $\ln \left(q - \frac{\mu}{m} y \right) = -\frac{\mu}{m} t + C_2$.

Taking into account that $y_0 = 0$ we will get $\ln \frac{q - \frac{\mu}{m} y}{q} = -\frac{\mu}{m} t$

Whence $1 - \frac{\mu}{qm} y = e^{-\frac{\mu}{m} t}$

i.e. $\frac{\mu}{qm} y = 1 - e^{-\frac{\mu}{m} t}$.

Whence $dy = \frac{qm}{\mu} \int \left(1 - e^{-\frac{\mu}{m} t} \right) dt$

Than $y = \frac{qm}{\mu} t + \frac{qm}{\mu} \cdot \frac{m}{\mu} e^{-\frac{\mu}{m} t} + C_3$

Taking into account that $y_0 = 0$ for C_3 we will get

$$C_3 = -\frac{qm}{\mu} \cdot \frac{m}{\mu}$$

Than

$$y = \frac{qm}{\mu} \left(t - \frac{m}{\mu} \left(1 - e^{-\frac{\mu}{m} t} \right) \right) \tag{11}$$

Formula (11) allows determining flight time of granule depending on height of disk placement (fig. 4).

Formula (10) allows determining the initial escaping velocity of granule, which provides required range of flight (bandwidth) l .

$$V_0 = \frac{(x-R)\mu}{m \left(1 - e^{-\frac{\mu}{m} t} \right)}$$

Thus, the initial velocity, which should provide the disk rotation, can be found from the flight analysis of the granule. The diameter of the disk is determined based on developed dependence shown in fig. 5.

A diagram that qualitatively describes the distribution of granules at the simultaneous screening of three edges is shown in fig.7.

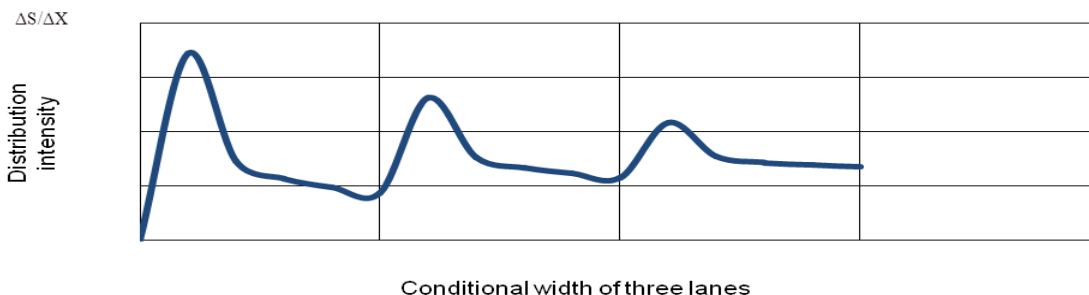


Fig. 7 - The distribution of the three streams

Square curve limited distribution intensity. On each of the three units, the width of the swath is approximately equal. Each strip has approximately the same number of pellets. Given the distribution pattern is idealized. All the pellets fly up from the surface of one of the ribs at the same distance. The reality is that the granules are not the same in shape and volume. They have different aerodynamic characteristics that provide a different range and improve the uniformity of their distribution.

CONCLUSIONS

- The distribution of fertilizer granules on field surface is a multifunctional dependence. Taking into account all input parameters, for an analytical study it is too complicated by mutual influence of factors one to other.
- The three-tier mineral fertilizer spreader designed to provide high-quality spreading without the intersection of streams that escapes from the current tier is substantiated.
- The mathematical model of the process of granules interaction with disk and subsequent spreading of granules is provided. Air resistance affects the final distribution of fertilizer granules on soil surface. Basically, the influence is shown in changing the flight range of individual granules.
- The calculation diagram of spreading disks diameters is shown. Analysis of possible variants of centrifugal working body constructions for mineral fertilizing allowed accepting the spreader scheme, construction of which involves the formation of granules streams location during loading.

ACKNOWLEDGEMENT

The work has been funded by the Ukrainian Ministry of Education and Science.

REFERENCES

- [1] Allaire S. E. and L. E. Parent, (2004), Physical Properties of Granular Organic-based Fertilisers, Part 1: Static Properties, *Biosystems Engineering*, 1, pp.79-87;
- [2] Ancza E., Gindert-Kele A., Hagymássy Z., (2009), The Effect of the Design of the Spreading Device on the Working Width and Evenness of Spreading in the Case of Centrifugal Spreaders Bulletin UASMV Agriculture, Print ISSN, 66 (1), pp.1843-5246;
- [3] Antille D.L., Gallar-Redondo L., Godwin R.J., (2013), Determining the particle size range of organo-mineral fertilisers based on the spreading characteristics of the material, *ASABE Annual International Meeting*, Paper n° 13-1620197;
- [4] Biocca M., Gallo P., Menesatti P., (2013), Aerodynamic properties of six organo-mineral fertiliser particles. *Journal of Agricultural Engineering*, volume XLIV(s2):e83: pp.411-414;
- [5] Dong X., Song J., Zhang J., Wang J., (2013), Working performance and experiment on granular fertilizer spreader with cone disk. in *Nongye Gongcheng Xuebao/Transactions of the Chinese Society of Agricultural Engineering* 29(19), pp.33-40;
- [6] Fulton J. P., Shearer S. A., Chabra G., Higgins S. F., (2001). Performance assessment and model development of a variable-rate, spinner-disc fertilizer applicator. *Transactions of the ASAE*. Vol. 44(5), pp.1071–1081;
- [7] Hijazi B., Cool S., Vangeyte J., Mertens K.C, Cointault F., Paindavoine M., Pieters J.G. (2014) High Speed Stereovision Setup for Position and Motion Estimation of Fertilizer Particles Leaving a Centrifugal Spreader; *Sensors* , 14, pp.21466-21482;
- [8] Hofstee J. W., (1992), Handling and spreading of fertilizers: part 2, physical properties of fertilizer, measuring methods and data. *Journal of Agricultural Engineering Research*, Vol. 53: pp.141–162;
- [9] Kravchuk V.I., Grytsigina M.I., Kovalya S.M., (2004), *Modern tendencies of construction development of agricultural technique (Сучасні тенденції розвитку конструкції сільськогосподарської техніки)*, Ed.Agrarian Science, p.396;
- [10] Ning S., Taosheng X., Liangtu S., Rujing W., & Yuanyuan, W, (2015), Variable rate fertilization system with adjustable active feed-roll length. *International Journal of Agricultural and Biological Engineering*, Vol. 8, Issue 4: pp.19–26;
- [11] Nukesheva S.O., Eskhozhina K.D., Tokusheva M.H., Zhazykbayeva Z.M., (2016), *Substantiation of the Parameters of the Central Distributor for Mineral Fertilizers*, *International journal of environmental & science education*, Vol. 11, №15, pp.7932-7945;

- [12] Petcu A., Ștefan V., Popa L., Toderasc P., Ciupercă R., (2014), Factors influencing the management of granular fertilizers, *Tehnomarket* nr.2, pp.20-21;
- [13] Petcu A.S., Popa L., Ștefan V., Ciuperca R., Nedelcu A., Girleanu I.C., Avramescu A.M., Veringa D., Zaica A., Lazar G., (2015), Theoretical research regarding the working process of the fertilizers managing systems by centrifugation. *Annals of the University of Craiova - Agriculture, Montanology, Cadastre Series*, Vol. XLV: pp.174-184,
- [14] Reumers J, Tijsskens E., Ramon H., (2003), "Experimental characterisation of the tangential and cylindrical fertiliser distribution pattern from a spinning disc : A parameter study," *Biosystems Engineering* 86(3), pp.327-337;
- [15] Šima T., Nozdrovický L., Krupička J., Dubeňová M., Koloman K. (2013), Granulometric study of dasa 26/13 fertiliser. *MENDELNET*, pp.882-887;
- [16] Tijsskens E., Van Liedekerke P., Piron E., Van Geyte J., Cointault F. et al., (2008), Recent results of experimental and Dem modeling of centrifugal fertilizer spreading. *Granular Matter*, Springer Verlag, 10 (4), pp.247 – 255;
- [17] Vasylieva, N. and Pugach, A., (2017); Economic assessment of technical maintenance in grain production of Ukrainian agriculture. *Bulgarian Journal of Agricultural Science*, 23(2), pp.198–203;
- [18] Velychko O., (2015), Logistical system Fortschrittzahlen in the management of the supply chain of a multi-functional grain cooperative, *Economics and Sociology*, Vol. 8, No.1: pp.127-146;
- [19] Vilette S., G Cointault F., Piron E., Chopinet B., (2005), Centrifugal spreading an Analytical Model for the Motion of Fertilizer Particles on a spinning disc, *Biosystems Engineering*, 92(2), pp.157-164.

SOWING MACHINES AND SYSTEMS BASED ON THE ELEMENTS OF FLUIDICS

ВИСІВНІ МАШИНИ ТА СИСТЕМИ НА ОСНОВІ ЕЛЕМЕНТІВ ПНЕВМОНІКИ

Prof. D.Sc. Eng. Aulin V.V., Prof. D.Sc. Eng. Chernovol M.I., Ph.D. Eng. Pankov A.O.,
Ph.D. Eng. Zamota T.M., Ph.D. Eng. Panayotov K.K.

Kirovograd National Technical University / Ukraine
Tel: +380950396372; E-mail: app.post@rambler.ru, aulin52@mail.ru

Keywords: *pneumatics, fluidics, stream element, sowing system*

ABSTRACT

On the basis of the research results it is established that to increase the productivity and quality, as well as to reduce the work intensity of planting machines it is necessary to unite the metering and timing system on one principle – the principle of discrete action. The rational basis for this is using of control and power fluidic devices, and active distribution of pneumatic devices and pneumatic power systems. On this basis, pneumatic seeding systems on the row and one grain sowing were developed, which also allows distributing seeds differentially when this seeding technology is used for precision farming.

РЕЗЮМЕ

На підставі результатів досліджень встановлено, що для підвищення продуктивності і якості, зниження енергоємності роботи посівних машин необхідно об'єднання висівного апарату і системи синхронізації на одному принципі – дискретної дії, а раціональною основою для цього є застосування керуючих і силових струменевих елементів, а також активних пневматичних розподільних пристроїв і пневматичної системи живлення. Виходячи з цього, розроблено пневмоструминні висівачі системи для рядової і однозернової сівби, що також дозволяють диференційовано розподіляти насіння при сівбі по технології точного землеробства.

INTRODUCTION

The traditional methods of agricultural technique production do not provide the increase of the labour productivity in proportion to expenses already, and also return of capital investments, and, at the same time, reduce efficiency of agricultural production. The state of Science and Technique presently allows finding principally new technical decisions.

At the same time, some systems of mechanization control and automation are working under trying conditions exploitations (at temperatures, different from normal, high accelerations, intensive oscillation and shock loadings, in the conditions of heavy dustiness, etc.). Therefore, search for the new technological and technical decisions, based on modern achievements of Science and Technique and proper socio-economic requirements, is required.

«Pneumatic» is a new direction in agricultural machinery. Pneumatics or pneumatic automation is an area of automation, based on the use of gas streams operation. A stream technique is analogical electronics in regard to both basic principles of construction and practical application. Devices and systems of stream technique do not have mobile details and are utilized in computers, pumps of heart-lungs, control the system rockets, submarine boats, metal-cutting machine-tools, etc. Jet elements are working on in relation to small overfalls of pressure. Jet techniques have a number of advantages before electronic. Its technique is maximum simple, lasting, cheap and reliable (Kassimov A., 2010). It is more reliable at high and low temperatures, and also at the high levels of radiation and steadier to the mechanical loadings and vibrations, which is very important in a mobile technique (Aulin V.V. et.al, 2016).

Jet techniques are a new direction of automation, but the perspective of its application in industrial and in agricultural engineering is great enough. In this connection there are many interesting questions yet to be solved, namely – possibilities of wider use of Jet elements and devices.

As generally known, the mortgage of high harvest at the low expenses of labour and facilities is timely and high-quality implementation of technological operations on agricultural crops tillage in accordance with agro technical requirements, in particular case sowing. For this purpose, the reliable, productive, high-quality working sets of technique are needed for all of operations in tillage technologies.

The study of the general state and prospects of the development of food stuff production technical providing shows that the extensive approach in relation to traditional facilities and mechanization process is unable to provide rationally the increase of amount and quality of products and works in the future, and also to the capacity requirement, adequate making progress capital investments, circulating cost and power expenses. The scopes of extensive growth are already obvious in the processes of traditional mechanization (*Kashubo N.D., 2007*).

The analysis of existing sowing machines and systems shows that the scientific thought was aimed at the original principles of sowing machines work. It allows improving the quality of the sowing process (*Firsov A.S. and Golubev V.V., 2013*). Lately, the decision on sowing process automation and its control has begun to appear (*Kobchenko S.N. and Medvedev E.Yu., 2015*). However, analysing the algorithmic models of technological processes of existing constructions of seed meters and systems for the different types of sowing and seeds, it is possible to draw a conclusion, namely that the operative algorithm of these constructions requires much more energy to overcome the friction of the materials, though less energy is required to fulfill the elementary operations of sowing.

Existing constructions of sowing machines still have high intensity, which results in using a lot of energy. It entails a high cost, insufficient reliability of machines, relatively large labour intensiveness of tuning, adjusting and maintenance of machines, and also restrains creation and applying in industry of new kinds of machine constructions. The analogical position is technique automation in agriculture.

The stake of the automated agricultural machines in the general volume of their output does not exceed 30%, the simplest means of control and management are used, together with hydraulic, mechanical and mixed devices. The application, for example, of microelectronics in the systems of automation of agricultural machinery separate groups is within the limits of 16%.

Further development of agriculture, its concentration, and consequently, the possibility of its intensification was put on an order-paper by new requirements to form the material and technical base of machine constructions.

Therefore, presently there is a question of development and applying in industry new, universal agricultural machines, including sowing, with minimum energy of production and exploitation, high reliability, automation of working process and possibility of its durability on every area of machine moving (*Garbers H., 2015; Alt V.V. et. al., 2008*).

To accomplish the set tasks, new direction is offered for creation of seed meters and devices on the basis of Jet elements. They are appropriate both for the ordinary sowing and for vegetable crops sowing, and also for the one seed sowing of the cultivated crops.

In agriculture, the information of Jet device on the basis of power Jet elements (Fig.1) can be used in seed sowing, the main new sowing systems being created as a result.

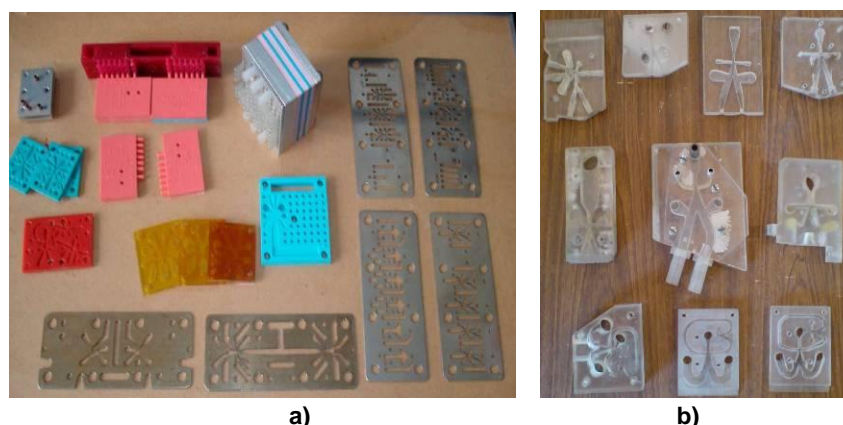


Fig. 1 - Power jet elements for sowing devices
a – for controlling, b - executive power elements

Hereupon, the task is to research the possibility to apply power Jet elements in devices for sowing different crops seeds.

Here we used the special tasks associated with the area of aeromechanics, the solution of which has led to the use of fluidic elements for sowing.

These tasks study the impact of economies of scale and modes of air movement in the development of fluidic devices that are designed to work in specialized seed devices.

To optimize the operation of the jet elements the dimensions of the cameras, the duct and the ratio between the values of pressure and flow control channels have to be rational (*Chernovol M.I. et.al., 2015*).

In addition, application of power stream elements restrains a device for a number of reasons - by their insufficient efficiency, by absence of the developed model standards as dimension, rows type etc. Therefore, for the removal of these retentive factors additional researches are required.

MATERIALS AND METHODS

During the research the following materials were used:

- models of seeding machines with elements of fluidics (look at Fig.2, 3, 6) and existing sowing machines N 126.13.000 (from planter SUPN-8);
- devices for flow measurement (G6PJI meter, rheometer-indicator, T-2-80) and instruments for measuring pressure (NWO-100Y3) and rarefaction (TMP-100Y3 and the manometer and U-shaped manometer); - stand "sticky tape" (see Fig. 3b);
- seed material: seeds of wheat, sunflower and sugar beet; - sowing machine to the tractor MTZ-80 (see Fig. 5). In the course of research designed planters used hydrostatic and hydrodynamic methods of determining pressure, flow and air velocity in seeding devices and systems as well as standard test methods of seeding machines and systems for dotted seed sowing in terms of seeding reliability and its conformity to the agronomic indicators. It is envisaged the definition of the following indicators:
 - the uniformity of seed distribution and the measurement of the intervals between the seeds on the sticky tape and in the groove on the germination of seeds;
 - seed damage by its visual inspection after sowing;
 - the stability and uniformity of sowing by weighing portions of seeds, which are sown at a distance of 100 meters;
 - the presence of twins near the seed and omissions of the individual seeds in the process of planting, visual inspection of seed number on the tape and germination after sowing.

RESULTS

Jet sowing system consists of sowing jet apparatus and the device for sowing synchronization with seeders' speed. A stream technique can work both in the power mode and in the mode of control.

Development of the given direction gives positive results presently. The standards of seed meters are created without mobile details on the basis of power elements and devices of stream pneumatic automation for ordinary crops sowing (Fig.2, a, b, Fig.3), (*Scheglov A.V., 2010; Scheglov A.V., 2011*).

It is also set (*Burkov Y. et.al., 2009; Kassimov A., 2010*) on the basis results of conducted analysis of the systems, that for the high-quality sowing of ordinary and cultivated crops the association of seed meter and system of synchronization is needed on one principle – discrete action, and rational basis for them is the pneumatic feed system. On this basis, the Jet sowing system is also developed including a seed meter with the drive of sowing drum (Fig.3).

In comparative tests of the new device ATV-7.02 and serial device N126.13.000 it was found that in the new apparatus the uniformity of seeding was better and the injury of seed was missing. Laboratory and field tests on the sowing system showed the high quality of seeds distribution and a perfect agreement with the seeders' agrotechnical requirements.

Comparison of apparatuses' operative quality shows that evenness of seed distribution ($\Delta\sigma$) is 2.7cm (for sunflower seeds) and 4cm (for sugar beet seeds, Fig.4).

Exactness of intervals at the developed and serial apparatus was: for the beet seed - 100 and 83%, for the sunflower seed - 100 and 85.4%. In addition, during the researches on the developed apparatus, unlike serial, there was not injuring of sowing material, as air stream fully purged suckers from seeds.

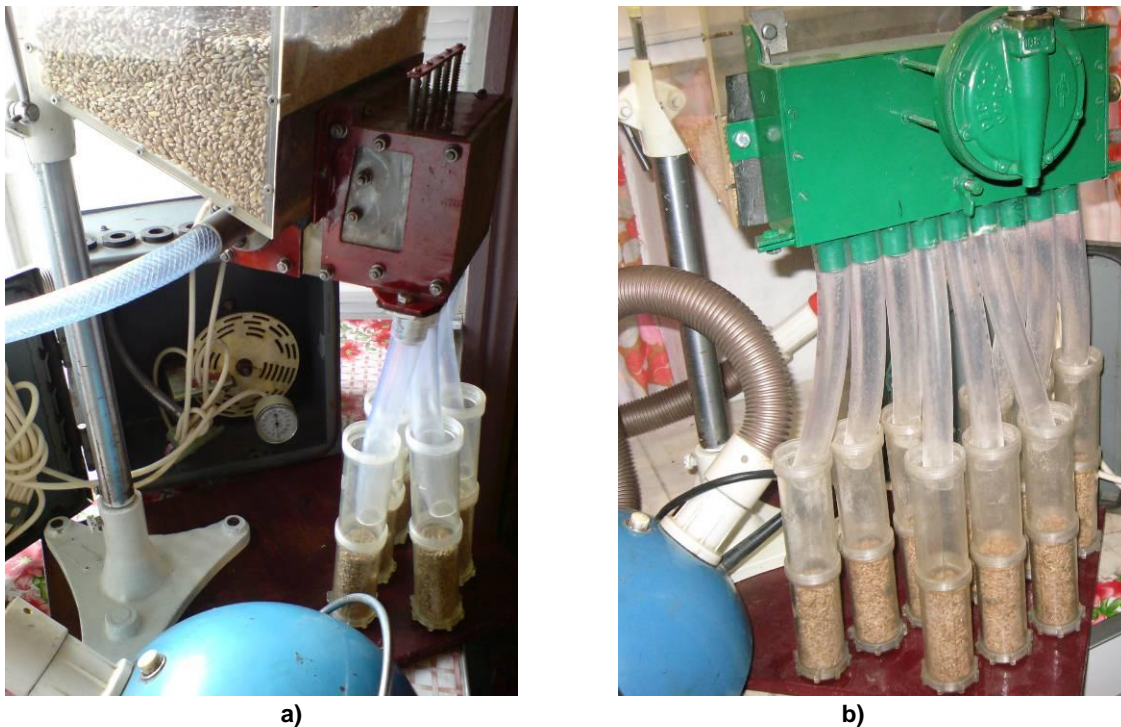


Fig. 2 - Seed meters based on pneumatic automation elements for ordinary crops sowing:
a - without moving details, for application in the systems of the centralized sowing (look at Fig.6),
b - for a layout chart there is an "apparatus – plowshare"

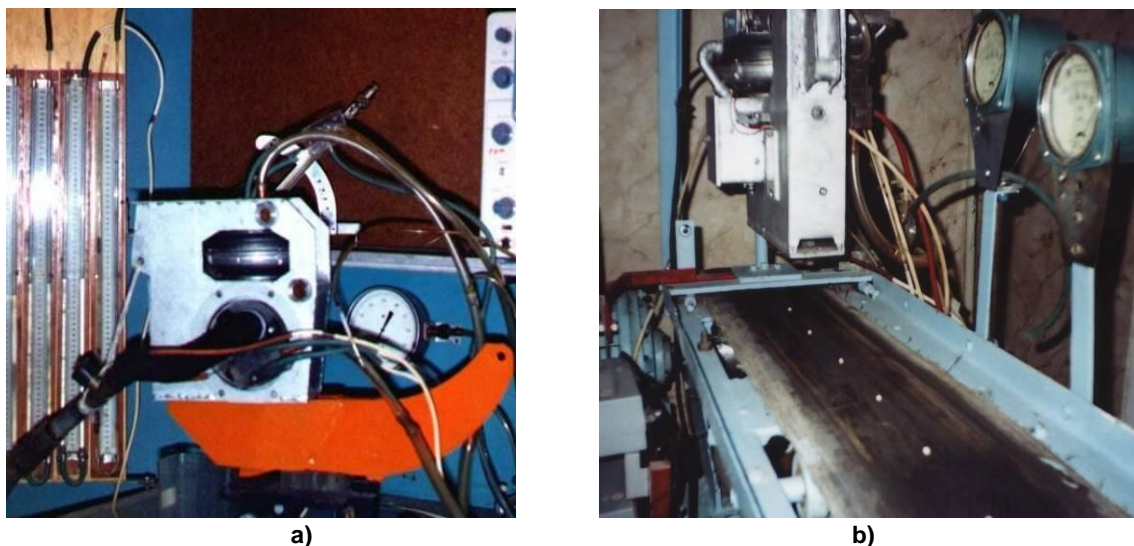


Fig. 3 - Seed meters based on pneumatic automation elements for one seed sowing:
a - an apparatus is testing the sowing stability,
b - a device is testing the uniformity of seeding on the sticky tape

Laboratory stand and production testing show high quality of seed distribution (the variation coefficient is 18.2-25.4% and exactness of intervals between plants growth is 86.7-85%), which conform to the agrotechnical requirements for precision seeding machines (*Belodedov V. et.al, 2013*).

The sowing systems also allow carrying out the differentiated seed sowing and distributing on an area in the technologies of exact agriculture.

In agriculture, sowing devices based on Jet elements can be also used for sowing of seed and distribution of mineral fertilizers; the creation of new universal planters appears as a result.

Seed meters and sensor-based systems based on stream pneumatic automation elements can work in the laboured external environments (at high accelerations, intensive oscillation and shock loadings).

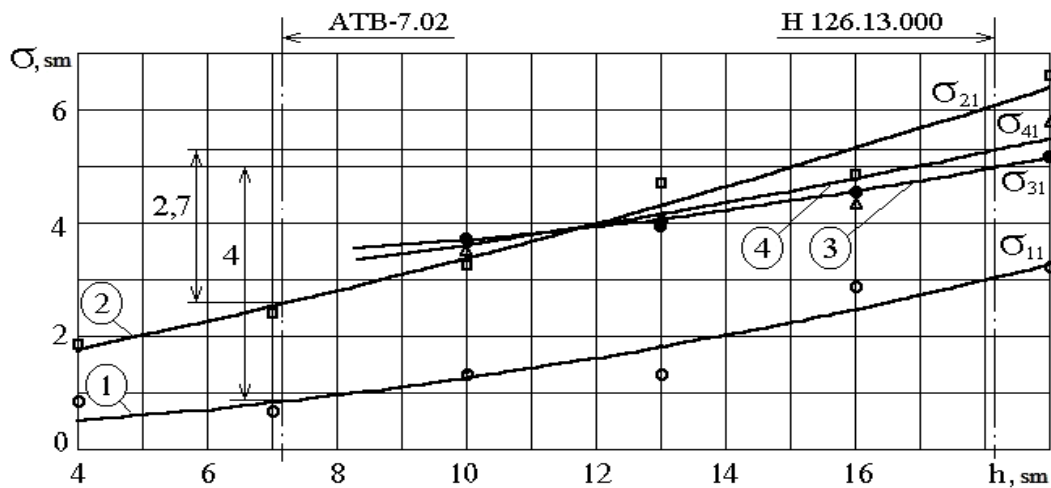


Fig. 4 - Dependence of rejection σ on intervals from the upcasting height "h" of seeds

1 and 2 - sugar beet and sunflower for the developed apparatus,

3 and 4 - sugar beet and sunflower for a serial apparatus

There are some other advantages of the sowing systems based on stream pneumatic automation elements, namely: high reliability and longevity; rather low cost of stuff details; simplicity of making technology (casting, unsealing on a 3D-printer); firmness to aggressive influences of environment; small resource-demanding, diminutiveness and fast-acting; a minimum of mobile mechanical and ground details; absence of individual regulations during setting of sowing norms; absence of driving mechanisms and gear boxes; absence of lubrication points; simplicity of tuning on the required sowing norm; simplicity of alteration on different sowing norms and charts; there is a high quality of sowing in all ranges of movement norms and rates; the sowing system requires a relatively small amount of energy; possibility of working process complete automation and control.

To further detail let us consider indexes related to process energy, namely to the power necessary for performing the working process. The comparative power analysis of seed meters and systems operation shows that on driving to the action and working process of Jet seed meters far less power expenses are required (Table 1). Comparison was made for the sowing machine of the ordinary sowing with the width of capture $B = 3m$ and number of plowshares $n_p = 24$.

Table 1

The energy costs of sowing systems operation

Type of seeding system	Power N_s summed up, (Watt)	Available power N_A , (Watt)	Fuel equivalent		System efficiency η
			(l/h)	(l/year)*	
Spool-type	440	2200	0.22	33.0	0.20
Pneumatic centralized	4272	12491	1.25	187.5	0.34
Sukhin sowing system	125	329	0.03	4.5	0.38
With elements of fluidics	144	421	0.04	6.3	0.34
Tilled seeder	1300	4632	0.46	69	0.28

* - when loading the planting machine 150 hours per year

It is known that for the proper culture, not including harvesters, it is necessary to have at least four separate machines, which have considerable steel intensity and cost, although they work during a limited period of the year. For example, the annual load of different planters reaches 50-160 hours, cultivators – 270-350 hours, etc. It is thus set that there is 116.1MJ of the materialized energy per one kilogram of agricultural machine mass, which corresponds to a heating value of approximately four litres of fuel.

It's obvious that a great deal of material energy which is paid for, doesn't do any work. The search of ways and possibilities is therefore required if not avoidance, minimization of such non-productive expenses of labour and facilities.

Also, one of the possible directions in researches is the creation of universal machines, due to the stream sowing systems which are considered better.

A machine (Fig.5) can have a frame of cultivator with add-on sections, pneumatic station the drive of which can be hydraulic or mechanical from a tractor, general control of the seed sowing or fertilizer distribution system and removable working knots, set on it; containers with sowing devices and devices covering seed with earth; plowshares, cultivation paws and rolling up wheels set on the add-on sections of the cultivator.

Thus, effectiveness of circulating costs, consisting in the decline of high power consumption of sowing process, takes place here. Also, as a result of replacing two machines by one, universal, the possibility to reduce expenses of the materialized energy or fixed assets is obtained.



Fig. 5 - Universal machine "seeder - cultivator"

It is necessary to point out that this is only one of the variants to apply Jet seed meters and systems. There are other possibilities of development in this direction:

- application in «precision» agriculture is easy enough adaptation to changing the line of sowing norms,
- possibility to create not only universal machines of type «seeder - cultivator» but also universal module which facilitates the mechanization of corn and cultivated crops tillage.

Also, one of perspective directions is the development of the pneumatic centralized sowing systems (PCSS). Their application allows promoting labour productivity on sowing and reducing sowing machines resource-demanding. But in terms of sowing quality, in particular the unevenness of sowing between plowshares, they do not always conform to the agro technical requirements.

One of reasons for such a position is that the dividing devices of known PCSS do not provide the required evenness of the sown material. At sowing machine inclinations and vibrations, under field conditions, there is the displacement of seed stream from the divisor axis of symmetry, so there is an increased unevenness as a result, while plant productivity largely depends on seed evenness on the sowing area. It is known that for this reason up to 20% of potential harvest is lost. The increased unevenness is due to an equal degree to the mechanical sowing machines with spool-type seed meters, which do not provide the high-quality sowing and distributing of seed, especially during work on slopes because of sowing material moving, which results in uneven distribution of plowshares.

From the review and analysis of literary sources it results that the most applied distributors - both vertical and horizontal type - are passive, which means that the negative effect of gravity, aerodynamic and the inertia forces on the seeds are not compensated. From here, their high technological "sensitiveness" results in external and internal influences, namely inclinations, vibrations, air pressure in the system, seed distribution, concentration of mixture etc. Besides, the distributors of horizontal type have a drawback which appears because of the effect of the so called "Galton board", which means that the main part of the seeds is in the center of the distributor. It is therefore necessary to create and improve distributive devices, providing

a high evenness of seeds on plowshares and possessing a sufficient technological “rudeness”, mostly eliminating negative influence of external and internal factors.

It is set that this requirement can be achieved by applying the seed active distribution on sowing boots. The constructions, where the active mechanical distributing, untwisting of seed stream is used on sending, under the influence of centrifugal forces, are already known. But in them there are failings - presence of mobile details and regulations, considerable resource-demanding, difficulty in making.

Therefore, for Jet of seed meters for ordinary sowing a divider pneumo-jet device is provided for the process of seed distribution in which takes place the rotation of materials – there is an air current with permanent speed into a cylinder under act of air-blast (Fig.6).

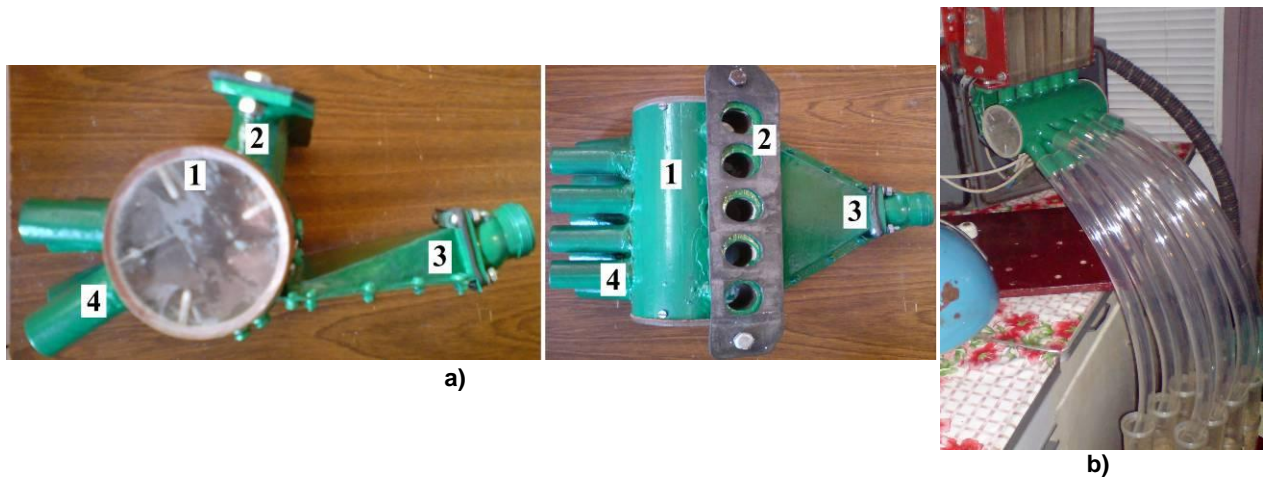


Fig. 6 - Jet sowing apparatus with the Jet distributor for centralized sowing systems:

a - distributor assembled; b - mounted on sowing apparatus

Seeds from a seed distributor are going to the cylindrical body 1 of the dispenser through the input unit nozzles 2. Air under pressure is fed tangentially into the cylindrical enclosure through the diffuser 3 and interacts with the seed, rotating them within the cylindrical body 1. As a result of exposure to centrifugal force which presses the seeds against the case, they fall into the outlet nozzle 4, where the air flow transports them to the coulters and the bottom of the furrow. The radius of the cylindrical housing 1 is selected so that the centrifugal force acting to the seed was greater than the force of gravity, which affects the seed and negatively affects the uniformity of distribution, particularly on the slopes of the fields. Thus, due to compensation of the force of gravity by centrifugal force, the uniformity of distribution of seeds increases.

On the lateral surfaces of cylinder, along its axis, ducting of seed input, chart of feed pressure and output ducting are located. Such distributor chart makes it active, compact and without locomotive parts. Thus, the particles of material under the action of centrifugal force reach the cylinder wall (vertical chamber) and move on it to the output. For distributor normal work, centrifugal forces must be stronger than gravity, displacing seed at inclinations, which reduces the degree of redistribution of sowing material because of inclinations and vibrations.

CONCLUSIONS

The new seeding system machines and their components can be built on entirely new principles, the basics of which are laid in fundamental research in hydraulics, pneumatics and aerodynamics.

Efficiency of seed technological sowing process rises with the use of seed meters based on executive and managing elements of stream pneumatic automation and also stream distributive devices.

Laboratory bench and production test showed high quality seed distribution (coefficient of variation is 18.2 to 25.4% and accuracy of the intervals between plant emergence – 86.7-85%) for the developed devices. For existing devices, these values are 25-30% and 80-82% respectively. The improved designed machine is due to a forced reset of the seeds on the bottom of the furrow and consequently the lack of seed rolling from the preset position.

The planting was sustainable. The uneven formation of the original flow on the devices and between the devices was less than 2% for developed, and 3% for existing machines. This is corresponding to the agro technical requirements for sowing machines.

Evenness of sowing or distribution of seed and plants is thus improved on an area in the same time with sowing machines decrease in energy - and resource-demanding (Table 1).

The use of the new sowing systems based on elements and devices of Jet technique opens the possibility to create universal multi-purpose machines (Fig.5).

REFERENCES

- [1] Alt V.V., Shchukin S.G., Valkov V.A., (2008), The concept of sowing machine development (Концепция развития посевных машин), *The achievements of Science and Technology AIC (Достижения Науки и Техники АПК)*, № 9, pp.44-48, Moscow/Russia;
- [2] Aulin V.V., Pankov A.A., Zamota T.N., (2016), Reliable work processes of agriculture technical equipment with elements of fluidics (Надёжность рабочих процессов технических средств АПК с элементами пневмоники), *Technical services agriculture, forestry and transport complexes (Технічний сервіс агропромислового, лісового та транспортного комплексів)*, № 5, pp.117-125, Kharkov/Ukraine;
- [3] Belodedov V., Nosko P., Boyko G., Fil P., Mazneva M., (2013), The optimisation settings of the dispenser for technical cultures tested at intervals of sowing, which are close to calculation, *TEKA Commission of Motorization and Power Industry in Agriculture*, vol.13, no.4, pp.18-24, Lublin/Poland;
- [4] Burkov Y., Goryunov V., Diachkov E., (2009), Use of inkjet technology for seed drills (Использование элементов струйной техники для высева семян сеялками), *Sensors and Systems (Датчики и системы)*, № 3, pp.30-32, Moscow/Russia;
- [5] Chernovol M.I., Aulin V.V., Pankov A.A., (2015), Simulation of power pneumojet elements of the sowing apparatus (Моделирование силовых пневмоструйных элементов высевающих аппаратов), *Bulletin of engineering Academy of Ukraine (Вісник інженерної Академії України)*, № 4, pp.175-179, Kiev/Ukraine;
- [6] Firsov A.S., Golubev V.V., (2013), The structural analysis of seed system for growing crops (Анализ конструкций высевающих аппаратов для возделывания сельскохозяйственных культур), *Bulletin of the Orenburg state agrarian university (Известия Оренбургского государственного аграрного университета)*, № 4(42), pp.85-88, Orenburg/Russia;
- [7] Garbers H., (2015), Digital future solutions, not buzzwords need (Digitale Zukunft braucht Lösungen, nicht Schlagworte), *Agricultural technique (Landtechnik)*, № 6, pp.218-220, Darmstadt/Germany;
- [8] Kashubo N.D., (2007), Management of innovative processes in agriculture (Управление инновационными процессами в АПК), *AIC: economics and management (АПК: экономика и управление)*, № 4, pp.51-56, Moscow/Russia;
- [9] Kassimov A., (2010), The development of pneumatic automation (Развитие пневматических средств автоматизации), *Proceedings of the conference "Hardware and software systems management, control and measurement" of the Institute of Control Sciences RAN (Труды конференции «Технические и программные средства систем управления, контроля и измерения» Института проблем управления РАН)*, pp.640-652, Moscow/Russia;
- [10] Kobchenko S.N., Medvedev E.Yu., (2015), Adaptive elements of precision seeders (Адаптивные элементы сеялок точного высева), *Actual problems of innovative activity in agroindustrial production (Актуальные проблемы и инновационная деятельность в агропромышленном производстве)*, pp.30-31, Kursk/Russia;
- [11] Scheglov A.V., (2010), Promising seeding system. Criteria scheme selection (Перспективная высевающая система. Критерии выбора схемы), *Scientific journal of LNAU, "Technoscience" (Науковий вісник ЛНАУ, «Технічні науки»)*, № 20. pp.202-206, Lugansk/Ukraine;
- [12] Scheglov A.V., (2011), Improvement of pneumatic sowing machines (Совершенствование пневматических высевающих аппаратов), *Scientific journal of LNAU, "Technoscience" (Науковий вісник ЛНАУ, «Технічні науки»)*, № 30, pp.338-341, Lugansk/Ukraine

**A NEW BLADE DESIGN OF ROTARY TILLER AND STATIC ANALYSIS
USING COMPUTER-AIDED TOOL**
/
**BİLGİSAYAR DESTEKLİ TASARIM İLE ROTOTİLLER İÇİN YENİ BİR BIÇAK
TASARIMI VE STATİK ANALİZİ**

Assist. Prof. Dr. Selvi K.Ç.^{*1)}

¹⁾Faculty of Agriculture, Ondokuz Mayıs University, Atakum / Turkey
Tel: + 90 362 3121919 / 1259; E-mail:kcselvi@omu.edu.tr

Keywords: rotary tiller, blade, static analysis, Von Mises stress

ABSTRACT

Soil tillage is one of the main points in agricultural application in plant production. It is defined as mechanical actions applied to the soil to change soil conditions in order to grow plants. Rotary tillers are a kind of soil-working machines that are used to mix soil and work by rotating their active parts. Nowadays, due to its simple structure and high efficiency, the potential for use is increasing day by day. In this study, a static analysis of a new type of blade, designed with 3 different material selections, was carried out using a solid modeling design program. As a result, it has been observed that the rotary tiller blade, which performs static analysis using different materials, can work well under the boundary conditions determined during the design stage.

ÖZET

Toprak işleme, bitki üretiminde ki tarımsal uygulamalarda temel esaslardan biridir. Bitkisel üretime uygun toprak koşullarının oluşturulması amacıyla toprağa uygulanan mekanik eylemler olarak tanımlanır. Toprak frezeleri toprağın karıştırılmasında kullanılan ve aktif organları dönerek çalışan toprak işleme makinalarıdır. Günümüzde, basit yapısı ve yüksek verimliliğinden dolayı kullanım potansiyeli gün geçtikçe artmaktadır. bu çalışmada, bir katı modelleme tasarım programı kullanılarak 3 farklı malzeme seçimi ile dizayn edilmiş yeni tip bir bıçağın statik çözümlemesine çalışılmıştır. Sonuç olarak, farklı malzemeler kullanarak statik analizi gerçekleştiren Rototiller bıçağının, tasarım aşamasında belirlenen sınır koşulları altında çalışabileceği görüşmüştür.

INTRODUCTION

Soil tillage is one of the essential points of agricultural application in crop production. It is defined as mechanical or soil-stirring actions exerted on soil to modify soil conditions for the purpose of nurturing crops (Köller, 2003). The tillage literature classifies soil tillage implements into two types as primary and secondary according to their impact on the soil and seedbed preparation. Although many studies have suggested that rototillers can be used as primary tillage tools (Bowers., 1992; Srivastava et al.2006; Cloutie et al. 2007), it can be seen as an advantage of this implement that primary and secondary tillage applications can be conjugated in one stage. It is a specialized mechanical tool used to plough the land by a series of blades which are used to swirl up the soil (Mandal et al. 2013). It has a huge capacity for cutting, mixing to topsoil preparing the seedbed directly and also it has more mixing capacity seven times than a plough (Shindeand Kajele, 2012).

It may be noticed, within the recent years, that the increasing number of the tools used for agrotechnological processing in the farms are not individual machines but multifunctional aggregates (e.g. tooth harrow and cage rollers). Their main function is to provide the crop cultivated with the best possible growing conditions, with the lowest number of machinery passes over the cultivated soil (Tucki and Sikora, 2016).

Despite of their high energy consumption, since rotary tillers have the ability of making several types of tillage applications in one stage, the total power needed for this equipment is low (Culpin., 1981). Because rotary tillers' power is directly transmitted to the tillage blades, the power transmission efficiency in rotary tillers is high. Moreover, the negative traction existence in rotary tillers causes the required tractive force to be decreased and consequently, smaller tractors could be used with this type of tillage implements for land

preparation (Zareiforoush et al. 2010). Although they are produced in different shape blades (L, I, C, J, etc.), usually L type blades are more common in rotary tiller because of its effectiveness especially over 'C' and 'J' type (Figure 1).



Fig. 1 - A Sample of L type blades

On the other hand, soil tillage applications require high energy inputs. As a consequence, producers tend to have less energy-cost systems and implements, especially due to increases in energy prices in recent years.

Thus, increasing the effectiveness of tillage tools, even by a small fraction, would amount to a huge saving in energy. It would be rather more economical to increase the productive rate of each machine than to increase the number of machines indiscriminately (Saimbhi et al., 2013). Due to these considerations, the design of tillage tools and especially the optimizations related to the design of the active parts become the priority subjects. The CAD (computer aided design) systems can enable simultaneous engineering applications and can have impressive roles on time, final product cost and labour saving considerably.

The objectives of this study are:

1. To prepare a new geometric solid model of rotary tillers blade by using CAD- software
2. To make a principle and Von Mises stress analysis of rotary tiller's blade

MATERIALS AND METHODS

A tractor of 60 hp was selected to be used in the calculations to perform the design of the blades. Prime mover forward speed (u) was selected 1.5 m/s while traction efficiency (η_c) and the coefficient of reservation (η_z) were 0.85, 0.75 respectively. A rotary tiller with 100 mm active work depth and 3000 mm width was selected for this study. The total power of the machine is distributed between the blades. The blade parameters affect the performance of Rotary tiller. 30 blades are used in this design to connect a blade to a flange. The blade was designed in 3 D CAD software and analysed with ANSYS for static solution and optimization. The shape and related parameters and values of the blade designed for this study are as follows (Figure 2; Table 1).

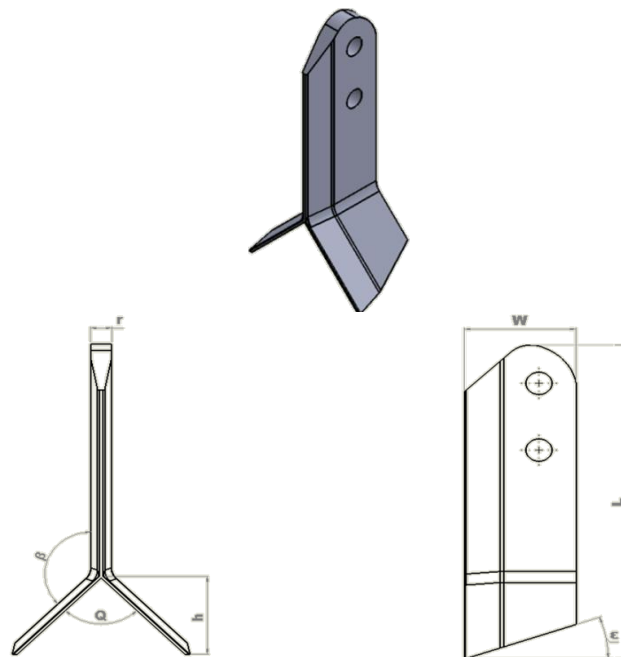


Fig. 2 - Blade shape and measurement

Table 1

Blade parameters and values

Nr	Parameters	Notations	Units	Values	
1.	W	Blade span	mm	60	
2.	L	Effective vertical length	mm	200	
3.	h	Vertical length of winglet	mm	50	
4.	r	Blade thickness	mm	Body blade	12
				Winglet blade	6
5.	Q	Angle between winglets	°	90	
6.	ε	Clearance angle	°	20	

The new design of the blades assembled with rotary shaft is shown in Fig. 3

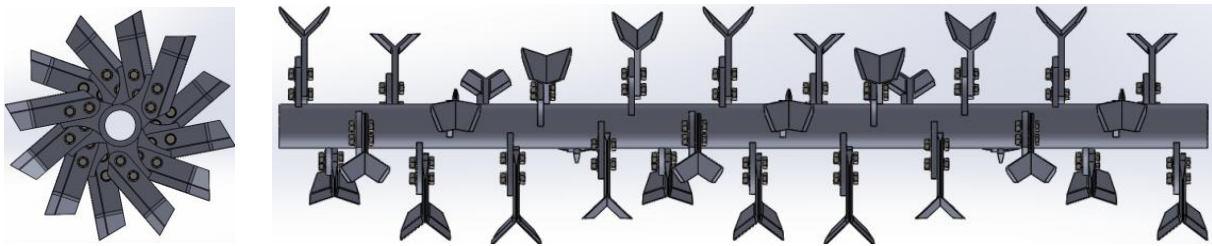


Fig. 3 - General view of blades arrangements and shaft

Based on the geometrical configuration of the designed blade, three different types of material were selected. Material properties used in the analysis are presented in Table 2.

Table 2

Material properties

	Young's module (Pa)	Poisson's ratio	Compressive yield strength (Pa)	Density (t/m ³)	Ultimate tensile strength (Pa)
Structural Steel	2.00 x e ¹¹	0.3	2.5 e ⁸	7.85 x e ⁻⁹	4.60xe ⁸
Stainless Steel	1.93 x e ¹¹	0.3	2.07 e ⁸	7.75 x e ⁻⁹	5.86xe ⁸
Mild Steel	2.10 x e ¹¹	0.3	2.5 e ⁸	7.87 x e ⁻⁹	4.40xe ⁸

The rotor shaft should be able to withstand the maximum force value. The maximum tangential force (Matani et al 2015; Mandal et al. 2015) occurs at the minimum of blades tangential speed, calculated using the following relation

$$K_s = C_s \frac{75 \cdot N_c \cdot \eta_c \cdot \eta_z}{u} \quad (1)$$

where:

K_s is the maximum tangential force (kg)

N_c is the prime mover tractor power (HP)

η_c is traction efficiency

η_z is reservation coefficient of tractor power

C_s is the reliability factor that is equal to 1.5 for non-rocky soils and 2 for rocky soils

U is prime mover forward speed (m/s)

The parameters used for static analysis are as follows.

Rotor rpm: 250, blade peripheral velocity: 6.56 m/s.

The soil force acting on each of blades (K_e) (Mandal et al. 2015) is calculated using the following equation:

$$K_e = \frac{K_s \cdot C_p}{i \cdot Z_e \cdot N_e} \quad (2)$$

Where:

K_e is the soil force acting perpendicularly on the cutting edges of each of the blades,

C_p - the coefficient of tangential force,

l - the number of flanges,

Z_e - the number of blades on each side of the flanges,

N_e - the number of blades with joint action on the soil.

As a result of the calculations and selected parameters given above, K_s and K_e are calculated as 2151 kg and 573.7 kg respectively. These values were used in the analysis by ANSYS. The results of the analysis performed by the ANSYS are given below.

When Using FEM software ANSYS Workbench 16.0, “Fixed support” method to fix two surfaces which contact with frame and use the “Frictionless support” method to fix locating hole on the shovel.

Force along the z direction is -5737N, and, as shown in Fig. 4, the number of nodes and elements were 15199 and 8022 respectively. Also, the element size was 4mm.

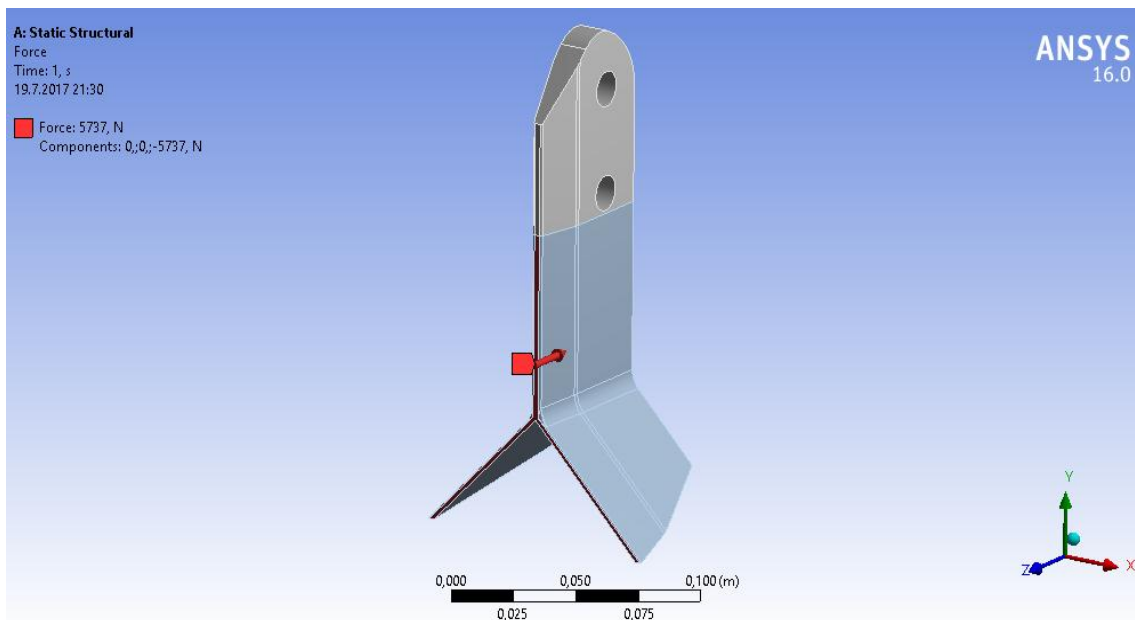


Fig. 4- Boundary constraint of Rotary tiller blade

RESULTS

Topakçiet al. (2010) worked on the optimization of the subsoiler. They used finite element method (FEM) to simulate stress solutions on the subsoiler tine.

According to the tines material yield stress point (355 MPa), plastic deformation was evident.

As a result of the optimization, they have achieved a reduction of 27.62% in the weight of the subsoiler platform.

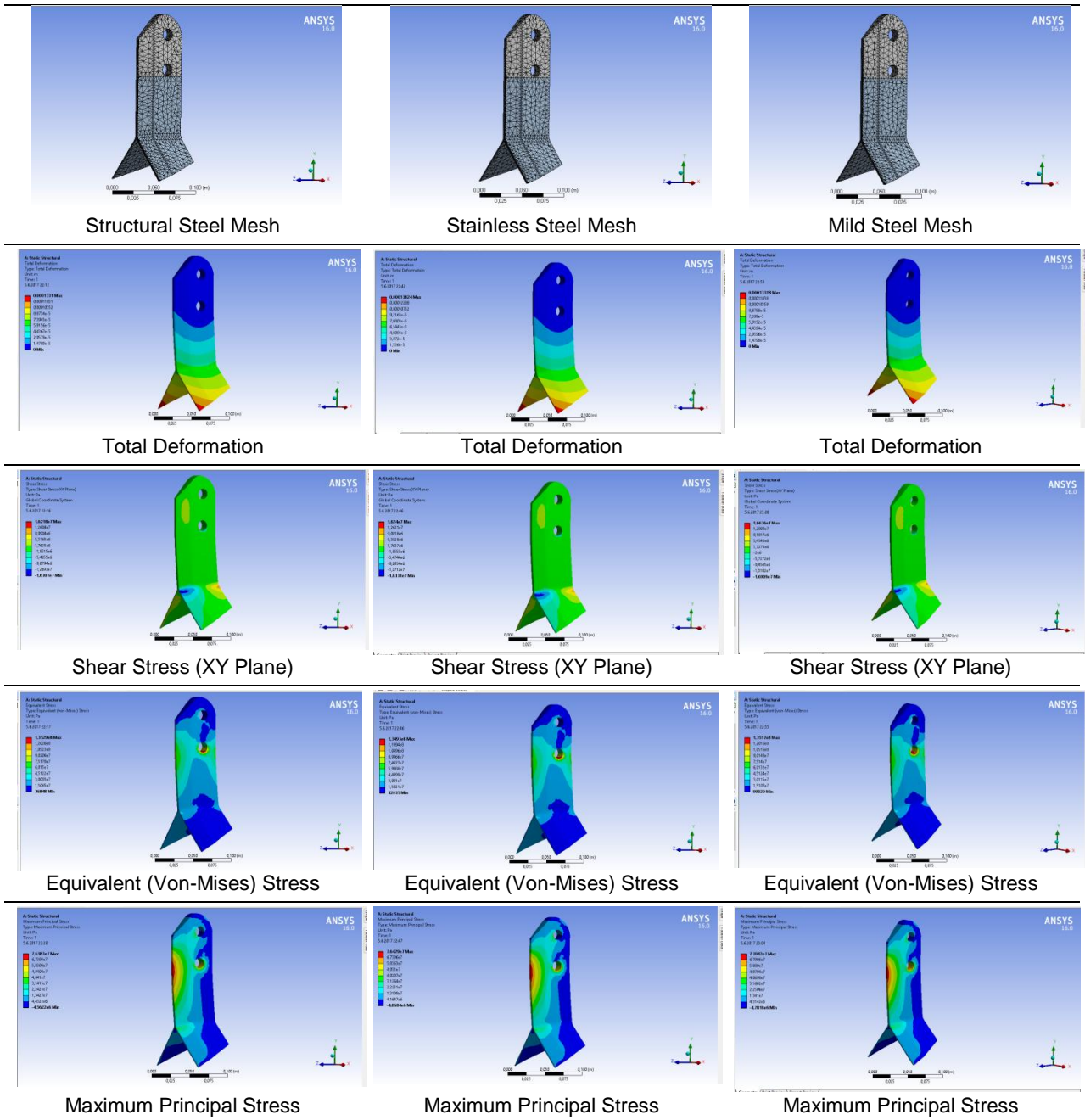
Birişet al. (2016) studied on stress and strains distribution in the frame of agricultural cultivators using the finite element method. They found that from the analysis, equivalent stress observed that under the effect of the applied external loads and finally, the structure of the frame does not deform in the plastic domain.

We studied the effect of different materials on blade and stress solution.

The meshes of the blades designed using different materials and the stress solutions of blades are given separately in the following tables.

Table3

Meshes and deformations of blades



The analysis results according to different materials are given in Table 4.

Table4

Blade material properties

	Total Deformation, (mm)	Shear Stress (XY Plane), (Pa)	Equivalent (Von- Mises) Stress, (Pa)	Max. Principal Stress, (Pa)
Structural Steel	0.1331	1.621×10^7	1.3529×10^8	7.6387×10^7
Stainless Steel	0.1382	1.624×10^7	1.3493×10^8	7.6429×10^7
Mild Steel	0.1331	1.663×10^7	1.3517×10^8	7.7082×10^7

The results showed that the maximum deformation (0.1382 mm) was achieved on the blade where the stainless steel was used. On the other hand, no significant changes were observed between the results on the basis of the parameters, despite the use of different materials.

These results may be due to the fact that the compressive yield strength (Pa) and density values of the selected materials are very close to each other. The total deformations were between 0.1331-0.1382 mm. The maximum principal stress (77 MPa) was achieved at mild steel material.

This stress value is less than the yield stress of blade material i.e. 250 MPa. Max. Von Mises stress found was between 134.9 MPa-135.3 MPa.

CONCLUSIONS

Finite element is a highly effective method of solving complex engineering problems with controllable components. It can be used efficiently in static analysis of soil processing tools as well as in many other areas. Integration of this method with a solid modeling program provides designers with advantages in terms of time, labour and material savings. The analysis of the rotary blades is reliable in terms of mechanical strength.

The selection of the cheaper material in market conditions will provide an economic advantage because each of the 3 materials used is below the limit values in terms of mechanical strength.

REFERENCES

- [1] Biriş S.Ş., Maican E., Vlăduţ V., Bungescu S.T., Ungureanu N., Vlăduţ D.I. (2016), Stress and strains distribution in the frame of agricultural cultivators using the finite element method. *44. Symposium "Actual Tasks on Agricultural Engineering"*, pp. 111-117, Opatja, Croatia;
- [2] Bowers, W, (1992), Energy in farm production. Vol.6, *Agricultural Field Equipment. Chapter 10*. Elsevier Science publishers. B.V., 384 p., ISBN 0-444-88681-8;
- [3] Cloutier D.C., Van der Weide R.Y., Peruzzi A., Leblanc M L, (2007), Non-chemical weed management principles, *Concepts and Technology. Mechanical Weed Management*. Chapter 8. Produced and typeset by columns design Ltd. Reading, UK. ISBN-13: 978 1 84593-290-9;
- [4] Culpin C, (1981), Farm machinery, 10th ed. *Granada Technical Books Press*, Spain;
- [5] Köller K, (2003), Soil tillage in agroecosystems. *Techniques of Soil Tillage. Chapter 1*. CRC Press. ISBN 0-8493-1228-0;
- [6] Mandal S K., Bhattacharya B., Mukherjee S, (2015), Design of rotary tiller's blade using specific work method (swm), *Journal of Applied Mechanical Engineering*, 4:3;
- [7] Mandal S.K., Bhattacharya B., Mukherjee S, (2013), Optimization of design parameters for rotary tiller's blade. *Proceedings of the 1st International and 16th National Conference on Machines and Mechanisms*, IIT Roorkee, India;
- [8] Matani A G., Bhishnurkar A D, (2015), Use of cad tool for design, analysis and development of rotary tillage tool. *International Journal of Science and Research*, vol.4, pp.215-217, (IJSR), India;
- [9] Saimbhi V.S., Wadhwa D.S., Grewal P.S, (2013), Development of a rotary tiller blade using three-dimensional computer graphics. *Biosystems Engineering* 89 (1), pp. 47–58, United Kingdom;
- [10] Shinde G. U. and Kajale S R, (2012), Design optimization in rotary tillage tool system components by computer aided engineering analysis. *International Journal of Environmental Science and Development*, Vol. 3, no.3, pp.279-282, Singapore;
- [11] Srivastava A K., Goering C.E., Rohrbach R.P., Buckmaster D.R, (2006), Engineering principles of agricultural machines, *Soil Tillage.Chapter 8*. 2nd ed., pp.169-229, St. Joseph, Michigan: ASABE, Copyright American Society of Agricultural and Biological Engineers;
- [12] Karol Tucki K., Sikora M, (2016). 3d design procedure, FEM analyses and optimization of the tiller's sprocket. *Econtechmod. An international quarterly journal*, Vol. 5, issue 3, pp. 59-70
- [13] Topakcı M., Celik H K., Canakcı M., Karayel D., Rennie A, (2010), Structural Optimization of a Subsoiler. *Pakistan Journal of Scientific and Industrial Research*, Vol. 53, issue 5, pp.281-287, Pakistan;
- [14] Zareiforoush H., Komarizadeh M H., Alizadeh M.R, (2010), Rotary tiller design proportional to a power tiller using specific work method (SWM). *Nature and Science*.8 (9), pp.40-45.

MODERN ASPECTS OF TILLED CROPS PRODUCTIVITY FORECASTING

/

СУЧАСНІ АСПЕКТИ ПРОГРАМУВАННЯ ВРОЖАЙНОСТІ ПРОСАПНИХ КУЛЬТУР

Lect. Ph.D. Biol. Mostypan M.I., Lect. Ph.D. Eng. Vasytkovska K.V.,
Lect. Ph.D. Agric. Andriyenko O.O., Lect. Ph.D. Agric. Reznichenko V.P.
Central Ukrainian National Technical University / Ukraine;
Tel: +380667103625; E-mail: vasytkovskakv@ukr.net

Keywords: crop forecasting, soil fertility, tilled crops, precision seeding, pneumatic and mechanical sowing device, versatility

ABSTRACT

The article presents the main application trends of the resource-saving agriculture and its implementation on the principles of crop forecasting. To intensify sowing operations a new pneumatic and mechanical seeding device with a peripheral layout of cells on the sowing disk and a passive device for removing excess seeds by a centrifugal method which ensures even seed distribution on the sowing area was proposed. This sowing device increases the technological efficiency of sowing tilled crops and reduces energy intensity. The research carried out on sugar beet seeds, soybean, sunflower and corn allowed asserting the versatility of the proposed sowing device. It has been found that one sowing disk can measure out in doses all the above-mentioned seeds of the tilled crops with a sufficient precision.

РЕЗЮМЕ

В статті наведені основні тенденції запровадження технологій ресурсозберігаючого землеробства та його реалізація на основі програмування врожаю з урахуванням принципів програмування врожаю. Для інтенсифікації посівних операцій розроблено новий пневмомеханічний висівний апарат з периферійним розташуванням комірок на висівному диску та пасивним пристроєм для видалення зайвого насіння відцентровим способом, що дозволяє забезпечити рівномірний розподіл насіння за площею живлення. Запропонований висівний апарат збільшує технологічну ефективність висіву насіння просапних культур та зменшує енергоємність процесу. Проведені дослідження на насінні цукрових буряків, сої, соняшнику та кукурудзи дозволили стверджувати про універсальність запропонованого висівного апарата. Встановлено, що один висівний диск дозволяє дозувати всі перераховані види насіння просапних культур з достатньою точністю.

INTRODUCTION

The basis for the effective implementation of productive technologies in agriculture is crop forecasting based on the system of soil fertility recovery and soil-protective technologies, quality preparation of highly-productive seeds, resource-saving mechanization and automation, effective protection of plants from diseases, pests and weeds.

It is well-known that fertility is the ability of soil to feed plants during vegetation with necessary quantity of nutrients, water, warmth and air (Sydorchuk O., 2014). Without proper care of the human, the agro-ecosystem will inevitably have a gradual impoverishment and degradation of its important part which is soil (Sysolin P.V., 2001).

Artificial agro-ecosystems differ from the natural range of specific features. They have sharply reduced the species diversity of organisms. Since the fields are grown alone, rarely - several species of plants, the species composition of animals and microorganisms in biocenosis is considerably impoverished and requires constant energy revenues from the human side, which creates conditions for the cultivation of cultural plant species (soil cultivation, fertilization, weed control, pests, diseases, etc.). Grown crop is removed and does not fall further in the food chain and energy exchange in agricultural ecosystems. Without proper care (return) of the human agro-ecosystem inevitably a gradual impoverishment and degradation of important part - soil occurs (Zlobin Yu.A., 2012).

Nowadays, the soil degrades in Ukraine as a result of intensive agricultural production, growing of monocultures and crop rotation supply with green crops which deplete the soil and pollute the environment reducing the amount of organic matter in the tilled layer. Another problem is the application of erosion-hazardous agricultural tools, etc. (Sviren M.O., 2012; Primak I.D. 2010).

Therefore, the search for new technologies and mechanization methods in order to preserve soil fertility and save energy, to improve the sustainability of agro-ecosystems, to preserve the environment will contribute to the cultivation of environmentally safe products and ensure sustainable harvests in future.

Productivity forecasting is an important and promising trend of production technologies, including tilled crops which allow efficiently using material, labour and energy resources for maximum yields of good quality (Vasylykovska K.V., 2016). Today, there are several trends of crop forecasting which, at different stages of the life cycle, help analysing and evaluating the quality of tilled crops growing, but they only partially fulfil the task of ensuring the quality and productivity (Osadchij S.I., 2014; Sviren M.O., 2016). The full application of crop forecasting techniques in the real economic conditions is restrained by a number of problems that require complex solutions.

One of the key problems is the choice of cultivation tools which will ensure the implementation of resource-saving and soil-protective technologies in the cultivation process. Another problem is the application of precision sowing as a uniform seed distribution is the basis of high yields in the future.

In order to apply crop forecasting in economic conditions there should be carried out gradual stages. The first stage towards crop forecasting is the choice of water-retaining, soil-protective and energy saving tillage (Vasylykovska K.V., 2016). The second stage is seed preparation for sowing and the third stage is to ensure a uniform seed placement on the sowing area (Salo V.M., 2014).

Tilled crops significantly change their productivity depending on predecessors with high edificatory properties such as perennial legumes. The mass and quality of postharvest root residues affect the processes of their transformation in soil, i.e. the formation of its fertility. The most valuable are the remains of leguminous perennial grasses and legumes (Primak I.D., 2010).

In the area of risk farming where moisture is the key factor of plant productivity, the main impact of predecessors is determined by water in the soil. The moisture remaining in the deeper layers after harvesting some crops has a positive effect on the productivity of the following crop rotation, and the deficiency of water leads to a significant harvest shortfall.

To improve seed germination there should be conducted qualitative cultivation which ensures the preservation of water by breaking compacted subsoil layer and stimulates efficient development of plant roots due to qualitative loosening of the cultivated layer.

In the technology of most tilled crops growing, an important role is played by the incrustation of seeds that contains some kind of pesticides, plant growth regulators and micronutrients. They improve the penetration of moisture through the cell membrane into the cell cytoplasm, accelerate their entry with water to the germ and stimulate the biochemical processes in tissues and enhance its field germination and livelihood, stimulate the growth of aboveground mass and root system of plants. Micronutrients can increase plant resistance to adverse environmental conditions (low temperatures, drought, etc.), stimulate the activity of most enzyme systems, improve the absorption of nutrients from soil and fertilizers and ultimately stimulate the growth of productivity and improve the quality of the received (grown) products.

The sowing of crops should be carried out at the optimum time. This affects the conditions of seedlings emergence, their further development and the depth of sowing that is related with humidity and temperature of the soil. Sowing into the insufficiently heated soil causes not only the extension of the period of "sowing - emergence" but leads to the loss of some seeds in the soil and uneven plant development. Applying optimum sowing time provides the highest germination energy and field germination of seeds that stimulates a uniform plant development and high performance of agroecosystem in general.

Sowing uniformity and evenness of its location in the line is the key to not only get good emergence, but to have excellent harvests in future. Moreover, the increase of seeds even distribution on the sowing area leads to a reduced level of weed-infested crops.

So, the issue of improving technical appliances for sowing may be the initial step of crop forecasting and the practical solution of the above-mentioned problem will increase competitiveness of crop production and will lead to soil-protective and resource-saving agriculture.

MATERIALS AND METHODS

Sowing machines that are used in mass production have insufficient dispensing capacity caused by limited seed disk rotary velocity and random uncontrolled redistribution of spacing between seeds in the furrow because of the high relative velocity of the seeds (Voytyuk P., 2005; Vasytkovska K.V., 2014). To increase the efficiency of precision seeding of cultivated crops the Department of Agricultural Engineering of Central Ukrainian National Technical University designed and manufactured a prototype of the new pneumatic and mechanical disk for sowing device (Fig.1) (Vasytkovska K., 2015; Vasytkovska K.V., 2016).

The main feature of the new sowing device is the application of sowing disk 1 with peripheral layout of cells 2. Behind the cells there are blades 3 on the inner surface of the disk for enforced seizure of seeds by the disk 9 in the chamber and their further transportation to the release place.

To remove excess seeds from the cells of seeding disk 1 at the top of the cylindrical surface of the body there is passive device 7 in the form of cavity which gets excess seeds and separates them from the disk and transports the seeds back to the filling zone. In the lower part of the housing surface there is seeding hole 6 which provides free release of the seeds to the furrow.

The design of the pneumatic and mechanical disk sowing device, due to the enforced seizure of seeds by blades 3, ensures the reliability of the process of filling the sowing disk cells and increases the efficiency of excess seeds removal by using the passive device 7. It makes reliable the process of releasing seeds from the cells in the sowing area. This ensures an even seed distribution in the furrow by dispensing process stabilization and seeds releasing from the sowing disk.

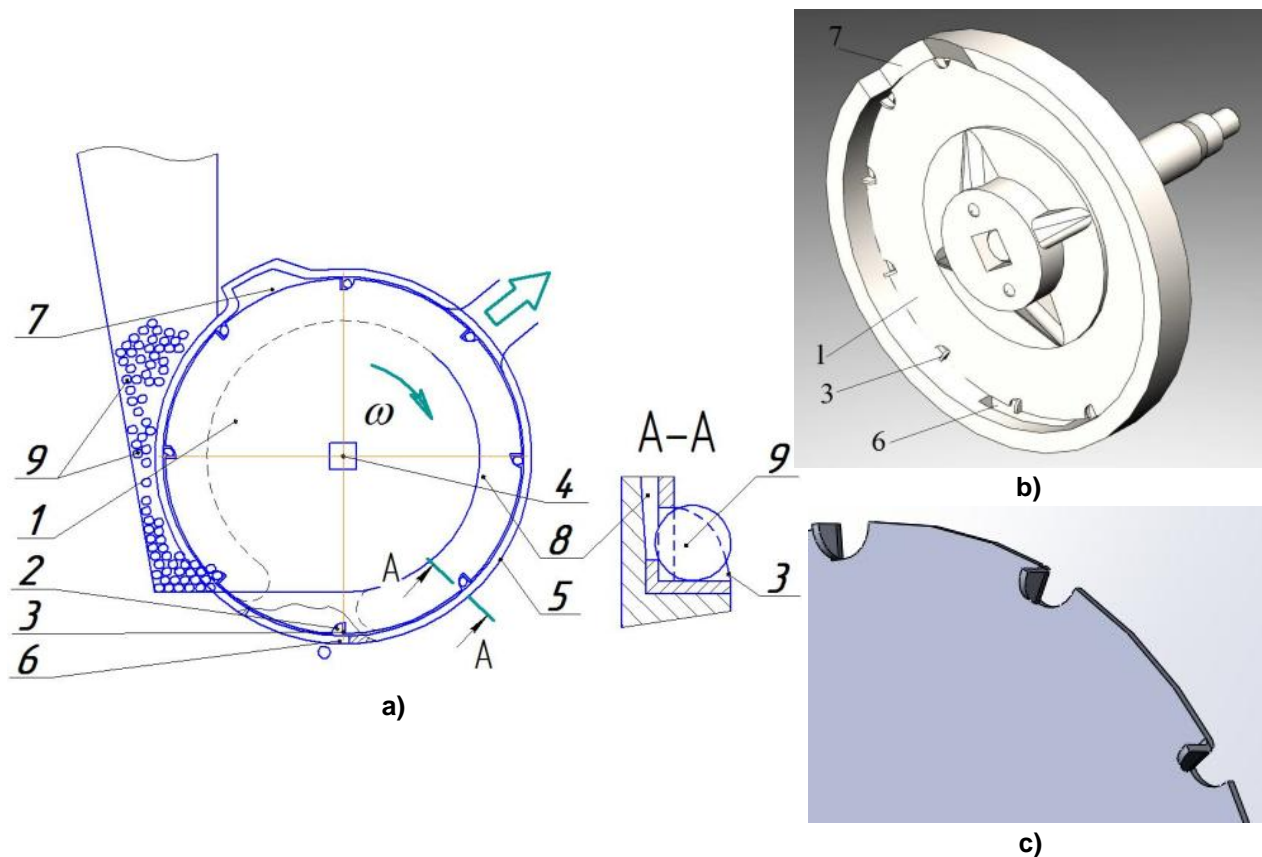


Fig. 1 – Pneumatic and mechanical sowing device

a – scheme; b – 3D model of the sowing device; c – 3D model of sowing disk fragment
 1 – sowing disk; 2 – cell; 3 – blade; 4 – drive shaft; 5 – housing; 6 – seeding hole;
 7 – passive device (container) for removing excess seeds; 8 – vacuum chamber; 9 – seeds

RESULTS

To prove the versatility of the suggested sowing device we performed the research on the seeds of sugar beets, soybeans, sunflower and maize. We received the dependences of the cell filling coefficient of the sowing disk K on the degree of thinning in the vacuum chamber ΔP for the corresponding types of seeds (Fig. 2).

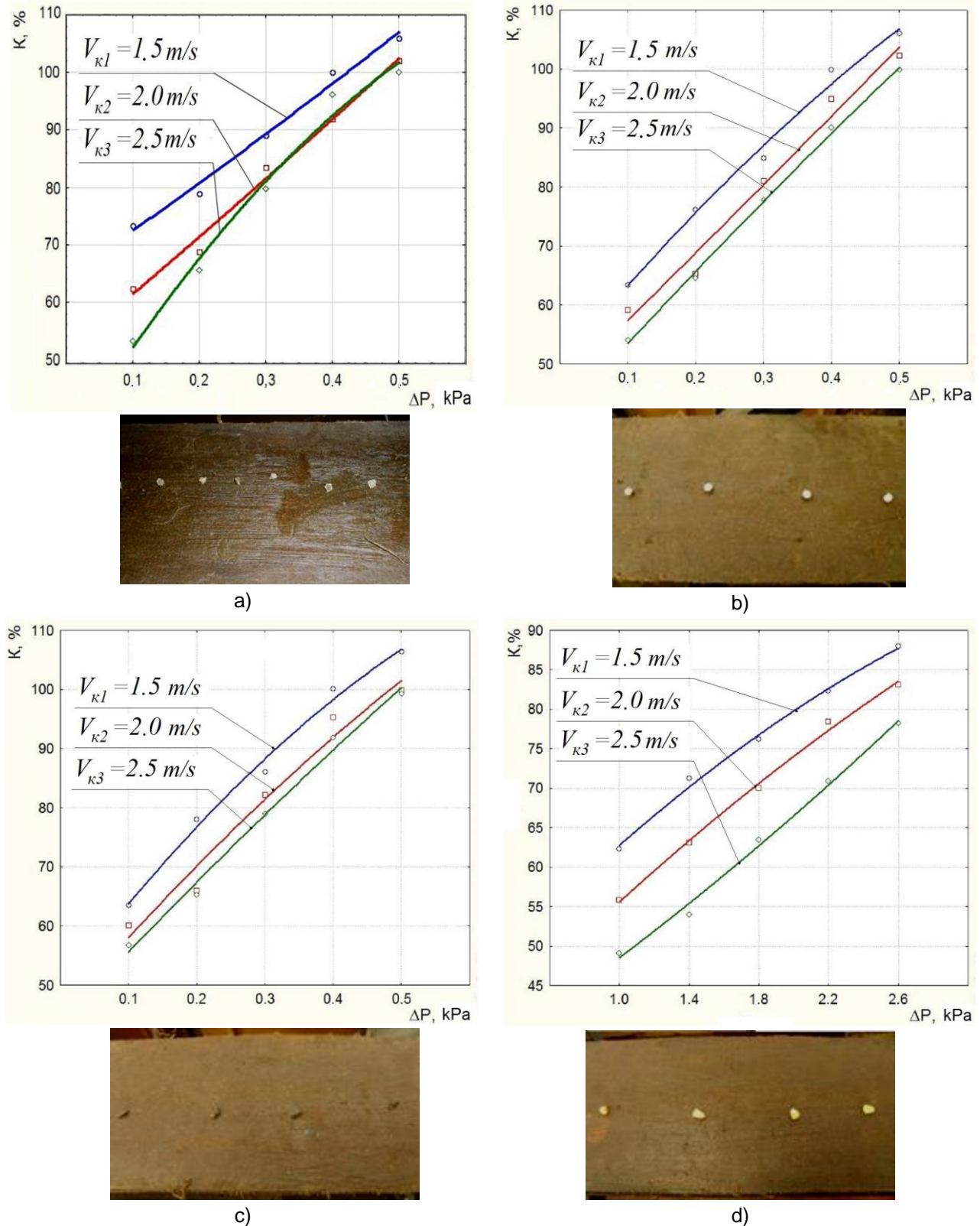


Fig. 2 –Dependence of the cells filling coefficient of the sowing disk K on the thinning degree in the vacuum chamber ΔP for the seeds:

*a – sugar beet; b – soybean;
c – sunflower; d – maize*

Having verified the versatility of the experimental sowing device we found that the disk with the cell hole radius $r = 6.0$ mm enables effective dispensing of sugar beets, soybeans and sun flower seeds.

The optimum value of the cells filling coefficient ($K = 100$ %) while dispensing the above-mentioned crops is achieved under the following parameters:

- sugar beets – $\Delta P = 0.2 \dots 0.3$ kPa, $V_k = 2.0 \dots 2.5$ m/s;
- soybean – $\Delta P = 0.4 \dots 0.5$ kPa, $V_k = 1.5 \dots 2.0$ m/s;
- sunflower – $\Delta P = 0.4 \dots 0.5$ kPa, $V_k = 1.5 \dots 2.5$ m/s.

The analysis of the dependence of the cells filling coefficient for maize seeds with the hole radius $r = 6.0$ mm is complicated by the big size of the seeds, so the maximum value of the cells filling coefficient $K = 88$ % is achieved if $\Delta P = 2.6$ kPa, $V_k = 1.5$ m/s. Therefore, a separate sowing disk with a bigger radius of the cell hole should be used for this kind of crop.

CONCLUSIONS

A consistent application of the developed technical tools in the processes of growing crops will practically implement some basic aspects of crop forecasting techniques in the system of soil-protective and resource-saving agriculture.

A special attention should be paid to ensure quality seed distribution on the sowing area while introducing soil-protective technologies, quality preparation of tilled crops highly productive seeds and resource-saving mechanization and automation of agricultural production.

The design of the new pneumatic and mechanical device increases the angular velocity of cells and reduces their number on the sowing disk and significantly reduces thinning in the vacuum chamber. Therefore, the proposed sowing device increases technological efficiency of seeding tilled crops and reduces energy intensity.

Also, having checked the versatility of the sowing device it was found that the disk with the cell hole radius $r = 6.0$ mm allows dispensing sugar beet seeds, soya and sunflower. The cell filling coefficient $K = 100\%$ is achieved by setting the following parameters: for sugar beet $-\Delta P = 0.2 \dots 0.3$ kPa, $V_c = 2.0 \dots 2.5$ m/s; soybean $-\Delta P = 0.4 \dots 0.5$ kPa, $V_c = 1.5 \dots 2.0$ m/s; for sunflower $-\Delta P = 0.4 \dots 0.5$ kPa, $V_c = 1.5 \dots 2.5$ m/s.

Sowing maize seeds with the cell hole radius $r = 6.0$ mm is complicated because of the big size of the seeds, so the maximum cellsfillingcoefficient $K = 88\%$ is achieved at $\Delta P = 2.6$ kPa, $V_c = 1.5$ m/s.

REFERENCES

- [1] Moroz N.V., (2011), Harvest forecasting and quality of grain cultures, *Bulletin of the National University "Lviv Polytechnic", "Computer systems and networks"*, №717, pp. 105-107, Lviv/Ukraine;
- [2] Osadchij S.I., Macuj A.M., Zubenko V.O., (2014), Modernized Multidimensional Wiener Filtering of Navigational Information with Correction of Noise, *IEEE 3rd International Conference «Methods and Systems of Navigation and Motion Control»*, pp.50-53, Kyiv/Ukraine;
- [3] Primak I.D. (2010), *Ecological problems of agriculture: study guide for university students*, 455 p., Kyiv / Ukraine;
- [4] Salo V.M., Bohatyrev D.V., Leshchenko S.M., Savytskyi, (2014), National technical support of modern processes in plant growing, *Engineering and Technology of APK. Scientific and production journal*, №10 (61), pp. 16-19, Kyiv / Ukraine;
- [5] Sviren M., Shmat S., Ivanko I., Amosov V., (2016), The impact of the geoelectromagnetic field energy on the increase of agricultural crops productivity, *Engineering and Technology of APK. Scientific and production journal*, №11 (62), pp. 26-28, Kyiv / Ukraine;
- [6] Sviren M.O., (2012), Scientific and technological bases of efficiency increase of seeding machines seeding devices: diss. Doc. of Sciences.: spec. 05.05.11. "Machinery and mechanization of agricultural production", p. 284, Kirovograd / Ukraine;

- [7] Sydorчук O., Lub P., Malanchuk O., (2014), Impact of metrological conditions on the need in adaptive performing of soil tillage and crop sowing technological operations, *ECONTECHMOD: an international quarterly journal on economics in technology, new technologies and modelling processes*. Vol. 3, No. 4, pp. 35-39, Lublin-Rzeszów / Poland;
- [8] Sysolin P.V., Salo V.M, Kropivnyy V.M., (2001), Agricultural machines: theoretical bases, design, engineering, Book 1. *Arable farming machines*, p.384, Edited by Chernovol M.I., Kyiv/Ukraine;
- [9] Vasytkovska K., Vasytkovskyy O., Anisimov O., Trykina N., (2015), Research of pneumatic sowing machine with peripheral cells location and inertial superfluous seeds extraction, *Econtechmod. An international quarterly journal*, Vol.4, No.4, pp. 85-89, Lublin-Rzeszów / Poland;
- [10] Vasytkovska K.V., Leshchenko S.M., Vasytkovskyi O.M., Petrenko D.I., (2016), Improvement of equipment for basic tillage and sowing as initial stage of harvest forecasting, *INMATEH - Agricultural Engineering*. Vol.50, No.3, pp. 13-20, Bucharest / Romania;
- [11] Vasytkovska K.V., Vasytkovskyy O.M. (2014), Influence of the shape and type of seed cells drive on the quality of dispensing seeds, *Eastern European Journal of latest technology*, Vol.6, No.7 (72),. pp. 33-36, Kharkov / Ukraine;
- [12] Voytyuk P., (2005), Preconditions of the future harvest of sugar beets: seeds quality, performance pre-sowing tillage and seeding. *Propozytsia*, № 4, pp. 17-19, Kyiv / Ukraine;
- [13] Zlobin Yu.A., Kochubei N.V. (2012), *General Ecology: Textbook*. p. 414, Sumy/ Ukraine.

CHICORY ROOT CROPS COMBINED HARVESTER

/

КОМБІНОВАНИЙ КОПАЧ КОРЕНЕПЛОДІВ ЦИКОРІЮ

Prof. Ph.D. Eng. Baranovsky V.M.¹⁾, P.G. Skalsky O.Ju.¹⁾, Assoc. Prof. Ph. D. Pankiv M.R.¹⁾,
Ph.D. Eng. Pastushenko A.S.²⁾

¹⁾Ternopil Ivan Puluj National Technical University, Ternopil / Ukraine;

²⁾Mykolayiv National Agrarian University, Mykolaiv / Ukraine

E-mail: baranovskyvm@rambler.ru

Keywords: root crops, disk digger, concave disc, cleaning roller, development algorithm, root crops harvesting adapted machine.

ABSTRACT

The stages of improvement, structure and modes of digging tools of root harvesters' transport-technology systems have been described in this paper. The main ways of improvement, development principles and construction algorithm of combined digging machine for chicory root crops harvesting have been considered on the basis of research objects identification (conventional types of diggers). It was found that the construction algorithm of chicory roots combined harvester functional design must be based on mono block technological-transport systems development where digging tools are supposed to perform related technological operations simultaneously, namely: preliminary and final root crops digging, their topping. The results of experimental researches, the regression equation describing the change in loss and damage chicory root crops depending on the parameters of the combined digger are presented. It is established that the condition providing generalized criteria (root crop loss less than 2.5%, root crop damage less than 15%) performed digger combined velocity of 1.5 m/s, rotational speed of the drive shaft 500 Rpm and depth of the ripper 16 cm.

РЕЗЮМЕ

Наведено етапи удосконалення, будову та принцип функціонування викопувальних робочих органів транспортно-технологічних систем коренезбиральних машин. На основі ідентифікації об'єктів дослідження (існуючих типів копачів) зазначено основні шляхи удосконалення, принципи розробки та алгоритм побудови конструктивно-компонувальної схеми комбінованого копача, призначеного для викопування коренеплодів цикорію. Визначено, що алгоритм побудови функціонально-конструктивної схеми комбінованого копача коренеплодів цикорію повинен базуватися на розробці моноблочних технологічно-транспортних систем, робочі органи яких передбачають одночасне виконання суміжних технологічних операцій попереднього підкопування та кінцевого викопування коренеплодів і відокремлення залишків гички з їх головок. За результатами експериментальних досліджень розроблено рівняння регресії, які характеризують зміну втрат і пошкоджень коренеплодів цикорію залежно від параметрів комбінованого копача. Встановлено, що умова забезпечення узагальнених критеріїв (втрати коренеплодів менше 2.5 %, пошкодження коренеплодів менше 15 %) виконується за швидкості руху комбінованого копача 1.5 м/с, частоти обертання приводного вала 500 об/хв, глибини ходу розрихлювача 16 см.

INTRODUCTION

Modern trends of root crops machinery include the development and implementation of highly efficient, energy-saving and technologically reliable harvesting systems and facilities in the agricultural production. The main criteria for meeting these demands are the digging quality and root crops impurities separation characteristics. The analysis of conventional root crops machinery showed that chicory roots damaging and losses while digging by the existing tools are 20...30% and 4...10% respectively, which significantly exceeds the present requirements of cleaning quality (Adamchuk V. et al., 2002; Baranovsky and Skalsky, 2016). The main current feature of the general trend of big root crops harvesting, especially sugar and fodder beet, is a large-scale use of single phase technology, which is implemented on the basis of energy intensive six-row self-propelled bunker combine harvesters use, with up to 40 m³ bunker capacity (Kravchuk V.I. et al., 2004).

Self-propelled combine harvesters do all phases of root crops harvesting (main tops cutting, tops unloading on the field, remaining tops cutting of root crops heads, root crops digging, root crops cleaning from impurities, root crops transportation and loading into bunker, clean root crops unloading on the harvested field in large piles, or on a vehicle), i.e. combining all phases of root crops harvesting into one sequential technological operation.

In the EU, this type of root-harvesting machine annually harvest up to 70% of the planted acreage of sugar beet roots and in Germany and France – much more. Due to some objective and subjective factors (economic conditions, soil and climate conditions of root crops harvesting, etc.) such harvesters used in Ukraine are not always effective – root crops cleaning quality doesn't sufficiently meet the agrotechnical requirements as there are a number of defects (*Dubrovin et al., 2013*).

However, despite the rather complex multi-joints transport technological systems of tools for root crops digging and cleaning, the diggers, together with the already dug root crops, load on the mentioned cleaning systems of root crops harvesting machinery a completely unacceptable amount of soil impurities (an average of 30...50 tons per 1 hectare).

As a result, after their cleaning by energy-intensive multi-stage cleaning systems from field impurities a great amount of fertile soil is carried, which is equivalent to 10...15 cm topsoil on 100 hectares of harvesting area, while the total length (technological length) of surfaces under cleaning is 8...10 m and more (*Pogorely and Tatyanko, 2004*).

The goal of this study is to increase the technical and economic parameters of chicory harvesting by using the improved digging-cleaning systems of root crops harvesting machinery.

MATERIALS AND METHODS

Significant damage and losses of chicory roots are the results of cutting and not digging the underground parts of root crops by tools that are not adapted for brittle roots digging, which lie in the soil in great (to 15...20 cm) depths (*Humentyk M. Ya., 2003*).

In addition, these types of harvesters structurally and technologically can't combine, while harvesting, two manufacturing operations – root crops digging and remaining head tops separation.

Therefore, a simultaneous combination of head tops separating with the process of roots digging is a further step in the development, research and implementation into production of digging-cleaning systems of combined chicory root crops diggers. Under economic management conditions of multipurpose farm, agricultural enterprises in Ukraine, which are engaged in growing not only chicory but sugar, red and fodder beet and carrot root crops as well, the most urgent technical and economic problem is the payback of technically complex and costly (from 150 to 350 thousand of UAH per unit) root crops machinery due to their limited climatic performance life (about one calendar month) in a small area (especially root crops of red and fodder beet, carrots and chicory), and 90% of the root crops total area is gathered in by separate, economically inefficient technology (*Baranovsky et al., 2014*).

Significant efficiency increase of multipurpose farms economic management can be achieved primarily due to some organizational measures such as the use of a root crop machine for different root crops gathering in and determination of necessary flexible and cyclic operation due dates regarding weather and climate, root crops different agrophysical characteristics and so on.

The basis of the scientific problem solving dealing with operational and agrotechnological characteristics increase of chicory root crops harvesting is the hypothesis of possible considerable intensification of root crops digging due to the development and substantiation of parameters and general design-engineering principles and aspects of the combined carrying and cleaning diggers use.

RESULTS

A variety of design schemes of digging tools greatly depend and are closely linked both with harvest method and with the technological requirements to harvest quality indicators of different crops and root crops, the main of which are the quality indicators of root crops digging and their heads cleaning from the head tops. The most common basic disadvantage of existing and technically implemented types of diggers (blade, forklift, two-disc, vibration), which are widely installed on mounted, trailed and self-propelled root crops machinery is considerable second's supply of soil both free and adhering to the root surface (7...10 kg/s) head tops on root crops heads (0.5 to 1.5 kg/s) per one running meter at operating speeds up to 1.6 m/s, which led to an increase in length and structural complexity of cleaning-transport systems (*Bulgakov et al., 2009*).

The major drawback of existing and technically implemented types of diggers is relatively high both percentage (up to 3% relative to the root crops weight) and a mass amount of soil adhering to the roots surface and also percentage (from 0.5 to 1.5% relative to the root crops weight) and mass of head tops on the root crops heads, which significantly reduce, depending on the crop, or in one case, the quality of raw sugar and sugar yield or, in another case – products storage life. In addition, together with root crops gathered on the fields approx. 1.5...3.0% of fertile soil is removed depending on crops yield (Baranovsky et al., 2014).

The objective reason of these diggers' technological imperfections is that the conventional diggers structurally and technologically can't combine two technological operations while digging – root crops digging and simultaneous removal of head tops. Algorithm for design-layout scheme constructing of transport-cleaning combined digger must be based on the use of mono block digging and cleaning combined tools in its technological scheme, the principles of which are based on common properties of multipurpose (all purposes to some degree) adapters use, their purpose and way of use while root crops gathering.

A large number of developed tools designs, assemblies and circuit layout of digging machines require a differentiated approach at the selection, calculation, design, research and implementation of new developments into production. Therefore, the ranked approach taking into consideration tools characteristics, their layout schemes and methods of operation can provide the possibility of identification (analysis and synthesis) of the necessary structural and technological scheme of digging-cleaning system for chicory root crops combined digger.

Of the whole digger variety, one-disk concave diggers, or the so-called "eurodisc" (Fig. 1a) are the simplest in design, and the least energy and metal consuming. Besides, they have a wide range of applications for the various root crops digging at satisfactory performance index. The axis of rotation 2 of concave 1 of a digger forms an angle of attack α in the horizontal plane reported to root crops row axis.

A significant drawback of their work, or the failure of simultaneous root crops digging and head tops cutting can predictably be eliminated by further structural and technological improvement of this digger type.

Operational characteristics and quality factors enhancement of conventional diggers, and all root crops machinery in general, is partly solved by using the improved digger (Fig. 1b) or by additional installation of the concave disc 1 in the front area, root guide 3 and horizontal drive cleaning shaft 4, where radial flanges 5 are fixed. Parallel axes 6 are consequently circle-wise set between the flanges, rotated relative to the cleaning shaft axis by a sharp angle. Flat elastic blades sections 7 are articulated on the parallel axes (Hurchenko et al., 1991).

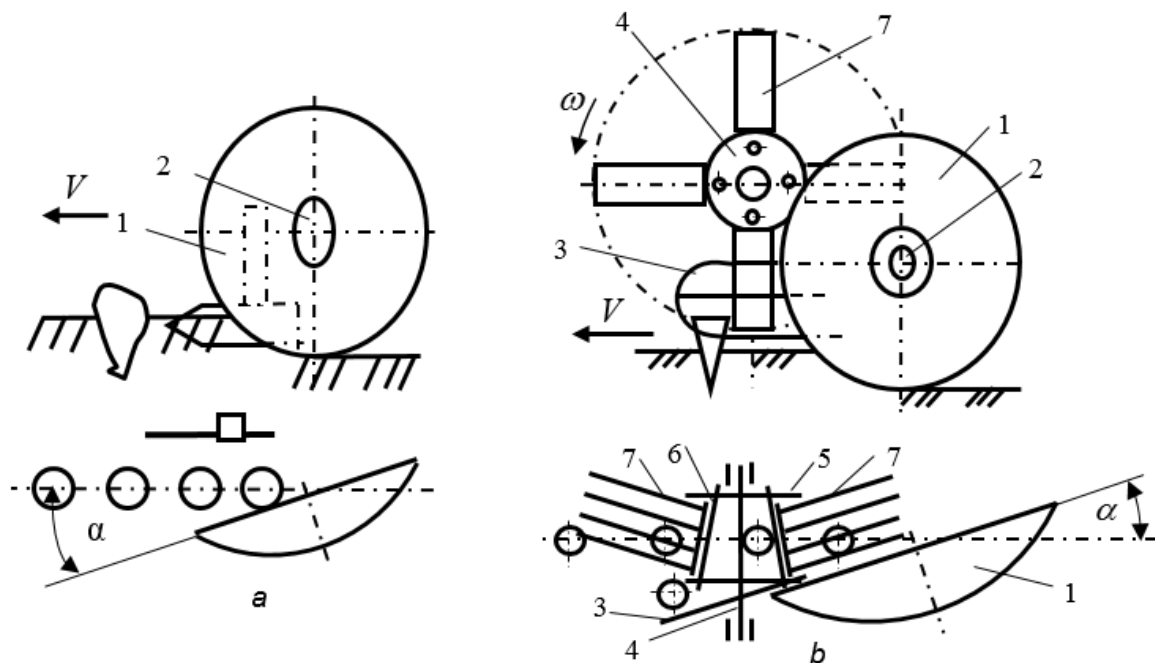


Fig. 1 – One-disk digger structural diagram

a – digger of "eurodisc" type; b – improved digger; 1 – disc; 2 – axis of rotation; 3 – root director; 4 – drive shaft; 5 – flange; 6 – axis; 7 – blade

When the digger is moving, root guide 3 is shifting the previously beaten root crops during crop tops cutting by toppers tools from the row to its centre, and concave disc 1 is digging the root crops. Simultaneously, while the root crops digging by a concave disk is taking place due to cleaning shaft 4 rotation, flat elastic blades 7 are in contact with the root crops heads, clean them from the head tops due to contact interaction of flat elastic blades with the head.

Parallel axes 6 rotation by a sharp angle relative to the axis of the cleaning shaft allows the flat elastic blades to strike the root heads aside of the row, which improves the roots of different height cleaning, as a high root crop doesn't cover a low one against oblique impact.

In addition, flat elastic blades simultaneously interact with soil clumps, destructing the latter and pushing the root crops to the next transportation systems, that results in enhancement of the technological potential of root crops machinery.

While root crops digging under dry hard soil conditions, root tails are damaged due to their cracking, because of lack of roots pushing vertical force and result root crops significant losses. To eliminate this cracking of root tails or their losses concave disc 1 (Fig. 2a) is set at a sharp angle φ and flange 5 – at an angle δ to the vertical plane, with the axis 6 in the lowest position on the flange, forming an angle ε equal or close to 90° with a plane passing through the concave disk blade.

Concave disc 1 digs root crops, which are in a row by lifting them up due to setting the concave disk at a sharp angle φ to the vertical and appearing additional lateral projection of lift force which is directed to a vertical plane. At the moment of flat elastic blades 7 impact on the root crop head or soil surface their rotation around their axes 6 is taking place and in the impact plane due to installing the flanges 5 at an angle φ to the vertical and rotated axes by an angle γ relative to the axis of the shaft 4. As the axes in the lower position are perpendicular to the plane passing through the concave disk blade or inclined to it at an angle close to the right, then flat elastic blades in the lower position are parallel to this plane and do not have a contact with the concave disc surface, which results in their wear reduction.

To increase the cutting degree of root crops head tops, particularly sugar beet and carrots, and the degree of soil lumps destruction by increasing the force of contact interaction (the force of direct central impact) of flat elastic blades on the root crops heads and soil lumps, parallel axes 6 (Fig. 2b) which are placed on the flanges 5 of horizontal cleaning shaft 4 and where flat elastic blades 7 are mounted, are installed parallel to the rotation axis of the cleaning shaft (Pankiv et al., 2009).

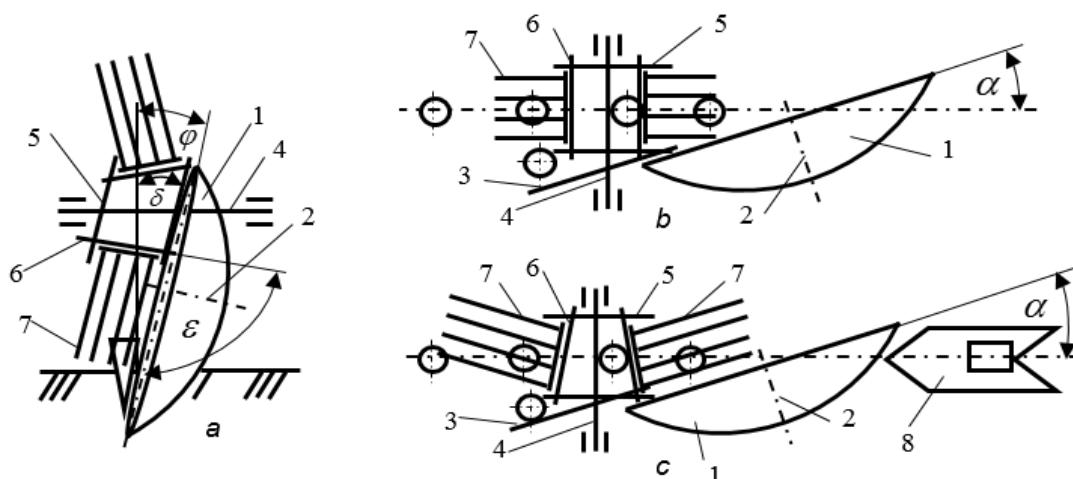


Fig. 2 – Structural diagram of one-disc digger

1 – disc; 2 – axis of rotation; 3 – root director; 4 – drive shaft; 5 – flange; 6 – axis; 7 – blade; 8 – ripper

Along with root crops digging, due to cleaning shaft 4 rotation, flat elastic blades 7 interact with root crops heads and soil lumps. In this case a direct impact of elastic flat blades takes place which results in head tops removal of root crops heads and soil lumps breaking up.

For digging root crops which are relatively deep relative to the soil surface (sugar beets, some kinds of carrots, chicory root crops) ripper 8 is used, which is set behind the concave disc 1 stroke (Fig. 2c) and can be designed as cultivating tine or chisel.

In the working process, ripper 8, while moving forward, lifts the roots a little, and the root crops-soil ties are getting damaged, i.e. the previous breaking up of soil layer is taking place. Then the root crops are easily dug from crumbled soil by the concave disc 1 and are displaced in the direction of a plane passing through the concave disk blade. In this case, we have the opportunity to dip the concave disc so as not to lose the root crops and load to transport-cleaning systems of root crop machinery the least amount of soil and plant heads.

On the basis of earlier diggers identification (analysis and synthesis) we have proposed an improved design of the two-disc (two-row) digger, which combines all positive aspects and benefits relative to the existing concave one-disc digger (Fig. 1). The structural diagram of two-row digger is shown in Fig. 3.

Two-row digger (Fig. 3a) consists of two loose concave discs 1 mounted on their axis of rotation 2 and located by angle α to the corresponding row axis of root crops. A root guide 3 is set in the front area of the attacking edge of each disc 1. Above the discs 1 the horizontal drive shaft 4 is mounted perpendicular to the digger motion operating speed V_k direction. The horizontal drive shaft includes a cylinder 5, bearing flanges 6. The horizontal shaft cylinder is divided into three sections. The axes 7, 8, 9 with flat elastic blade 10, 11 are set consequently between the flanges of the cylinder circle-wise. Axes 7 and 8 of two boundary sections 12, 13 of the cylinder form a truncated cone, and sections 12, 13 are directed to each other by smaller bases. Axes 9 of middle section 14 form a cylinder. The planes crossing the axes 7, 9 or 8, 9 of contiguous sections 12, 14 or 13, 14 form an obtuse angle.

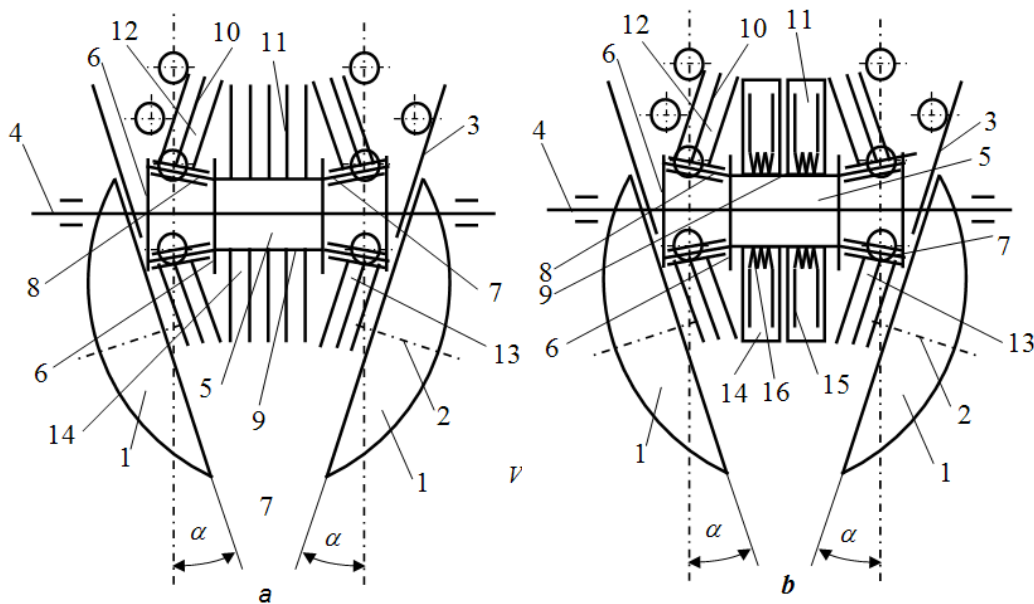


Fig. 3 – Structural diagram of two-row disc digger

1 – disc; 2 – axis of rotation; 3 – root guide; 4 – drive shaft; 5 – cylinder; 6 – flange; 7, 8, 9 – axis;
10, 11 – blade; 12, 13 – boundary section; 14 – middle section; 14 – spring-loaded; 15 – two-section spring

While the digger is moving, root guide 3 is displacing the root crops dug out of the row to its centre and concave disc 1 is digging the roots out. Along with roots digging out, due to horizontal drive shaft 4 rotation, flat elastic blades of 10 two boundary sections 12, 13 interact with the roots heads. In this case roots heads cleaning of head tops from two adjacent rows and breaking up of soil lumps take place simultaneously. In addition, flat elastic elements 11 of middle section 14 also interact simultaneously with roots and soil lumps, thus the roots surface cleaning of adhering soil and soil lumps breaking up take place together with pushing the thrashed heap in the concave discs 1 at the same time, in this way accelerating its supply to the next technological systems of root harvesting machinery.

To reduce the supply of soil contaminants during two-row digger operation under dry and hard soil conditions on the outer side of each flat elastic blade 11 (Fig. 4) of middle section 14 spring-loaded rod 15 is mounted which is designed as a two-section spring 16. Two-section spring is firmly fixed on each axis 9 of middle section 14 (Kravchenko et al., 2013).

To adjust the contact force of flat elastic blades 10 (Fig. 4) of two boundary sections 12, 13 with the head of root crops during their digging, or to provide the highest degree of root crops cleaning of head tops

and simultaneous agreement on roots damage degree that should not exceed the limit according to agrotechnical requirements, we propose to install a spring-loaded rod 17 on the outer side of each flat elastic blade of two boundary sections 12, 13 of three-section cylinder 5, which is designed as a two-piece spring 18. Two-section spring is firmly fixed on each axis 7, 8 of the three-section cylinder. The contact force of flat blades of two boundary sections is regulated by turning each section axis, which results in changing the twisting of two-section springs and spring-loaded rod pressing.

Along with roots digging due to horizontal drive shaft 4 rotating, flat elastic blades 10 of two boundary sections 12, 13 get in contact with the roots heads and flat elastic blades 11 of middle section 14 – with soil lumps dug out by concave discs 1. In this case, the cleaning root crop heads of head tops of two adjacent root rows and soil lumps intense breaking up, due to the impact contact of inner side of the flat elastic blades 11 with lumps of soil, take place simultaneously.

In addition, the flat elastic blades of middle section not only break up the soil lumps but push the thrashed heap dug out by concave disks, located in the space between them, thereby accelerating its move to the next technological systems of the machine.

On the basis of conventional diggers identification (analysis and synthesis), we have proposed an improved design of transport and cleaning system of chicory root combined digger taking into consideration all the positive aspects and advantages of concave two-disc digger (Fig. 3, 4).

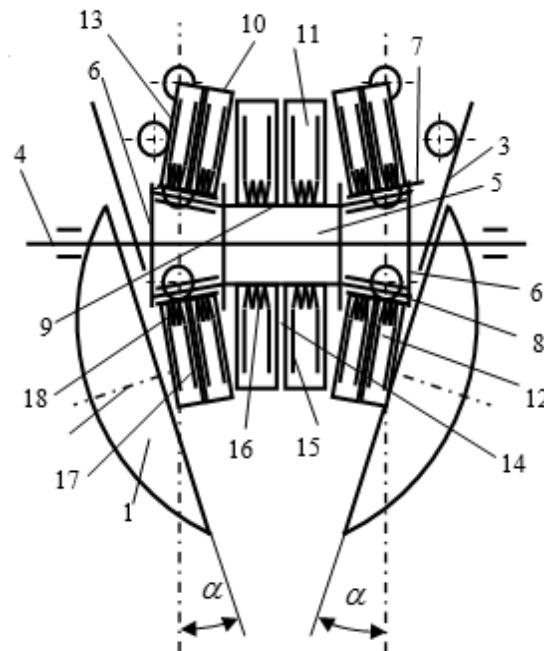


Fig. 4 – Structural diagram of two-row disc digger

1 – disc; 2 – axis of rotation; 3 – root guide; 4 – drive shaft; 5 – cylinder; 6 – flange; 7, 8, 9 – axis; 10, 11 – blade; 12, 13 – boundary section; 14 – middle section; 15, 17 – spring-loaded; 16, 18 – two-section spring

The proposed transport-cleaning system of combined digger allows intensifying the process of chicory root crops digging under considerable rooting depth conditions. The structural diagram of transport and cleaning system of combined chicory root digger is shown in Fig. 5.

Combined root crops digger consists of two adjacent concave discs 1 which are loose on their axes of rotation 2 and are mounted by angle α to the root crops row axis. In the front area of cutting edge 3 of each of the two concave disks a root guide 4 and hollow guide tube 5 are set horizontally. The latter is placed above the two concave discs and between them perpendicular to the roots row, or to the digger motion operating speed V_k direction. Bearings 6 are set inside the hollow guide tubes, where drive shaft 7 is mounted. The separate cylinders 10 and 11 are fixed on the frontal edges 8 and 9 of the drive shaft, designed as radial flanges 12 installed on the horizontal drive shaft. Between the flanges of each of the cylinders the axes 13, 14 are fixed on their generators in series and parallel, where flat elastic elements 15 are set. The axes are turned about the axis of the drive shaft by an acute angle. Two supporting plates 17 are mounted radially to the external bottom of the hollow tube 16 where horizontal finger 18 is fixed. Pivoting

slide rest 19 is hinged on the fixed horizontal finger where the ripper 20 is assembled which is placed in the space between rows. Pivoting slide rest of the ripper is made of springy type thanks to spring 21, one end of which is fixed on the top of the pivoting slide rest 22, and the second – on the digger frame 23. The pivoting slide rest rotation on the fixed horizontal finger is limited by the stop 24 fixed on the supporting plates.

The ripper running depth is more than running depth of concave disks. The drive shaft direction of rotation V_k is the same as the combined digger.

Combined root chicory harvester operating principle is as follows. While at combined harvester motion, the ripper 20 due to the soil environment resistance is stretching the spring 21 and is deviating in the opposite direction on the horizontal fixed finger 18 to the support 24. The ripper simultaneous translational motion in the soil environment and spring reverse compression create two recurring opposite acting forces the action of which causes forced oscillations around roots soil environment. These cyclic fluctuations lead to the breaking ties of chicory root crops with soil on the rooting depth, i.e. the ripping intensification of soil environment and root crops partial digging take place. Also, along with roots digging up by a ripper, two related processes take place, i.e. chicory roots final digging out by adjacent concave disks 1 due to their free rotation on their axes 2 in the soil environment and root heads cleaning of head tops of two adjacent root rows by rotating cylinders 10 and 11 of the drive shaft 7 or interactions of flat elastic elements 15 with root crops heads. Root guide 4 is shifting the chicory roots previously broken up of the row to its centre and adjacent concave disks pick up the roots dug out of soil. Besides, flat elastic elements also break up the soil lumps and at the same time push the thrashed heap, located in the space of adjacent concave disks, accelerating its supply to the next technological systems of root harvesting machinery.

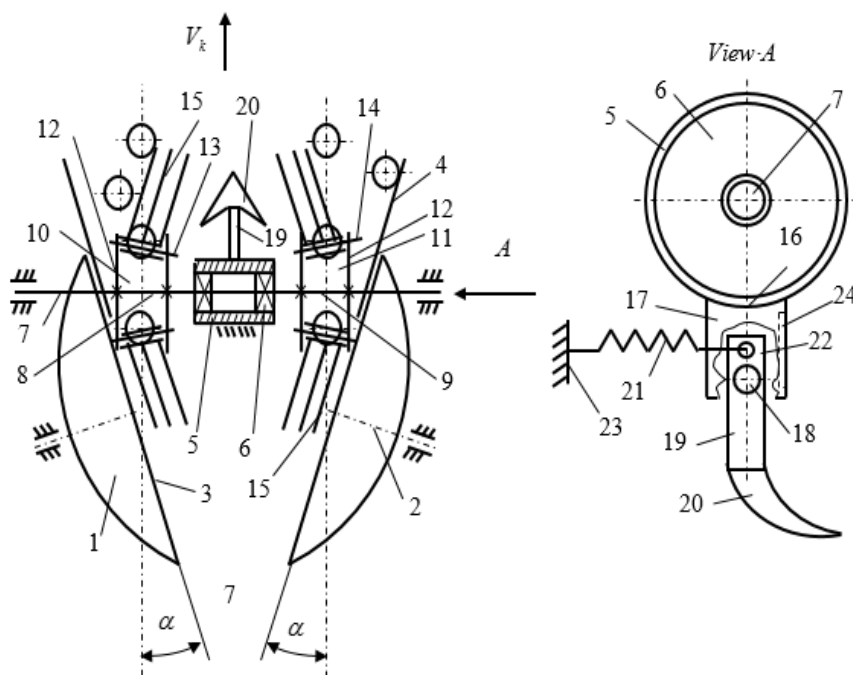


Fig. 5 – Structural diagram of combined digger transport and cleaning system

1 – disc; 2 – axis of rotation; 3 – edge; 4 – root guide; 5 – guiding tube; 6 – bearing; 7 – shaft; 8, 9 – shaft end; 10, 11 – cylinder; 12 – flange; 13, 14 – axis; 15 – spring element; 16 – low outer part of guiding tube; 17 – support plate; 18 – finger; 19 – swivel carriage; 20 – ripper; 21 – spring; 22 – swivel carriage top; 23 – frame; 24 – support

To confirm the technological efficiency of the combined digger in the composition of the root-harvesting machine (Fig. 6), field comparative experimental studies were carried out on the digging of chicory roots of the variety "Alexandrite".

The dependences of the quality indices of the work-loss w_k and damage p_k of the chicory root crops for two cases were investigated with the use of a ripper 6 (Fig. 6), which is performed in the loosening loos and without the use of a pest. The performance indicators w_k and p_k were determined according to the standard procedure and relative to the common root crop of one experiment.

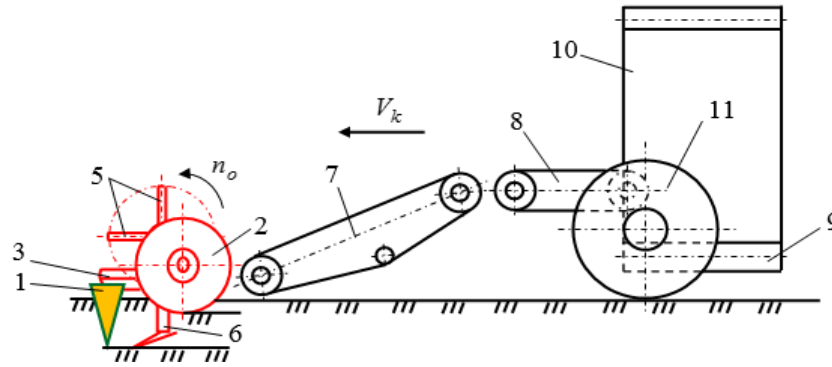


Fig. 6 – Structural diagram of field installation

1 – root crop; 2 – disc; 3 – axis of rotation; 4 – root guide; 5 – drive shaft; 6 – spring blades; 7 – ripper; 8, 9, 10, 11 – conveyors; 12 – support wheel

After processing the experimental values, final regression equations are obtained in natural quantities, that characterize the dependence of changes in losses and damages of chicory root crops on their digging out of the constructive-kinematic parameters of the combined digger:

$$\left. \begin{aligned} w_k &= 94,19 - 38,06V_k - 7,36a_k + 13,24V_k^2 + 0,15 \cdot 10^{-4} n_o^2 - 0,76 \cdot 10^{-3} n_o a_k + 0,22a_k^2; \\ p_k &= 4,51 + 1,28V_k + 1,001n_o + 1,003a_k \end{aligned} \right\}, \quad (1)$$

where V_k – speed of the root machine, [m/s];

a_k – depth of the ripper stroke, [cm];

n_o – rotational speed of drive shaft, [rpm].

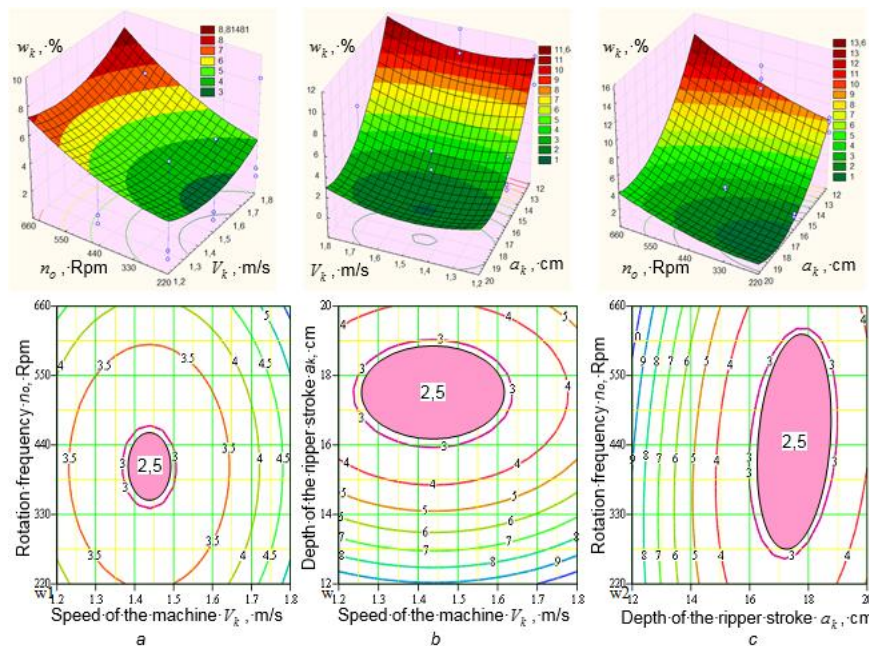


Fig. 7 – The response surface and the two-dimensional section of the response surface

$$a - w_k = f_{w_k}(V_k; a_k); \quad b - w_k = f_{w_k}(V_k; n_o); \quad c - w_k = f_{w_k}(n_o; a_k)$$

In Fig. 7, 8 is shown the response surface and the response surface two-dimensional section of losses w_k and damage p_k of chicory root crops from the movement speed of the root harvesting machine V_k ($1.2 \leq V_k \leq 1.8$ m/s), the speed of the drive shaft n_o ($220 \leq n_o \leq 660$ rpm), the depth of the ripper stroke a_k ($12 \leq a_k \leq 20$ cm), which are constructed according to the regression equations (1).

The dominant factors that functionally characterize the loss w_k of chicory root crops (Fig. 7) are the speed V_k and the ripper's stroke depth of the combined digger. The functional change w_k in root crop losses has an optimum - the minimum values of the response function $w_k = f_{w_k}(V_k; n_o; a_k)$, which are in the range of 1.5 to 2.5%, are provided for the movement speed of the root harvesting machine in the range $1.4 \leq V_k \leq 1.5$ m/s, the depth of the ripper stroke – $16 \leq a_k \leq 20$ cm, the speed of the drive shaft – $400 \leq n_o \leq 500$ rpm. It has been established that the smallest values of the chicory root crops loss ($w_k \Rightarrow \min$) correspond to the values of factors $V_k = 1.45$ m/s, $n_o = 450$ rpm, $a_k = 18$ cm. The optimization criterion for the minimum point w_k , which is calculated using the first regression equation (1), is 1.2% at this point.

The maximum permissible damage to the chicory roots ($p_k \leq 15\%$ according to agrotechnical requirements) corresponds to the rotational speed of the drive shaft not more than $n_o \leq 500$ rpm and the established limits of variation of V_k and a_k (Fig. 8).

Based on the analysis of empirical dependencies and graphical constructions (Figures 7, 8), which characterize the change in the performance indicators of the combined digger in the form of functionals $w_k; p_k = f_i(V_k; n_o; a_k)$, we can state that the condition for storing generalized optimization criteria $w_k \leq 2.5\%$ and $p_k \leq 15\%$ is fulfilled for the following constructive-kinematic parameters: $V_k = 1.5$ m/s, $n_o = 500$ rpm, $a_k = 16$ cm.

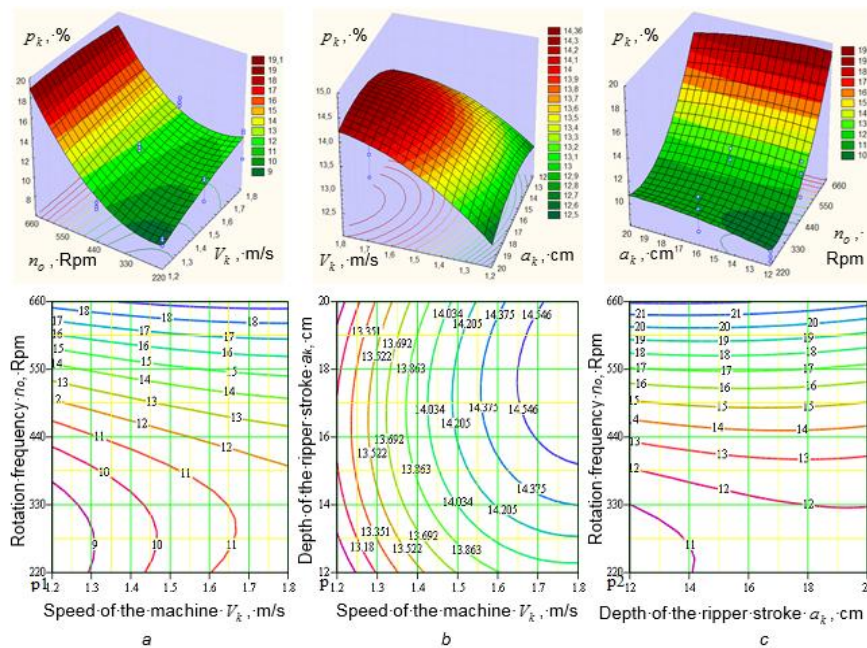


Fig. 8 – The response surface and the two-dimensional section of the response surface
 $a - p_k = f_{p_k}(V_k; a_k)$; $b - p_k = f_{p_k}(V_k; n_o)$; $c - p_k = f_{p_k}(n_o; a_k)$

The rational constructive-kinematic parameters of the combined digger in conducting comparative studies were as follows: diameter of the spherical disk 0.45 cm; the angle of attack of the disk is 30 degrees; the depth of the disc is 9 cm; the diameter of the drive shaft is 0.6 m; rotation speed of the drive shaft 500 Rpm; the depth of the ripper 16 cm.

It was found that the total losses of chicory root crops, which were excavated by a combined digger, were 1.6 times lower compared to the basic digger (without setting the ripper) - from 3.5% in the basic digger to 2.2% in the modernized digger. A significant reduction in the losses of chicory root crops is achieved due to the additional installation of the ripper, which also reserves a 2.1-fold decrease in the number of untreated (unrecovered and left in the soil) root crops – 2.9% in the base crop and 1.4% in the combined digger.

A significant reduction in the damage to root vegetables of chicory (approximately 2 times - 20.3% in the base versus 10.1% in the combined digger) also confirms the technological feasibility of its use for the rooting of roots. This allows us to improve the technological process of digging out the crumbling roots.

CONCLUSIONS

Thus, it can be stated that the mounted drive shaft with flat blades installed on it, allows two operations (root crops digging and root heads cleaning of head tops) to take place simultaneously. This provides the reducing of second supply of soil and plant impurities due to contact interaction of flat blades with thrashed heap components. Moreover, hinged ripper use mounted on a horizontal finger and made a spring-loaded, can intensify roots with soil environment ties breaking up. As a result, the losses of chicory roots are decreasing due to the number of damaged root tails reducing, energy consumption while root crops digging saving and technological reliability growth of the digger and root crop machinery in general. It has been established that chicory root losses are reduced by digging with a combined digger in 1.6, and the damage is approximately 2-fold compared to a baseline (serial) digger. In this case, the number of dug roots with a broken tail is reduced by approximately 2.6 times.

REFERENCES

- [1] Adamchuk V, Bulgakov V, Ivanyshyn V (2002), About the development and creation in Ukraine of modern agricultural machinery (Про розробку і створення в Україні сільськогосподарських машин сучасного рівня), *Scientific works of Vinnitsa National Agricultural University (Збірник наукових праць Вінницького національного аграрного університету)*, vol. 66 (11), pp. 8-14, Vinnitsa/Ukraine;
- [2] Baranovsky V.M., (2012), Transport and technological systems of excavation working bodies of the adapted root-cutting machine (Транспортно-технологічні системи викопувальних робочих органів адаптованої коренезбиральної машини), *Design, production and operation of agricultural machinery (Конструювання, виробництво та експлуатація сільськогосподарських машин)*, vol. 42, pp. 79-86, Kirovograd/Ukraine;
- [3] Baranovsky V.M., Pidhursky M.I., Pankiv M.R., Tesljuk V.V., Onithenko V.B., (2014), *Through the development of adapted transport and technological systems root crop machinery (Основи розробки адаптованих транспортно-технологічних систем коренезбиральних машин)*, ISBN 978-966-305-061-4, TNTU, Ternopil/Ukraine;
- [4] Baranovsky V.M., Skalsky O.Ju., (2016), The analysis of constructive-technological aspects function of root crops diggers (Аналіз конструктивно-технологічних аспектів функціонування копачів коренеплодів), *Innovative solutions in modern science*, no.1(1), pp. 147-154, ISSN 2416-6714, Dubai/ United Arab Emirates;
- [5] Bulgakov V.M., Chernovol, M.I., Sviren N. A., (2009), *Theory of beet-lifting machines: monograph (Теорія свеклоуборочних машин)*, Kirovograd, ISBN 978-966-1508-01-08, Kirovograd/Ukraine;
- [6] Dubrovin V., Golub G., Baranovsky V., Tesliyk V., (2013), Identification of the development process of machines adapted for harvesting root crops (Идентификация процесса разработки адаптированной корнеуборочной машины), *MOTROL, Engineering Sciences*, vol.15, no.3, ISSN 1730-8658, pp. 243-255, Lublin-Rzeszow/Poland;
- [7] Humentyk M.Ya., (2003), Features of chicory root cultivation and agricultural technology (Особливості цикорію кореневого і агротехніка його вирощування), *coll. scient. works ICB UAAN (зб. наук. праць ІЦБ УААН)*, Kyiv/Ukraine;
- [8] Hurchenko A.P., Baranovsky V.N., Zavorodniy A.F., Hurchenko L.A., Bulgakov V.M., (1991), *Device for root crops extraction (Устройство для выкапывания корнеплодов)*, Author certificate, No 1672964, SU;
- [9] Kravchenko I.E., Baranovsky V.M., Pidhursky M.I., Pankiv V.R., Trushanska O.O., (2013), *Combine root digger (Комбінований копач коренеплодів)*, Patent, No 77568, UA;
- [10] Kravchuk V.I., Grytsigina M.I., Kovalya S.M., (2004), *Modern tendencies of agricultural technique construction development (Сучасні тенденції розвитку конструкції сільськогосподарської техніки)*, Ed.Agrarian Science, 396 p.;
- [11] Pankiv M.R., Herasymchuk H.A. Baranovsky V.M., Ramsh V.U., (2009), Device for root excavate (Пристрій для викопування коренеплодів). Patent, No 44747, UA;
- [12] Pogoreliy L.V., Tatyanko N.V., (2004), *Beet machines: history, design, theory, forecast (Свеклоуборочные машины: история, конструкция, теория, прогноз)*, "Phoenix" Publishing, ISBN 966-651-167-3, Kyiv/Ukraine.
- [13] Storozhuk I.M. Pankiv V.R. (2015), Research results of harvesting haulm remnants of root crops, *INMATEH-Agricultural Engineering*, vol.46. no.2, pp.101-108, Bucharest/Romania.

RESEARCH OF THE DYNAMIC MODEL OF THE FLAX STEMS LINE ARRANGING MECHANISM

ДОСЛІДЖЕННЯ ДИНАМІЧНОЇ МОДЕЛІ МЕХАНІЗМУ ПІДБИВАННЯ СТРИЧКИ СТЕБЕЛ ЛЬОНУ-ДОВГУНЦЯ

Prof. Ph.D. Eng. Nalobina O.O.¹⁾, Ph.D. Eng. Gerasymchuk O.P.¹⁾, Ph.D. Eng. Puts V.S.¹⁾,
Prof. Ph.D. Eng. Marchuk M.M.²⁾

¹⁾ Lutsk National Technical University / Lvivska str., 75, Lutsk / Ukraine;

²⁾ National University of Water Management and Nature Resources Use, Rivne / Ukraine
Tel: 0727651064; E-mail: nalobina08@rambler.ru

Keywords: common flax, flax line, length, arranging mechanism, kinematic pair, jaw, belt.

ABSTRACT

The article deals with the dynamics of mechanism for arranging the flax stems line on the conveyor belt. There were developed the equations of the kinematic pair which is included as a compound of mechanism. The equation for calculating the conveyor belt length was developed.

РЕЗЮМЕ

У статті розглянуто динаміку механізму підбивання стебел стрічки льону, яка поступає на транспортер підбирача стрічок льону-довгунця. Виведені рівняння для опису динаміки кінематичної пари, яка входить до складу механізму підбивання та отримано вираз для визначення довжини транспортеру стрічок.

INTRODUCTION

Flax is traditionally grown in Ukraine and it provides a lot of benefit. People use flax fiber, seeds and by-products. The flax fiber is used to produce highly persistent household or technical clothes. Flaxseed oil is used in food industry as well as for technical aims (to produce varnishes, oil paints and lacquers) and for electrical, pharmaceutical, rubber and leather production. The value of flax fiber is higher than the value of other fiber plants, such as cotton, hemp, kenaph. Flax fiber is healthy, nice and putrefaction resistant; it has taken on market all over the world. Flax press cake with around 36% of protein is used in farm industry as animal feeding stuff. Flax by-products (oakum, shove) serve as source for paper and building material production.

The areas of flax plantings have been decreased recently. In 1990 there were 172 500,00 hectare of them, but in the following years these areas became smaller because of various reasons; in 2015 there were 1, 91 thousand hectare (*Statistical bulletin, 2015*).

Flax cultivation should be renewed in Ukraine. A lot of measures are necessary to raise the amount of flax production.

Taking into consideration all above, we formulate the task for the flax industry – development of modern technologies of growing, cropping and manufacturing of flax in order to increase the quality and decrease the wastes. Ukrainian agriculture will need more machines for flax cultivation and cropping if the areas of flax plantings increase. It is especially important to mechanize the flax cropping process because it is labour-consuming.

The researches of Ukrainian and Russian scientists (*Nalobina O.O., 2004; Nalobina O.O., Gerasimchuk O.P., 2014; Nalobina O.O. and Muravynets Y.V., 2012; Nalobina O.O., Puts V.S., 2013; Zincov O.N., 2016*) have proved that the index of the length of flax stem line influences the final product of flax industry. This index is formed in several stages: during flax taking, transporting by the combine working tool, while making a line, lying, making retted straw.

The analyses of exciting research has shown that one of the possible ways to reduce the flax line length is to introduce the operation of arranging the stems in the line either during cropping or unrolling at the stage of primary machining. It is necessary to have special piling (arranging) mechanisms to perform this operation. Some works (*Chernikov V.H., Rostovtsev R.A., Konokhov V.J, 2004; Chernikov V.H., Rostovtsev R.A., 2005; Konokhov V.J, 2004; Nalobina O.O., Puts V.S., Tolstushko N.N., 2014; Rostovtsev R.A., Konokhov V.Y., 2006; Zincov O.N., 2007*) research these mechanisms. The authors suggest reducing the

line length by affecting the stems with different mechanisms, but they haven't taken into consideration the fact that the stems in the line are usually intertwined.

They researched parallel and not intertwined stems that don't correspond to reality.

The authors of this work got a technical task to provide the arranging of flax stem line where the stems may be intertwined and lopsided; they have constructionally completed this task.

In order to complete the above mentioned task, they have performed the system research that allowed analyzing the behaviour of the complex physical system, consisting of data sets, technical and planting components. It is well-known that system research involves performing two tasks – analyses and synthesis (Sydoruk O.V., Nalobina O.O., Demyduk N. A. et al., 2011). We have analyzed the system that consists of flax cropping machines and the plants of flax, this system works under the influence of various external and internal factors (Hylleys H.A., Konovaliuk D.M., 1992; Nalobina O.O., 2012).

The authors have discovered that cropping of the vertical flax stems by combines gives the high index of flax straw quality. However, the experience of harvest works in different regions of Ukraine, Belorussia and other countries has shown some drawbacks of combines: great length of flax stem line, parallel misalignment, damages; these defects can be eliminated due to the improvement of design parameters of flax cropping machines.

This article presents the results of theoretical work aimed to perform the systemic syntheses and as result the authors have made the real model of the apparatus for arranging the flax stem line; it allowed to research the working dynamics of the arranging mechanism (Hylleys H.A., Nalobina O.O. et al. 2001); this mechanism helps to make the stem flax line smaller, arrange the flax stems in parallel.

MATERIALS AND METHODS

The work presents the research based on the principles of theoretic mechanics and kinetics of material systems. Figure 1 shows the scheme of the apparatus for arranging the flax stem line.

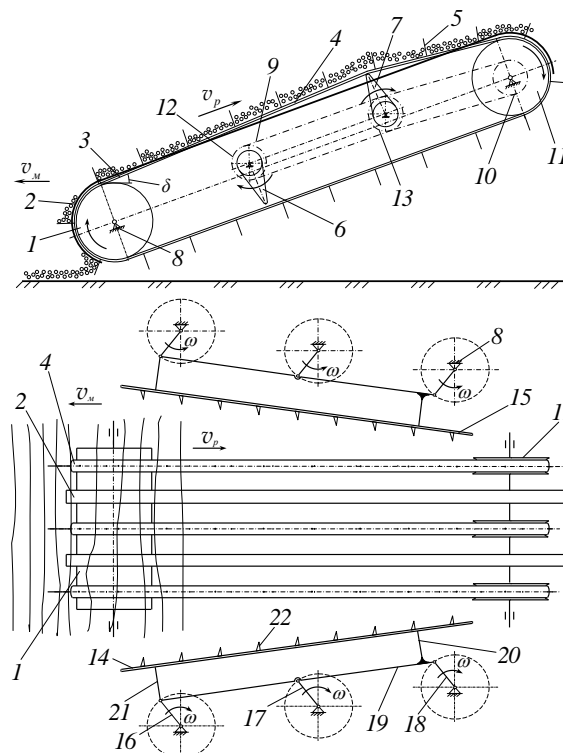


Fig. 1 - Scheme of the apparatus for flax stems arranging

1 – drum, 2 – guideway, 3 – conveyor, 4 – conveyor belt, 5 – pin, 6, 7 – jaws, 8 – frame, 9 – chain, 10 – drive sprocket, 11 – shaft, 12, 13 – driven sprockets, 14, 15 – crash protectors, 16, 17, 18 – crank shafts, 19 – piston rod, 20, 21 – planks, 22 – ribs.

The apparatus consists of two mechanisms: shaking mechanism and piling mechanism. The shaking mechanism consists of the jaws 6, 7 and the drive gear made of the chain 9, the drive sprocket 10 fixed to the drive pulley of the shaft 11, the driven sprocket 12 with the jaw 6 fixed to the shaft, the transition sprocket 13 fixed to the same shaft that the jaw 7. On the both sides of the conveyor the two crash protectors 14 and

15 are symmetrically situated, they are the parallel link motions consisting of the crank shafts 16, 17, 18 and the piston-rod 19 with the adjustable spring plank 20 at one of its edge.

The same spring plank 21 is fixed to the edge of another piston-rod by linkage joint. The plank height is regulated with the nut. Each plank contains the spring hidden inside the pinion carrier. The planks 20, 21 from the other side are fixed to the ribbed crash protectors 14, 15 by linkage joints. The mechanisms are installed within the frame and they are driven with the shaft offtake from the tractor.

Figure 1 shows the arranging system of the conveyor that includes the drum 1, guideways 2, conveyor 3, continuous belts 4 with the pins fixed on them.

In order to increase the arranging effectiveness, the conveyor that runs on the belts 4 and guideways 2, is shaken periodically. The stems are tossed and separated, that is why the crash protectors can arrange them easier. The tossing is caused by the sequential jaws kicks upon the upper conveyor track. The arrangement of the flax line starts in the A-A zone (fig. 1) and finishes in zone B-B.

Pilling transporter and arranging apparatus are in the harvesting unit in front of the press or tying device, and the drum is situated in front of the stem line. This part of the machine should be under the machine operator's control all the time. The center conveyor slot should function in the conveyor belt zone where the stem centers are situated.

The jaw (figure 2) rotates with the rotational velocity around the axle in order to shake the conveyor belt. The axle can change the position due to the spring plank variations.

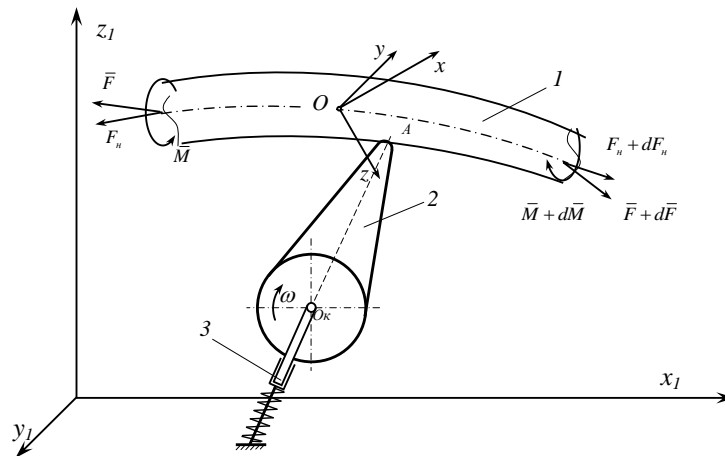


Fig. 2 - Dynamic model of the kinematic pair: conveyor belt – jaw outer surface

1 – belt, 2 – jaw, 3 – adjustable spring plank

The point on the jaw outer surface moves with the speed $V = O_{\kappa}A \cdot \omega$ in the moment when it touches the conveyor belt, where $O_{\kappa}A$ is the distance between the jaw rotation centre and the point on the jaw outer surface touching the conveyor belt in the moment. When the jaw surface moves along the belt, it turns to the angle $\alpha = \omega t$, where t is time, sec.

Figure 2 shows the element of the conveyor track of the flax line, which is influenced by the forces: F – cross-axle force and stretching force F_H , M – bending moment that appears under the jaw action in the surface element of the conveyor: $M = EI/r$, where r – radius of belt bending due to the contact with the jaw, E – power module of belt material, I - inertia moment. The moment can cause slight displacement of the conveyor belt. However, the moment will not have the considerable influence of the conveyor work if the belt tension is correct. The belt bents and becomes longer under the influence of the jaw. The belt prolongation is calculated (Svetlitskii V.A., Stasenko I.V., 1994).

$$\Delta l = r_d \beta_1 - r_s \beta_2 \quad (1)$$

r_d , r_s - are radiuses of the drum and shaft (drawing 1), [m];

β_1 , β_2 - deviation from equilibrium of the corresponding belt areas, [grad].

RESULTS

Let's assume that the belt moves with the speed V , m/s; resulting force of F and F_H is R ; the length of belt element under the influence is l , m.

Thus, we can write the equation of belt movement on jaw outer surface with forces on the axel ZYX (fig.2):

$$\left. \begin{aligned} m_n \frac{dV}{dt} - m_n V_{z_1} \omega_{y_1} &= \frac{\partial R_z}{\partial x} - \frac{R_z}{r} + \frac{T_x}{l}, \\ m_n \frac{dV_z}{dt} - m_n V \omega_{y_1} &= \frac{\partial R_z}{\partial x} + \frac{R_x}{r} + \frac{T_z}{l}, \end{aligned} \right\} \quad (2)$$

m_n – belt weigh, [kg];

T – jaw tension on the belt, [mPa].

The speed of the belt element moving in a certain moment directly on the jaw outer surface will be different from V_A , because of deformation and fluctuation. Taking the fluctuations into account, we can assume that they will cause some slight shifts of equilibrium: s and s_z . Considering this, we will substitute expression in the equation (2):

$$\left. \begin{aligned} V &= \frac{\partial s}{\partial t}, \\ V &= \frac{\partial s_z}{\partial t}. \end{aligned} \right\} \quad (3)$$

The jaws rotates with the speed ω . There should be a contact between the pin in the outer surface of the jaw and the inner surface of the conveyor belt to shake the conveyor belt and, correspondingly, the flax stem line. In order to assure this condition the distance from the rotation centre of the jaw to the conveyor belt in the moment when the pin A neither touches the belt nor deforms it should be chosen with regard to the following condition:

$$h = O_\kappa A - \Delta \quad (4)$$

Δ is the spring deformation in the moment when the curve of the jaw nut rises the belt to the highest position (fig.2), [mm].

The flax stems will be torn from the ground if they get acceleration $a = \frac{dV}{dt}$ from the jaw hit.

Thus, the speed of the conveyor belt transport V must be higher than the product $V_{C_1} \operatorname{tg} \delta$, where V_{C_1} is the initial speed of the stems and the conveyor surface in the moment when the nut of the jaw touches them, δ is the bending angle of the conveyor belt (fig.1).

The bending angle of the conveyor upper track δ respective the horizon equals: $\arcsin \frac{H}{L}$, where H is the stem line height, L is the distance that the stems pass, and they are risen κ times by the jaws.

In order to reason the belt length L_b we assume that minimal required distance between the axels of the drum and the drive pulley is L_{min} .

Thus, the minimum conveyor length is calculated

$$L_{b \min} = L_{\min} + r_d + r_s \quad (5)$$

where $L_{\min} = \kappa n$ here κ – number of jaws, n is distance between them.

CONCLUSIONS

The authors have constructed flax stem line arranging mechanism that allows reducing the length of the flax stem line or flax stem roll during cultivating.

The authors have specified efficient elements of this machine taking into consideration the stems tearing from the conveyor belt, the differential equation (2) of dynamic pair jaw-belt, and the equation (5) and the design of the flax stem pickup with arranging mechanism.

REFERENCES

- [1] Chernikov V.H., Rostovtsev R.A., Konokhov V.J., (2004), Analyses of flax line arrangement process (Анализ процесса выравнивания лент льна), *Improvement of mechanical technologies of flax products manufacturing and processing. Materials of the international scientific and practical conference (Интенсификация машинных технологий производства и переработки льнопродукции. Материалы Международной научно-практической конференции)*, VIM Publishing House («Издательство ВИМ»), ISBN 978-5-7609-1162-9, pp. 111-123, Moscow/Russia;
- [2] Chernikov V.H., Rostovtsev R.A., (2005), Research the device for aligning the stems of flax (Исследование устройства для выравнивания стеблей льна), *New technologies and technology for resource saving and labor productivity increase in agricultural production. Materials of the international scientific and practical conference (Новые технологии и техника для ресурсосбережения и повышения производительности труда в сельскохозяйственном производстве. Материалы Международной научно-практической конференции)*, pp.45-48, Moscow / Russia;
- [3] Hylleys H.A. & Konovaliuk D.M., (1992), *Backgrounds of agricultural machines projecting and research (Основи проектування і дослідження сільськогосподарських машин)*, NMK VO (НМК ВО), p.320, Kyiv/Ukraine;
- [4] Hylleys H.A., Nalobina O.O. and others, (2001), *Flax stem arranging machine (Вирівнювач стебел льону)*, Patent № 40899 Ukraine;
- [5] Konokhov V., (2004), Background Technology of Straw Butting (Технологические основы комлеподбивания), *Achievements of Agriculture for Agro-Industrial Complex. Materials of the International Scientific and Practical Conference. Collection of Scientific Works TGSNA (Достижения сельскохозяйственной науки – развитию агропромышленного комплекса. Материалы Международной научно-практической конференции, Сборник научных трудов ТГСНА)*, pp.282-284, Tver/Russia;
- [6] Nalobina O.O., (2004) *Combines for flax gathering (background theory, mechanism calculations and exploitation): monograph (Льнозбиральні комбайни (основи теорії і розрахунку механізмів та питання експлуатації: монографія)*, (LDTU), p. 208 Lutsk/Ukraine;
- [7] Nalobina O.O., (2012), *Improvement of technical systems – basis of flax gathering machines modernization (Удосконалення технічних систем – основа модернізації льнозбиральних машин)*, *Mechanization and electrification of agriculture. Interdisciplinary thematic collection of works (Механізація та електрифікація сільського господарства. Міжвідомчий тематичний збірник)*, Issue 96, ISSN 0202-1927, pp.96-112, Hlevakha/Ukraine;
- [8] Nalobina O.O., Gerasimchuk O.P., (2014), *Theoretical bases of designing dividers of flax cutting machines with curvilinear surface (Теоретичні основи проектування подільників льнозбиральних машин із криволінійною поверхнею)*, *Mechanization and electrification of agriculture. Interdisciplinary thematic collection of works (Механізація та електрифікація сільського господарства. Міжвідомчий тематичний збірник)*, Issue 99 (1), ISSN 0202-1927, pp.184-193, Hlevakha/Ukraine;
- [9] Nalobina O.O., Muravynets Y.V., (2012), Analyses of factors that influence the technological effectiveness of getting long fiber (Аналіз факторів впливу на технологічну ефективність отримання довгого волокна), *Merchandising reporter. Collection of scientific works (Товарознавчий вісник: збірник наукових праць)*, Vol. 5, ISSN:23 10-5283, pp.99-105, Lutsk/Ukraine;
- [10] Nalobina O.O., Puts V.S., (2013), *Research of the process of flax line arrangement during the operation of pickup (Дослідження процесу підвінювання стрічки льону під час виконання операції її підбирання)*, *Reporter of National University of Water Management and Supplies. Collection of Scientific Works. Technical sciences (Вісник Національного університету водного господарства та природокористування. Збірник наукових праць. Технічні науки)*, Issue 3 (63), ISSN 2306-5475, pp.216-226, Rivne/Ukraine;

- [11] Nalobina O.O., Puts V.S., Tolstushko N.N., (2014), *Parasnal device lonsberry machines: monograph (Підрівнюючі пристрої льонозбиральних машин: монографія)*, (LNTU), ISBN 978-617-672-072-0 : 10.00., p. 172, Lutsk/Ukraine;
- [12] Rostovtsev R.A., Konokhov V.Y., (2006), *Reasoning of centrifugal unbalanced straw-butting machine settings (Обоснование некоторых параметров центробежного дебалансового комлеподбивателя)*, *Achievements of science and technique in agriculture (Достижения науки и техники АПК)*, Vol. 4, ISSN 0235-2451, pp.30-31, Moscow/Russia;
- [13] Svetlitskii V.A. , Stasenko I.V., (1994), *Collection of tasks in oscillation theory (Сборник задач по теории колебаний: учебное пособие)*, High School, ISBN 5-7038-0893-6, pp.266-267, Moscow/Russia;
- [14] Sydorchuk O.V., Nalobina O.O., Demyduk N.A. and others, (2011), *System-technological approach of project management in modernization of technical objects (Системно-технологічний метод управління проектами модернізації технічних об'єктів)*, *Computer-integrated technology: education, science, industry (Комп'ютерно-інтегровані технології: освіта, наука, виробництво)*, Vol.7, ISSN 2524-0552, pp.125-130, Lutsk/Ukraine;
- [15] Zincov O.N., (2007), *Increasing the efficiency of flax harvesting technology by improving the design of the device for leveling the stems in a belt (Повышение эффективности технологии уборки льна путем совершенствования конструкции устройства для выравнивания стеблей в ленте)*, PhD dissertation, Scientific Research Institute of Agricultural Machine Building. V.P. Goryachkina, Moscow/Russia;
- [16] Zincov O.N., (2016), *On the decrease in the stretching of stems in ribbons of flax-fiber during wrapping (Об уменьшении растянутости стеблей в лентах льна-долгунца при оборачивании)*, *Innovative developments in the production and processing of bast cultures. Materials of the International Scientific and Practical Conference (Инновационные разработки производства и переработки лубяных культур: материалы Международной научно-практической конференции)*, ISBN 978-5-7609-1162-9, pp.194 - 198, Tver/Russia;
- [17] *** Areas under crops in agriculture in 2015, (2015) (Посівні площі сільськогосподарських культур під урожай 2015 року), *Statistical bulletin (Статистичний бюлетень)*, p.53, Kyiv/Ukraine.

SIMULATION OF BULK MATERIALS SEPARATION PROCESS IN SPIRAL SEPARATOR

/

МОДЕЛЮВАННЯ ПРОЦЕСУ СЕПАРАЦІЇ СИПКИХ МАТЕРІАЛІВ НА СПІРАЛЬНОМУ СЕПАРАТОРІ

Lect. Ph.D. Eng. Dudarev I., Lect. Ph.D. Eng. Kirchuk R.

Lutsk National Technical University / Ukraine

Tel: +38(0332)74-61-32; Fax: +38(0332)74-61-31; E-mail: i_dudarev@ukr.net

Keywords: simulation, separation process, spiral separator, bulk materials

ABSTRACT

The design of spiral separator in question is based on the analysis of bulk materials separators. It has advantages over the known devices. Spiral separator is maintenance-friendly compact mechanism with a simple drive. As a tool, the spiral separating screen is used. This allows intensifying the separation process and separate bulk materials into several fractions.

The empirical and theoretical dependence for describing the process of bulk materials separation by spiral separator is obtained. The methodology of definition coefficients of mathematical equations is developed. They depend on the material fractional composition and its initial settings. The experimental research for defining the separation coefficients is conducted. The processed pellets and flax fibre shives are used. The mathematical model of bulk materials separation by spiral separator is obtained and the method of determining bulk materials separation coefficients by designing a type of spiral separator is developed. The concept of spiral separator efficiency coefficient characterizing the separation degree of the bulk material fine fraction is introduced. The dependence to justify the length of the spiral separator cage is obtained.

РЕЗЮМЕ

На основі аналізу конструкцій сепараторів сипких матеріалів запропонована конструкція спірального сепаратора, що має низку переваг над відомими конструкціями. Зокрема, спіральний сепаратор є компактним, має простий привод та зручний в обслуговуванні. Крім того, використання у якості робочого органу спіралеподібного решета дозволяє інтенсифікувати процес сепарації та здійснювати розділення сипкого матеріалу чи суміші матеріалів на кілька фракцій.

Одержані емпірико-теоретичні залежності для опису процесу сепарації сипкого матеріалу на спіральному сепараторі. Розроблено методика для визначення коефіцієнтів сепарації, які входять в отримані рівняння і залежать від фракційного складу матеріалу та початкових параметрів шару матеріалу. За розробленою методикою здійснено експериментальні дослідження, що дозволили на прикладі паливних гранул та костриці льону-довгунця визначити значення коефіцієнтів сепарації для цих матеріалів. Проведений комплекс теоретичних та експериментальних досліджень дозволив описати перебіг процесу сепарації сипких матеріалів (паливних гранул, костриці льону-довгунця) на спіральному сепараторі. Отримана математична модель процесу сепарації сипких матеріалів на спіральному сепараторі та розроблена методика визначення коефіцієнтів сепарації придатні для опису процесу сепарації і інших сипких матеріалів на спіральному сепараторі запропонованої конструкції. Введено поняття коефіцієнта ефективності роботи спірального сепаратора, що характеризує ступінь відокремлення дрібної фракції з сипкого матеріалу. Отримано залежність для обґрунтування довжини спіралеподібного решета сепаратора.

INTRODUCTION

To separate materials into fractions by size, shape, weight and aerodynamic properties in agriculture, manufacturing and food processing, various separators are used. The most common are separators with flat and drum cage. The vibratory separators and air separators with helical surfaces are used as well (Ciobanu V. et al., 2015; Dadak V., 2015; Falko O., 2014; Ivancu B. et al., 2015; Kartashevich, S., 2001; Paraschiv G. and Manole C., 2015). Most of the separators combine several separation types. The famous

design have a number of drawbacks: big sizes and high metal content (characteristic of separators with flat and drum cages); complex driving system of working bodies (characteristic of vibratory separators); low degree of chamber filling and productivity (characteristic of air separators, separators with drum cages, spiral bodies and surfaces).

Scientific research is aimed at finding new technological and technical solutions to intensify the process of bulk materials separation (Falko O., 2014; Kartashevich, S., 2001). The key to a successful solution to this problem is the development of mathematical models describing the separation process of bulk materials that would justify the rational design-technological parameters of separators. Development of mathematical models is based on the analysis of the separation process and determining the factors that most influence its course.

During the theoretical description of the separation process the following factors must be considered:

- separation type;
- separator design peculiarities;
- uneven distribution of particles of different material size or its components;
- a wide range of particle sizes and particle mass of bulk material or mixture of materials;
- different physical-mechanical properties of the material;
- variation of separation intensity depending on the material parameters (material layer width, the feeding rate, etc.) and movement along the working bodies or surfaces;
- fraction content in the initial material layer or its mixture.

In most cases, the separation process is described using empirical and theoretical or empirical dependences with ratios determined experimentally. Typically, these dependencies are not universal and are suitable to describe the separation process of bulk material or mixture of materials. Thus, to describe the separation process of bulk materials carried out with the modern separators it is necessary to conduct additional theoretical and experimental investigations.

MATERIALS AND METHODS

Two types of bulk materials were used in the research: processed pellets and flax fibre shive. According to EN 14961-2 the content of fine fraction in the pallets packaging unit should not increase 1.0 %. During production process of pallets this parameter exceeds the norm. Taking this into account, it is necessary to separate the fine fractions from pellets before packaging.

Quality of pellets and briquettes made from flax shive depend on the raw material properties. One of the major characteristics of the raw material is its fraction. The best mechanical properties of the pellets and briquettes are achieved if the fraction is less than 10 mm. If it is not in line with this requirement – the shive should be pre-processed, i.e. necessary fractions should be separated.

The method of determining separation factors for bulk materials (pellets, shive) in a spiral separator study included the investigation of bulk material fractional composition with the help of particle-size analysis (Khaylis G. and Fedorus Y., 2004). Fractional composition was determined as the ratio of individual fractions mass to the total weight of bulk material:

$$N_j = \frac{M_j}{M_m} \cdot 100\% , \quad (1)$$

where N_j – quantity of bulk material particle of j fraction, [%];

M_j – j fraction mass of bulk material, [kg];

M_m – total weight of bulk material, [kg].

As a result, the content of fine fractions, below 10 mm, is 29.5%. Fine fraction content, below 10 mm, which should be separated, is 39.8%.

After the fraction content was defined, a portion of the bulk material was weighed and loaded into the spiral separator (figure 1) (Dudarev I., 2016). The spiral cage was adjusted to the fraction to be separated with sizes 0.9x10 mm.

The spiral separator is equipped with two spiral cages, with similar separation processes. During separation, the bulk material was moved with the disc. Fine fractions went through the cage holes into the container. Separation intensity was defined with the coefficient μ :

$$\mu_i = \frac{m_i}{M_{oi} \cdot l_i}, \tag{2}$$

where μ_i – the separation coefficient on section i of the spiral cage, [m⁻¹];

M_{oi} – mass of fine fraction in the bulk material before separation on section i of the spiral cage, [kg];

m_i – fine fraction mass separated on section i of the spiral cage with the length l_i , [kg];

l_i – length of section i of the spiral cage, [m].

Theoretical investigations included the major statements of bulk materials separation theory and own investigation outcome (Dudarev I., 2016; Khaylis G. and Konovaliuk D., 1991).

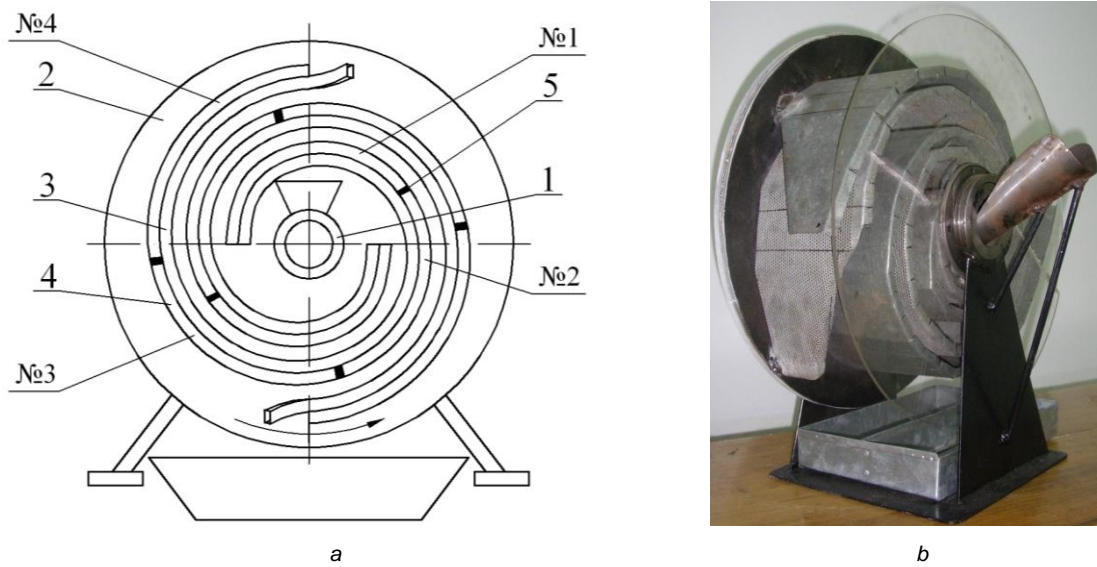


Fig. 1 – Scheme (a) and picture (b) of spiral separator laboratory machine

1 – bin; 2 – disc; 3 – spiral cage; 4 – spiral container; 5 – dividing plates; №1, №2, №3, №4 – sectors

RESULTS

The spiral separator (figure 2) contains a frame, driving unit, bin, disc with two similar spiral cages and spiral containers for fine fractions as well as buffers for big and fine fractions.

The operation of the spiral separator is shown on the example on one of the spiral cage, since the second cage is operated similarly. The bulk material is fed to the bin and moved through the spiral cage. The fine fraction material goes through the cage holes into the spiral container. Big fraction material is moved to the end of the spiral cage and then to the big fraction material buffer, fine fraction material goes to the fine fraction material buffer.

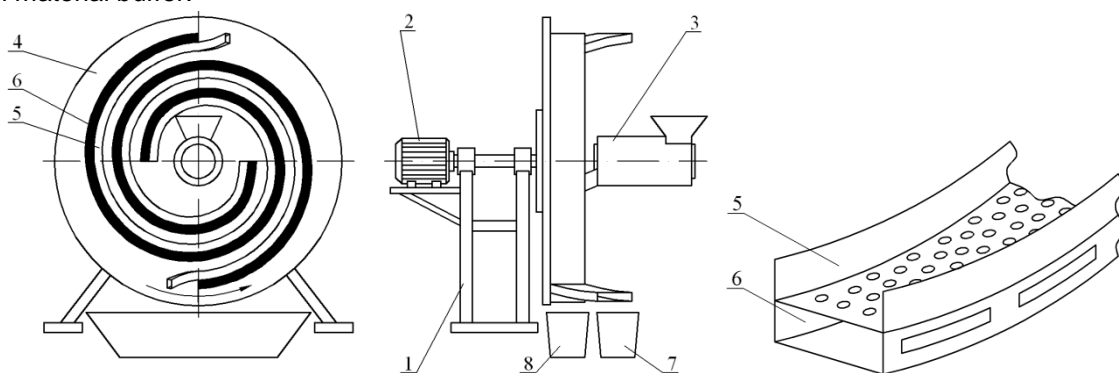


Fig. 2 – Spiral separator

1 – frame; 2 – drive; 3 – buffer; 4 – disc; 5 – spiral cage; 6 – spiral container; 7 – big fraction container; 8 – fine fraction container

The separation process is complex in terms of description, because the location of particles of different materials or sizes is random. Besides, the particles to be separated are reduced in the process, making the process description even more complicated and requiring introduction of assumptions.

Since the separation coefficient changes according the cage length, in order to provide a more detailed description, the spiral cage should be divided into similar sections $l_1 = l_2 = \dots = l_i = l$. Every section is assumed to have a constant separation value $\mu = \text{const}$.

Let's investigate a portion of bulk material, fed to the separator, containing fine fraction M_0 to be separated. During short time span dt the bulk material layer will pass the surface of the spiral cage with the length dl . The probability of fine fraction separation is μdl . At the beginning, the fine fraction to be separated was M_0 , and after it passed the spiral cage section with the length $l + dl$ (where l – is the length of the spiral cage section passed by the material layer, [m]; dl – increase of the spiral cage section, [m]), fine fraction mass became $M_0 - dM$. Thus, dM is the separation value (mass of the bulk material separated fine fraction). Then, dM / M_0 will be the relevant separation value. The equation of relevant separation value dM / M_0 and separation probability describes separation process in the spiral separator as follows:

$$-\frac{dM}{M_0} = \mu dl \tag{3}$$

The experimental value of the separation value μ is defined at a certain width of material layer, because it influences significantly the separation coefficient. The bigger the width, the worse the separation process is. That is why, in order to achieve required separator productivity, the cage width should be increased. In this case, better separation conditions are possible for the same material volume fed to the separator at similar intervals.

Using the separation equation (3), let's define the mass of the fine fraction material M_i , which remains unseparated in the i -section of the spiral cage with length l_i :

$$M_i = M_{i-1} e^{-\mu l_i}, \quad i = \overline{1, n} \tag{4}$$

where n – number of sections with the length l of the spiral cage and spiral container.

Mass of the separated fine fraction material m_i during bulk material separation of each spiral cage section:

$$m_i = M_{i-1} - M_i \tag{5}$$

Total mass m_Σ of the bulk material separated fine fraction on the spiral cage:

$$m_\Sigma = \sum_{i=1}^n m_i = M_0 - M_n \tag{6}$$

The previous investigations determined the appropriateness of the cage spiralling according to the logarithmic spiral with equation $\rho(\varepsilon) = \rho_0 e^{m^* \varepsilon}$, here $m^* = (\rho - \rho_0) / l$ (where l – spiral cage length between the radii ρ_0 and ρ , [m]; ρ_0 – the smallest radius of the spiral cage, [m]; ε – angle of spiral, [rad.]).

Let us define the separation process changing the spiral cage radius. The length of a section can be defined as $l_i = \frac{1}{m^*} (\rho_i - \rho_{i-1})$ (where ρ_{i-1} and ρ_i – radii at the beginning and the end of the i -section of spiral cage).

Considering the presented dependences, the equation (4) will be:

$$M_i = M_{i-1} \cdot e^{-\frac{\mu (\rho_i - \rho_{i-1})}{m^*}} \tag{7}$$

The radii values of the spiral cage for the equation (7) are defined with the equation $\rho(\varepsilon) = \rho_0 e^{m^* \varepsilon}$. The angle of the cage spiral is defined as follows:

$$l_i = \int_{\varepsilon_{i-1}}^{\varepsilon_i} \sqrt{\rho^2(\varepsilon) + \rho'^2(\varepsilon)} d\varepsilon = \frac{\rho_0 \sqrt{1 + m^{*2}}}{m^*} (e^{m^* \varepsilon_i} - e^{m^* \varepsilon_{i-1}}), \tag{8}$$

from where we obtain:

$$\varepsilon_i = \frac{1}{m^*} \ln \left[\frac{m^* l_i}{\rho_0 \sqrt{1+m^{*2}}} + e^{m^* \varepsilon_{i-1}} \right]. \quad (9)$$

Applying the obtained dependences (7) – (9), and separation values μ_i , the fine fraction mass M variation diagrams depending on the radius ρ of the spiral cage in each section of the length l are built (figure 3).

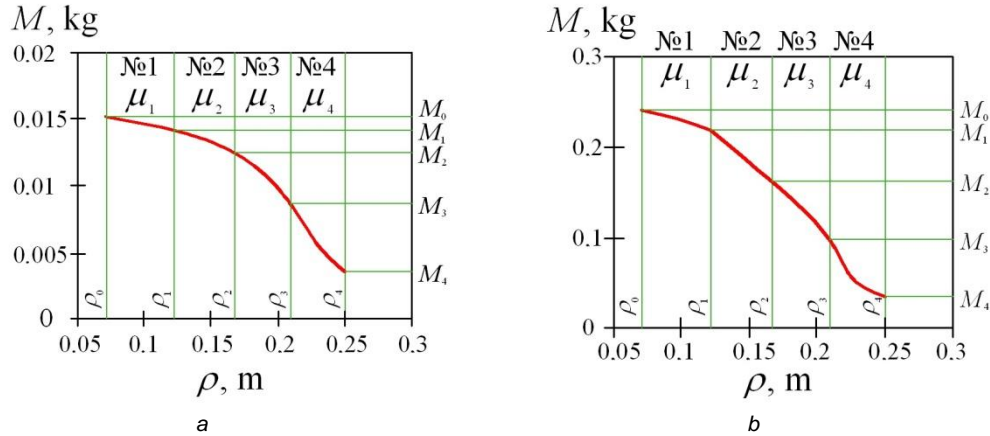


Fig. 3 – Fine fraction mass M variation diagrams in the separation process depending on the radius ρ of the spiral cage in sections with $\rho_0 = 0.07 \text{ m}$ and $m^* = 0.18$

- a – separation of the pellets with $\mu_1 = 0.263 \text{ m}^{-1}$; $\mu_2 = 0.507 \text{ m}^{-1}$; $\mu_3 = 1.323 \text{ m}^{-1}$; $\mu_4 = 4 \text{ m}^{-1}$;*
- b – separation of the flax fibre shive with $\mu_1 = 0.4 \text{ m}^{-1}$; $\mu_2 = 1.11 \text{ m}^{-1}$; $\mu_3 = 1.97 \text{ m}^{-1}$; $\mu_4 = 4 \text{ m}^{-1}$*

In order to show the length of the spiral cage L_s where the fine fraction will be separated from the bulk material, we take the logarithm of equation (4):

$$\ln(M) = \ln(M_0 e^{-\mu_m L_s}), \quad (10)$$

Where: M – mass of the fine fraction material remaining in the bulk material after separation on the spiral cage with the length L_s , [kg];

M_0 – mass of fine fraction in the bulk material before separation, [kg];

μ_m – average value of bulk material separation coefficient per spiral cage length L_s , [m^{-1}];

L_s – spiral cage length, [m].

Having transformed the equation (10), we obtain:

$$L_s = -\frac{1}{\mu_m} \cdot \ln\left(\frac{M}{M_0}\right), \quad (11)$$

Mass of fine fraction in the bulk material before separation is determined according to dependence (1):

$$M_0 = \frac{M_m N}{100}, \quad (12)$$

where N – number of fine fraction particles in the bulk material before separation, [%];

M_m – total mass of bulk material before separation, [kg].

The average value of the bulk material separation coefficient per spiral cage length is defined as follows:

$$\mu_m = \sum_{i=1}^n \frac{\mu_i}{n}. \quad (13)$$

Let's introduce the efficiency coefficient of spiral separator, to characterize separation degree of fine fractions from the bulk material. The coefficient value is defined as follows:

$$K_s = \frac{M}{M_0}. \quad (14)$$

The lower the coefficient value K_s , the more efficient the separator operates. If, for example, the efficiency coefficient is $K_s = 0.03$, it means that 3% of fine fraction material remained unseparated, and 97% was separated. Substituting the average separation coefficient μ_m and spiral separator efficiency coefficient K_s in the equation (11), we obtain:

$$L_s = -\frac{\ln(K_s)}{\sum_{i=1}^n \frac{\mu_i}{n}} \tag{15}$$

Based on the equation (15) the diagrams are built (figure 4), which show impact of coefficients μ_m and K_s on the spiral cage length L_s , where the necessary degree of the fine fraction separation should be obtained. At reduction of the spiral separator efficiency coefficient K_s and separation coefficient μ_m the spiral cage length L_s increases.

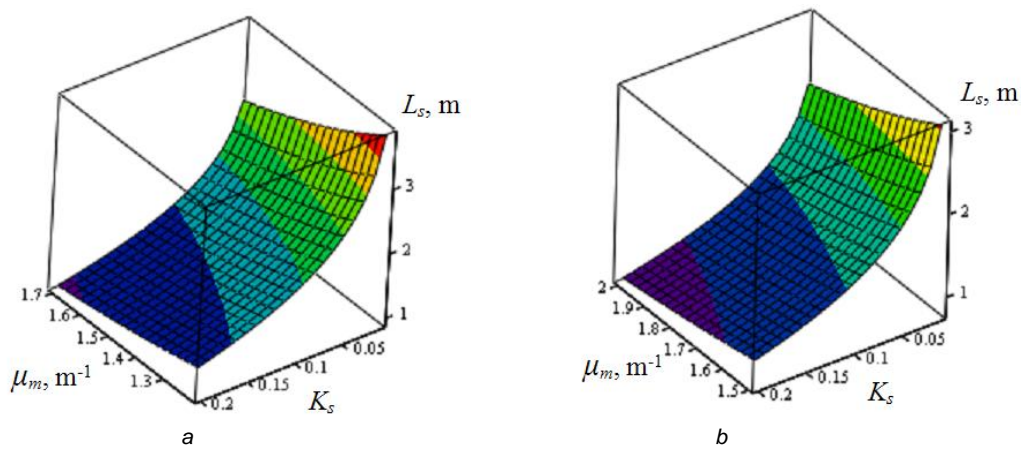


Fig. 4 – Diagrams showing the impact of the coefficients μ_m and K_s on the lengths L_s of the spiral cage
 a – for pellets; b – for flax fibre shive

The calculations made according to the equation (15) allowed us to demonstrate the length of the separator spiral cage: 1) for pellets with $\mu_m = 1.523 \text{ m}^{-1}$ and $K_s = 0.03$ the length of the cage should be $L_s = 2.3 \text{ m}$; 2) for flax fibre shive with $\mu_m = 1.87 \text{ m}^{-1}$ and $K_s = 0.05$ the length of the cage should be $L_s = 1.6 \text{ m}$. The defined spiral cage will ensure the required separation degree of fine fractions in the bulk material. The conducted investigations allowed obtaining the mathematical model of bulk material separation in the spiral separator which will be represented in coordinates xyM :

$$\left. \begin{aligned} x &= \rho_0 e^{m^* \varepsilon} \sin \varepsilon; \\ y &= \rho_0 e^{m^* \varepsilon} \cos \varepsilon; \\ M &= M_0 e^{-\mu_m \frac{\rho_0 \sqrt{1+m^{*2}}}{m^*} (e^{m^* \varepsilon} - e^{-m^* \varepsilon})} \end{aligned} \right\} \tag{16}$$

where $\varepsilon \in [\varepsilon_0; \varepsilon_{\max}]$, $\varepsilon_{\max} = \frac{1}{m^*} \ln \left[\frac{m^* L_s}{\rho_0 \sqrt{1+m^{*2}}} + e^{m^* \varepsilon_0} \right]$.

The first and the second equation of the system (16) show the spiral of the cage. By means of the mathematical model (16) and equations (4), (7) the diagrams are built (figure 5 and figure 6) showing the separation model.

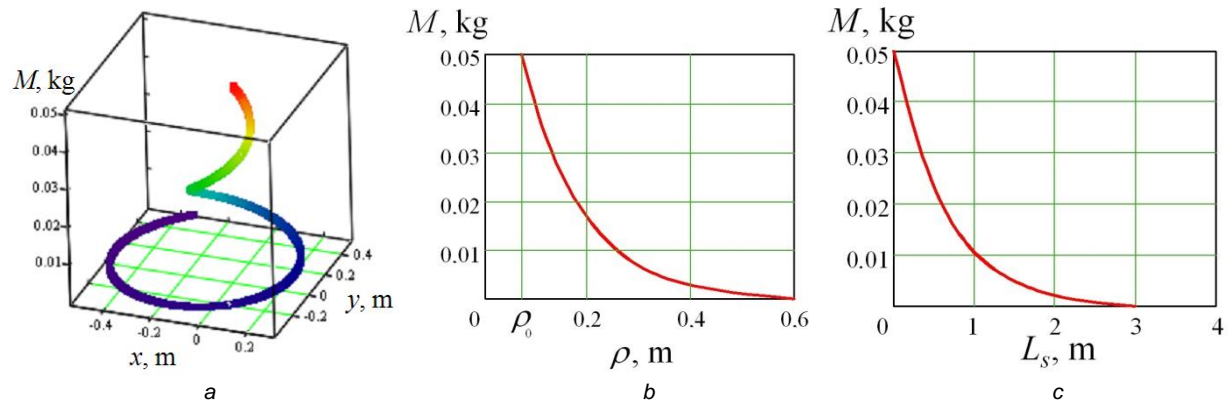


Fig. 5 – The curves showing separation of the pellets in the spiral separator with

$$K_s = 0.01; \mu_m = 1.523 \text{ m}^{-1}; M_0 = 0.05 \text{ kg}; \varepsilon_0 = 0 \text{ rad.}; \rho_0 = 0.07 \text{ m and } m^* = 0.18$$

a – fine fraction mass M variation diagram in the material along the spiral cage; b – fine fraction mass M variation in the material with changed radius ρ of the spiral cage; c – fine fraction mass M variation in the material with changed length L_s of the spiral cage

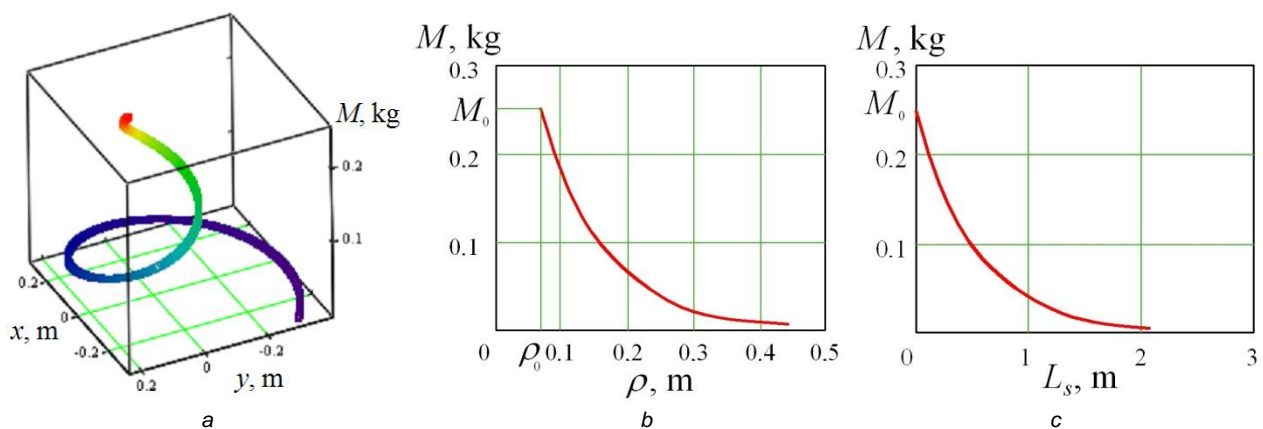


Fig. 6 – The curves showing separation of the flax fiber shive in the spiral separator with

$$K_s = 0.02; \mu_m = 1.87 \text{ m}^{-1}; M_0 = 0.25 \text{ kg}; \varepsilon_0 = 0 \text{ rad.}; \rho_0 = 0.07 \text{ m and } m^* = 0.18$$

a – fine fraction mass M variation diagram in the material along the spiral cage; b – fine fraction mass M variation in the material with changed radius ρ of the spiral cage; c – fine fraction mass M variation in the material with changed length L_s of the spiral cage

CONCLUSIONS

The design of spiral separator in question allows reducing sizes of the separator due to the installation of the spiral unit and reducing metal and power consumption. Besides, the spiral separator is ergonomic and ensures high level separation.

The conducted investigations allowed describing the bulk material separation process (pellets and flax fibre shive) with the spiral separator. The mathematical model of the bulk material separation with the spiral separator is obtained; the method for coefficient definition is developed, which can also be applied for other materials.

The definition of spiral separator efficiency coefficient is introduced, characterizing the degree of separation of the fine fractions. The dependence representing the spiral cage length is obtained.

REFERENCES

- [1] Ciobanu V., Casandroi T., Persu C., Paun A., Muraru V., (2015), Experimental aspects regarding seed separation with mechanical separating machines with drums, *INMATEH – Agricultural Engineering*, vol. 46, no.2 / 2015, ISSN 2068-2239, pp.125-132, INMA Bucharest/Romania;
- [2] Dadak V.O., (2015), *Grounding of parameters and operating modes of small-seeded mixtures air separator mill (Обґрунтування параметрів та режимів роботи пневмосепаратора дрібно насінневих сумішей)*, PhD dissertation, Lviv National Agrarian University, p.174, Lviv/Ukraine;

- [3] Dudarev I.M., (2016), *Scientific principles development of resource-saving technology of primary bast crops processing (Розвиток наукових основ ресурсозберігаючої технології первинної обробки луб'яних культур)*, Doctor of Engineering Science dissertation, Lutsk National Technical University, p.370, Lutsk/Ukraine;
- [4] Dudarev I.M. (2016), *Spiral separator (Спіральний сепаратор)*. Patent, No. 111203, Ukraine;
- [5] Dudarev I.M. (2016), *Spiral separator (Спіральний сепаратор)*. Patent, No. 111130, Ukraine;
- [6] Falko O.L., (2014), *The scientific base of vegetative raw materials fractionation process (Наукове обґрунтування процесу фракціонування рослинної сировини)*, Doctor of Engineering Science thesis, National University of Food Technologies, p.46, Kyiv/Ukraine;
- [7] Ivancu B., Voicu Gh., Bracacescu C., Persu C., Zaica Al., (2015), Theoretical research on determining the vibrations isolation degree of a vibrating separator, *INMATEH – Agricultural Engineering*, vol. 45, no.1 / 2015, ISSN 2068-2239, pp.59-64, INMA Bucharest/Romania;
- [8] Kartashevich, S. (2001), *Mechanical and technological bases of efficiency increase of the mechanical complexes after grain and seed harvesting treatment (Механико-технологические основы повышения эффективности механизированных комплексов для послеуборочной обработки зерна и семян)*, RUP "BelNIIlagroenergo" Publ., p.288, Minsk/Belarus;
- [9] Khaylis G.A., Fedorus Y.V., (2004), *Mechanics of plant materials (Механіка рослинних матеріалів)*, ISBN 966-7667-47-2, RVV LDTU Publ., p.302, Lutsk/Ukraine;
- [10] Khaylis G.A., Konovaliuk D.M., (1991), *Calculation of harvesting machine working bodies (Розрахунок робочих органів збиральних машин)*, NМК VO Publ., p.200, Kyiv/Ukraine;
- [11] Paraschiv G., Manole C., (2015), Explaining the phenomenon of separation into fractions of a mixture of particulate matter by applying the principle of minimum energy, *INMATEH – Agricultural Engineering*, vol. 45, no.1 / 2015, ISSN 2068-2239, pp.65-70, INMA Bucharest/Romania.

ANALYTICAL ASSESSMENT OF THE PNEUMATIC SEPARATION QUALITY IN THE PROCESS OF GRAIN MULTILAYER FEEDING

/

АНАЛІТИЧНА ОЦІНКА ЯКОСТІ ПНЕВМОСЕПАРАЦІЇ ПРИ БАГАТОРІВНЕВОМУ ВВЕДЕННІ ЗЕРНА

As. Nesterenko A.V., Lect. Ph.D. Eng. Leshchenko S.M.,
Lect. Ph.D. Eng. Vasylovskiy O.M., Lect. Ph.D. Eng. Petrenko D.I.

Central Ukrainian National Technical University / Ukraine

Tel: +380505691338; E-mail: nov_78@ukr.net

Keywords: *pneumatic separation, grain, feeding device, multilayer feeding*

ABSTRACT

The design of a pneumatic separator with the feeding device for grain multilayer feeding was suggested in this paper. The application of the device enables increasing the uniformity of the airflow field velocity and the quality separation indicators. In order to determine the impact of grain multilayer feeding on the quality of grain cleaning we conducted a quantitative distribution of light grain impurities in the operating separation area. As a result, a statistical model of the probability of light impurities passing through the grain layers in the process of grain multilayer feeding in pneumatic and separating channel was obtained and the influence of specific load on the quality of grain cleaning was analytically determined.

РЕЗЮМЕ

Запропоновано конструкцію пневмосепаратора з живильним пристроєм для багаторівневого введення зернового матеріалу, використання якого дозволяє підвищити рівномірність поля швидкостей повітряного потоку та якісні показники сепарації. З метою визначення впливу багаторівневого введення зернового матеріалу на якість очищення зерна проведено кількісний розподіл легких домішок в робочій зоні сепарації. В результаті отримано статистичну модель ймовірності проходження легких домішок через зернові шари при багаторівневному введенні зернового матеріалу в пневмосепаруючому каналі та аналітично визначено вплив питомого навантаження на якість очищення зерна.

INTRODUCTION

Today Ukraine is one of the leading countries in the production of grain and one of the three world exporters of grain crops (Materynska O.A., 2013). That requires introducing new production technologies that can provide high performance of grain cleaning and its compliance with the standards of cleanliness and humidity (Grabar I.G., 2013).

The required quality of food grain can be achieved only through the effective and timely grain cleaning from impurities which substantially affect the terms of storage and selling conditions. In this case the pneumatic separation is very important. It separates a significant amount of impurities at various stages of grain cleaning (Vasylovskiy M.I., 2006).

Air separation is one of the most common ways of grain cleaning. This process is versatile due to the separation of any material – from the smallest grain (alfalfa, poppy, etc) to the largest (corn, beans) and can partially reduce its moisture content and minimize damage (Dryncha V.M., 2006). However, the efficiency of the air flow depends on many factors: the size of specific grain load, aerodynamic properties of the components, airflow velocity, geometrical parameters of the pneumatic separating channel and others. (Kroulík M., 2016, Lukaszuk J., 2008).

But, despite the widespread application and versatility of pneumatic separation, the efficiency of the air flow is significantly reduced due to uneven grain location in the operating separation area. The increase of grain specific feeding causes the increase of aerodynamic resistance in the area of grain input and output, which in its turn increases the uneven airflow velocity in the cross section of the pneumatic separating channel (Kovrikov I. T., 2003, Burkov A. I., 2000).

The increase of evenness of the air flow velocity field can be achieved by using the feeding devices of the pneumatic separating channels (Saitov A. V., 2015). This improves interaction of the grain components

and the air flow, thereby increasing the quality of separation, which improves the efficiency of the air flow and the quality of grain cleaning (Panasiewicz M., 2008, Leshchenko S.M., 2008).

Despite a large number of works on theoretical research of the pneumatic separation quality (Hamuev V.G., 2016, Leshchenko S.M., 2012), the problem of quality indicators analytic assessment is very important and requires a detailed analysis of the process especially in the conditions of grain contact interaction in the operating separation area.

So, the research is to study the impact of grain interaction on pneumatic separation quality indicators while applying feeding devices. That will improve the air flow efficiency and reduce the power consumption for grain cleaning.

MATERIALS AND METHODS

The analysis of feeding devices operation led to the conclusion that the main disadvantage of active feeders used in the pneumatic grain cleaning machines is the additional energy, thereby increasing the power consumption and complexity of the pneumatic separating channel design. Therefore, among all types of feeders the gravity feeders are widely used due to their simplicity of design and reliability. These feeders are used in grain cleaning machines and some feeders became the result of scientific research (Baldanov V.B., 2015, Levdanskyi E.Yu., 2012, Doshi J.S., 2013).

On the basis of the research analysis of pneumatic separation and of feeding devices designs, the Department of Agricultural Engineering of the Central Ukrainian National Technical University designed and manufactured a prototype of a new pneumatic separator with the feeding device for grain multilayer feeding (Patent of Ukraine №8058A, 2005) (Fig. 1). The design of the pneumatic separator ensures even distribution of grain material in the operating separation area and significantly reduces air flow resistance in the input and output zones and makes velocity field uniform (Nesterenko O.V., 2015).

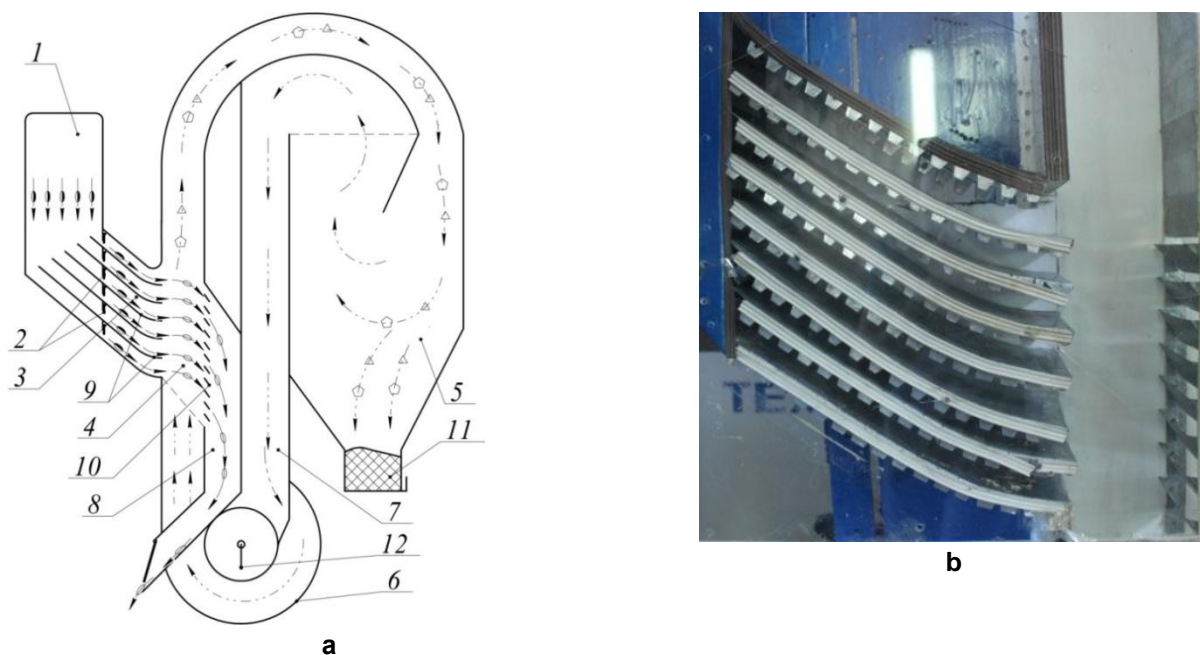


Fig. 1 – Experimental air separator

a – functional scheme of pneumatic separator; b – multilayer feeding device

1 – batcher; 2 – batch gates; 3 – multilayer feeding device; 4 – pneumatic separating channel; 5 – settling chamber;

6 – fan; 7 – air channel; 8 – airproof outlet channel; 9 – indirect gravity curves; 10 – louver type unit;

11 – impurity receiving collector; 12 – adjusting air velocity shutter

The main specific feature of the new pneumatic separator is the application of a gravitational multilayer feeding device. As a result, there is a separation of the inlet grain flow into several single-layer air streams that are delivered to different height operating areas of the pneumatic separating channel (Nesterenko O.V., 2012). In this case, the output of the cleaned grain out of the separation area is carried out through the louver bar and the airproof outlet channel.

Accordingly, while using the design of the pneumatic separator it is necessary to determine the quality characteristics of grain cleaning as ascending trajectories of light impurities from the lower layers will

intersect with the descending trajectories of grain fractions. Therefore, to determine the effect of the multilayer inlet of grain material on the quality of separation we studied the quantitative distribution of light impurities in the operating separation area.

In the case of grain multilayer feeding into the pneumatic separating channel, there will be a contact action among some light impurities and taking into account that the trajectory of the impurity will be changed after the contact with the grain we may observe the least positive situation for impurities of the lowest layer (Fig. 2b).

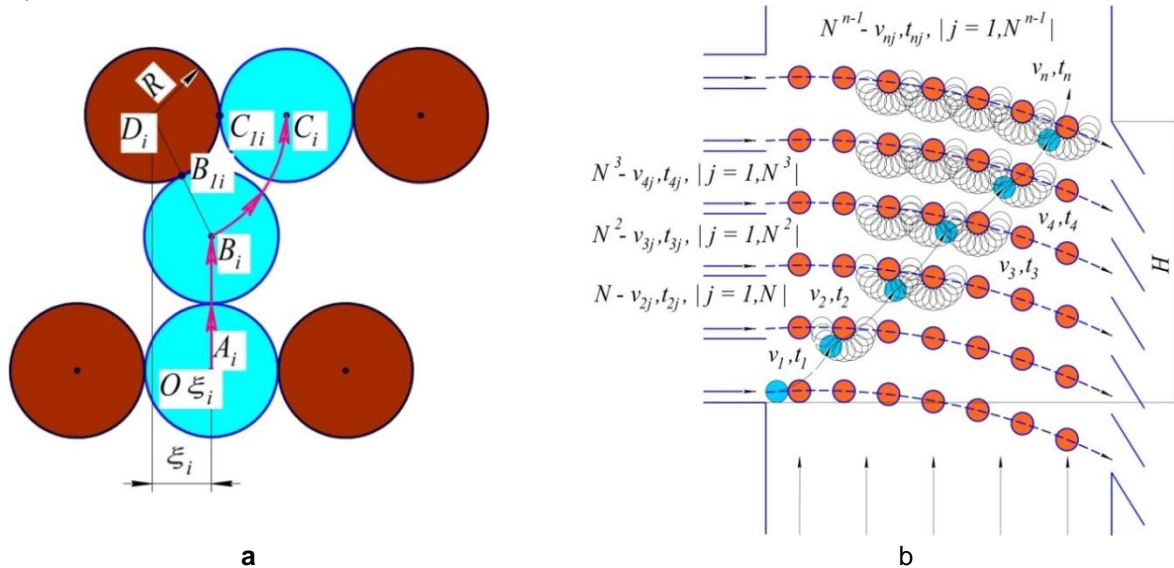


Fig. 2 – The scheme of passing impurity with grain multilayer feeding:
a – through the grain layer; b – from the lower grain layer.

The contact action of the impurity in the multilayer grain flow is multistaged. In this case, the motion of the centre of impurity mass O_{ξ_i} consists of three successive stages (Fig. 2 A):

- contactless motion of impurities between the layers –section $A_i B_i$;
- contact of impurities with grain at the point B_{1i} ;
- the motion of impurities in grain and the point of contact traces the trajectory $B_{1i} C_{1i}$ and the mass centre of a separate particle of impurities will be $B_i C_i$.

Since the motion trajectory and the time of impurities motion between grain layers depends on the initial horizontal displacement ξ_i of the impurity and grain mass centre, which is a random variable and can have any value in the range $[0; 2R]$, then for quantitative distribution of light impurities we need to distinguish their kinematic characteristics at the output from every subsequent layer, which depends on the contact point of impurities with grains from another upper layer.

In this case, the section $\xi_i \in [0; 2R]$, $i=1, N$ is divided into N similar equal intervals $(\xi_{i,j-1}; \xi_{i,j})$, $j=1, N$ with the length $2R/N$ (Fig. 2b).

Then, the impurities from the first layer after passing:

- the second layer will be distributed into N equal by quantity groups. Each group will have its own kinematic characteristics – $V_{2,j} \cdot t_{2,j}, j=1, N$. At the same time, some of the groups may have similar kinematic characteristics;

- the third layer will be divided into N^2 groups – $V_{3,j} \cdot t_{3,j}, j=1, N^2$;
- the fourth layer will be divided into N^3 groups – $V_{4,j} \cdot t_{4,j}, j=1, N^3$; ...;
- the n layer will be divided into N^{n-1} groups – $V_{n,j} \cdot t_{n,j}, j=1, N^{n-1}$.

Since the duration of impurities motion for some groups is longer during the time of grain passing the depth of the pneumatic separating channel, then the number of groups for grain layers can be significantly lower. The probability to select such impurities is considerably reduced as since reaching the louver unit they can get into the airproof channel for receiving clean grains and they will not be processed in the following layers.

According to these circumstances, the height of lifting impurities depends on the contact point with the grain. Setting the scale height of lifting impurities, we make analysis of the process of impurity passing

through the grain layer and determine its final elevation point. That is which n grain layer the impurity reaches, and in this case the impurities from all grain layers are added according to the height levels.

The scale of the impurities elevation height is calculated by the formula:

$$\Delta Y = \frac{Y_{\max} - Y_{\min}}{n}, \quad (1)$$

where, Y_{\max} is the maximum elevation height (the impurities from the upper layer move easily upward); Y_{\min} is the minimum elevation height (the impurities from the lower layer collide with the grains from all layers in the worst case).

This distribution is made for the grain flow in which the distance between the surfaces of the grains in the direction of the grain flow is equal to their size ($2R$). For the rarefied grain flow, we introduced the coefficient of rarefaction $f_p = l/2R$, which characterises the density of grain position in the horizontal motion in the pneumatic separating channel.

As a result, the productivity of the pneumatic separating channel (taking into account the rarefaction of the grain flow) is determined by the formula:

$$q_B = 3600 \frac{\pi}{6} (B \cdot v \cdot n \cdot R \cdot \gamma) \cdot \frac{2}{1 + f_p}. \quad (2)$$

Where B is the width of the channel, m;

v – the velocity of feeding the grain into the pneumatic separating channel, m/s;

n – number of layers, pieces;

R – grain radius, m;

γ – grain volume weight, kg/m³;

f_p – the coefficient of rarefaction of the grain flow in the pneumatic separating channel.

Modelling of light impurities quantitative distribution with a multilayer feeding of grain material was carried out using the Mathcad software.

RESULTS

The results of the research helped us obtain the statistical probability model of light impurities passing through grain layers in the grain multilayer feeding into the pneumatic separating channel (Fig. 3).

The analysis of variation characteristics of light impurities distribution (Fig. 3), which were obtained for each layer of grain material input, enables asserting that at six-layer feeding with maximum specific load, the highest percentage of impurities remaining in the cleaned grain appear from the first and second (located lower) feeding layers, 15% and 12.8% respectively. Thus, light impurities appear in the cleaned grain only from the three lowest layers of grain feeding and a full selection of light impurities takes place from IV to VI feeding layers (located the highest). Under such conditions the installation place of the louver unit top depends on the number of layers involved in the feeding device. The louver unit will be located at the height $H = 0.05 \dots 0.055$ m.

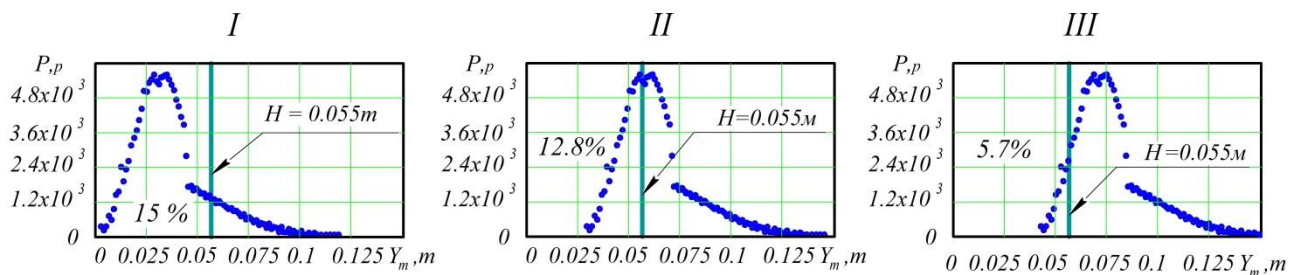


Fig. 3 – Quantitative characteristics of impurities in the cleaned grain with a multilayer feeding

I – III – the ordinal number of grain feeding layer

Taking into consideration the rarefaction coefficient and the number of layers used in the feeding device and according to distribution results, we obtained analytical dependence of separation completeness of light impurities ε on the productivity of the pneumatic separating channel q_B with a multilayer feeding of grain material (Fig.4).

The given dependences were obtained at specific load on the layer of the feeding device $q_{bF} = 250 \dots 350 \text{ kg/dm}\cdot\text{hour}$ at which the single-layer feeding of the grain is carried out.

The analysis of the dependence (Fig. 4) shows that with increasing specific load q_B and, consequently, increasing the number of feeding layers, the completeness of separation ε decreases. Thus, the number of layers used in the feeding device depends on the purpose of cleaning and its rational meaning is within $n = 4 \dots 6$ pcs.

Reducing the separation quality can be explained by the increasing number of probable contacts of light particles that move from the lower grain layers, respectively, the output velocity decreasing with each passed layer. The time to pass through the depth of the channel also decreases.

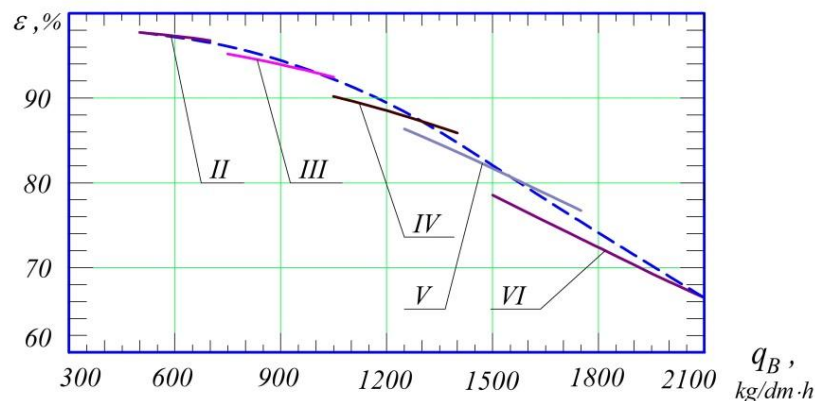


**Fig. 4 – Analytical dependence of the separation completeness of grain material on the specific load value of the pneumatic separating channel, $\varepsilon = f(q_B)$:
II – VI is the number of used feeding layers**

With the introduction of two feeding layers, the separation completeness is $\varepsilon = 97 \dots 98\%$, with specific load q_B varying from $500 \dots 700 \text{ kg/dm}\cdot\text{hour}$.

With the introduction of four feeding layers the separation completeness is $\varepsilon = 86 \dots 91\%$, with the specific load being able to be set from 1000 to $1400 \text{ kg/dm}\cdot\text{hour}$; using six feeding layers, we get $\varepsilon = 66 \dots 78\%$, with specific load $q_B = 1500 \dots 2100 \text{ kg/dm}\cdot\text{hour}$.

The results of experimental studies of the impact of a multilayer feeding on the light impurities separation completeness (Nesterenko O.V., 2015) sufficiently prove the analytical studies with correlation values ranging from $7 \dots 9\%$.

CONCLUSIONS

As a result of the analytical analysis, the possibility to apply a multilayer feeding in pneumatic systems of grain cleaning machines was grounded. That allows equalizing the velocity field of the airflow in the operating separation area and increasing the separation quality compared to the traditional grain feeding.

The undertaken studies allow reaching the conclusion that reducing the number of used layers from 6 to 2 improves the quality of separation by $22 \dots 30\%$, but the value of the specific load decreases by $1000 \dots 1600 \text{ kg/dm}\cdot\text{hour}$ and the productivity of the pneumatic separator. However, the number of layers used also depends on the purpose of cleaning with the rational value $n = 4 \dots 6$ pcs.

It was determined that the separation probability of light impurities with a multilayer feeding of grain material depends on the time and velocity of their passage through grain layers that vary depending on the contact point of the impurities with grain and the instalment position of the louver unit top. In this case, the increase of the distance between grain particles $2R$ in the horizontal direction improves the quality of the material separation, but the separation productivity decreases.

ACKNOWLEDGEMENT

The work has been funded by the Sectorial Operational Programme Human Resources Development 2007-2013 of the Romanian Ministry of Labour, Family and Social Protection through the Financial Agreement POSDRU/107/1.5/S.76903.

REFERENCES

- [1] Baldanov V.B., Yampilov S.S., Khandakova G.Zh., (2015), The impact of the main parameters of gravitational separator on the efficiency of grain cleaning from small impurities, *Newsletter of VSGUTU*, № 3(54), pp.14-21, Ulan-Ude/Russia;
- [2] Burkov A.I., Sychugov N.P., (2000), Grain cleaning machines. *Design, research, valuation and testing*, NSIA of the North-East, pp. 261, Kirov/Russia;
- [3] Doshi J.S., Patel V.B., Patel J.B., Patel J.A., (2013), Quantification of Quality Improvement in Wheat Seed Processing, *Journal of Agricultural Engineering*, Vol. 50(4), pp.83-86, Anand/India;
- [4] Dryncha V.M., (2006), Research of grain separation and elaboration of machine technologies for their preparation, Publishing house *NPO «MODEK»*, pp.384, Voronezh/Russia;
- [5] Grabar I.G., Derevyanko D.A., Geruk S.M., (2010), The influence of the factors of grain after-harvesting treatment on seed material quality, *Design, production and exploitation of agricultural machines: national cross-sectional scientific technical collection*, Edition 40, Part 1, pp.3-6, Kirovohrad/Ukraine;
- [6] Khamuev V.G., (2016), The intensity of light impurities separation in the vertical ascending air flow, *Agricultural machines and technologies*, N5, pp.12-16, Moscow/Russia;
- [7] Kovrikov I.T., Tavtilov I.Sh., (2003), Research trends and design of feeders for grain separation in the vertical airflow, *Newsletter of OSU*, №7, pp.198-201, Orenburg/Russia;
- [8] Kroulík M., Hůla J., Rybka A., Honzík I., (2016), Pneumatic conveying characteristics of seeds in a vertical ascending airstream, *Research in Agricultural Engineering*, Vol.62, pp.56-63, Prague/Czech Republic;
- [9] Leschenko S.M., (2008), The results of experimental research of a multi-stream feeding of the material into the air-inertial grain cleaning machines of the closed cycle, *Design, production and exploitation of agricultural machines: national cross-sectional scientific technical collection*, Edition 38, pp.199-205;
- [10] Leschenko S.M., Salo V.M., Vasylykovskiy O.M., et al., (2012), Analytical assessment of the separation quality on the basis of the algorithm of grain cleaning machines functioning, *Machines in agricultural production, industry machine building, automation: collection of scientific works*, Issue 25, part 1, pp. 68-73, Kirovohrad/Ukraine;
- [11] Levdanskiy E.I., Levdanskiy A.E., Chyrkun D.I., Opyrnakh E.V., (2012), Design and research of grain cleaning machine with air separator, *Scientific works of Odesa national academy of food technologies*, Issue. 41(2), pp.124-129, Odesa/Ukraine;
- [12] Lukaszuk J., Molenda M., Horabik J., Szot B., Montross M.D., (2008) Air flow resistance of wheat bedding as influenced by the filling method. *Research in Agricultural Engineering*, Vol.54, pp.50-57, Lublin/Poland;
- [13] Materynska O.A., (2013), Production and export of grain in Ukraine, *Economy of the Agro-industrial Complex*, №10, pp.49-53, Vinnytsya/Ukraine;
- [14] Nesterenko O.V., Leschenko S.M., Petrenko D.I., (2015), Research of the air flow evenness in the pneumatic separating channel with the multilayer input of grain, *Newsletter of Kharkiv National Technical University named after P. Vasylenko, Technical Sciences*, Issue 156, pp.35-42; Nesterenko O.V., Leschenko S.M., Petrenko D.I., (2015), Research on quality indicators of pneumatic separation with grain multilayer feeding, *Agricultural machines*, Issue 32, pp.143-151, Lutsk/Ukraine;
- [15] Nesterenko O.V., Vasylykovskiy O.M., Leschenko S.M., Petrenko D.I., Bohatyryov D.V., (2012), The perspective trend of intensification of grain air separation, *Machines in agricultural production, industrial machine building and automation*, Issue 25, Part1, pp.49-53, Kirovohrad/Ukraine;
- [16] Panasiewicz M., Zawiślak K., Kusińska E., Sobczak P., (2008), Purification and separation of loose material in pneumatic system with vertical air stream. *TEKA Kom. Mot. Energ. Roln.*, Vol.8, pp.171-176, Lublin/Poland;
- [17] Patent of Ukraine №8058A, Published 15.07.2005, Bulletin №7, *Air separator*, Vasylykovskiy M.I., Vasylykovskiy O.M., Moroz S.M., Leschenko S.M., Nesterenko O.V., Kirovohrad/Ukraine;
- [18] Saitov A.V., Farafonov V.G., Saitov V.E., (2015), Efficiency improvement of pneumatic separating channel operation, *Modern Hi-tech technologies*, № 6, pp.31-35, Vyatka/Russia;
- [19] Vasylykovskiy M.I., Honcharova S.Y., Leschenko S.M., Nesterenko O.V., (2006), The analysis of the up-to-date situation of grain air separation, *Design, production and exploitation of agricultural machines: national cross-sectional scientific technical collection*, Edition 36, pp.111-114, Kirovohrad/Ukraine.

DEVELOPMENT AND EXPERIMENTAL STUDY OF INFRARED BELT DRYER FOR RAPESEED

用于油菜籽干燥的红外带式干燥机研制和实验

Prof. Ph.D. Eng. Yang M.J.¹⁾, Ms. Stud. Eng. Liu B.¹⁾, Ms. Stud. Eng. Yang Z.R.¹⁾, Ms. Eng. Ding Z.Y.¹⁾,
Prof. Ph.D. Eng. Yang L.¹⁾, Prof. Ph.D. Eng. Xie S.Y.¹⁾, Prof. Eng. Chen X.B.²⁾

¹⁾ Southwest University, College of Engineering and Technology, Chongqing Key Laboratory of Agricultural Equipment for Hilly and Mountainous Regions / P. R. China;

²⁾ Agricultural Machinery Quality Control and Inspection Technology Centre, Nanjing Research Institute for Agricultural Mechanization
Ministry of Agriculture / P. R. China
Tel: 8613883002509; E-mail: ymingjin@swu.edu.cn

Keywords: belt dryer, infrared drying, mathematic model, rapeseed, design and development

ABSTRACT

According to matches of radiation properties of infrared heater and rapeseed, a small-scale infrared belt dryer was developed and its drying performance was tested and validated. Control factor of layer thickness has the highest significant level of impact on rapeseed effective moisture diffusivity and it is followed by factors of temperature, initial moisture content and radiation distance, sequentially. Two-term model gives the best fit to experimental data of moisture ratio, and it is followed by Page model. Both models are effective to predict moisture ratio of rapeseed infrared drying, with coefficient of correlation higher than 0.999.

摘要

基于红外加热元件辐射特点和油菜籽的匹配关系，开发了一套小型红外带式干燥机，并测试和验证了它的干燥性能。研究表明，料层厚度对油菜籽有效水分扩散系数影响最显著，其次是温度和初始含水率，辐射距离影响最小。Two-term 模型对水分比实验值的拟合度最好，Page 模型次之，两模型都具有很好的拟合效果，其相关系数均大于 0.999。

INTRODUCTION

Rape (*Brassica campestris* L.) is planted for oil production, protein, forage, nectar and energy. Rapeseed is the third-leading source of vegetable oil and second-leading source of protein worldwide. China is a major country of rapeseed production and consumption, while the region of Yangtze River is the main rape planting area, rape (*Brassica napus* L.) as the main species, where harvest period often runs into rainy season of high temperature and high humidity. The freshly harvested rapeseed of high moisture content is susceptible to subject to deteriorations such as overheat, acidification and mildew, primarily due to its high-water activity (Gao *et al.*, 2016; Yang *et al.*, 2012).

Artificial drying is required for the safe post-harvest process and storage of rapeseed. Solar drying, especially open sun drying and hot-air drying are still main options for rapeseed. Even though open sun drying offers low capital and operating costs and little expertise is required, its major disadvantages being extremely dependency on weather and large land areas needed for the shallow drying layer (Aghbashlo *et al.*, 2013). As for hot air drying, it involves product exposure to a continuous air flow to remove moisture, which leads to high energy demand (Onwude *et al.*, 2016). Compared to hot air drying, infrared radiation heating has many advantages such as greater energy efficiency, heat transfer rate and heat flux, which results in reduced drying time and higher drying rate (Kayran *et al.*, 2017). Infrared energy can be transferred from source to product surface directly without heating the surrounding air. However, when it falls on the other parts (such as tray) apart from product surface, they get heated, and as a result, the temperature of the surrounding increases, which helps reduce the moisture of the product (Pawar *et al.*, 2017).

Infrared drying is particularly suitable for thin layers of product with large surface exposed to radiation, and it has gained popularity as an alternative drying method for a variety of agricultural products (Kayran *et al.*, 2017). Infrared drying either alone or combined with others offers many advantages (such as greater energy efficiency, higher drying rate and better quality of dried product) over convective air drying under similar drying conditions. Because of a synergistic effect, the combination of infrared drying and hot

air drying has recently received much attention as novel thermal heat drying method, either to augment or completely replace the conventional drying method to improve overall process efficiency (Onwude *et al.*, 2016; Zhang *et al.*, 2015).

Many studies have reported on the applications of infrared drying or combination with others such as strawberry (Adak *et al.*, 2017), red pepper (Zhou *et al.* 2016), tomato (Kocabiyik *et al.* 2016), bean seeds (Doymaz, 2015), rice (Okeyo *et al.*, 2017) and others. However, there is no information in the literature about infrared drying of rapeseed. The main objectives of this study were to develop a small-scale infrared belt dryer and investigate the effect of process parameters on the drying performance, fit the experimental data to 5 thin-layer drying models and compute effective moisture diffusivity of rapeseeds.

MATERIALS AND METHODS

DESIGN AND DEVELOPMENT OF THE DRYER

Overall Design

Considering physical properties of rapeseed and scale-up purpose of the infrared belt dryer, a small-scale infrared belt dryer was designed and developed, with dimensions of length 1.0 m, width 0.4 m, and height 0.6 m, as shown in Fig.1. The wet rapeseed is fed from feed port and flows onto the upper conveyer belt. There is a baffle plate in the feed port that acts as a cushion to the fall of the seed. The seed is delivered by conveyer belts in the upper and lower sections of the drying chamber sequentially, and in midway of the delivering, seed passes through a guide chute. During delivering, seed gets heated mainly by the infrared radiation, and the surrounding air is heated mainly by other heated parts in the drying chamber (such as belts, walls, etc.). The synergistic effect of infrared radiation and hot air benefits the moisture removal of the rapeseed. The delivery speed of the seed is controlled by a microcontroller based control system as required and the infrared radiation distance is adjustable by manipulating the thread screw.

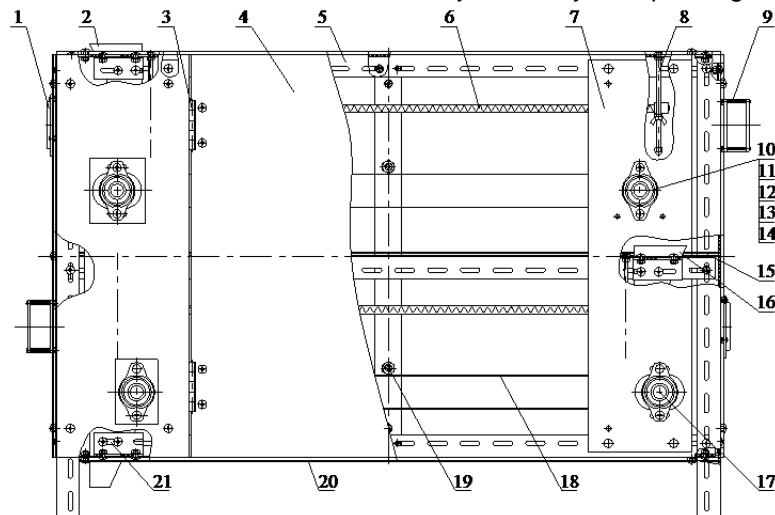


Fig. 1 - Structure diagram of the infrared belt dryer

- 1 – vent; 2 – feed port; 3 – hinge; 4 – opening; 5 – v-shaped steel; 6 – infrared heater; 7 – side plate; 8 – thread screw; 9 – axial flow fan; 10 – drive roller; 11 – bearing seat; 12 – coupling; 13 – stepping motor; 14 – motor bracket; 15 – baffle plate; 16 – guide chute; 17 – driven roller; 18 – conveyer belt; 19 – temperature sensor; 20 – wall; 21 – discharge port

Main Structure Design

Infrared heating system

Rapeseed is an unsaturated porous medium with sorptivity. According to matches of radiation properties of infrared heater and the product to be dried, since absorptivity of agricultural products at spectral range higher than 3 μm have their maximum absorptivity (Pan *et al.*, 2007), infrared heaters of wavelength of 3.3 μm were adopted for the radiation heating. Then, the surface temperature of the infrared heaters can be calculated as 878 K by the following expression (Wien's displacement law):

$$\lambda_{\max} T = 2897.8, [\mu\text{K}] \quad (1)$$

where:

λ_{\max} is wavelength of maximum emissivity, [μm];

T – absolute temperature, [K].

Radiation distance between infrared heater and the product affects drying efficiency and final quality of the dried product. The smaller the radiation distance is, the higher the radiant emittance will be, and the higher drying efficiency becomes, but the final quality of the dried product degrades. The irradiance of product can be calculated by the following expression (Zhang *et al.*, 2013):

$$M_e = H^2 E_e, [W/m^2] \quad (2)$$

where:

M_e is radiant emittance ("e" for "energetic"), $[W/m^2]$;

H – radiation distance, $[m]$;

E_e – irradiance at distance H , $[W/m^2]$.

The radiant flux can be controlled by adjusting the radiation distance. According to pre-experiments, a range of radiation distance 50-100 mm was defined for the infrared belt dryer in this study.

The power (or radiant power, radiant flux) of each infrared heater can be calculated as 795 W by the following expression (Wang, 2003):

$$P = E_e A, [W] \quad (3)$$

where:

P is radiant power, $[W]$;

A – area of irradiance at distance H , $[m^2]$.

Irradiance 3000 kW/m^2 and area of irradiance 0.265 m^2 were defined in this study.

Conveying system

The conveying system of the infrared belt dryer comprises an upper chamber unit and a lower chamber unit (as shown in Fig. 2), and each unit is composed of conveyer belt, drive roller, driven roller, bearing seat, coupling, motor bracket, and stepping motor. The conveyer belt is made of polytetrafluoroethylene (Teflon®), with evenly distributed square holes of side size 1 mm. The conveyer belt is driven by the stepping motor. Then, the rapeseed on the conveyer belts moves forward, as shown by the arrows in Fig. 2.

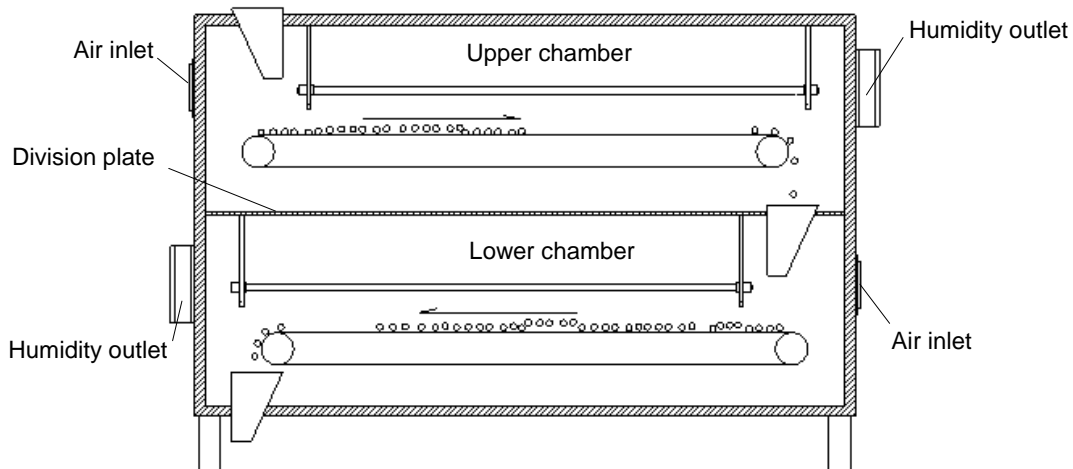


Fig. 2 - Conveying and ventilation diagram of the infrared belt dryer

Ventilation system

The ventilations in the upper chamber and lower chamber are separated by a division plate, as shown in Fig. 2. The axial flow fans 2B08038B12S (made by Asia Vital Components Co., Ltd) are installed at both humidity outlets, with parameters: operation voltage 12 V; maximum rotating speed 7000 r/min; maximum air flow rate $437 \text{ m}^3/\text{h}$. The air velocity and air flow rate can be controlled by means of frequency modulation. Moreover, there are evenly distributed holes on the conveyer belts which are beneficial to the ventilation in the drying chamber, especially in the thin layer product being processed.

Control System

The control system of the infrared belt dryer consists of modules of infrared heating, temperature sampling, motor control, ventilation, LCD display and keyboard input, and microcontroller STM32F407ZGT6 (made by STMicroelectronics) is the core platform of the system. Two temperature sensors WZP-187 PT100 (made by Shanghai Jiamin Instrument, Co. Ltd) are built at suitable positions above the product.

They sample the temperature information in the upper chamber and lower chamber individually. The feedback of temperature information is compared with pre-defined values and processed by the microcontroller. Then, based on the output of the process, the power of each infrared heater can be controlled (heating on/off) to obtain the pre-defined temperature in the drying chamber. The speed of the conveyer belts is driven by stepping motors and controlled by the motor control module. Since the speed of the conveyer belts is correlated to process time of the product in the drying chamber, the process time is controllable. Similarly, the air velocity and air flow rate in the drying chamber is controlled by the ventilation module.

RESULTS

PERFORMANCE STUDY OF THE DRYER

Experimental Procedures

The rapeseed (*Brassica napus* L.), Zhongzaliang 16, was harvested in Zhongxiang, Hubei Province, China. The impurities, cracked, germinated, mouldy seed and seed with green colour were manually removed so as to obtain uniform test samples. The initial moisture content (MC) of rapeseed was determined according to Chinese standard GB/T14489.1-2008 (China National standardizing committee, 2008). According to the initial MC 8.68 %d.b., test samples of the dry rapeseed were rewetted to MCs of 20 %d.b., 25 %d.b. or 30 %d.b. as required, by using the same method detailed in literature (Gao *et al.*, 2016).

Orthogonal Factorial Experiment Design technique based on Taguchi methodology was used to arrange experiments. Taking temperature, radiation distance, initial MC and layer thickness as control factors, and effective moisture diffusivity as evaluation index, levels of control factors were defined, as shown in Table 1. Experiments are designed in accordance with appropriate orthogonal array $L_9(3^4)$, a 3-level 4-factor array with 9 runs, and their arrangement is shown in Table 2.

Table 1

Levels of control factor				
Level	Temperature A	Radiation distance B	Initial MC C	Layer thickness D
	[°C]	[mm]	[%d.b.]	[mm]
1	95	80	20	4
2	100	100	25	6
3	105	120	30	8

Table 2

Experiment arrangements and results of effective moisture diffusivity D_{eff}					
No.	Factor A	Factor B	Factor C	Factor D	D_{eff} [$10^{-9} \text{m}^2/\text{s}$]
1	1	1	1	1	1.863
2	1	2	2	2	3.371
3	1	3	3	3	4.029
4	2	1	2	3	4.758
5	2	2	3	1	1.917
6	2	3	1	2	3.726
7	3	1	3	2	3.956
8	3	2	1	3	5.165
9	3	3	2	1	2.036

Effective moisture diffusivity can be calculated by the following expression (Yang *et al.*, 2014):

$$\ln MR = \ln \frac{8}{\pi^2} - \frac{\pi^2 D_{\text{eff}} t}{L^2}, \text{ [dimensionless]} \quad (4)$$

where:

MR is moisture ratio, [dimensionless]; $MR = (M - M_e) / (M_i - M_e)$, M is the instantaneous MC, [%d.b.];

M_i is the initial MC, [%d.b.]; M_e is the equilibrium MC, [%d.b.];

D_{eff} – effective moisture diffusivity, [m^2/s];

t – drying time, [s];

L – layer thickness, [m].

For simplification, it was assumed that the surface of kernel remained dry throughout the drying process, then $M_e=0$ (Thakor et al., 1999). Effective moisture diffusivity is typically determined by plotting experimental drying data in terms of $\ln MR$ versus drying time t in Equation (4), because the plot gives a straight line with a slope as follows: $\pi^2 D_{\text{eff}} / L^2$.

Drying Characteristics

The experimental moisture ratios of rapeseed versus drying time for different runs were plotted, as shown in Fig. 3. The drying characteristics curves of rapeseed under different combinations of drying conditions largely show a same tendency of change with drying time, namely, that moisture ratio exponentially decreases with drying time. No obvious constant rate drying stage is observed during the infrared drying of rapeseed, moisture removal is mainly processed during falling rate drying stage, and most of the moisture removal is finished in the first half stage. After drying of 30 min, the moisture ratios of all runs in Table 2 are less than 0.4 (the corresponding MCs are less than 9 %d.b.) which is a qualified MC level to safe storage of rapeseed in China.

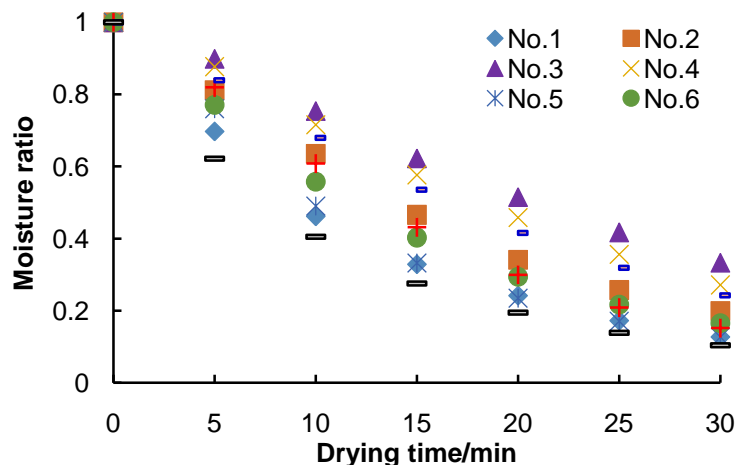


Fig. 3 - Experimental moisture ratios of rapeseed, for different runs

Statistical analyses of range and variance were performed to obtain the impacts and their significance of each control factor on the effective moisture diffusivity of rapeseed during infrared drying. Range analysis results were shown in Table 3, and variance analysis results were shown in Table 4. The values in cells of each level of the control factors in Table 3 represent mean diffusivities of the corresponding levels and factors. The delta values of each factor represent the biggest change of mean diffusivities of the factor, namely the impact level of each factor. The numbers in the rank row indicate the impact significance of the control factors. The reason why control factor of radiation distance of infrared heater has the lowest significance of impact on the effective moisture diffusivity can be explained as: even though radiation distance affects the irradiance of infrared heating, the on/off of the heater is controlled by temperature information, which determines the total radiant emittance.

Range analysis and variance analysis show that: the factor of layer thickness has the highest significant level of impact on rapeseed effective moisture diffusivity during infrared drying and it is followed by factors of temperature, initial MC and radiation distance, sequentially. The F -ratio of each control factor was compared to a critical value corresponding to a certain pre-selected probability, resulting in probabilities of 99.0 %, 83.6 %, and 51.6 % that control factors are in fact due to chance because of layer thickness, temperature, and initial MC, respectively. $A_3B_1C_1D_3$ and $A_1B_3C_3D_1$ are the optimal level combination and the worst level combination of the control factors that benefits to the effective moisture diffusivity, respectively.

According to optimal engineering average strategy (Wang, 2004), the effective moisture diffusivities of any level combinations of the control factors can be calculated. The calculated diffusivities of combinations of $A_3B_1C_1D_3$ and $A_1B_3C_3D_1$ were obtained and compared with tested data, as shown in Table 5. Of which, the tested diffusivities of combinations of $A_3B_1C_1D_3$ and $A_1B_3C_3D_1$ were obtained by following the same experimental method aforementioned. As can be seen in Table 5, the optimal level combination, namely $A_3B_1C_1D_3$, shows better performance for moisture removal than any level combination in Table 2.

Table 3

Level	Factor A	Factor B	Factor C	Factor D
1	3.088	3.526	3.585	1.939
2	3.467	3.484	3.388	3.684
3	3.719	3.264	3.301	4.651
Delta	0.631	0.262	0.284	2.712
Rank	2	4	3	1

Table 4

Source of variance	Degree of freedom	Sum of squares	Mean sum of squares	F-ratio	Critical F-ratio
Factor A	2	0.606	0.303	5.090	$F_{0.25}(2,2)=3.0$
Factor B	2	0.119	0.060	Error	$F_{0.10}(2,2)=9.0$
Factor C	2	0.127	0.063	1.066	$F_{0.01}(2,2)=99.0$
Factor D	2	11.336	5.668	95.224	/
Total	8	12.188	/	/	/

Table 5

Combinations	Tested diffusivity	Calculated diffusivity	Relative error
	$[10^{-9}m^2/s]$	$[10^{-9}m^2/s]$	$[\%]$
$A_3B_1C_1D_3$	5.586	5.206	6.80
$A_1B_3C_3D_1$	1.528	1.317	13.81

Mathematical Modelling

For further investigation of the drying performance, the experimental drying data of rapeseed moisture ratio under different conditions were fitted into 5 commonly used thin-layer drying models. The statistical results of the different models, including the drying model coefficients and the comparison criteria used to evaluate goodness of fit, namely, coefficient of correlation (R^2), reduced chi-square (χ^2) and root mean square error (RMSE), are listed in Table 6.

The coefficient of correlation, the reduced chi-square and the root mean square error can be calculated as follows:

$$R^2 = 1 - \frac{\sum_1^N (MR_{exp,i} - MR_{pre,i})^2}{\sum_1^N (MR_{exp} - Mr_{pre,i})^2}, \text{ [dimensionless]} \quad (5)$$

$$\chi^2 = \frac{\sum_1^N (MR_{exp,i} - MR_{pre,i})^2}{N-n}, \text{ [dimensionless]} \quad (6)$$

$$RMSE = \sqrt{\frac{\sum_1^N (MR_{exp,i} - MR_{pre,i})^2}{N}}, \text{ [dimensionless]} \quad (7)$$

where:

$MR_{exp,i}$ is the i th experimental moisture ratio, and $MR_{pre,i}$ is the i th predicted moisture ratio;

N – the number of observation;

n – the number of constants in the mathematical model.

Table 6

Statistical results obtained from different models

Model	Parameter									Mean value
	Run 1	Run 2	Run 3	Run 4	Run 5	Run 6	Run 7	Run 8	Run 9	
1 Newton: $MR=\exp(-kt)$										
k	0.073	0.051	0.033	0.039	0.070	0.060	0.057	0.043	0.086	/
R^2	0.9986	0.9924	0.9808	0.9816	0.9940	0.9980	0.9834	0.9911	0.9961	0.9907
χ^2	0.000146	0.000612	0.000994	0.001131	0.000599	0.000178	0.001448	0.000613	0.000437	0.000684
RMSE	0.0112	0.0229	0.0292	0.0311	0.0227	0.0124	0.0352	0.0229	0.0194	0.0230
2 Page: $MR=\exp(-kt^n)$										
k	0.082	0.033	0.016	0.018	0.054	0.049	0.028	0.026	0.118	/
n	0.957	1.158	1.254	1.254	1.097	1.070	1.251	1.177	0.878	/
R^2	0.9991	0.9993	0.9996	0.9999	0.9966	0.9994	0.9995	1.0000	0.9998	0.9992
χ^2	0.000114	0.000074	0.000029	0.000011	0.000433	0.000067	0.000058	0.000002	0.000028	0.000091
RMSE	0.0090	0.0073	0.0046	0.0028	0.0176	0.0069	0.0064	0.0012	0.0045	0.0067
3 Henderson and Pabis: $MR=a\exp(-kt)$										
a	0.996	1.025	1.036	1.037	1.020	1.013	1.039	1.026	0.983	/
k	0.073	0.053	0.035	0.041	0.071	0.061	0.059	0.045	0.084	/
R^2	0.9986	0.9947	0.9890	0.9888	0.9952	0.9985	0.9888	0.9940	0.9965	0.9938
χ^2	0.000170	0.000555	0.000784	0.000940	0.000614	0.000165	0.001309	0.000536	0.000457	0.000614
RMSE	0.0110	0.0199	0.0237	0.0259	0.0209	0.0109	0.0306	0.0196	0.0181	0.0201
4 Logarithmic: $MR=a\exp(-kt)+c$										
a	0.962	1.176	1.946	1.700	1.035	1.044	1.260	1.345	0.934	/
k	0.080	0.040	0.015	0.019	0.069	0.057	0.041	0.028	0.100	/
c	0.041	-0.165	-0.932	-0.687	-0.018	-0.035	-0.241	-0.338	0.063	/
R^2	0.9995	0.9976	0.9976	0.9981	0.9953	0.9988	0.9960	0.9993	0.9998	0.9980
χ^2	0.000083	0.000315	0.000223	0.000205	0.000749	0.000168	0.000614	0.000085	0.000034	0.000275
RMSE	0.0069	0.0134	0.0113	0.0108	0.0207	0.0098	0.0187	0.0070	0.0044	0.0114
5 Two-term: $MR=a\exp(-k_0t)+b\exp(-k_1t)$										
a	0.028	1.171	1.186	1.351	1.101	1.055	1.302	1.655	0.458	/
k_0	-0.010	0.060	0.042	0.053	0.077	0.063	0.073	0.061	0.053	/
b	0.975	-0.171	-0.186	-0.350	-0.101	-0.055	-0.302	-0.655	0.542	/
k_1	0.079	0.244	0.211	0.151	6.558	6.184	0.254	0.108	0.139	/
R^2	0.9995	0.9995	0.9998	0.9999	0.9983	0.9998	0.9999	1.0000	1.0000	0.9996
χ^2	0.000107	0.000110	0.000022	0.000020	0.000361	0.000034	0.000015	0.000000	0.000001	0.000074
RMSE	0.0068	0.0069	0.0031	0.0030	0.0124	0.0038	0.0025	0.0001	0.0006	0.0044

Notes: k , k_0 , k_1 , n , a , b and c are model constants.

In this study, the nonlinear regression analysis was performed with statistical software, SPSS16.0. The higher the R^2 values and the lower the χ^2 and $RMSE$ values, the better the goodness of fit (Wang *et al.*, 2007). As it can be seen in Table 6, the Two-term model gives the best fit to experimental data of moisture ratio, with R^2 0.9996, χ^2 0.000074 and $RMSE$ 0.0044; it is followed by the Page model, with R^2 0.9992, χ^2 0.000091 and $RMSE$ 0.0067.

Experimental moisture ratio values of the optimal level combination, namely $A_3B_1C_1D_3$, were employed to validate the effectiveness of the Two-term model and Page model. The predicted moisture ratio values of these two models were compared with experimental values, as shown in Fig. 4. The Two-term model and Page model both fit very well the experimental data: R^2 0.9996, χ^2 0.00067 and $RMSE$ 0.0054 for the former model and R^2 0.9993, χ^2 0.000072 and $RMSE$ 0.0072 for the latter model. However, to simplify the mathematical model, the convenience for process control and optimization of drying technology, the Page model is preferred to the rapeseed infrared drying.

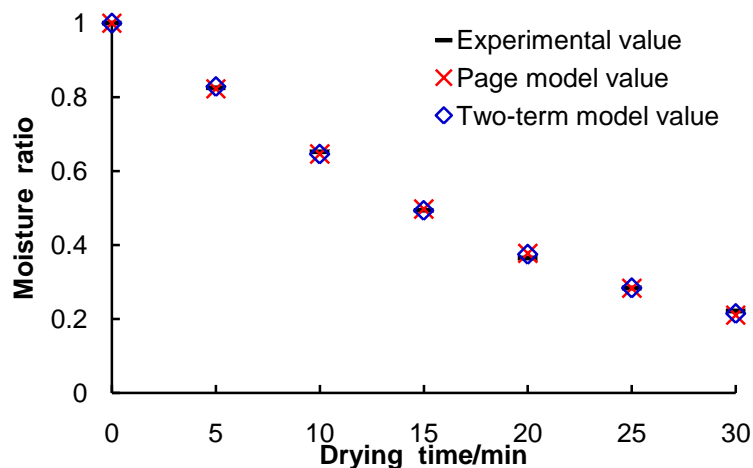


Fig. 4 - Validation of mathematical models

Continuous Drying Experiment

According to the optimal level combination ($A_3B_1C_1D_3$) of drying parameters, namely temperature 105 °C, radiation distance 80 mm, initial MC 20%d.b. and layer thickness 8 mm, rapeseed of 1.109 kg was loaded into the infrared belt dryer for continuous drying experiments (as shown in Fig. 5). The drying time was set as 30 min via keyboard input, and all the drying operations were controlled by the control system of the infrared belt dryer. The experimental results show that the mass of the dried rapeseed was 0.967 kg, namely its MC was 4.63%d.b. which is much less than the qualified MC level to safe storage of rapeseed in China.



Fig. 5 - Continuous drying experiment

CONCLUSIONS

According to matches of radiation properties of infrared heater and rapeseed, a small-scale infrared belt dryer was developed. The effect of process parameters on the drying performance of rapeseed was investigated, the goodness of fit of selected mathematical models for infrared drying was evaluated, and the continuous drying experiment was conducted. The main conclusions are as follows:

- during rapeseed infrared drying, no obvious constant rate drying stage is observed, moisture removal is mainly processed during falling rate drying stage, and rapeseed moisture ratio exponentially decreases with drying time.
- control factor of layer thickness has the highest significant level of impact on rapeseed effective moisture diffusivity during infrared drying, and it is followed by factors of temperature, initial MC and radiation distance, sequentially.
- Two-term model gives the best fit to experimental data of moisture ratio, with coefficient of correlation 0.9996, reduced chi-square 0.000074 and RMSE 0.0044; it is followed by the Page model, with coefficient of correlation 0.9992, reduced chi-square 0.000091 and RMSE 0.0067, which shows that both models are effective to predict the moisture ratio of rapeseed infrared drying.
- To simplify the mathematical model, the convenience for process control and optimization of the drying technology, the Page model is preferred to rapeseed infrared drying.

ACKNOWLEDGEMENTS

The study has been funded by the National Natural Science Foundation of China (No. 31301575), Ph.D. Research Project of Southwest University (No. SWU115011), and Fund from Key Laboratory of Modern Agricultural Equipment, Ministry of Agriculture, China (No. 201601001).

REFERENCES

- [1] Adak N., Heybeli N. and Ertekin C., (2017), Infrared drying of strawberry, *Food Chemistry*, vol. 219, pp. 109-116, Ed. Elsevier, London/U.K.;
- [2] Aghbashlo M., Mobli H., Rafiee S. and Madadlou A., (2013), A review on exergy analysis of drying processes and systems, *Renewable & Sustainable Energy Reviews*, vol. 22, pp. 1-22, Ed. Elsevier, London/U.K.;
- [3] Doymaz I., (2015), Infrared drying characteristics of bean seeds, *Journal of Food Processing and Preservation*, vol. 39, issue 6, pp. 933-939, Ed. Wiley, Malden/U.S.A.;
- [4] Gao B., Guo M.B., Yang L., Wu D.K. and Yang M.J., (2016), Heat and mass transfer during hot-air drying of rapeseed: CFD approach and evaluation, *INMATEH Agricultural Engineering Journal*, vol. 50, issue 3, pp. 73-82, Ed. INMA Bucharest, Bucharest/Romania;
- [5] Kayran S., and Doymaz I., (2017), Infrared drying and effective moisture diffusivity of apricot halves: influence of pre-treatment and infrared power, *Journal of Food Processing and Preservation*, vol. 41, issue 2, pp. 1-8, Ed. Wiley, Malden/U.S.A.;
- [6] Kocabiyik H., Yilmaz N., Tuncel N.B., Sumer S.K., and Buyukcan M.B., (2016), Quality properties, mass transfer characteristics and energy consumption during shortwave infrared radiation drying of tomato, *Quality Assurance and Safety of Crops & Foods*, vol. 8, issue 3, pp. 447-456, Ed. Wageningen Academic Publishers, Wageningen/Netherlands;
- [7] Okeyo A., Olatunde G., Atungulu G., Sadaka S., and Mckay T., (2017), Infrared drying characteristics of long-grain hybrid, long-grain pureline, and medium-grain rice cultivars, *Cereal Chemistry*, vol. 94, issue 2, pp. 251-261, Ed. AACC International, St Paul/U.S.A.;
- [8] Onwude D.I., Hashim N., and Chen G.N., (2016), Recent advances of novel thermal combined hot air drying of agricultural crops, *Trends in Food Science & Technology*, vol. 57, pp. 132-145;
- [9] Pan Y.K., Wang X.Z., and Liu X.D., (2007), *Modern drying technology (现代干燥技术)*, ISBN 978-7-5025-9361-2, Chemical Industry Press, Beijing/P.R.C.;
- [10] Pawar S.B. and Pratape V.M., (2017), Fundamentals of infrared heating and its application in drying of food materials: a review, *Journal of Food Process Engineering*, vol. 40, issue 1, pp. 1-15, Ed. Wiley, Malden/U.S.A.;
- [11] Thakor N.J., Sokhansanj S., Sosulski F.W., and Yannacopoulos S., (1999), Mass and dimensional changes of single canola kernels during drying, *Journal of Food Engineering*, vol. 40, pp. 153-160, Ed. Elsevier, London/U.K.;

- [12] Wang W.Z., (2004). *Design of experiments and analysis (试验设计与分析)*. Higher Education Press, Beijing/P.R.C.;
- [13] Wang X.B., (2003), *Theoretical analysis and experimental study on combined convective and infrared radiation drying (红外辐射与对流联合干燥的理论分析及试验研究)*, PhD dissertation, China Agricultural University, Beijing/P.R.C.;
- [14] Wang Z.F., Sun J.H., Liao X.J., Chen F., Zhao G.H., Xu J.H., and Hu X.S., (2007), Mathematical modelling on hot air drying of thin layer apple pomace, *Food Research International*, vol. 40, pp. 39-46, Ed. Elsevier Science Bv, Amsterdam/Netherlands;
- [15] Yang G., He S., and Ding C., (2013), Study of the rapeseeds' quality storage after hot-air drying (油菜籽热风干燥后储藏品质的研究), *Journal of the Chinese Cereal and Oils Association*. vol. 28, issue 9, pp. 97-102, Ed. Chinese Cereal and Oils Association, Beijing/P.R.C.;
- [16] Zhang M., Chen H.Z., Mujumdar A.S., Zhong Q.F., and Sun J.C., (2015), Recent developments in high-quality drying with energy-saving characteristic for fresh foods, *Drying Technology*, vol. 33, issue 13, pp. 1590-1600, Ed. Taylor & Francis Inc., Philadelphia/U.S.A.;
- [17] Zhang Q.Q., Wen H.X., and Yuan Y.J., (2013), Research and design far infrared with drying equipment in vacuum (远红外联合低温真空干燥设备研究与设计), *Food & Machinery*, vol. 29, issue 1, pp. 157-160, Ed. Changsha University of Science and Technology, Changsha/P.R.C.;
- [18] Zhou L.Y., Cao Z.Z., Bi J.F., Yi J.Y., Chen Q.Q., Wu, X.Y., and Zhou M., (2016), Degradation kinetics of total phenolic compounds, capsaicinoids and antioxidant activity in red pepper during hot air and infrared drying process, *International Journal of Food Science & Technology*, vol. 51, issue 4, pp. 842-853, Ed. Wiley, Hoboken/U.S.A.;
- [19] *** China National standardizing committee, (2008), *Oilseeds - Determination of moisture and volatile matter content, GB/T14489.1-2008 (油料 水分及挥发物含量测定, GB/T14489.1-2008)*, Chinese Standard Press, Beijing/P.R.C.

DETERMINATION OF PERFORMANCE CHARACTERISTICS OF HORIZONTAL WIND TUNNEL IN THE CLEANING OF CORN-COB MIX

MISIR-KOÇAN KARIŞIMININ TEMİZLENMESİNDE YATAY HAVA TÜNELİNİN PERFORMANS KARAKTERİSTİKLERİNİN BELİRLENMESİ

Ress.Assist. Karaköse T. ^{*1)}, Assist.Prof.Dr. Tekgüler A. ²⁾

¹⁾Ondokuz Mayıs University, Faculty of Agriculture, Atakum / Turkey

²⁾Ondokuz Mayıs University, Samsun Vocational School, İlkadım / Turkey

Tel: +903623121919; E-mail: tugba.karakose@omu.edu.tr

Keywords: horizontal air tunnel; cleaning efficiency; loss ration

ABSTRACT

In the cleaning process, different relative velocities of the grains through the air stream are utilized. The purpose of this study is to determine parameters such as fan angle, material feed rate and air velocity which will ensure separation of corn. Cleaning efficiency increased with increasing fan angle and air velocity and decreased with increasing feed rate. Loss rate increased with increasing fan angle and air velocity, and decreased with increasing feed rate.

It can be said that the most appropriate combination (89.79% cleaning efficiency and 0.24% loss rate) was the application at 30° fan angle, 1152 kg⁻¹ feed rate and 15 ms⁻¹ air velocity.

ÖZET

Aerodinamik temizlemede, hava akımı içinde tanelerin farklı bağıl hızlarından yararlanılır. Bu çalışmada, mısırın temizlenmesini sağlayacak; fan açısı, materyal besleme oranı ve hava hızı gibi parametreleri belirlemektir. Temizleme etkinliği, fan açısı ve hava hızı arttıkça artmakta, besleme oranı arttıkça azalmaktadır. Fan açısı ve hava hızı arttıkça kayıp oranı artmakta, besleme oranı arttıkça kayıp oranı azalmaktadır.

En uygun kombinasyonun (%89.79 temizleme etkinliğine %0.24 kayıporanı) 30° fan açısında, 1152 kg⁻¹ besleme oranında ve 15 ms⁻¹ hava hızındaki uygulama olduğu söylenebilir.

INTRODUCTION

A great majority of food needs are met from the grains. In the world, corn is in the third place after the wheat and paddy in terms of production areas, and the first in the production amount (URL-1). In Turkey, according to the data of 2014, it is in the 3rd place in the production of cereals, in terms of production area and amount of production (URL-2).

Corn usage areas increase day by day. In addition to this, it is more important than other grains for reasons such as being easy to grow and drought-tolerant, effective photosynthesis even at low CO₂ ratios, being more resistant to diseases and damages, having high ability to use light intensity and high water use efficiency.

Even if the most modern harvesting machines are used, grain products cannot be assessed immediately as they are obtained (Tekin Y., 1995). Agricultural products need a sequence of processes such as cleaning, classification, drying, storage, etc. in order to make them available. These processes preserve the nutritional and commercial value of the product (Yağcıoğlu A K, 2009). Cleaning is separation of the straw, mud, stone, soil, foreign seed etc. material in the product from the original product. Cleaning and classification of granular products can be performed according to different physico-mechanical properties. These are geometric properties, aerodynamic properties, surface structure, mechanical properties, specific gravity, electrical and optical properties.

According to the aerodynamic characteristics, different relative velocities of the grains are utilized in the airflow during cleaning (Berber S, 2007). Air velocity that can suspend grain in the air is called critical speed. If the critical speeds of each material forming any mixture are sufficiently different from each other, these materials can be separated from each other (Yağcıoğlu A K, 2009). If there is a big difference between the critical speeds, it increases the success of the separation process (Pasikatanand Quick, 1995; Tabatabaeefar et al., 2003).

Air flow separators or pneumatic cleaners are used to clean products from foreign materials by means of air flow. In the pneumatic cleaning process, the flow direction of the air can be horizontally between 0°-90°. In pneumatic cleaners where the air flow is in the vertical direction (90°), the suspension of main materials within the air flow is made use of. Pneumatic cleaners where the air flow is in the horizontal direction (0°) make use of materials that enter the air in the direction perpendicular to the flow and of their being dragged away by drawing different orbits horizontally.

Pneumatic cleaners consist essentially of air canal and air flow generators (fans). These cleaners operate according to the principle of absorption or pressurization of air to air canal. The air velocities in each section taken along the length and width of the air channel are wanted equal to each other, in order to ensure high separation efficiency and low seed loss during cleaning (Evcim Ü, 1991; Yağcıoğlu A K, 1996).

In Adewumi's (2008) study, horizontal air tunnel was used to classify cowpea, according to size and density in terms of aerodynamic principles. The results showed that 12 ms⁻¹ air velocity and 22.5° fan angle were most appropriate.

Simonyan and Yiljep (2008) used the cleaning unit of traditional thresher to determine the separation and clean up efficiency values of sorghum. Cleaning losses increased with increasing feed rate and air velocity. The highest separation efficiency was found as 99.85%. Air velocity raise increased with the loss rate and up to 54% lost product was observed in different feed amount.

Rouzegar et al. (2013) used a horizontal air tunnel to determine the effect of humidity, air velocity and feed rate on rice separation efficiency. They achieved the highest separation efficiency at 850 rpm fan speed. Separation efficiency increased with rising humidity and feed ratio. Compared to a mechanical system, they reported that this machine, operating according to pneumatic principles, is economical because of its high separation efficiency, low loss rate and low power consumption. Beyhanve Erol (1993) has made a study to determine the aerodynamic characteristics of some hazelnut varieties of grains and hazelnuts. In the study, they found that the critical rates of grain and hazelnuts varied between 7-14 m s⁻¹.

The purpose of this study, is to determine design parameters such as fan angle, material feed rate, air velocity and air tunnel length to provide separation of corn mixture consisting of grain and cob parts.

MATERIALS AND METHODS

An experimental mechanism has been prepared in which air velocity, fan angle and feed rate can be adjusted (Fig. 1). Mechanism consists of the fan, the product storage, the feeding unit, the air canal and collection boxes.



Fig. 1 - Experimental mechanism

Fan characteristics used to obtain airflow are given in Table 1.

Table 1

Fan characteristics	
Number of wings (number)	8
Air outlet section (mm)	190x70
Internal diameter of fan (mm)	150
External diameter of fan (mm)	400
Width (mm)	200
Rotation(min^{-1})	1100-1300-1500-1750-1950
Flow (m^3s^{-1})	0.1995-0.2394-0.2793-0.3192-0.3591

The power of the electric motors acting on the fan and the supply units are 0.75 kW and 3 kW, respectively. The experimental mechanism is used for uniform material flow. The length of the air tunnel is 800 mm. Two different product collection boxes of 400 and 800 mm from storage outlet section were used.

Experiments were conducted with *zea mays indentata sturt* corn grains and their cobs. The sizes of corn cobs are reduced by crushing in the hammer mill. During the course of the experiment, the grain moisture varied between 15-16%. A mixture of 8 kg was prepared. It was arranged so as to include 85% corn and 15% stubble. The amount of this mixture was kept constant throughout all experiments.

Feed rates of 240, 576, 822, 1152 and 1600 kg h^{-1} were created by changing the sections of the storage outlet. Experiments used air velocities of 15, 18, 21, 24 and 27 ms^{-1} . These air velocities were obtained with the frequency converter shown in figure 2.2, by varying the revolutions per minute of the electric motor which drives the fan. Anemometer was used to measure air velocities.

The position of the fan with the test mechanism can be adjusted to make horizontal angles of 15°, 30° and 45°. The mixture of corn and cob, which falls into the air canal from storage and encounters the air flow provided by the fan, falls into the product collection boxes at different distances. The grains and cobs collected in these boxes were separately weighed with a precision scale.

The product cleaning efficiency and loss ratio of grain-cob quantities obtained as a result of the weighing were determined using the following equations (Simonyanand Yiljep, 2008).

Cleaning efficiency:

$$CE = \left(\frac{Go}{G1} \right) * 100 \quad (1)$$

Where:

CE- the cleaning efficiency (%)

Go - grain weight at outlet (kg)

G1 -total mixture weight at outlet (kg)

Loss ratio:

$$LR = \frac{Gi}{Gw} * 100 \quad (2)$$

Where:

LR - Rate of grain loss in cleaning units (%)

Gi - Weight of grain thrown out of the air tunnel (kg)

Gw - Grain weight in the mixture filled in the feeding unit (kg)

For each application of 5 different feed rates, 5 different air speeds and 3 different fan angles were made with four repetitions. To determine the effect of these factors, the obtained data were analysed according to the 3-factorial design in randomized blocks in the JUMP 5.0.1 statistical program. The results were compared with the LSD test.

RESULTS

According to the analysis of variance, interactions of the fan angle, feed rate and air velocity were found to be significant for clearing efficiency (CE) and loss ratio (LR) ($p < 0.01$). CE for the first collection box varied between 85-100%, LR varied between 0.24-93.01 %.

The CE and LR variations at 45°, 30° and 15° fan angles are given in Fig. 2. At 45° fan angle, CE values varied between 99.65-89.58 % and LR values varied between 92.42-3.21%. The highest CE value (99.65%) was detected at the feed rate of 576 kg h^{-1} and at the air velocity of 21 ms^{-1} while the lowest LR value (15.2%) was detected at the feed rate of 1152 kg h^{-1} and the air velocity of 15 ms^{-1} .

At 30° fan angle, CE values varied between 99.16-87.17% and LR values varied between 50.70-0.24%. The highest CE value (99.16%) was detected at the feed rate of 822 kg h^{-1} and the air velocity of 27 ms^{-1} , while the lowest LR value (0.24%) was detected at the feed rate of 1152 kg h^{-1} and the air velocity of 15 ms^{-1} .

At 15° fan angle, CE values varied between 95.86-85.06% and LR values varied between 18.73-0.39%. The highest CE value (95.87%) was detected at the feed rate of 576 kg h^{-1} and the air velocity of 27 ms^{-1} , while the lowest LR value (0.39%) was detected at the feed rate of 240 kg h^{-1} and the air velocity of 15 ms^{-1} .

In previous studies, cleaning efficacy values were determined as 42-80% for corn (Hurburgh *et al.*, 1989) 80%, 94%, 98% for oat, wheat and rye respectively (Uhl and Lamp, 1966), 93% for Chickpea (Tabatabaefar *et al.*, 2003), 99.85% for sorghum (Simonyan, Yiljep, 2008), 87.2% for the yellow bitter variety (Amulet lupine) (Panasiewicz *et al.*, 2011).

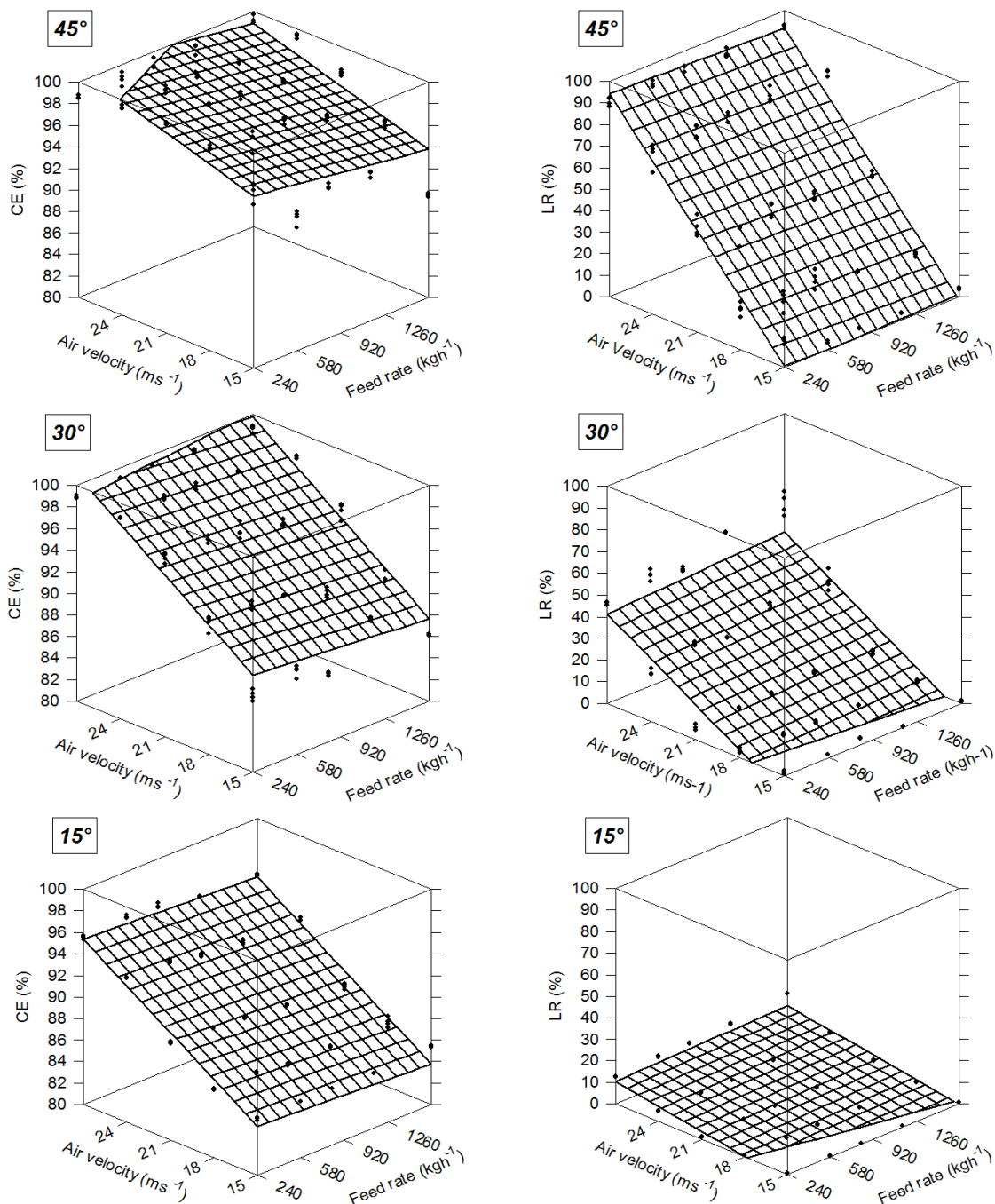


Fig. 2 - The first collecting box, CE and LR variation at 45°, 30° and 15° fan angles

CE for the second collection box varied between 85-100%, LR varied between 0.13-70%.

Fig.3 shows the change of CE and LR at 45°, 30° and 15° fan angles according to the feed rate and air velocity.

At 45° fan angle, CE values varied between 98.73-86.45 % and LR values varied between 69.17-1.85%. The highest CE value (98.74%) was detected at the feed rate of 576 kg⁻¹ and the air velocity of 21 ms⁻¹, while the lowest LR value (1.85%) was detected at the feed rate of 1152 kg⁻¹ and the air velocity of 15 ms⁻¹.

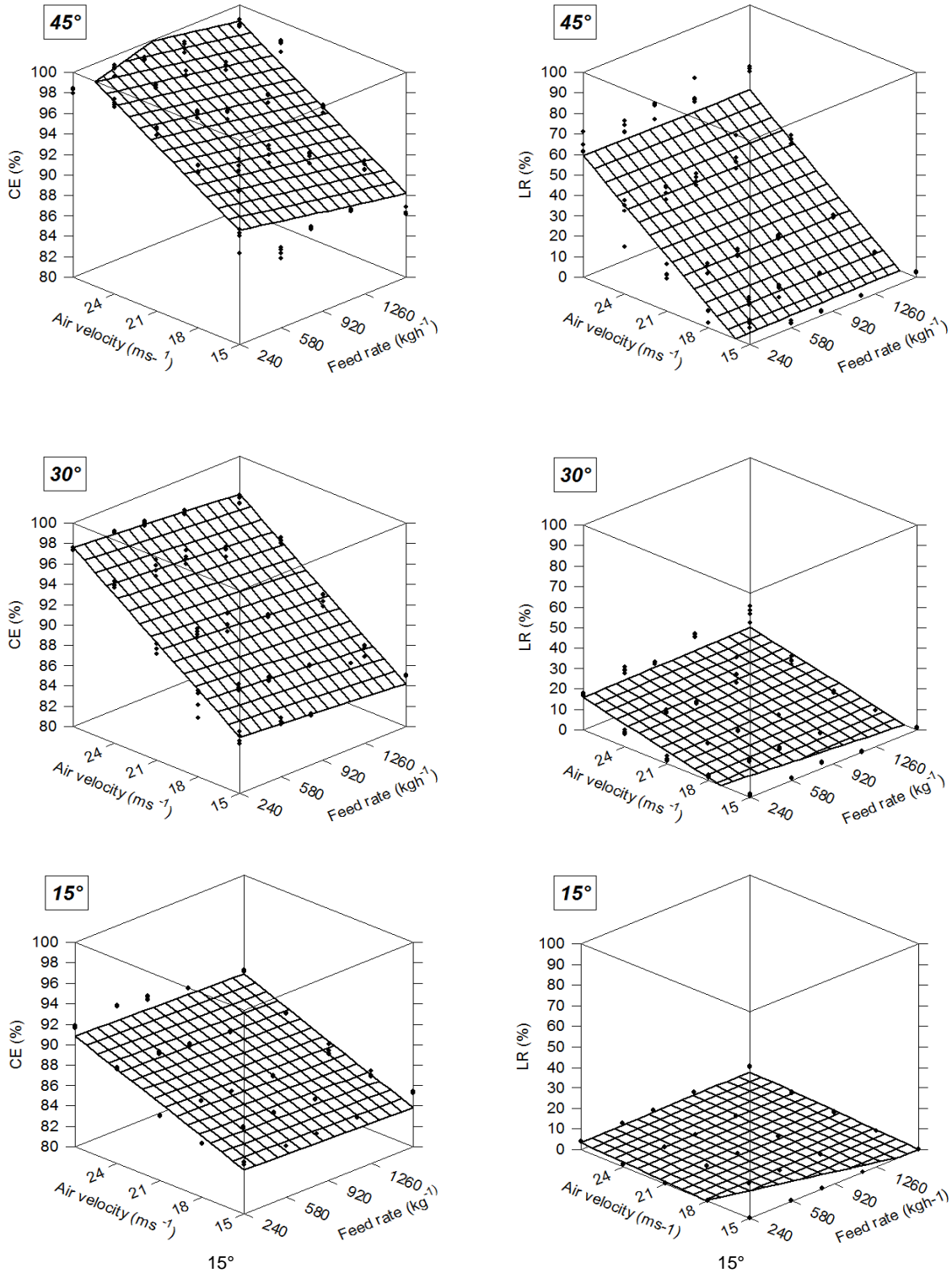


Fig. 3 - The second collecting box, CE and LR variation at 45°, 30° and 15° fan angles

At 30° fan angle, CE values varied between 97.58-85.01% and LR values varied between 24.50-0.13%. The highest CE value (98.59 %) was detected at the feed rate of 576 kg^h⁻¹ and the air velocity of 27 ms⁻¹, while the lowest LR value (0.13 %) was detected at the feed rate of 1152 kg^h⁻¹ and the air velocity of 15 ms⁻¹.

At 15° fan angle, CE values varied between 92.21-85.00% and LR values varied between 7.22- 0.15%. The highest CE value (92.21%) was detected at the feed rate of 576 kg^h⁻¹ and the air velocity of 27 ms⁻¹, while the lowest LR value (0.15%) was detected at the feed rate of 24 kg^h⁻¹ and the air velocity of 15 ms⁻¹.

CE values in the first box were higher than in the second box, while LR values were lower. For the first collecting box, the highest CE value (99.65%) was seen at 45° fan angle, 576 kg^h⁻¹ feed rate and 21 ms⁻¹ air velocity while the lowest CE value (85.07%) was observed at 15° of fan angle, 1152 kg^h⁻¹ of feed rate and 15 ms⁻¹ of air velocity.

For the second collecting box, the highest CE value (98.74%) was seen at 45° fan angle, 576 kg^h⁻¹ feed rate and 27 ms⁻¹ air velocity while the lowest CE value (85.01%) was observed at 15° of fan angle, 240 and 576 kg^h⁻¹ of feed rate and 15 ms⁻¹ of air velocity.

For the first collecting box, the highest LR value (93.01%) was seen at 45° fan angle, 1600 kg^h⁻¹ feed rate and 27 ms⁻¹ air velocity while the lowest LR value (0.24%) was observed at 30° of fan angle, 1152 kg^h⁻¹ of feed rate and 15 ms⁻¹ of air velocity.

For the second collecting box, the highest LR value (69.17%) was seen at 45° fan angle, 1600 kg^h⁻¹ feed rate and 27 ms⁻¹ air velocity while the lowest LR value (0.13%) was observed at 30° of fan angle, 1152 kg^h⁻¹ of feed rate and 15 ms⁻¹ of air velocity. Cleaned products reduce product loss due to the increased air tunnel length from the feed outlet side.

Sorghum has been found to have product loss up to 54% (Simonyan and Yiljep, 2008). Uhland Lamp (1966) stated that it is not possible to clean corn without loss of grain.

CONCLUSIONS

In the study for corn cleaning in the horizontal air tunnel, CE and LR values varied depending on the length of the air tunnel, air speed, feed rate and fan angle. The highest CE (99.65%) was determined at 45° fan angle, 576 kg^h⁻¹ feed rate and 21 ms⁻¹ air velocity in the first collection box. The least LR (0.13%) was determined at 30° fan angle, 1152 kg^h⁻¹ feed rate and 15 ms⁻¹ air velocity in the second collection box.

The applications below 1% of LR in the first collection box, in which CE is high, are given in Table 2.

Table 2

Best applications in the first box according to cleaning efficiency and loss rate

CE (%)	LR (%)	Fan angle (°)	Feed rate (kg ^h ⁻¹)	Air velocity (ms ⁻¹)
89.79465	0.24173	30	1152	15
86.33599	0.53313	15	240	18
86.23009	0.59268	15	576	18
85.86218	0.89735	15	1152	18
85.84654	0.98743	15	822	18
85.39345	0.82482	15	1600	15
85.26317	0.39235	15	240	15
85.23333	0.58316	15	822	15
85.23089	0.49364	15	576	15
85.06529	0.58882	15	1152	15

As it can be seen in Table 2, we can say that the best application were at the fan angle of 30°, feed rate of 1152 kg^h⁻¹ and air velocity of 15 ms⁻¹ (89.79% CE and 0.24% LR).

As a result of the study findings evaluation, we can list the suggestions as follows:

- 15-21 ms⁻¹ air velocity was found suitable for separation of corn-cob mixture in the horizontal air tunnel. LR increases at higher speeds.

- CE values are higher at 45° fan angle because the air entering the air canal at a more vertical angle causes the product to be cleaned more effectively. However, LR values were found to be high at this angle.
- There are differences between collection boxes in terms of CE and LR. While CE increases in the first box, LR decreases in the second box. If the product evaluated as loss can be returned to the storage, the first box (40 cm) should be preferred because of higher CE.

ACKNOWLEDGEMENT

This study was the summary of the master thesis which was directed by Ass.Prof.Dr. Ali TEKGÜLER and was accepted in the Institute of Science of Ondokuz Mayıs University in 2016.

REFERENCES

- [1] Adewumi B.A., (2008), 2D Modeling of grain transport and separation in the horizontal air stream, *ASABE Publication, Food Processing Automation Conference CD-Rom, Proceedings of the 28-29 June 2008 Conference, Providence, Rhode Island, ASABE Publication Number 701P0508cd*;
- [2] Adewumi B.A., Sathyendra Rao B.V., Kiran Kumar N.L., Pratape V.M., Srinivas A., (2007). Grain classification using aerodynamic principles, *African Crop Science Conference Proceedings*, Vol.8, pp.1799-1801;
- [3] Adewumi B., Ademosun O., Ogunlowo A., (2006), Preliminary investigation on the distribution and spread pattern of cowpea in a cross flow grain separator. *Agricultural Engineering International: The CIGR E journal*. Manuscript FP 06 020, Vol. VIII, pp.1-12, India;
- [4] Berber S., (2007), *Determination of aerodynamic properties of safflower (Carthamus Tinctorious. L.) seeds*, M.Sc. Thesis. Gaziosmanpaşa University. Institute of Science and Technology. Tokat;
- [5] Beyhan M.A., Erol M.A., (1993). The aerodynamic characteristics of husk and grain of some hazelnut varieties, *Proceedings of 5th Int. Cong. On Mechanization and Energy in Agriculture*, pp.472-483, Kuşadası / Turkey;
- [6] Evcim Ü., (1991), *Product cleaning and sorting technology*, Ege University Agricultural Faculty Press, p.110, İzmir;
- [7] Hurburgh C.R., Bern C.J., Brumm T.J., (1989), Efficiency of rotary grain cleaners in dry corn, *Transactions of the ASAE*, 32 (6), pp. 2073-2077;
- [8] Panasiewicz M., Zawiślak K., Kusińska E., Sobczak P., (2008), Purification and separation of loose materials in a pneumatic system with vertical air stream, *TEKA Kom. Mot. Energ. Roln.–OL PAN*, vol:8, pp.171–176;
- [9] Panasiewicz M., Sobczak P., Mazur J., Zawisłak K., Andrejko D., (2011), The technique and analysis of the process of separation and cleaning grain materials, *Journal of Food Engineering*, vol.109, pp.603–608, Elsevier;
- [10] Pasikatan M.C., Quick G.R., (1995), A review of oscillating screen-blower cleaners for grains, *Philippine Engineering Journal XVI* (2): pp.77-97, Philippines;
- [11] Pasikatan. M.C., Quick. G. R., Barredo I. R., Lantin. R. M., (1996), *A Compact triple airstream. triple-screen rice seed cleaner*, Philipp J. CropSci., 21 (3), pp.53-60;
- [12] Rajabipour A., (2004), Moisture-dependent terminal velocity of wheat and rice varieties, *ASAE/CSAE Annual International Meeting*. paper number:046008, Ottawa. Ontario, Canada;
- [13] Rouzegar M. R., Asli-Ardeh E. A., Abbaspour-Gilandeh Y., Khalifeh A. A., (2013). Study effects of moisture content, feed rate and fan revolution on separation efficiency in a paddy laboratory winnower, *International Journal of Agriculture and Crop Sciences (IJACS)*, Vol. 5(21), pp.2576-2578, Elsevier;
- [14] Simonyan K.J., Yiljep Y.D., (2008). Investigating grain separation and cleaning efficiency distribution of a conventional stationary rasp-bar sorghum thresher, *Agricultural Engineering International: The CIGR E-journal Manuscript PM 07 028*. Vol. X, pp.1-13;
- [15] Tabatabaeefar A., Aghagoolzadeh H., Mobli H., (2003). Design and development of an auxiliary chickpea second sieving and grading machine, *Agricultural Engineering International: CIGR Journal of Scientific Research and Development*. Manuscript FP 03 005, Vol.V, 1-8;
- [16] Tekin Y., (1995), Product cleaning and sorting technology, Özdaş K., *Agricultural Tools and Machinery*, 4th edition, pp.297-318, Anadolu University, Eskişehir;
- [17] Uhl J.B., Lamp. B.J., (1966), Pneumatic separation of grain and straw mixtures. *Transactions of the ASAE*, vol.9, pp.244-246.

- [18] Yağcıođlu A.K., (2009), Post-harvest processing technology, Editor: Prof. Dr. G. Güneş, Agricultural machines, 1st edition, Nobel Publication and distribution, Ankara, pp.488-491;
- [19] URL-1 <http://www.tmo.gov.tr/Upload/Document/hububat/hububat%20raporu.pdf>(ZiyaretTarihi:02.06.2016/ 10.04);
- [20] URL-2 <http://www.tuik.gov.tr/UstMenu.9do?metod=temelist>(ZiyaretTarihi:02.06.2016/ 10.11).

GRAIN CROPS INJURIES AND DRYING MODES DURING SEEDS PREPARATION

ТРАВМУВАННЯ ЗЕРНІВОК ТА РЕЖИМИ ПІДСУШУВАННЯ ПРИ
ПІДГОТОВЛЕННІ НАСІННЯ

Ph.D. Eng. Derevjnko D., Ph.D. Eng. Sukmaniuk E, Stud. Derevjnko O.

Zhytomyr National Agroecological University / Ukraine

E-mail: sukmanyukolena@gmail.com**Keywords:** seed, mode, injuries, quality, moisture**ABSTRACT**

The article deals with the technological process of seed drying beginning with the bottom layer, where the heated air enters, which is quickly saturated with moisture from the grains. The higher the seed layers are placed, the less they are drying, which is the main cause of uneven quality for a certain time and can cause cracks, injury and deterioration of quality. In the work, the diagrams of forces' influence on grains are shown while moving along with the auger screw turns. The speed of the screw, the pressure of the seed to the body and the angle of the screw spiral, which influence the seeds injury, were studied. Optimal and proper drying conditions for seeds of different crops are established, which are the main factors in obtaining high quality seeds, especially of high energy and similarity.

РЕЗЮМЕ

В статті розглянуто технологічний процес підсушування насіння, який розпочинається з нижнього шару, куди надходить нагріте повітря, яке швидко насичується вологою від зернівок. Чим вище розміщені шари насіння, тим менше в них проходить підсушування, що буде основною причиною нерівномірної якості протягом певного часу і може викликати утворення тріщин, травмування та погіршення показників якості. В роботі показано схеми впливу сил на зернівку при переміщенні вздовж витків гвинта шнека. Досліджено частоту обертів гвинта, притиснення насіння до корпусу та кут нахилу спіралі гвинта, які впливають на травмування насіння. Встановлено оптимальні та правильні режими підсушування для насіння різних культур, які є головним чинником отримання високоякісного насіння, особливо високої енергії та схожості.

INTRODUCTION

For many decades, and especially in the second half of the last century, researchers, breeders, and manufacturers proved and substantiated that only high quality seeds, for all other similar opportunities, provide a significant part of the future harvest, so there is an urgent need for high-quality seeds that play a large role in the country food security.

Studies show that the improvement of the influence of technical means working elements in technological processes on reducing the seeds injury, contributes to a significant improvement in the quality of seeds and the growth of grain yields.

Injuries, damage and total destruction of grain crops are the result of mechanical loads effect of many elements of the technological process from harvesting to sowing.

Researchers (Strona I.G., 1974; Derevianko D. A., 2015; Derevyanko D. A. et al. 2012; Tarasenko A.P., 2003; Pugachev A.N., 1976; Chazov S.A. and Plaksin V.F. 1974; Chazov S.A. et al. 1981; Fadeev L.V., 2015) have proved that the grain crops injury during grinding reaches 20% and even more, and while finishing the grain pile, preparing the seeds and sowing, it significantly grows to 60-80%.

According to V. M. Drinch (Drinch V.M., 2006), the grain crops injury during threshing sometimes reaches 30-35%, and during the preparation of seeds, even more than 50%, depending on the moisture content and structure of the grain pile.

In recent years, considerable work has been carried out by L.V Fadeev (Fadeev L.V., 2015) on the development and introduction into the production of fundamentally new cleaning and calibration technical equipment and technical lines.

In creating the scientific foundation of the theory of interaction between the mechanisms' working surfaces and various materials, including grain mass, scientists such as P.M. Vasilenko (*Vasilenko P.M., 1960*), V.M. Drincha (*Drincha V. M. and Sukonin L. M., 1997*), V.V. Adamchuk (*Adamchuk V.V., 2010*), L.M. Tishchenko (*Tishchenko L.N. et. al., 2011*), A.P. Tarasenko (*Tarasenko A.P., 2003*), P.M. Zaika (*Zaika P.M., 2006*), and E. S. Goncharov (*Goncharov E.S., 1963*) had significant contribution.

Thus, a deep and comprehensive study of the physico-mechanical and biological characteristics of the seeds, the development of new technologies and the modernization of the working bodies that will provide the minimum amount of grain crops injury, is the basis for obtaining high quality seeds in accordance with the agro-technical requirements and state standards.

MATERIALS AND METHODS

Using the method of mathematical modeling of machines, working elements and technological processes, using calculated differential equations, transformations and graphic determinations based on the mechanical laws usage, we consider the processes of transportation and loading by screw, scraper, conveyor belts or other technical means, which leads to grain crops injury and their quality decrease.

It is important to study the influence of the angle of the turns' inclination on the force of seed pressure to the body of engagement, on the centrifugal force, grain crop weight and grain friction force of the seed with an auger.

The essence of the seed movement physical characteristics on the turns during the rotation of the screw shows that as the angle of spiral lifting increases, the forces of resistance to the seed movement increase, too.

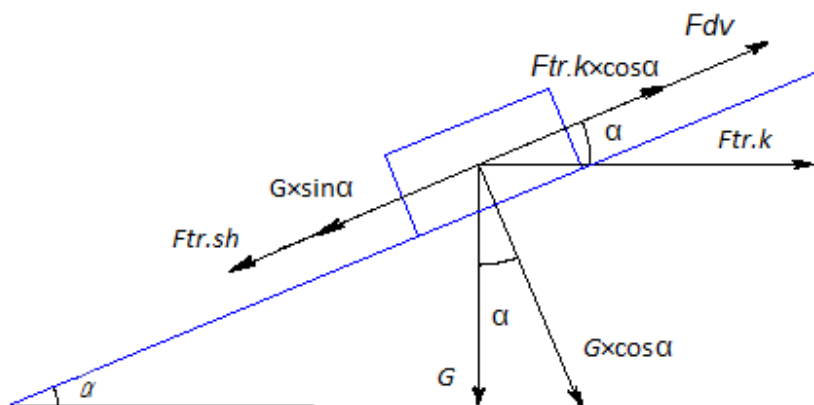


Fig. 1 – Scheme of the force effect on the corn grain when moving along the turns of the screw

From this scheme of forces acting on a certain number of seeds between the rods along the screw (fig. 1) it is evident that the force that promotes the movement of the seeds upwards the coils of the screw is the friction with the casing $F_{tr,k}$, but counteract this frictional force with the rotation of the screw $F_{tr,sh}$ and weight force $G \times \sin \alpha$. So, the difference between the first and the sum of the two others allows you to determine the force that drives the seeds by turning the screw up:

$$F_r = m \cdot \left[\omega_{sh}^2 R \cos \alpha \cdot f_k - g(\sin \alpha + \cos \alpha \cdot f_{sh}) \right] \quad (1)$$

Where ω_{sh} – the angle of the auger speed;

R – auger radius;

α – the angle of auger lifting;

f_k – friction coefficient of the seed with the body;

f_{sh} – friction coefficient of the seed with the auger.

The analysis of the change in the intensity of the motion force, depending on the turn lifting angle, indicates that this indicator is a variable quantity and the smallest intensity is in the range $\alpha = 5 - 10^\circ$, and starting with $\alpha = 15^\circ$, the intensity increases in proportion to the angle of lifting the turns of the screw.

RESULTS

The following factors, such as the value of the screw spiral inclination angle, the pressure of the seed to the body, the critical speed of the screw, etc., affect the corn seed injury when the technological processes are carried out by screw conveyors during their inclined or vertical placement.

Studies show that the seed volume between the turns has a linear dependence on the area of the screw cross section, so the analytical dependence for the calculation of seed volume will be:

$$V_n = K_{ob} \cdot D \cdot n_{sh} \quad (2)$$

Where K_{ob} – the coefficient, which depends on the density of the seed and the distance between the turns, that is a step;

D – auger diameter, [m].

n_{sh} – auger speed [r/min.].

These studies suggest that not only the friction force but also the centrifugal force F_c acting on the seed during the rotation of the screw affects the damage of the corn grains (fig. 2).

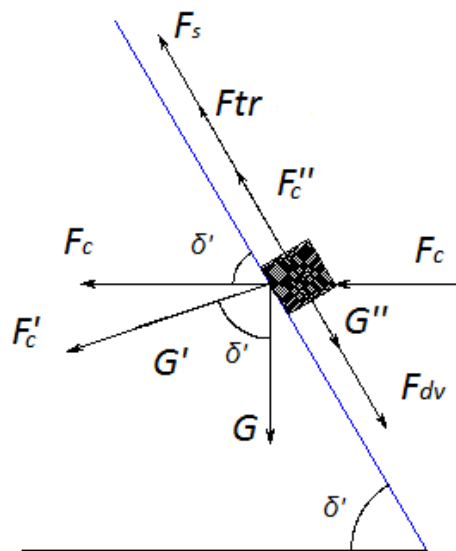


Fig. 2 – Scheme of the influence of forces on the corn grain at the rotation of the auger screw

If we show the forces of action on the corn grains, as the product of pressure on the area, we obtain an equation of the general case that describes the movement of the seed layer in a vertical screw conveyor, taking into account the angular velocity.

On the basis of the forces scheme analysis acting on the corn grains across the turn, we obtain the dependence on the calculation of the effort of pressing the seed to the working surface of the screw and the possibility of its injury (fig. 3).

$$F_{pr} = m \times [\omega_{sh}^2 \times p(\cos \gamma + \sin \gamma \times f_{sh}) + g(\sin \gamma - \cos \gamma \times f_{sh})] \quad (3)$$

Where γ – the angle of inclination of the spindle to the auger axis;

p – the resistivity.

Calculations according to the expression (3) show that the turns inclined from the axis to the periphery of the auger, the growth of the seeds to the body pressing force, compared with the variant, where the turns in the cross section of the auger are horizontal, is 5–38%, depending on the auger speed.

Thus, the expression (3) allows determining analytically the dependence of the angle γ on the friction coefficient of grains with the auger.

Due to the fact that the first component of this formula practically does not depend on the angle γ at the permissible limit of 5° – 20° , the increase in the force of pressing the seeds to the shell will be zero if $\sin \gamma = \cos \gamma \times f_{sh}$ we have:

$$\gamma = \arctg f_{sh} \quad (4)$$

When making an auger, the working surface of the screw is thoroughly treated, the coefficient of the corn grains friction with this surface in the majority will be 0.2–0.3, therefore the proposed inclination angle of the spindle relative to the auger axis will be within 10 – 15° .

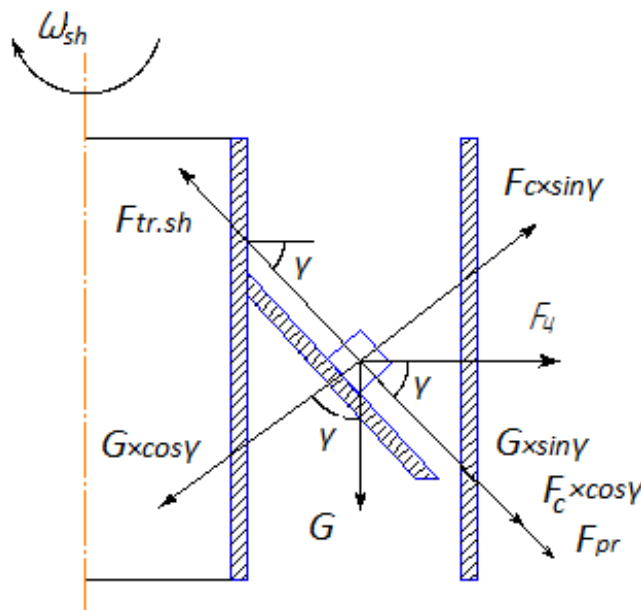


Fig. 3 – Scheme of forces acting on a corn grain on an inclined turn of a screw

As a result of thinning, the corn grain enters the stream in the presence of an under-mature seed, ventilated to accelerate the maturation process and increase the energy of germination and similarity, and in storage, this must be done to preserve the viability of the seed material.

With further movement of air, its ability to enrich with moisture decreases, relative humidity gradually increases and when the equilibrium with the grain is reached, the moisture passes through the rest of the grain mass and does not dry it, while in the upper layers it is possible even to leave the moisture. The grain moisture difference in the upper and lower layers can reach 15%.

Uneven drying of layers for a long time of operation is the main cause of cracks and deterioration of seed quality, which is manifested differently in different cultures. Thus, over-drying in the lower layers can lead to cracks while in the upper layers there will be mould and which generates self-warming, microorganism damage and quality degradation.

Drying of a small height grain layer is provided by heating the outside air with the temperature of the coolant up to 30 – 35°C . A further increase in the temperature of the air may be dangerous, as there may be cracks. Consequently, to obtain high quality seeds it is inadmissible to obtain cracking corn grains, which means that overheating during drying cannot be achieved by maintaining the required air temperature parameters. Maximum permissible temperatures for air heating with active ventilation are given in table 1.

Table 1

Culture	Maximum allowable air temperature during seed drying	
	Temperature at the moisture content of the seeds, %	
	18	24
Barley, oats	56	52
Pea	36	32

This temperature mode in combination with the rate of air consumption to 1000–1500 m³/h. per ton of grain with a thickness of 0.6-0.8 m for grain crops, 0.5-0.6 m for legumes and 0.3–0.5 m for corn grain should form the basis of the technology of drying seeds by active ventilation.

The supply of heated air stops when the average moisture content of the seeds reaches 12–14%, in this case the moisture content of the upper layer, which is dried, reaches 16–18%, while the bottom – 10-12%.

To avoid unwanted drying of grain in the lower layers during the process with the use of heated air, it is necessary to observe the parameters of the treatment layer thickness, the height of which should not exceed 100 cm.

During the drying of barley on the floor dryer, the number of cracks increased by 2–3 %, and the study of Canadians showed that the best quality of the seeds of barley is obtained at a low-temperature mode of drying in a thin layer. To study the temperature-humidity regime, drying of barley was carried out with a humidity of 17.0% at an air temperature of 7–38 °C, a relative humidity of 37–78 % and a velocity of 0.3–0.6 m/s. The results of the obtained data showed that the drying rate had the greatest influence on the temperature of the air, while the humidity of the air had a slight effect on this index.

CONCLUSIONS

To produce high-quality seeds, it is necessary to achieve uniform drying of seed mass layers during the entire technological process. Violation of this requirement will contribute to the formation of cracks, destruction and deterioration of quality indicators. The speed of the screw, pressing the seeds to the body and the angle of the screw spiral also affect the injury of the seed.

To determine the optimal drying conditions, it is necessary to correctly determine the height of the seed layer, the flow rate, air temperature and the corresponding amount of seeds for a certain period of time.

The application of special drying regimes, even longer in time, with a decrease in seeds moisture content of less than 6%, will negatively affect the quality of seeds, especially their similarity.

REFERENCES

- [1] Adamchuk V.V., (2010), Theory of centrifugal robotic organs of machines for applying mineral fertilizers. *Agr. Nauka*, 177 p., Kiev/Ukraine;
- [2] Chazov S.A., Shelepen P., Votsky Z., (1981), Injury of seeds and ways of reduction in mechanized processing, threshing, sorting. *Ukrainian fields*, Vol. 8. pp.41-43, Kiev/Ukraine;
- [3] Chazov S.A., Plaksin V.F., (1974), Research results of a pneumatic installation with a polyethylene pipeline for transportation of seed grain. *Biology and technology of seeds*. pp.16-19. Kharkov/Ukraine;
- [4] Derevyanko D. A., Tarasenko O.P., Orobinsky V.I., (2012), Influence of Injuries on the Quality of Cereal Crop Seeds: Monograph. (Вплив травмування на якість насіння зернових культур: Монографія), *Zhytomyr: Polissya*, 438 p., Zhytomyr/ Ukraine;
- [5] Derevyanko D. A., (2015), Influence of technical means and technological processes on seeds injury and quality: Monograph, (Вплив технічних засобів та технологічних процесів на травмування і якість насіння: Монографія), *Zhytomyr: Polissya*, p.774, Zhytomyr/ Ukraine;
- [6] Drincha V.M., (2006), Seed separation studies and development of machine technologies for their preparation, 382 p., Voronezh/Russia;
- [7] Drincha V. M., Sukonin L. M., (1997), Technology and complex of machines for cleaning grains and seeds, *Agriculture*, Vol. 3, pp. 34-35, Voronezh/Russia;
- [8] Fadeev L.V., (2015), Strong seeds for each field, *SPETS EMM*, 176 p., Kharkov/ Ukraine;
- [9] Fadeev L.V., (2015), Grain cannot be beaten - it is the basis of human life, *SPETS EMM*, 96 p., Kharkov/ Ukraine;
- [10] Golovach I.V., Derevyanko D.A., Derevyanko O.D., (2017), Injury of seeds during drying by technical means, *Allukr Scientific-Technical Journal, Vinnitsa National Agrarian University*, (Всеукр. наук.-технічний журнал, Вінницького національного аграрного університету), Vol. 1 (96), pp. 78-82, Vinnitsa / Ukraine;
- [11] Golovach I.V., Derevyanko D.A., Derevyanko O.D., (2016), Reducing of seeds injury when using rubber materials and improved cleaning. *Allukr Scientific-Technical Journal, Vinnitsa National Agrarian University*, Vol. 3 (95), pp. 26-30, Vinnitsa / Ukraine;

- [12] Goncharov E.S., (1963), *Research on the separation process of grain materials by centrifugal-vibrating sieves*. Dissertation for the academic degree in technical sciences-Abstract, 40 p., Kiev/Ukraine;
- [13] Pugachev A.N., (1976), Grain damage by machines. *Mechanical Engineering*, p. 320, Moscow/Russia;
- [14] Strona I.G., (1974), Injury of grain crop seeds and harvest. *Biology and technology of seeds*, pp.122-129, Kharkov/Ukraine;
- [15] Tarasenko A.P., (2003), Reduction of seeds injury during harvesting and post-harvest processing p. 301, Voronezh/Russia;
- [16] Tishchenko L.N., Olshansky V.P., Olshansky S.V., (2011), Vibro-silicate separation of grain mixtures, *Miskdruk*, p. 280, Kharkov/Ukraine;
- [17] Vasilenko P.M., (1960), Theory of particle motion over rough surfaces of agricultural machines. *To: UASH.*, p. 284, Kiev/Ukraine;
- [18] Zaika P.M., (2006), The theory of agricultural machines, *OKO*, Vol.3, 408 p., Kharkov/Ukraine;
- [19] Zoltzman A., Schmilovitch Z., Mizrach A., (1985), Separating flower bulbs and stones in fluidized bed, *Agricultural Engineering*, Vol. 237, Issue 2, pp. 63-67.

MICROWAVE DEHYDRATION OF SUGAR CUBE: THERMOPHYSICAL INVESTIGATION AND FINITE ELEMENT SOLUTION

آبزدایی از حبه قند با مایکروویو: بررسی ترموفیزیکی و حل المان محدود

Ph.D. Stud. Eng. Hazervazifeh A.¹⁾, Assoc.Prof. Ph.D. Eng. Nikbakht A.M.^{*1)},
Assoc.Prof. Ph.D. Eng. Moghaddam P.A.¹⁾, Assist.Prof. Ph.D. Eng. Sharifian F.¹⁾

¹⁾Department of Mechanical Engineering of Biosystems, Urmia University / Iran
Tel: +98 44 2770555, P.O.Box: 165 ; E-mail: a.nikbakht@urmia.ac.ir

Keywords: sugar cube, finite element method, temperature distribution, moisture removal pattern, colour analysis.

ABSTRACT

Finite element numerical solution was employed to solve coupled model of electromagnetic, heat and mass transfer phenomena in microwave dehydration of sugar cube. For microwave power 880 W, pulsing ratios 1.5, 2.5, 4.5 and 10 were applied to prevent thermal runaway. Colour quality of dried sugar cubes was assessed by calculating whiteness, yellowness and total colour difference. Results revealed that uniform heating as a major issue of drying was improved with pulsing ratio. Moreover, low pulsing ratios yielded to lower colour quality. Thus, preferable pulsing ratio based on heating uniformity and colour quality of dried sugar cube is 10.

چکیده

برای حل مدل ترکیبی الکترومغناطیس، انتقال حرارت و جرمدر فرآیند آبزدایی از حبه قند با استفاده از مایکروویو از روش عددی المان محدود استفاده گردید. توان مایکروویو 880 W انتخاب شد که برای جلوگیری از افزایش بیش از حد دمای حبه قندها در طی فرآیند خشک کردن، نسبت های پالسی 1/5، 2/5، 4/5 و 10 اعمال گردید. کیفیت رنگ محصول خشک شده با محاسبه سفیدی، زردی و اختلاف رنگ کل مورد بررسی قرار گرفت. نتایج نشان داد گرمایش یکنواخت به عنوان یک موضوع مهم در فرآیند خشک کردن، با افزایش نسبت پالسی، بهبود می یابد. از طرفی دیگر نسبت پالسی کم، سبب کاهش کیفیت رنگ محصول خشک شده می گردد. بنابراین نسبت پالسی مطلوب بر اساس گرمایش یکنواخت و کیفیت رنگ حبه قند خشک شده، 10 می باشد.

Nomenclature			
PR	Pulsing ratio	P_V	Conversion of microwave power per unit volume ($W m^{-3}$)
t_{on}	On time cycle microwave power, (s)	f	Frequency (Hz)
t_{off}	Off time cycle microwave power, (s)	ϵ_0	Free space permittivity ($8.85 \times 10^{-12} Fm^{-1}$)
E	Electric field intensity (Vm^{-1})	ϵ'	Dielectric constant
H	Magnetic field intensity (Am^{-1})	ϵ''	Dielectric loss factor
D	Electric displacement ($NV^{-1} m^{-1}$)	D_e	Effective diffusivity
B	Magnetic induction (T)	c	Water concentration ($mol m^{-3}$)
μ	Permeability (Hm^{-1})	x	Depth from the surface of sample (m)
ϵ^*	Complex relative permittivity	$P(x)$	power dissipation value at depth x (W)
ρ	Density ($kg m^{-3}$)	P_0	Incident power at the surface (W)
C_p	Specific heat capacity ($J kg^{-1} K^{-1}$)	β	Attenuation constant (m^{-1})
T	Temperature ($^{\circ}C$)	WI_{CIE}	Whiteness index
t	Drying time (s)	YI_{FC}	Yellowness index
K	Thermal conductivity ($W m^{-1} K^{-1}$)	ΔE^*	Total colour difference with respect to undried sample
ω	Angular frequency (radians s^{-1})		

INTRODUCTION

Sucrose is commercially extracted from cane or beets and then refined to produce the white crystalline grains that is named sugar (deMan, 1999). Sugar cube, is also produced from wetting and pressing sugar crystals. These compressed sugar crystals are then dehydrated to avoid the cube conglutination (Skočllas et al., 2016). Hot air drying is a most common method for dehydrating sugar cubes (Skočllas et al., 2016). In this method, heat transfer is strongly dependent on the conduction and considering the low thermal conductivity of the biological products, penetration of heat into the flesh is regarded as a major concern

increasing the drying period. Therefore hot air flow drying of sugar cube faces major drawbacks such as long drying time and colour degradation of a dried product since thermal damages to the product is directly proportional to temperature and heating time (Akosman, 2004; Kocabiyik and Tezer, 2009). The desire to eliminate these problems convinced researchers to seek new technologies such as microwave dryers to optimize the heat transfer systems (Kassem et al., 2011). This method is gaining popularity in food processing, because of fast heating rate, efficient heat transfer, uniform temperature distribution and high product quality in comparison to conventional heating (Hazervazifeh, Moghaddam, et al., 2016; Karaaslan and Tunçer, 2008). Microwaves are a form of electromagnetic waves within the frequency ranging from 300 MHz to 300GHz and wavelengths ranging from 1 m to 1 mm, respectively (Metaxas and Meredith, 1983). These waves are not in the form of heat but, rather, a form of energy that the absorption of microwaves by a dielectric material results in the microwaves giving up their energy to the material, with a consequential rise in temperature. The two important mechanisms that explain heat generation in a material placed in a microwave field are ionic polarization and dipole rotation that are generally due to collisions between the ions of material and friction between the molecules of material heat is generated (Singh and Heldman, 2001). As mentioned before, microwave heating offers many advantages, so there is a growing interest in industrial microwave systems in respect to microwave heating simulation (Knoerzer et al., 2008; Pitchai, 2011; Romano et al., 2005), comparing microwave drying with hot air drying (Arslan and Musa Özcan, 2010; Gowen et al., 2008; Hazervazifeh, Nikbakht, et al., 2016) temperature distribution analysis in microwave drying (Knoerzer et al., 2008; Vadivambal and Jayas, 2010; Wang et al., 2008), colour analysis of products being dried by microwave (Arslan and Musa Özcan, 2010; Botha et al., 2012; Celen and Kahveci, 2013).

Results in literature indicate that minimum drying time and higher drying rate is revealed in microwave drying in comparison to hot air method. Moreover, microwave drying presented better colour values in the dried products and the colour quality of the product deteriorates significantly with the increase of the microwave power. Furthermore results show that microwave heating is non-uniform and different factors affect the heating uniformity such as food shape and size, dielectric properties of food, microwave power and cycling.

Despite numerous studies on sugar production technologies, there is only a limited number of studies on sugar cube dehydration using mostly hot air flow method (Akosman, 2004; Skočillas et al., 2016). Sucrose melts and forms glucose and fructose anhydride (Levulosan) at 160°C (deMan, 1999). In microwave drying process at a fixed level of microwave power, when almost free water of product is vaporized, product temperature rises sharply; this is known as thermal runaway, due to an increase in the specific microwave energy input (ratio of microwave energy to unit mass of wet product) and a decrease in the specific heat of the product (Botha et al., 2012). Therefore, there is a potential risk of thermal runaway in sugar cube drying process using microwave. Cycling or pulsed radiation is often used to control product temperature and overheating at high and fixed level of microwave powers. Moreover, pulsed heating model is extensively studied (Changrue et al., 2008; Gunasekaran and Yang, 2007; Soysal et al., 2009). The need for improvement in engineering design and process optimization for microwave drying has stimulated the development of computer simulation techniques to predict, electromagnetic field, temperature and moisture distribution in materials (Kadem et al., 2014). Coupled electromagnetic and thermal PDE equations of three-dimensional coordinates with boundary conditions cannot be solved analytically and require iterative numerical methods (Pitchai, 2011). Two methods mainly applied to model the heat transfer are finite difference method (FDM) and finite element method (FEM). FEM has been extensively used to solve the microwave heating process in food due to its flexibility in handling irregular geometrical configurations and material properties, depending on the temperature and moisture (Romano et al., 2005).

The present study furnishes detailed information on the 3-D temperature distribution and moisture removal pattern of microwave sugar cube dehydration. Moreover, colour analysis of dried sugar cube was conducted to determine optimal pulsing ratio for microwave sugar cube dehydration.

MATERIALS AND METHODS

Sample preparation

Sugar cubes (1.5 cm) before dehydration were prepared by a sugar factory in West Azerbaijan Province, Iran, and stored at 4°C in a closed container to avoid demoiurization. Average initial moisture content of the samples in three replications at the temperature of 70°C and vacuum pressure of 1 bar was determined to be 3.23% (wet basis).

Equipment

Sugar cubes were dried with a domestic microwave oven operating at the frequency of 2.45 GHz with pulsed radiation.

Pulsing ratio (on-off ratio)

Pulsing ratio is expressed as Eq. 1 (Sharifian et al., 2012) and summarized in table 1:

$$PR = \frac{(t_{on} + t_{off})}{t_{on}} \quad (1)$$

Table 1

On and Off time cycle microwave power at different pulsing ratios		
Pulsing ratio	On time (s)	Off time (s)
1.5	22	7
2.5	12	17
4.5	6	23
10	3	27

Computer simulation

In this work, Maxwell equations for electromagnetic field were coupled with Fourier's law and Fick's second law for heat and mass transfer, respectively. Subsequently, the coupled model as a set of partial differential equations (PDE) is integrated by Finite Element Method (FEM). The package COMSOL Multiphysics 5.2 was used for the simulations (Knoerzer et al., 2008; Navarrete et al., 2012). Maxwell's equations inside the microwave cavity including the food for constant permittivity and permeability and with no sources can be written as: (Geedipalli et al., 2007).

$$\nabla \times E = -j\omega\mu H \quad (2)$$

$$\nabla \times H = j\omega\varepsilon_0\varepsilon^* E \quad (3)$$

$$\nabla \cdot D = 0 \quad (4)$$

$$\nabla \cdot B = 0 \quad (5)$$

The complex relative permittivity is defined as:

$$\varepsilon^* = \varepsilon' - j\varepsilon'' \quad (6)$$

Fourier's law with microwave term source is expressed as: (Navarrete et al., 2012).

$$\rho C_p \frac{\partial T}{\partial t} = \nabla \cdot (k \nabla T) + P_V \quad (7)$$

The conversion of microwave energy to heat is defined by the following equation (Vadivambal and Jayas, 2010).

$$P_V = \omega \varepsilon_0 \varepsilon'' E^2 = 2\pi f \varepsilon_0 \varepsilon'' E^2 \quad (8)$$

Fick's second law can be written as: (Haghi and Amanifard, 2008).

$$\frac{\partial c}{\partial t} = D_e \nabla^2 c \quad (9)$$

Colour analysis

The colour analysis of the product was conducted by a Hunter Lab colorimeter to obtain some knowledge about the quality of the dried product. Three random readings for undried samples and each treatment (pulsing ratios 10, 4.5 and 2.5) were recorded. Three colour parameters, L*, a*, and b*, were used to study the colour changes. The L* refers to the lightness of the samples and ranges from black = 0 to white = 100. The negative value of a* indicates green, while the positive a* indicates red colours. The positive b* indicates yellow and the negative b* indicates blue colour (Celen and Kahveci, 2013). Whiteness is an important characteristic of many food products as a colour quality. Deviation from whiteness may be perceived as yellowness. These parameters describe the perceptual change of the white and yellowish of colour of the product being processed (Hirschler, 2012). In the food industry, the most frequently used whiteness index is expressed as Eq10: (Judd and Wyszecki, 1963).

$$WI_{JUDD} = 100 - [(100 - L^*)^2 + (a^*)^2 + (b^*)^2]^{\frac{1}{2}} \quad (10)$$

Yellowness index is unduly neglected in the publications and it is reported in a few cases (Hirschler, 2012) which is defined by Eq.11 (Francis and Clydesdale, 1975).

$$YI_{FC} = 142.86 \frac{b^*}{L^*} \quad (11)$$

The total colour difference was also calculated by following equation with respect to the undried product (Celen and Kahveci, 2013).

$$\Delta E^* = \sqrt{(L_{undried}^* - L^*)^2 + (a_{undried}^* - a^*)^2 + (b_{undried}^* - b^*)^2} \quad (12)$$

One way analysis (ANOVA) was conducted to estimate the significant effect of pulsing ratio on the colour quality of the dried products. In addition Dunnett t-test method was applied to comparison of means.

Evaluation procedure

Before experimentation, samples in the closed container were taken out of the fridge to adapt to ambient temperature. Temperature and relative humidity of the ambient were 18°C and 50%, respectively. Experiments were conducted in three treatments with the microwave power of 880 W and pulsing ratios of 1.5, 2.5, 4.5, 10, in three replications, where 1 sugar cube weighing 4.5 g was dried until sample moisture dropped to 0.06% (wet basis). Colour parameters of the dried product were measured and recorded to assess the quality of the dried product. Moreover, temperature distribution and moisture removal pattern of sugar cube were analyzed by spatial simulation contours in COMSOL. Furthermore the Moist sugar cube (3.23% w.b) properties needed for simulation of drying process in COMSOL are calculated from experimental values and listed in Table 2. Specific heat capacity and thermal conductivity were assumed as a function of moisture content of cube. Low moisture content of sugar cube is the main reason of why dielectric parameters can be assumed constant during the drying in spite of their moisture and temperature dependency (Singh and Heldman, 2001).

Table 2

Dielectric and thermal properties of sugar cube		
property	Value	Model
ϵ^* at 2.45 GHz	11.82 - 0.19 j	-
ρ (kg m ⁻³)	1400	-
C_p (J kg ⁻¹ K ⁻¹)	-	1243.12797+(0.79835c)-(0.346451e-3c ²)
K (W m ⁻¹ K ⁻¹)	-	0.24861058013516+ (0.974352e-4c)-(0.422829e-7c ²)

RESULTS

Temperature distribution

Fig.1 presents the spatial distribution of temperature in the sugar cube. As observed, temperature distribution in microwave drying of cubes is intrinsically non-uniform due to the basic non-uniformity of electromagnetic radiation in a medium (Fig.2). However, the general pattern of temperature distribution is analogous in four contours (Fig.1-a, b, c, d).

As the first point, it is evident that the pattern of temperature variation is independent of pulsing ratio and simply the magnitude of temperature is changing. Furthermore, in pulsing ratio of 1.5 which means longer microwave radiation time, a bigger range of minimum-maximum temperature over the body (120°C-170°C respectively) resulted. Therefore, decreased pulsing ratio prolongs microwave radiation and thus temperature and non-uniform heating tend to increase. Technically speaking, in pulsed radiation method, when there is no radiation, variation of product temperature at the radiation period is balanced due to heat transfer, and because of reduced hot spots on the product, temperature differences are minimized. So, higher pulsing ratio gives more chance to conduct the heat over the body. This is in agreement with the findings of Yang and Gunasekaran (2004) (Yang and Gunasekaran, 2004).

It is already accepted that better quality is obtained at uniform and low temperature dried products.

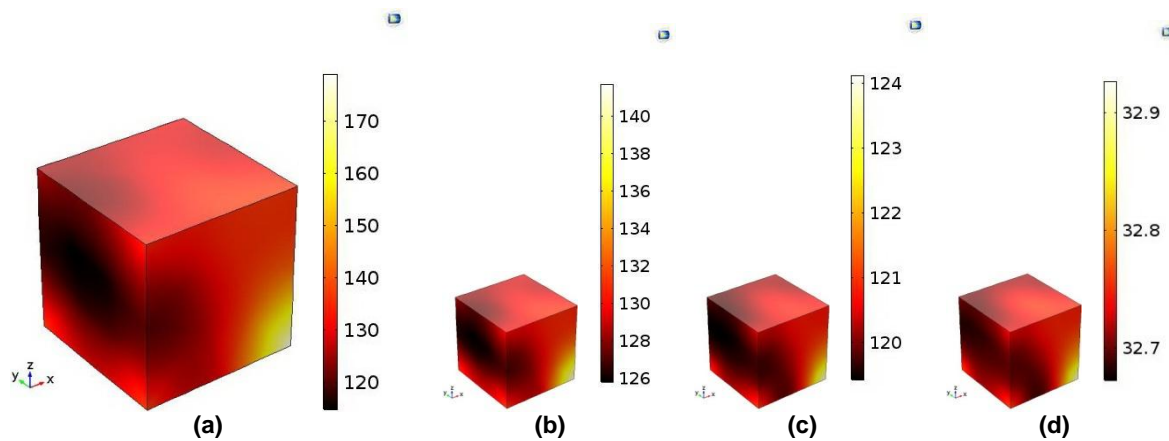


Fig. 1 - Temperature distribution ($^{\circ}\text{C}$) in sugar cube at the end of microwave drying process at different pulsing ratios: a) 1.5, b) 2.5, c) 4.5, d) 10

From Fig.1, it can be conferred that cube corners have the highest temperature values owing to reception of microwave radiation from three faces.

A proof of this claim is reported by Liu et al., 2013. Additionally, the corner exposed to the magnetron lamp benefits the highest temperature rise as it can be seen in Fig.1. This is consistent for moisture removal as shown in Fig.3.

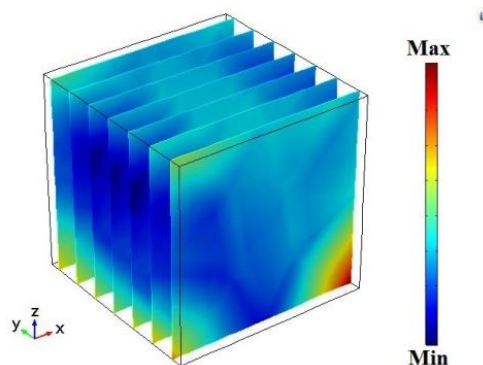


Fig. 2 - Electromagnetic field distribution (Vm^{-1}) in sugar cube at 2.45 GHz frequency and 880 W microwave power

Moisture removal

An important issue to be noted here is that moisture, temperature and electromagnetic distribution patterns in the sugar cube are adaptable due to their strict interactions during the drying (Fig.1, 2, 3). While, as expected, the bottom face of sugar cubes had the highest values of moisture content due to cubes' positioning on the tray. Similar to temperature spatial variation, moisture variation pattern is also independent of pulsing ratios. Fig.3-a and Fig.3-b illustrate the moisture variation of sugars at the beginning and end of the process respectively. The moisture content has been reduced to the desired value, 2.33 molm^{-3} , which is quite comparable with experimentations.

Moisture concentration is further shown in three layers of the product at the end of the process (Fig.3-c). Contours shown in the figures reveal that as we move to the inner layers of the sugar, moisture concentration is higher. The reason is that, if one-dimensional analysis is considered and the incident microwave radiation is assumed to be normal to the surface of cube, the microwave power would be dissipated by the exponential decay of the incident power along that direction as a function of sample depth ($P = P_0 e^{-2\beta x}$) (Yang and Gunasekaran, 2004).

Therefore, microwave power decreases with penetration within the product. This phenomenon is otherwise described; the low effective diffusivity of sugar cube can be stated as the main barrier to mass transfer from the centre zones of the product to outer layers keeping the distribution pattern as detailed in Fig.3-b, c.

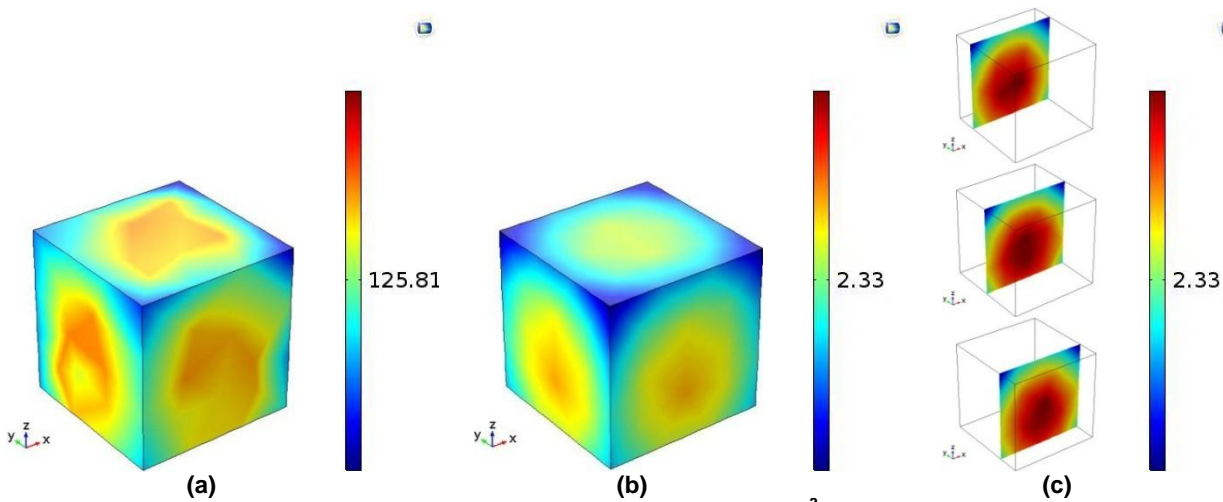


Fig. 3 – Water concentration distribution (mol/m³) in sugar cube at the a) first and b, c) end of microwave drying process

Colour analysis

Table 3 details the average colour features of sugar cubes as indicators of quality during the drying process. Colour has a direct correlation with cosmetic appearance and consumer acceptability. In order to get a better perception of colour features, more commercial parameters have been plotted in Fig. 4.

The analysis of the colour quality can be made according to the similarity of the values of the dried product colour parameters to those of the undried one (Celen and Kahveci, 2013). ANOVA analysis indicated that the effect of pulsing ratio on whiteness, yellowness and total colour difference is significant (p < 0.001).

Table 3

Average colour features for undried and dried sugar cubes using microwave at different pulsing ratios				
Colour feature	Undried sample	Pulsing ratio		
		10	4.5	2.5
L*	90.26	89.49	87.26	86.4
a*	-4.62	-4.76	-4.99	-5.31
b*	5.34	5.4	6.4	12.44

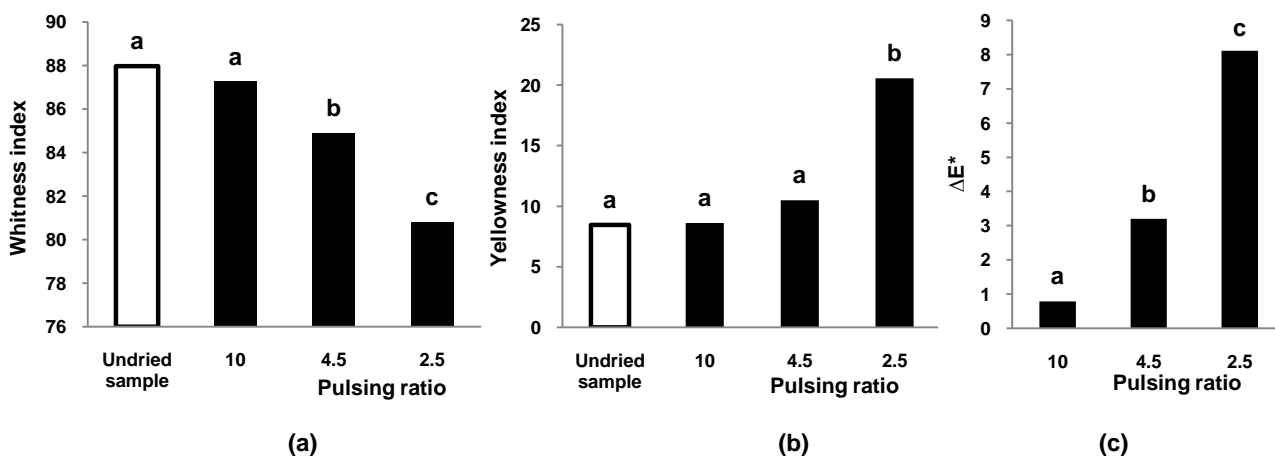


Fig. 4 - Whiteness, yellowness and total colour difference features for undried and dried sugar cubes using microwave at different pulsing ratios.

(Different letters state statistical significance at the 0.05 level using Dunnett t-test)

It is clearly demonstrated that higher pulsing ratio results in better whiteness, yellowness and total colour difference value which simply stated as white cube, less yellow final product and low colour difference to undried one (Fig.4). As inferred from Fig.1, higher radiation time, or lower pulsing ratio, leads to intense

temperature rise and over burning of the cubes which means higher yellowness and worse appearance and marketability. The colour features of the dried sugar cube with pulsing ratio 10 are relatively much closer to those of the undried ones (Fig.4-c). Therefore, it can be inferred that the most preferable pulsing ratio (at 880 W microwave power) relative to colour quality is 10. In addition, yellow spots develop in the product due to burning at the pulsing ratio of 2.5 (Fig.4-b). Therefore, the pulsing ratio higher than 2.5 (at 880 W microwave power) has to be preferred to prevent the product burning and repulsive appearance.

CONCLUSIONS

An integrated electromagnetic-thermal-moisture concentration model has been developed for simulating the microwave drying of sugar cube at different pulsing ratios 1.5, 2.5, 4.5 and 10. The model has been solved with finite element method using COMSOL Multiphysics 5.2. Electromagnetic field, temperature and moisture distribution within sugar cube at the end of drying process were analyzed. Results presented in this study show the maximum absorbed microwave power, and then the highest temperatures and lowest moisture concentration at the corners of cube. Therefore, high interaction between electromagnetic field, temperature and moisture concentration was found in the microwave drying process. Moreover at the bottom corners, moisture concentration was more than top corners due to sugar cube positioning on the tray. Highest temperature heterogeneities occurred at lowest pulsing ratio 1.5. So, decreased microwave radiation reduces heating uniformity. Colour quality of dried sugar cubes was studied by measuring colour features L^* , a^* and b^* and calculating whiteness, yellowness and total colour difference. Results revealed that higher radiation time, or lower pulsing ratio, leads to lower whiteness, higher yellowness, higher total colour difference and worse appearance and marketability. Thus, the preferable pulsing ratio based on colour indices and heating uniformity is 10.

REFERENCES

- [1] Akosman C., (2004), Determination of Drying Characteristics and Effective Diffusivity for Sugar Cubes. *Chemical Engineering & Technology*, Vol.27 (11), pp.1222-1226;
- [2] Arslan D., Musa Özcan M., (2010), Study the effect of sun, oven and microwave drying on quality of onion slices. *LWT-Food Science and Technology*, Vol.43 (7), pp.1121-1127,
- [3] Botha G E., Oliveira J C., Ahrné L., (2012), Microwave assisted air drying of osmotically treated pineapple with variable power programmes. *Journal of Food Engineering*, Vol.108(2), pp.304-311;
- [4] Celen S., Kahveci K., (2013), Microwave Drying Behaviour of Tomato Slices. *Czech Journal of Food Science*, Vol.31(2), pp.132-138;
- [5] Changrue V., Orsat V., Raghavan G S V., (2008), Osmotically dehydrated microwave-vacuum drying of strawberries. *Journal of Food Processing and Preservation*, Vol.32(5), pp.798-816;
- [6] DeMan J M., (1999), *Principles of Food Chemistry* (third ed.). Gaithersburg, Maryland: Aspen Publishers;
- [7] Francis F J., Clydesdale F M., (1975), *Food colorimetry: theory and applications*: AVI Publishing Co. Inc.;
- [8] Geedipalli S S R., Rakesh V., Datta A K., (2007), Modeling the heating uniformity contributed by a rotating turntable in microwave ovens. *Journal of Food Engineering*, Vol.82(3), pp.359-368;
- [9] Gowen A A., Abu-Ghannam N., Frias J, et al., (2008), Modeling dehydration and rehydration of cooked soybeans subjected to combined microwave–hot-air drying. *Innovative Food Science & Emerging Technologies*, Vol.9(1), pp.129-137;
- [10] Gunasekaran S., Yang H-W., (2007), Effect of experimental parameters on temperature distribution during continuous and pulsed microwave heating. *Journal of Food Engineering*, Vol.78(4), pp.1452-1456;
- [11] Haghi A K., Amanifard N., (2008), Analysis of heat and mass transfer during microwave drying of food products. *Brazilian Journal of Chemical Engineering*, Vol.25(3), pp.491-501;
- [12] Hazervazifeh A., Moghaddam P A., Nikbakht A M., (2016), Microwave dehydration of apple fruit: Investigation of drying efficiency and energy costs. *Journal of Food Process Engineering*;
- [13] Hazervazifeh A., Nikbakht A M., Moghaddam P A., (2016), Novel hybridized drying methods for processing of apple fruit: Energy conservation approach. *Energy*, Vol.103, pp.679-687;
- [14] Hirschler R., (2012), *Color in Food. Technological and Psychophysical Aspects*. Boca Raton: Taylor & Francis Group;

- [15] Judd D B., Wyszecski G., (1963), Color in business, science and industry, 3rd Ed., New York, pp.438-461;
- [16] Kadem S., Younsi R., Lachemet A., (2016), Computational analysis of heat and mass transfer during microwave drying of timber. *Thermal Science*, Vol.20(5), pp.1447-1455;
- [17] Karaaslan S N., Tunçer İ K., (2008), Development of a drying model for combined microwave–fan-assisted convection drying of spinach. *Biosystems Engineering*, Vol.100(1), pp.44-52;
- [18] Kassem A S., Shokr A Z., El-Mahdy A R, et al., (2011), Comparison of drying characteristics of Thompson seedless grapes using combined microwave oven and hot air drying. *Journal of the Saudi Society of Agricultural Sciences*, Vol.10(1), pp.33-40;
- [19] Knoerzer K., Regier M., Schubert H., (2008), A computational model for calculating temperature distributions in microwave food applications. *Innovative Food Science & Emerging Technologies*, Vol.9(3), pp.374-384;
- [20] Kocabiyik H., Tezer D., (2009), Drying of carrot slices using infrared radiation. *International Journal of Food Science & Technology*, Vol.44(5), pp.953-959;
- [21] Metaxas A C., Meredith R J., (1983), *Industrial Microwave Heating*: P. Peregrinus, IEE power engineering series. London. 1983;
- [22] Navarrete A., Mato R B., Cocero M J., (2012), A predictive approach in modeling and simulation of heat and mass transfer during microwave heating. Application to SFME of essential oil of Lavandin Super. *Chemical engineering science*, Vol.68(1), pp.192-201;
- [23] Pitchai K., (2011), *Electromagnetic and Heat Transfer Modeling of Microwave Heating in Domestic Ovens*, Thesis for Degree of Master of Science Lincoln, Nebraska: May, 2011;
- [24] Romano V R., Marra F., Tammara U., (2005), Modelling of microwave heating of foodstuff: study on the influence of sample dimensions with a FEM approach. *Journal of Food Engineering*, Vol.71(3), pp.233-241;
- [25] Sharifian F., Motlagh A M., Nikbakht A M., (2012), Pulsed microwave drying kinetics of fig fruit ('Ficus carica'L.). *Australian Journal of Crop Science*, Vol.6(10), pp.1441-1447;
- [26] Singh R P., Heldman D R., (2001), *Introduction to food engineering*: Gulf Professional Publishing.
- [27] Skočillas J A N., Solnař S., Aidossuly M., (2016), Analysis of Cube Sugar Drying in a Convective Dryer. *Czech Journal of Food Science*, Vol.34(5);
- [28] Soysal Y., Ayhan Z., Eştürk O., et al., (2009), Intermittent microwave–convective drying of red pepper: Drying kinetics, physical (colour and texture) and sensory quality. *Biosystems Engineering*, Vol.103(4), pp.455-463;
- [29] Vadivambal R., Jayas D S., (2010), Non-uniform Temperature Distribution During Microwave Heating of Food Materials—A Review. *Food and Bioprocess Technology*, Vol.3(2), pp.161-171;
- [30] Wang S., Luechapattanaorn K., Tang J., (2008), Experimental methods for evaluating heating uniformity in radio frequency systems. *Biosystems Engineering*, Vol.100(1), pp.58-65;
- [31] Yang H W., Gunasekaran S., (2004), Comparison of temperature distribution in model food cylinders based on Maxwell's equations and Lambert's law during pulsed microwave heating. *Journal of Food Engineering*, Vol.64(4), pp.445-453.

EXPERIMENTAL SETUP OF SOLAR DISH COLLECTOR WITH CHANGEABLE STRUCTURE

واحد آزمایشی کلکتور بشقابی خورشیدی با ساختار متغیر

Ph.D. Stud. Eng. Feizolahzadeh M.*¹, Lect. Ph.D. Eng. Modarres Motlagh A.¹, Lect. Ph.D. Eng. Banakar A.²

¹ Urmia University, Department of Mechanical Engineering of Biosystems / Iran;

² Tarbiat Modarres University, Department of Mechanical Engineering of Biosystems / Tehran

Tel: 0989371436521; E-mail: mazynas@gmail.com

Keywords: solar dish collector, optic, changeable structure

ABSTRACT

This paper proposes the design, construction and testing of a solar dish collector with changeable structure and evaluates its overall thermal conversion performance. The changeable parameters of the parabolic dish collector are as follows: focal length of the dish (f), aperture diameter of dish (D), dish rim angle (φ), area of the receiver (A) and concentration ratio (C_R). Results show that the solar dish collector system could reach a power output of 1973 W in a typical setup. Using the mentioned setup, 1 kg of water will be boiled in 2.5 minutes, which is enough to produce 192 kg boiling water per day that will be used at night for greenhouse heating.

چکیده

این مقاله طراحی، ساخت و آزمون یک کلکتور بشقابی خورشیدی را با ساختار متغیر ارائه داده و عملکرد تبدیل حرارت کلی آن را ارزیابی می‌نماید. مشخصه‌های متغیر گیرنده بشقابی سهموی بصورت مقابل هستند: فاصله کانونی بشقاب (f)، قطر دهانه بشقاب (D)، زاویه دهانه بشقاب (φ)، مساحت گیرنده (A) و نسبت تراکم (C_R). نتایج نشان می‌دهد که سیستم کلکتور بشقابی خورشیدی قابلیت دستیابی به توان خروجی 1973 وات در یک نمونه برپا شده را دارا می‌باشد. با استفاده از نمونه برپا شده مذکور، 1 کیلوگرم آب در 2/5 دقیقه به جوش خواهد آمد که برای تولید 192 کیلوگرم آب جوش در روز کافی است که در شب برای گرمایش گلخانه استفاده خواهد شد.

INTRODUCTION

Solar dish collectors (SDC) offer the highest thermal and optical efficiencies of all the current concentrator options (Lovegrove et al., 2011). Solar dish collector (SDC) have been widely used to concentrate solar radiation and convert it into medium or high temperature heat, including solar cooker (Abu-Malouh et al., 2011; Kumar et al., 2012), solar hydrogen production (Furler et al., 2012), and Dish–Stirling system to generate electricity (Mancini et al., 2003; Mills, 2004). Coventry and Andraka (2017) reviewed parabolic dish technology and focused on the evolution of dish design, by examining features such as mode of tracking, structure and mirror design. The review includes a brief summary of power generation options as well as a discussion about options for storage and hybridisation.

Sun is not a point source of light and 0.32° non-parallelism of natural sunlight and imperfections of the collector can provide a reduction in the solar radiation intercepted by the receiver (Stine and Harrigan, 1985). Hence, improving the optical performance is the main step to optimize the SDC (Li et al., 2013).

Considerable theoretical and experimental works on SDC for a large range of industrial applications have been carried out in recent years (Cui et al., 2003; Li et al., 2011; Lovegrove et al., 2011; Reddy and Kumar, 2009; Shuai et al., 2008; Wang and Siddiqui, 2010; Wu et al., 2010a, 2010b; Wua et al., 2010).

Solar dishes are very attractive due to their high concentration ratios and versatility (Poullikkas et al., 2010). High concentration ratios allow to control the thermal losses and therefore to obtain high conversion efficiencies (Andraka and Powell, 2008). Also, conversion efficiencies severely depend on the optical properties of the reflective surfaces. Errors affect the intercept factor, which is defined as the ratio of the energy intercepted by the receiver to the energy reflected by the reflector (Sodha et al., 1984). The ideal optical configuration for the dish concentrator is a paraboloidal mirror which is very expensive to fabricate, its costs increase rapidly with aperture area. However, in practice, it is easier to fabricate a dish concentrator from small elementary mirrors. The elementary components are known as reflecting petals or facets (Kaushika and Reddy, 2000).

During the last decade, several innovations in the design and materials of dish technology have been reported: Glass-metal, Aluminized film, Silver-polymer/silver-steel and Stretched membrane technology. Silvered mirror was adopted as reflective material as it combines both high reflectance and good mechanical properties (Poullikkas *et al.*, 2010). Compared with other mirror types, it is preferred for its high reflectance, good specularity and durability. Rafeeu and Ab Kadir, (2012) presented three experimental models with various geometrical sizes and diameter of about 0.5 m of SDC to analyse the effect of geometry on a solar irradiation and temperature and in maximizing the solar fraction.

According to the effects of optical and geometrical parameters on thermal performance of the concentrating collectors, the aim of this work is to design and manufacture a solar dish collector as an experimental setup with changeable geometrical and optical structure to investigate various parameters which it is impossible with prevalent unchangeable collectors and also to carry out the performance analysis of SDC to heat the water located at the focal point of the concentrator and finally heating a typical greenhouse.

MATERIALS AND METHODS

SOLAR DISH COLLECTOR DESIGN

A common SDC is mainly composed of a parabola provided with an absorber placed by some arms at the focal position. A reflector embedded in a nacelle rotatable around two axes: the horizontal axis (elevation angle) from the support sustained by a mast and the second is the vertical axis (azimuth angle). The SDC is fixed to the ground (Fig.1) and is constructed from small elementary mirrors of square form (Fig.1 and Fig.2). As indicated in Fig.1, the main frame supports the aluminium frame and the optical units have translational movement along aluminium frame to adjust distance between mirrors. Also, the aluminium frame is expandable to provide various aperture diameter of dish for different research applications. Fig.1 shows a row of optical units mounted on the aluminium frame and fixed in appropriate position by a typical holder.

As illustrated in Fig.2 the optical unit consists of three main parts with mirror dimension of 50×50 mm, the arm length varying in the range of 50-400 mm and it is made of wood covered with impermeable layer. The joint connects mirror and arm by two screws and also provide rotational degree of freedom (DOF) along two axes. The optical unit has 5 degrees of freedom that provide precision in adjustment of mirror position (Fig.3) and contrary to constant connection, installing errors were reduced. Also, it is possible to change the number of installed optical units on the main frame, which subsequently results in changing the aperture area of the dish in a wider range.

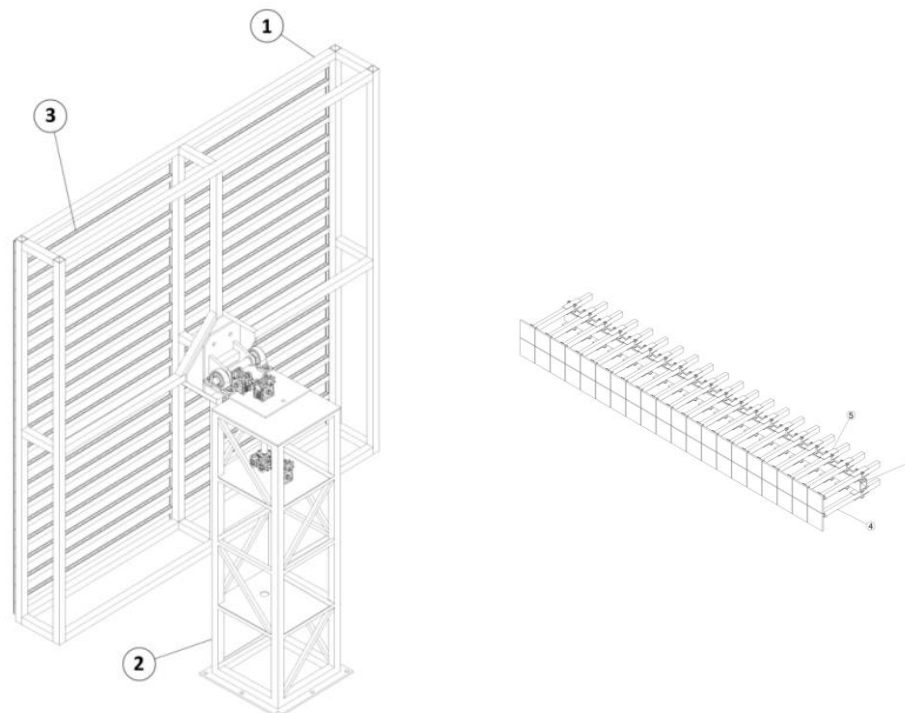


Fig. 1 - Components of SDC

1-main frame; 2- mast; 3- aluminium frame; 4-optical unit; 5-holder; 6-aluminum profile

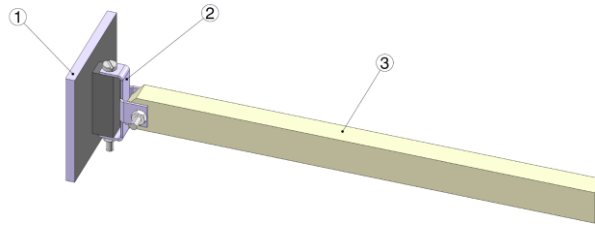


Fig. 2 - Optical unit
1- mirror; 2-joint; 3-arm

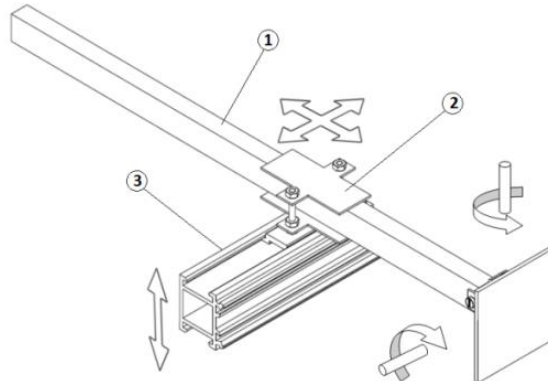


Fig. 3 - Degree of freedom of each unit
1-optical unit; 2-holder; 3-aluminum profile

The characteristics of the SDC (aperture diameter of dish, Depth of the dish and Focal distance) which are changeable are indicated in Table 1. These ranges are enough for an extensive application such as heat and electricity production, researches, etc.

Table 1

Changeable characteristics of the SDC

Parameters	Range
Focal distance (f)	500-2500 (mm)
Aperture diameter of dish (D)	500-4000 (mm)
Depth of the Dish (d)	50-500 (mm)
Aperture area of the dish (A_a)	0.25-16 (m^2)
Entrance aperture area of receiver (A_r)	176.7-706.8(cm^2)
Number of mirrors	100-6400 (unit)

In Fig.4, a pilot model of the assembled SDC illustrates the arrangement of 100 mirrors on main frame with 500 mm dish aperture diameter, 750 mm focal distance and 65 mm of the dish depth.

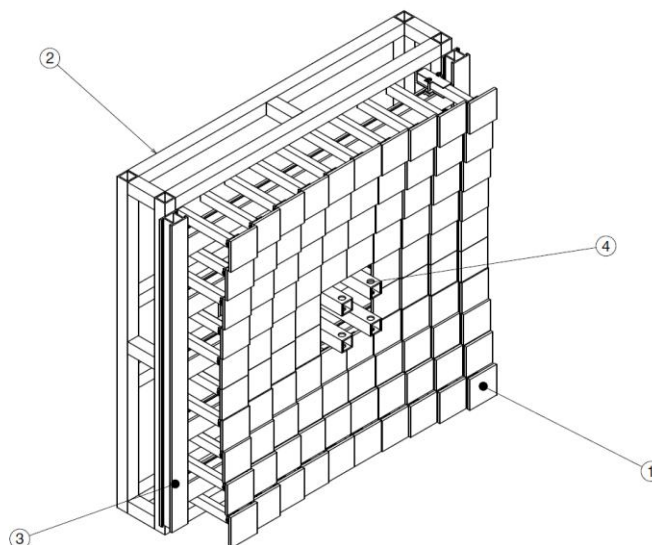


Fig. 4 - Pilot model of changeable collector
1-optical unit 2-main frame 3-aluminium profile 4-receiver joints

SOLAR TRACKING SYSTEM

Basics of solar geometry can be found in several texts on solar energy (Duffie and Beckman, 2013). Two most commonly used configurations in two-axis sun-tracking system are azimuth-elevation and tilt-roll (or polar) tracking system. In an optical mirror mount, azimuth-elevation system is the most popular sun-tracking system used in various solar energy applications (Mousazadeh et al., 2009; Beltran et al., 2007; Georgiev et al., 2004; Luque and Andreev, 2007, Hafez et al., 2017). In the azimuth-elevation tracking, the collector must be free to rotate about the zenith-axis and the axis parallel to the surface of the earth.

The tracking angle about the zenith-axis is the solar azimuth angle and the tracking angle about the horizontal axis is the solar elevation angle (Stine and Harrigan., 1985). The sun altitude or elevations (γ) and sun azimuth (α) define the position of the sun as shown in Fig. 5. The sun altitude is defined as the angle between the centre of the sun and the horizontal seen by the observer. The azimuth angle of the sun describes the angle between geographical north and the vertical through the centre of the sun (Quaschnig, 2005).

Many fast algorithms for the calculation of the solar position, used in engineering application, can be found in the literature. All these algorithms work correctly for limited periods of time. There are high-precision astronomical algorithms, such as the numerical algorithm proposed by Meeus (1988), which has been reviewed in a form suitable for solar application by Reda and Andreas (2004) and is known as SPA (solar position algorithm). This algorithm has a maximal error smaller than 0.0003° for a very long period of time (2000 b.C.–6000 a.C.), but it requires a large amount of calculations.

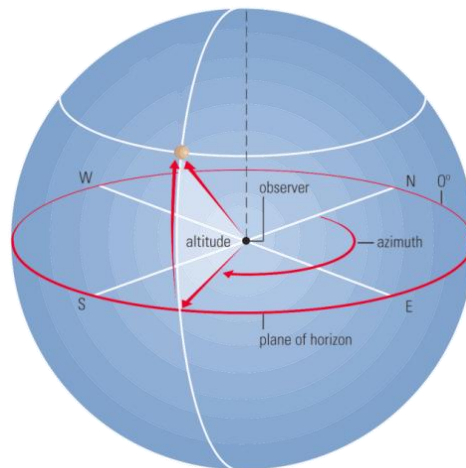


Fig. 5 - Position of the sun

- **Solar azimuth angle**

For a specific longitude and altitude the sun begins a race from east to west. This is the angle between the line that points to the sun and south. The angle is negative to the east and positive to the west. This angle is 0° at noon. It is probably close to -90° at sunrise and 90° at sunset, depending on the season. The azimuth angle is calculated according to the following equation (Chassériaux, 1979):

$$\sin \alpha = \frac{\cos \delta \sin \omega}{\cos h} \quad (1)$$

- **Solar altitude angle**

The solar altitude angle is the angle between the line that points to the sun and the horizontal. It is the complement of the zenith angle. This angle is 0° at sunrise and sunset. The altitude angle is calculated using to the following equation (Chassériaux, 1979).

$$\sin h = \cos \varphi \cos \delta \cos \omega + \sin \varphi \sin \delta \quad (2)$$

Two axes sun tracking system

The solar tracking system consists of four parts: mechanical design, electrical design, electronic design and a control program. In this work an algorithm for the computation of the solar position with high precision (maximal error 0.0027° over the period 2003–2023) and of small complexity are used which are presented by Grena (2008). This precision is enough for a wide range of solar applications.

FOCAL RECEIVER

The focal absorber receives the concentrated solar radiation and transforms it to thermal energy to be used in a subsequent process (Kaushika and Reddy, 2000). The basic feature of a receiver is to absorb the maximum amount of the reflected solar energy and transfer it as heat, with minimum losses, to the working fluid. A cavity receiver is used to accomplish this purpose. The position of cavity receiver should be varying to achieve the preferred performance of collector in different setups. Hence, a cavity receiver with a glass window or not is studied and mounted on a rail to provide transitional motion in direction of collector axis (Fig. 6).

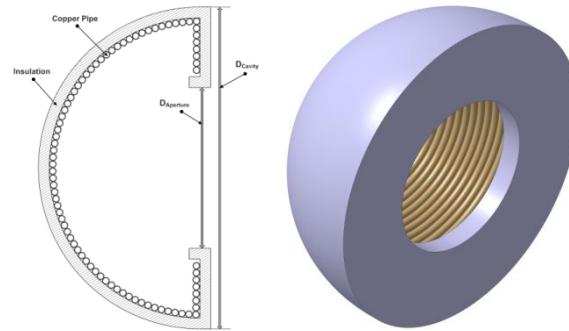


Fig. 6 - Cavity receiver

EXPERIMENTAL SETUP

The changeable parameters of the parabolic dish collector system are as follows: focal length of the dish (f), aperture diameter of dish (D), dish rim angle (φ), area of the receiver (A) and concentration ratio (C_R). The fundamental parts of the experimental SDC are: the solar concentrating system, the absorber (solar heat exchanger), the data acquisition system, instrumentation and solar tracking system (Fig. 8).

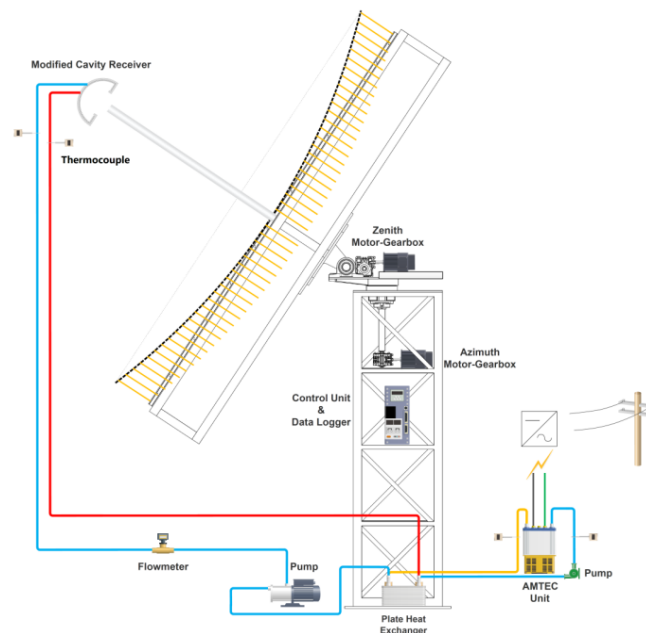


Fig. 7 - Schematic of experimental setup of changeable solar dish collector

OPTICAL CALIBRATION

The diode technique, a simple and cheap method, consists of a laser diode that emits a narrow beam that is made to be incident onto the reflecting surface of the dish. The diode emits light in the wavelength range of 640–660 nm. Mlatho et al. (2010) showed that a laser diode technique, which is relatively cheap when compared to the radiometer technique, can be used to determine the spatial extent of the focal point with fairly good accuracy. In this study laser beam is used to be assured that reflected ray incident on focal point. For this purpose, a laser beam source placed parallel to collector axis and the entire mirrors adjusted manually and fixed in appropriate position by two screws. This method not only provides a changeable structure but also increases the precision of concentration.

RESULTS

The concentration ratio (C) is defined as the ratio of the aperture area (A_a) to the entrance aperture area of receiver or absorber area (A_r); (Duffie and Beckman, 2013). The area concentration ratio is:

$$C_R = \frac{A_a}{A_r} \quad (3)$$

The results showed that the concentration ratio in the range of 3.5-800 is achievable. It is possible by changing the receiver area through different dimension of cavity aperture.

The useful heat delivered by a solar collector system was prepared according to the procedure used by Wu *et al.* (2010a) under steady state conditions and is equal to the energy absorbed by the heat transfer fluid, which is determined by the radiant solar energy falling on the receiver minus the direct or indirect heat losses from the receiver to the surroundings. That is,

$$\dot{Q}_u = \dot{Q}_r - \dot{Q}_l \quad (4)$$

Where \dot{Q}_u is the rate of useful heat gain, \dot{Q}_r and \dot{Q}_l are radiation falling on the receiver and total heat loss rate of the receiver respectively.

The radiant solar energy falling on the receiver can be defined as:

$$\dot{Q}_r = \eta_0 \dot{Q}_s \quad (5)$$

Where η_0 is the optical efficiency of concentrator and is defined by Wu *et al.* (2010a) as:

$$\eta_0 = \Gamma \tau \alpha \rho \gamma \cos \theta \quad (6)$$

where Γ is the factor of un-shading, ρ is dish reflectance, $\tau \alpha$ is transmittance–absorptance product, γ is the intercept factor of receiver, which is defined as the ratio of the energy intercepted by the receiver to the energy reflected by the focusing device, i.e. parabola dish, θ is angle of incidence. As the solar parabolic dish concentrator maintains its optical axis, always pointing directly towards the sun to reflect the beam, which means the incidence angle of solar beam into the dish is zero degree, and the cosine loss equals to zero (Palavras and Bakos, 2006). That is:

$$\eta_0 = \Gamma \tau \alpha \rho \gamma \quad (7)$$

A clean mirror made of low-iron glass with a silver back-coat should provide a reflectivity (ρ) of 90–94% (Kribus *et al.*, 2006). In this study, a transparent window is placed at the receiver entrance to reduce heat losses, hence the transmission–absorption loss of the receiver is assumed to have about 6–12% loss.

$$\Gamma = \frac{A_a - A_r}{A_a} \quad (8)$$

Based on the analysis above, the optical efficiency used in the current study, including all of these losses, is then assumed as a value of 0.847, which is close to the representative value of 0.85 reported in (Kribus *et al.*, 2006; Feuermann and Gordon, 2001; Wu *et al.*, 2010a).

The net solar heat transferred Q_s is proportional to A_a , and the direct normal insolation (DNI) per unit of collector area I_s :

$$\dot{Q}_s = I_s A_a \quad (9)$$

Substituting Eq. (6 and 5) into Eq. (4):

$$\dot{Q}_u = \dot{Q}_r - \dot{Q}_l = \eta_0 \dot{Q}_s - \dot{Q}_l = \Gamma \tau \alpha \rho \gamma I_s A_a - \dot{Q}_l \quad (10)$$

The total heat loss rate includes three parts and can be expressed as:

$$\dot{Q}_l = \dot{Q}_{lk} + \dot{Q}_{lc} + \dot{Q}_{lr} \quad (11)$$

where \dot{Q}_{lk} , \dot{Q}_{lc} , \dot{Q}_{lr} are Conduction, Convection and Radiation heat loss, respectively.

Researches show that the conductive loss is normally insignificant, compared to the convection and radiation losses (Wu *et al.*, 2010a). Therefore, $\dot{Q}_{lk} = 0$ convection heat loss is a major contributor to the total energy loss. Hence, its characteristic has been extensively investigated and various models have proposed to predict convection heat loss of cavity receivers (Le Quere *et al.*, 1981, Koenig and Marvin 1981, Siebers and Kraabel, 1984, Clausing, 1987, Stine and McDonald, 1989, Paitoonsurikarn *et al.*, 2004, Azzouzi *et al.*, 2016). As in this study, a transparent window is installed at the receiver aperture, thus natural convection heat loss becomes the dominant loss. Finally, the equations applied by Paitoonsurikarn *et al.* (2004) and Wu *et al.*, (2010a) are used to evaluate convective and radiation heat loss from the receiver. Finally, for a typical setup the following results were obtained (Table 2):

Table 2

Changeable characteristics of the SDC and achieved results

Parameters	value
Focal distance (f)	1250 (mm)
Aperture diameter of dish (D)	2000 (mm)
Depth of the Dish (d)	190 (mm)
Aperture area of the dish (A_a)	3.68 (m ²)
Entrance aperture area of receiver (A_r)	314.16(cm ²)
Number of mirrors	1600 (unit)
I_s	700 (w/ m ²)
\dot{Q}_s	2576 (w)
η_0	0.847
\dot{Q}_r	2183 (w)
\dot{Q}_l (max)	210 (w)
\dot{Q}_u	1973 (w)

It results from table 3 that the obtained value of \dot{Q}_u is high enough to boiling water with a rate of 0.397 kg/min. In other words, with the mentioned setup we can produce 1 kg hot water (100°C) in 2.5 minutes.

APPLICATION IN GREENHOUSE

The easiest and most common way to even out the temperature of greenhouse is to use thermal mass, also called a heat sink. The size of the thermal mass depends on the heat capacity of the material and it's mass. The most common way to use thermal mass is water, because it has such a high heat capacity (4.18 J/cm³K at 77 F). Using the designed Collector, we were able to control the greenhouse temperature in recommended range during April to October in West Azerbaijan, Urmia. In this study, a 250m² greenhouse with twin-wall polycarbonate considered (Fig. 8). The recommended temperature in greenhouse is 22°C.



Fig. 8 - Spanish design greenhouse, Urmia University, Agricultural Faculty

According to 10 years metrological data of Urmia, the monthly average temperatures are presented in Table 3. Also, the solar power incident on a surface averages 700 W/m² and 10 years average 8.5 sun hours. It is shown in this table that during April to October the average temperature is about 10 degrees below the recommended temperature in greenhouse. So, the calculation is based on $\Delta T=10^\circ$.

Table 3

Monthly average temperature, Urmia

Year	Jan	Feb	Mar	Apr	May	Jun	Jul	Aug	Sep	Oct	Nov	Dec
2004	0.4	1.8	7.8	9.9	14.8	20.4	22.1	23.2	18.4	13.3	5.9	-2.6
2005	-2.7	-2.1	6.5	12.2	15.2	20.3	24.8	23.6	18.9	12.3	5.3	2.4
2006	-2.7	0.8	7	12.2	16.3	23.1	23.5	24.7	18.7	13.2	3.6	-2.7
2007	-4.2	0.6	4.9	9	17.4	21.1	23.3	23.3	19.8	13	6.5	-0.4
2008	-7.3	-2.7	9.9	14.3	15.9	21.3	24.4	24.4	18.9	12.3	5.6	0.2
2009	-2.4	3.5	5.9	9.5	16.2	19.6	23.3	21.5	16.9	12.9	5.9	2.9
2010	2.8	3.8	8.5	11	15.5	22.7	25.3	23.3	20.5	14.6	6.2	2.3
2011	-2.8	0.9	5.4	11.6	15.6	21.2	24.9	22.8	18.1	11	1.3	-1.7
2012	-1.1	-0.6	2.6	12.9	17.5	22	23.9	24.6	18.9	13.4	7.6	0.6
2013	-0.4	3.8	7.4	12.2	15.4	20.9	24	22.8	19	11.2	7.3	-5.9
2014	-2.5	0.8	8	12.6	17.3	21.8	24.9	25	20.1	11.4	4.4	2.2

Considering 250m² greenhouse, a gas heater consumes 6 m³/h fuel, that its annual amount will be 25920 m³ gases. Taking into account the cost of the gas as 0.072\$/m³ in Iran, the annual cost will be 1866 \$. However, the total cost estimate of the proposed experimental setup of collector is 1750 \$. The results obtained from the preliminary calculations of useful heat delivered by a solar collector system are presented in

Table 2. For 8.5 hours received solar energy is:

$$700 \text{ W/m}^2 \times 8 \text{ hours} = 5600 \text{ Wh/m}^2 = 5.6 \text{ kWh/m}^2 = 5.6 \text{ PSH (Peak Sun Hours)}$$

According to results we produced 192 kg boiling water that will be used at night. It starts releasing that energy, thereby 'heating' the greenhouse.

CONCLUSIONS

This project was undertaken to design an experimental setup to investigate the effect of geometrical parameters on optical and thermal performance of a solar dish collector and evaluate its application. The characteristics of the SDC such as aperture diameter of dish, depth of the dish, focal distance and cavity area are changeable. This experimental setup has assembly and disassembly capability and can act as a research tool to investigate different configurations of SDC systems. Also different type of receivers, parabolic dishes and other type of collectors can be tested by the experimental setup and it can be used as a main structure for any type of collectors for solar applications. The major limitation of this study is the mirror sizes, which limited to 5×5cm mirrors. Useful heat delivered by solar collector system is 1973 W which is enough to produce 192 kg boiling water per day. Produced water will store in thermal mass that will be used at night for heating the greenhouse. This research will serve as a base for the future studies and for domestic solar thermal applications like indoor solar cooking and indoor solar water heating or electricity generation. This device can be used for different applications like desalination, pasteurization, detoxication and vapour production by adjustment of the working fluid flow through receiver. Taken together, these wide ranges of investigations suggest that the cost of experimental setup in comparison with its applications is justifiable. This would be a fruitful area for further works.

REFERENCE

- [1] Abu-Malouh A., Abdallah S., Muslih I. M., (2011), Design, construction and operation of spherical solar cooker with automatic sun tracking system. *Energy Conversion and Management*, vol.52, pp.615–620;
- [2] Andraka C.E., Powell M.P., (2008), Dish stirling development for utility scale commercialization, *14th Biennial CSP SolarPACES Symposium*, Las Vegas, NV;
- [3] Azzouzi D., Boumeddane B., Abene A., (2016), Experimental and analytical thermal analysis of cylindrical cavity receiver 1 for solar dish, *Renewable Energy*, vol.106, pp.111-121, Elsevier;
- [4] Beltran JA, Gonzalez Rubio JLS, Garcia-Beltran CD., (2007), Design, manufacturing and performance test of a solar tracker made by an embedded control, *Electronics, robotics and automotive mechanics conference*, pp.129–34;
- [5] Chassériaux J.M., (1979), *Thermal conversion of solar radiation*. French Agency for Energy Control, France;
- [6] Chong KK, Wong CW., (2009), General formula for on-axis sun-tracking system and its application in improving tracking accuracy of solar collector. *Solar Energy*; vol.83, pp.298–305;
- [7] Clausing AM, Waldvogel JM, Lister LD., (1978), Natural convection from isothermal cubical cavities with a variety of side-facing apertures, *ASME J Heat Transfer*, vol.109(2), pp.407–12;
- [8] Coventry J, Andraka C., (2017), Dish systems for CSP, *Solar Energy*, vol.152, pp.140-170, Elsevier;
- [9] Cui H, Yuan X, Hou X., (2003), Thermal performance analysis for a heat receiver using multiple phase change materials. *Applied Thermal Engineering*, vol.23, pp.353–361;
- [10] Duffie J.A., Beckman W.A., (2013), *Solar engineering of thermal processes*. John Wiley & Sons, Inc.
- [11] Feuermann D, Gordon J.M., (2001), High-concentration photovoltaic designs based on miniature parabolic dishes. *Sol Energy*; vol.70(5), pp.423–430;
- [12] Furler P., Scheffe J.R., Steinfeld A., (2012), Syngas production by simultaneous splitting of H₂O and CO₂ via ceria redox reactions in a high-temperature solar reactor. *Energy & Environmental Science*, 5 (3), pp.6098–6103;
- [13] Georgiev A, Roth P, Boudinov H., (2004), Design and construction of a system for sun tracking. *Renewable Energy*; 29, pp.393–402;

- [14] Grena R., (2008). An algorithm for the computation of the solar position. *Solar Energy* 82 (2008) 462–470;
- [15] Hafez A.Z., Soliman A., El-Metwally K.A. Ismail I.M., (2017); Tilt and azimuth angles in solar energy applications – A review. *Renewable and Sustainable Energy Reviews* 77, pp.147–168;
- [16] Hein M, Dimroth F, Siefer G, Bett AW., (2003), Characterisation of a 300 photovoltaic concentrator system with one-axis tracking. *Solar Energy Materials & Solar Cells*; vol.75, pp.277–283;
- [17] Kaushika N.D., Reddy K.S., (2000), Performance of a low cost solar paraboloidal dish steam generating system. *Energy Convers Manage*, 41(7), pp.713–726;
- [18] Koenig A.A., Marvin M., (1981), Convection heat loss sensitivity in open cavity solar receivers. Final report, DOE Contract No: EG77-C-04-3985, *Department of Energy*, USA;
- [19] Kribus A., Kaftori D., Mittelman G., Hirshfeld A., Flitsanov Y., Dayan A., (2006). A miniature concentrating photovoltaic and thermal system. *Energy Convers Manage*; vol.47(20), pp.3582–3590;
- [20] Kuma N., Vishwanath G., Gupta A., (2012), An exergy based unified test protocol for solar cookers of different geometries. *Renewable Energy*, vol.44, pp.457-462;
- [21] Le Quere P., Penot F., Mirenayat M., (1981), Experimental study of heat loss through natural convection from an isothermal cubic open cavity. *Sandia National Laboratories Report*, SAND81-8014;
- [22] Li Z, Tang D, Du J, Li T., (2011), Study on the radiation flux and temperature distributions of the concentrator–receiver system in a solar dish/Stirling power facility. *Applied Thermal Engineering*; 31:1780–9;
- [23] Li H., Huang W., Huang F., Hub P., Chen Z., (2013), Optical analysis and optimization of parabolic dish solar concentrator with a cavity receiver. *Solar Energy*, 92, pp.288–297;
- [24] Lovegrove K, Burgess G, Pye J., (2011), A new 500 m² paraboloidal dish solar concentrator. *Solar Energy*; 85:620–6;
- [25] Luque A., Andreev V., (2007), *Concentrator photovoltaics*. Berlin Heidelberg, New York: Springer,;
- [26] Mancini T., Heller P., Butler B. et al., (2003). Dish–Stirling systems: an overview of development and status. *Journal of Solar Energy Engineering-Transactions of the ASME* 125 (2), pp.135–151;
- [27] Meeus J., (1988), *Astronomical Algorithms*, second ed. Willmann-Bell Inc.;
- [28] Mills D., (2004), Advances in solar thermal electricity technology. *Solar Energy*, 76 (1–3), pp.19–31;
- [29] Mlatho J.S.P., McPherson M., Mawire A., Van den Heetkamp R.J.J., (2010), Determination of the spatial extent of the focal point of a parabolic dish reflector using a red laser diode. *Renewable Energy* 35, pp.1982–1990;
- [30] Mousazadeh H., Keyhani A., Javadi A., Mobli H., Abrinia K., Sharifi A., (2009), A review of principle and sun-tracking methods for maximizing solar systems output. *Renewable and Sustainable Energy Reviews*; 13:1800–18;
- [31] Paitoonsurikarn S., Taumoefolau T., Lovegrove K., (2004), Estimation of convection loss from paraboloidal dish cavity receivers. In: *Proceedings of 42nd conference of the Australia and New Zealand solar energy society (ANZSES)*, Perth, Australia;
- [32] Palavras I., Bakos G.C., (2006), Development of a low-cost dish solar concentrator and its application in zeolite desorption. *Renewable Energy*; 31(15):2422–31;
- [33] Poullikkas A., Kourtis G., Hadjipaschalis I., (2010), Parametric analysis for the installation of solar dish technologies in Mediterranean regions. *Renewable and Sustainable Energy Reviews* 14, pp.2772–2783;
- [34] Quaschnig V., (2005), *Understanding renewable energy systems*. UK: Bath Press;
- [35] Rafeeu Y., Kadira M., (2012), Thermal performance of parabolic concentrators under Malaysian environment: a case study. *Renewable and Sustainable Energy Reviews*; 16: 3826–3835;
- [36] Reda I., Andreas A., (2004), Solar position algorithm for solar radiation applications. *Solar Energy* 76 (5), 577–589;
- [37] Reddy K.S., Kumar N.S., (2009), An improved model for natural convection heat loss from modified cavity receiver of solar dish concentrator. *Solar Energy*; 83:1884–92;
- [38] Shuai Y., Xia X., Tan H., (2008), Radiation performance of dish solar concentrator/cavity receiver systems. *Solar Energy*; 82:13–21;
- [39] Siebers D.L., Kraabel J.S., (1984), Estimating convective energy losses from solar central receivers. *Sandia National Laboratories Report*, SAND 84-8717;
- [40] Sodha M.S., Mathur S.S., Malik M.A.S., (1984), *Review of Renewable Energy Resources*, vol. 2. Wiley Eastern Ltd;

- [41] Stine W.B., Harrigan R.W., (1985), *Solar energy fundamentals and design*. first ed. New York: Wiley Interscience;
- [42] Stine W.B., McDonald C.G., (1989), Cavity receiver convective heat loss. In: *Proceedings of the international solar energy society (ISES) solar world conference*, Kobe, Japan;
- [43] Wang M., Siddiqui K., (2010), The impact of geometrical parameters on the thermal performance of a solar receiver of dish-type concentrated solar energy system. *Renewable Energy*, 35:2501–13;
- [44] Wu S., Xiao L., Cao Y., Li Y., (2010a), A parabolic dish/AMTEC solar thermal power system and its performance evaluation. *Applied Energy*, 87:452–62;
- [45] Wu S., Xiao L., Cao Y., Li Y., (2010b), Convection heat loss from cavity receiver in parabolic dish solar thermal power system: a review. *Solar Energy*, 84:1342–55;
- [46] Wua Z., Caliot C., Bai F., Flamant G., Wang Z., Zhang J., Tian C., (2010), Experimental and numerical studies of the pressure drop in ceramic foams for volumetric solar receiver applications. *Applied Energy*, 87:504–13.

MACHINING METHOD WITH EVENLY DISTRIBUTED ALLOWANCE BASED ON THE NORMAL LINKAGE MODEL OF NON-CIRCULAR GEAR SHAPING

基于法向插削联动模型的非圆齿轮齿面余量匀化加工方法

As. Ph.D. Stud. Eng. Gao T.¹⁾, Prof. Ph.D. Eng. Han J.¹⁾, Ph.D. Eng. Tian X.Q.^{1,2)}, Prof. Ph.D. Eng. Xia L.^{*1)}

¹⁾ School of Mechanical Engineering, Hefei University of Technology, Hefei / China; ²⁾ S. M. Wu Manufacturing Research Centre, University of Michigan, Ann Arbor / United States
Tel: +8615905697463; E-mail: hfutgt@163.com

Keywords: non-circular gear, shaping, normal linkage model, micro-topography

ABSTRACT

Non-circular gears are important parts of agricultural machinery, such as transplanters and plant setters. The uneven distribution of allowance in the machining process seriously affects the machining accuracy and working performance of non-circular gears. Therefore, this study considered non-circular gear shaping as the research subject to solve the uneven distribution of allowance caused by the change of the curvature of the gear blank's pitch curve in non-circular gear machining. The influence of the radial motion on allowance distribution was determined by analyzing the geometric relationship between the shaper cutter and the gear blank in the machining process. Then, a normal linkage model of non-circular gear shaping was established, and the virtual and actual machining experiments were conducted. Finally, the machining method with evenly distributed allowance was simulated and validated. Results of the machining and testing show that the average unevenness of the allowance can be reduced from 110.21% to 4.95% through the machining method with evenly distributed allowance, meanwhile, the surface roughness S_a can be reduced from 3.18 μm to 1.26 μm . The proposed machining method can evenly distribute the allowance in the machining process, as well as remarkably improve the machining accuracy and surface quality of non-circular gears. The conclusions of this study provide significant references for the optimization and performance evaluation of non-circular gear machining methods.

摘要

非圆齿轮是取苗机、移栽机等农用机械的重要零件，其在加工过程中存在齿面余量分布不均问题，严重影响齿轮的加工精度与工作性能。因此，针对非圆齿轮加工中由齿坯节曲线曲率变化所引发的齿面余量分布不均问题，本文以非圆齿轮插齿加工为例，分析了加工过程中刀具与齿坯的几何位置关系，得到了径向进给运动对齿面余量分布的影响关系，建立了非圆齿轮法向插削联动模型，并进行了虚拟加工和实际加工试验，验证了齿面余量匀化加工方法。加工与检测结果表明，采用齿面余量匀化加工方法可将齿面余量不均匀度均值由110.21%降低至4.95%，齿面粗糙度 S_a 由3.18 μm 降至1.26 μm ，该方法能够有效均布非圆齿轮齿面余量，并显著提高非圆齿轮加工精度与表面质量。研究成果可以为非圆齿轮加工方法的优化和性能评估提供参考依据。

INTRODUCTION

Non-circular gears synthesize the advantages of circular gears and cam mechanisms and can be designed according to the working requirements to realize the variable ratio drive; these gears have the advantages of compact structure, stable transmission, and easy realization of dynamic balance, all of which are important parts of agricultural machinery (G.H. Yu et al., 2015; M. Zhou et al., 2014). The machining accuracy of non-circular gears determines the accuracy and durability of the transmission mechanism, so that improving the accuracy of non-circular gears is an important method for ensuring the working accuracy and service life of agricultural machinery products (Pathak S et al., 2014).

Gear hobbing and shaping are the common machining methods of non-circular gears. Gear hobbing is efficient but can only be used for non-circular gears with full convex pitch curves and is easy to undercut (B. Li et al., 2016). By contrast, gear shaping is a general method of non-circular gear machining that can overcome the limitations of gear hobbing. It can be used for non-circular external gears with concave pitch curves and non-circular internal gears and has high machining efficiency. In non-circular gear shaping, the pitch curve of the gear blank and the pitch circle of the shaper cutter in actual rough shaping are changed because of the constant change of the curvature of the gear blank's pitch curve (X.T. Wu and H.G. Wang, 1997), thus, the uneven machining allowance appears. In actual machining, the uneven allowance on each tooth surface can cause unequal cutting force and cutting vibration, which has a serious influence on the

service life of machines and the machining quality of gears (Y. Zhang, 2015). If the allowance on one side of the tooth surface is small or non-existent, then finish machining (finish shaping, grinding, and skiving) cannot be performed efficiently and the gear blank will likely be scrapped (X.T. Wu and H.G. Wang, 1997).

Based on this scenario, certain researchers conducted numerous analyses and studies on the machining principle and process of non-circular gear shaping. Litvin analyzed the generation process of the enveloping surface of an elliptical gear and proposed a matrix method to solve the involute equation. Then, he used a rack cutter, a hob, and a shaper as examples to illustrate the proposed method and established a machining theory of non-circular gears. However, the performances of the machining methods are disregarded (Litvin F et al., 2007). Zheng established the linkage model of non-circular gear shaping based on three-axis machine tools, discussed the machining process of non-circular gears, and suggested a general shaping method. However, the different linkage models are not analyzed comparatively (F. Zheng et al., 2017; F. Zheng et al., 2016). Xia deduced the mathematical model of non-circular gear meshing based on pure rolling contact theory and conducted the equal pole angle and arc length shaping simulations by setting different pole angles. However, the performances of the shaping methods are also ignored (L. Xia et al., 2013). Liu proposed a variety of shaping strategies by adjusting the speed relationship between the shaper cutter and the gear blank, conducted the machining experiments, and then selected the optimal speed linkage model. However, the influences of the machining methods on machining accuracy are disregarded (Y.Y. Liu, 2014). He J. installed the form-grinding wheel on a three-axis gear shaper and proposed a machining strategy to control the form-grinding process according to the linkage model of non-circular gear shaping. His work provided a method for realizing the finish machining on the non-circular gear shaper. However, this strategy is unverified by simulation or machining experiments (J.L. He et al., 2007). Erkorkmaz proposed a linkage model that could accurately predict the chip shape and the cutting force. Therefore, the contact between the shaper cutter and the cylindrical gear was predicted based on the DEXEL model, and the linkage model was verified by kinematics modeling. However, the meshing process of non-circular gears is more complicated, and optimizing the machining accuracy of non-circular gears through this method is difficult (Erkorkmaz K et al., 2016). Tarapanov analyzed the kinematic parameters of non-involute internal gear in the shaping process and studied the effect of the tool root contour on machining accuracy in terms of cutting thickness, cutting force component and surface roughness. However, the method for improving machining accuracy is not proposed (Tarapanov A et al., 2015).

All these research results are mainly concerned with the realization of non-circular gear machining and the processing technology of cylindrical gear machining. However, research on the processing technology of non-circular gear machining is minimal, especially the influences of the machining methods on distributing allowance and surface quality. Therefore, the existing research results can hardly improve the machining accuracy of non-circular gears. Machining accuracy and surface quality of non-circular gears have important influences on the stability, accuracy, and service life of the transmission mechanism of agricultural machinery. Thus, studying the processing technology of non-circular gear machining and improving the quality of non-circular gears are important means of improving the working performance of agricultural machinery. Predicting the influence of the linkage model on distributing allowance evenly is an urgent problem that needs to be addressed.

This study proposes a machining method with evenly distributed allowance. First, the origin of the uneven distribution of allowance is analyzed by deducing the position relationship between the shaper cutter and the gear blank in the shaping process. Second, a normal linkage model of non-circular gear shaping is established for the allowance to be distributed evenly by adjusting the geometric position relationship between the shaper cutter and the gear blank in real time. Third, the accuracy and feasibility of the machining method with evenly distributed allowance are verified by virtual and actual machining experiments. Finally, the non-circular gears obtained by the actual machining experiments are measured via micro-topography analysis. Thus, the effectiveness of the proposed method is verified, and the influences of the machining methods on the surface quality of non-circular gears are analyzed, providing references for the optimization and performance evaluation of non-circular gear machining methods.

MATERIALS AND METHODS

Analysis of the origin of uneven allowance

Non-circular gear shaping is performed by rough shaping with multiple cutting cycles and (semi) finish shaping in the last cutting cycle. Fig. 1 shows a set-up of the coordinate system $S(O_cXY)$, where the

rotation centres of the gear blank and the shaper cutter are O_c and O_b respectively, the rotation speeds of the gear blank and the shaper cutter are ω_c and ω_b respectively, and the velocity of the shaper cutter along O_bO_c is v_x .

In finish shaping, the starting point is A . At any time, the pitch circle of the shaper cutter and the pitch curve of the gear blank are tangent at point P . The angle between the polar radius r and the tangent of the pitch curve of the gear blank is μ . The angle between the polar radius of the gear blank r and O_bO_c is α , and the angle between the radius of the shaper cutter r_c and O_bO_c is β , as expressed in Eq. (1):

$$\begin{cases} \alpha = \arctan \frac{r_c \cos \mu}{r + r_c \sin \mu} \\ \beta = \arctan \frac{r \cos \mu}{r \sin \mu + r_c} \end{cases} \quad (1)$$

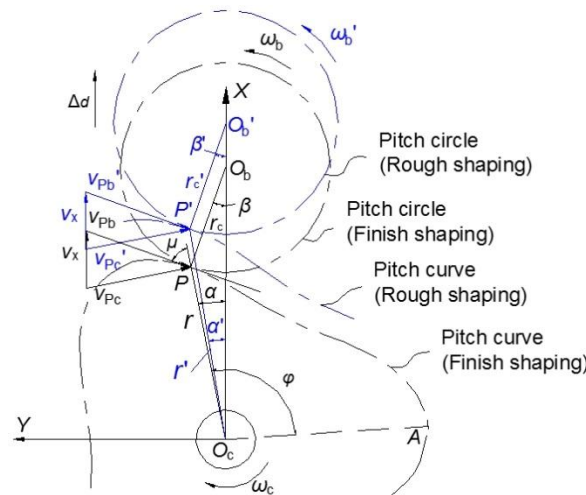


Fig. 1 - Geometric relationship between shaper cutter and gear blank in non-circular gear shaping

Point P is the relative velocity instantaneous centre according to the purely rolling between the pitch circle of the shaper cutter and the pitch curve of the gear blank. The velocity of point P relative to point O_b is v_{Pb} , and the velocity of point P relative to point O_c is v_{Pc} . From the velocity triangle in Fig. 1:

$$v_x = r_c \omega_b \sin \beta + r \omega_c \sin \alpha \quad (2)$$

In Fig. 1:

$$r_c \sin \beta = r \sin \alpha \quad (3)$$

Eq. (3) is substituted in Eq. (2), and thus:

$$v_x = r \sin \alpha (\omega_b + \omega_c) = r_c \sin \beta (\omega_b + \omega_c) \quad (4)$$

In Fig. 1, the distance between the shaper cutter and the gear blank in rough shaping increases Δd along O_bO_c compared with that in finish shaping. The rotation centre of the shaper cutter is point O'_b , the relative velocity instantaneous centre is point P' . The angle between the polar radius of the gear blank r' and $O'_bO'_c$ is α' , and the angle between the radius of the shaper cutter r'_c and $O'_bO'_c$ is β' . From the velocity triangle in Fig. 1:

$$v_x = r'_c \omega_b \sin \beta' + r' \omega_c \sin \alpha' \quad (5)$$

In Fig.1:

$$r'_c \sin \beta' = r' \sin \alpha' \quad (6)$$

Eq. (6) is substituted in Eq. (5), and thus:

$$v_x = r' \sin \alpha' (\omega_b + \omega_c) = r'_c \sin \beta' (\omega_b + \omega_c) \quad (7)$$

From Eqs. (4) and (7):

$$\begin{cases} r \sin \alpha = r' \sin \alpha' \\ r_c \sin \beta = r'_c \sin \beta' \end{cases} \quad (8)$$

From Eq. (8), point P' is above point P on the X -axis. The radial motion deviates from the normal direction of the gear blank's pitch curve. Accordingly, the uneven allowance appears after each cutting cycle, even the small allowance or the non-allowance, as depicted in Fig. 2.

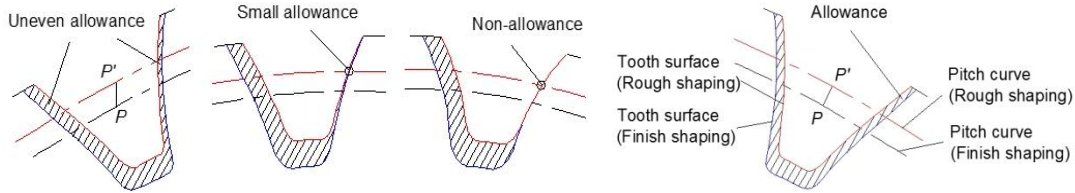


Fig. 2 - Distribution of allowance

Fig. 3 - Principle of the machining method

Machining method with evenly distributed allowance of non-circular gear

In rough shaping, each position of the shaper cutter has a one-to-one correspondence with the position in finish shaping along the normal direction of the gear blank's pitch curve by changing the generation motion to ensure that the shaper cutter is constantly machining in the normal direction of the gear blank's pitch curve. The principle of the machining method with evenly distributed allowance is illustrated in Fig. 3.

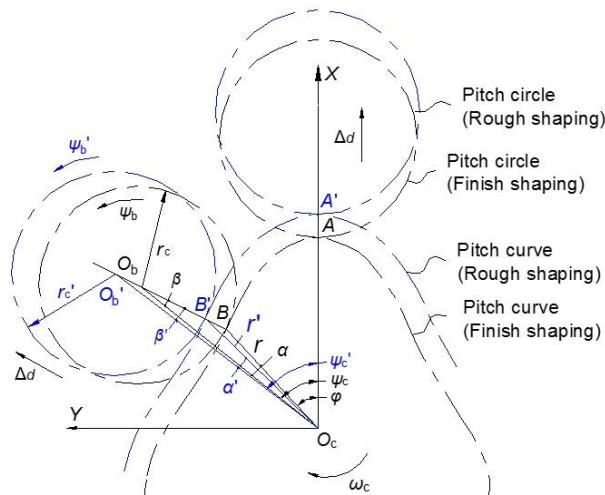


Fig. 4 - Normal linkage model of non-circular gear shaping

In Fig. 4, the coordinate system $S(O_c XY)$ is set up and the rotation centres of the gear blank and the shaper cutter are O_c and O_b respectively. In rough shaping, the distance between the shaper cutter and the gear blank increases Δd along the normal direction of the gear blank's pitch curve in each position compared with that in finish shaping. The rotation centre of the shaper cutter is point O_b' , the relative velocity instantaneous centre is point B' . The angle between the polar radius of the gear blank r' and $O_b'O_c$ is α' , and the angle between the radius of the shaper cutter r_c' and $O_b'O_c$ is β' , as expressed in Eq. (9):

$$\begin{cases} \alpha' = \arctan \frac{(r_c + \Delta d) \cos \mu}{r + (r_c + \Delta d) \sin \mu} \\ \beta' = \arctan \frac{r \cos \mu}{r \sin \mu + (r_c + \Delta d)} \end{cases} \quad (9)$$

The rotation angle of the shaper cutter around point O_b is ψ_b' ($\psi_b' = \psi_b$), the rotation angle of the gear blank around point O_c is ψ_c' , and the distance between points O_b' and O_c is i' , as follows:

$$\begin{cases} \psi_b' = S_{AB}/r_c - \beta \\ \psi_c' = \varphi - \alpha' \\ i' = r \cos \alpha' + (r_c + \Delta d) \cos \beta' \end{cases} \quad (10)$$

The arc length S_{AB} from points A to B is as follows:

$$S_{AB} = \int_0^\varphi \sqrt{r^2 + (dr/d\varphi)^2} d\varphi \quad (11)$$

Eqs. (1), (9), and (11) are substituted in Eq. (10). Thus, the normal linkage model of non-circular gear shaping is as follows:

$$\left\{ \begin{aligned} \psi_b^i &= \frac{\int_0^\varphi \sqrt{r^2 + (dr/d\varphi)^2} d\varphi}{r_c} - \arctan \frac{r \cos \mu}{r \sin \mu + r_c} \\ \psi_c^i &= \varphi - \arctan \frac{(r_c + \Delta d) \cos \mu}{r + (r_c + \Delta d) \sin \mu} \\ i &= r \cos \left[\arctan \frac{(r_c + \Delta d) \cos \mu}{r + (r_c + \Delta d) \sin \mu} \right] + \\ &\quad (r_c + \Delta d) \cos \left[\arctan \frac{r \cos \mu}{r \sin \mu + (r_c + \Delta d)} \right] \end{aligned} \right. \quad (12)$$

RESULTS

Validation example

A third-order elliptical gear is used as an example for verification. The equation of the pitch curve is as follows:

$$r(\varphi) = \frac{A(1 - k^2)}{1 - k \cos 3\varphi} \quad (13)$$

where A is the calculated semi-major axis, k is the eccentricity, and φ is the polar angle. The parameters are listed in Table 1.

Table 1

Parameters of third-order elliptical gear and shaper cutter

Parameters of gear	Value	Parameters of shaper cutter	Value
Number of teeth Z	42	Number of teeth Z_0	20
Normal module m_n [mm]	3	Normal module m_0 [mm]	3
Pressure angle α [°]	20	Pressure angle α_0 [°]	20
Order n	3	Helix angle β_0 [°]	0
Eccentricity k	0.1348		
Semi-major axis A [mm]	61.11		
Tooth width B [mm]	30		

Verification of the machining method with evenly distributed allowance based on virtual machining

Given that the rotation angle ψ_c^i of the gear blank is known, the polar angle φ of the gear blank can be obtained by Eq. (12) with the Steffensen iteration. If each cutting cycle is completed with N steps, the rotation angle of the gear blank in each step will be $\Delta\psi_c^i = 2\pi / N$, and the rotation angle of the gear blank in non-circular gear shaping will be $\psi_c^i(i) = (i-1)\Delta\psi_c^i$, where $i = 1, 2, \dots, N+1$. Thus, $\psi_b^i(i)$ and $l^i(i)$ can be obtained. The rotation and moving amounts of the shaper cutter in each step are $\Delta\psi_b^i(i) = \psi_b^i(i+1) - \psi_b^i(i)$ and $\Delta l^i(i) = l^i(i+1) - l^i(i)$ respectively, where $i = 1, 2, \dots, N$.

The software platform used in this study is SolidWorks and the control program is written to call the application program interface functions (API) by using visual basic for applications (VBA) to develop the CAM system of non-circular gear shaping. Then, the virtual machining is performed. Fig. 5 shows the flow of virtual machining, as follows: the shaper cutter and the non-circular gear blank are modelled, the two parts are controlled to move progressively with the motion data, and the Boolean difference is performed after each step (D.W. Liu et al., 2015; D.Z. Li et al., 2014). The shaper cutter envelops all the teeth of the non-circular gear after a single rotation by the gear blank. The process of the virtual machining is demonstrated in Fig. 6.

The parameters of the gear and the shaper cutter are inputted. As shown in Fig. 7, when $\Delta d = 2$ mm, the virtual machining will be performed according to the traditional and normal linkage models of shaping, in turn, the models of rough shaping are obtained, when $\Delta d = 0$, the model of finish shaping is obtained.

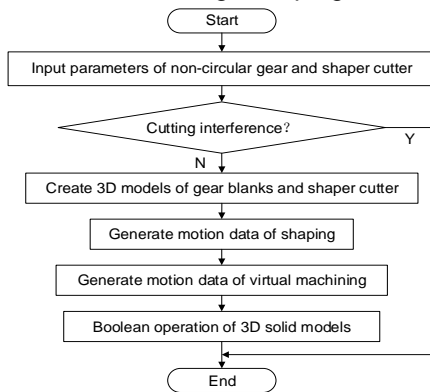


Fig. 5 - Flowchart of virtual machining

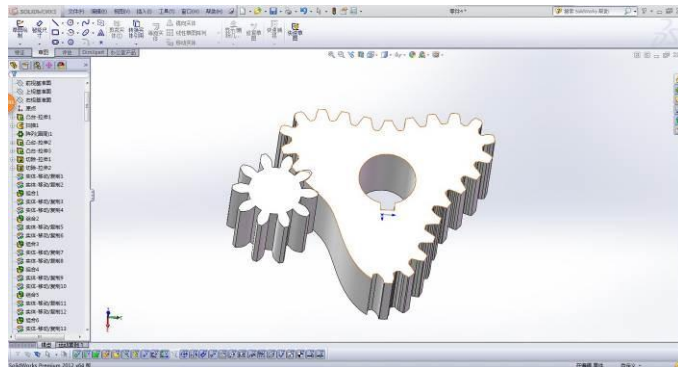


Fig. 6 - Process of virtual machining

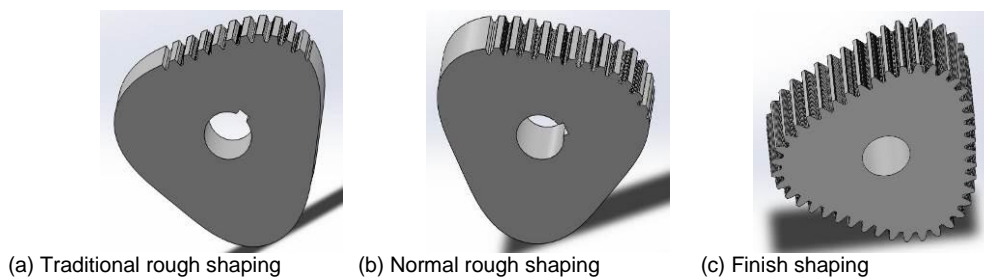


Fig. 7 - Gear models obtained by virtual machining

The models of rough shaping are compared with the model of finish shaping, and the distribution of the allowance is analyzed as illustrated in Fig. 8. The distribution of the allowance after the traditional rough shaping is uneven, whereas that after the normal rough shaping is even.

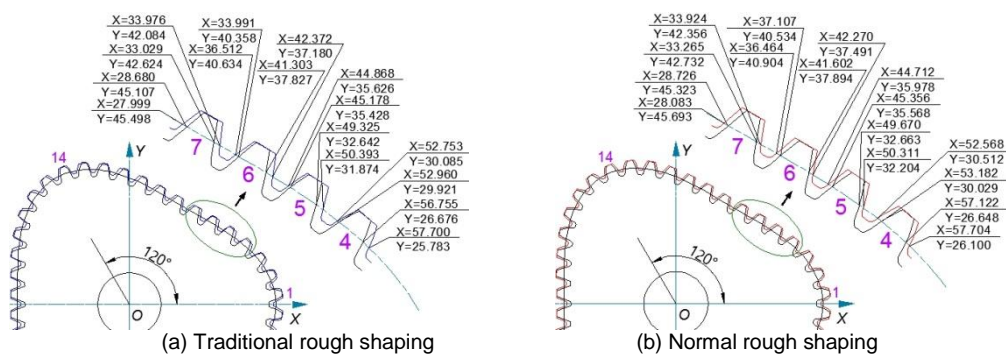


Fig. 8 - Distribution of allowance after rough shaping

In Fig. 9, points *A* and *D* are the intersections of the pitch curve with the rough model, points *B* and *C* are the intersections of the pitch curve with the finish model, while the chord lengths of *AB* and *CD* are defined as the allowance of the left and right tooth surfaces respectively. Thus, the unevenness of the allowance δ is as follows:

$$\delta = 2 \frac{|L_{AB} - L_{CD}|}{L_{AB} + L_{CD}} \cdot 100\% \tag{14}$$

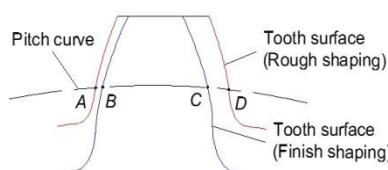


Fig. 9 - Definition of the unevenness of allowance

The coordinates of the intersection points are derived by the CAM system of non-circular gear shaping, a part of these coordinates are displayed in Table 2.

Table 2

Coordinates of intersection points			
Teeth	Points	Traditional shaping	Normal shaping
		[mm]	[mm]
1	A	(69.040, 7.627)	(69.216, 8.005)
	B	(69.165, 7.146)	(69.426, 7.223)
	C	(69.925, 2.212)	(70.208, 2.114)
	D	(69.977, 1.352)	(70.257, 1.273)
2	A	(65.424, 16.158)	(65.437, 16.632)
	B	(65.589, 15.875)	(65.845, 15.942)
	C	(67.781, 11.387)	(68.108, 11.283)
	D	(68.135, 10.467)	(68.397, 10.525)

The teeth in the first period $[0, 2\pi/3]$ are selected for analysis because of the periodical symmetry of the pitch curve of the third-order elliptical gear. The coordinates of the intersections are substituted in Eq. (14) and the unevenness of the allowance is presented in Fig. 10.

The maximum and average unevenness of the allowance after the traditional rough shaping are 132.47% and 91.2344%. The maximum and average unevenness of the allowance after the normal rough shaping are 5.03% and 2.7606%; compared with the traditional shaping, the maximum and average unevenness are reduced by 127.44% and 88.4738% respectively.

The results show that the machining method with evenly distributed allowance can greatly reduce the unevenness of the allowance in non-circular gear shaping; the method is correct and feasible.

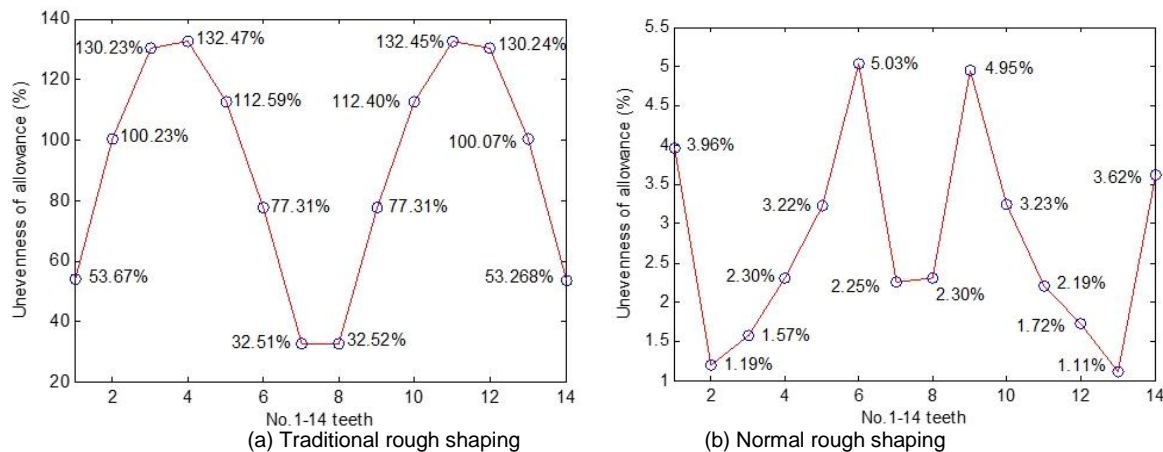


Fig. 10 - Unevenness of allowance in virtual machining

Verification of the machining method with evenly distributed allowance based on machining experiments

ARM+DSP+FPGA is used as the hardware platform of the CNC system, the code G84 for high-order elliptical gear shaping is developed by using the flexible electronic gearbox technology (X.Q. Tian et al., 2015). G84 is defined as $G84 A_N_K_R_D_S$, where A is the semi-major axis, N is the number of the order, K is the eccentricity, R is the radius of the pitch circle of the shaper cutter, D is the polar angle of the start point, and S is the residual feeding amount.

The elliptical gear used in the transplanting mechanism of a high-speed transplanter is taken as an example and the parameters are presented in Table 1.

The machining experiments are conducted on the YKS5132B CNC gear shaper.

The traditional and normal shaping is performed as illustrated in Fig. 11.



(a) Shaping process (b) Third-order elliptical gear obtained by machining experiments

Fig. 11 - Machining experiments of third-order elliptical gear

The non-circular gears obtained by the machining experiments are placed on the TESA Micro-Hite 3D coordinate measuring machine (CMM). The tooth profiles in the first period $[0, 2\pi/3]$ are reconstructed according to the discrete points obtained from the CMM. The coordinates of the intersections of the tooth surfaces with the pitch curve are substituted in Eq.14, the unevenness of the allowance is presented in Fig.12.

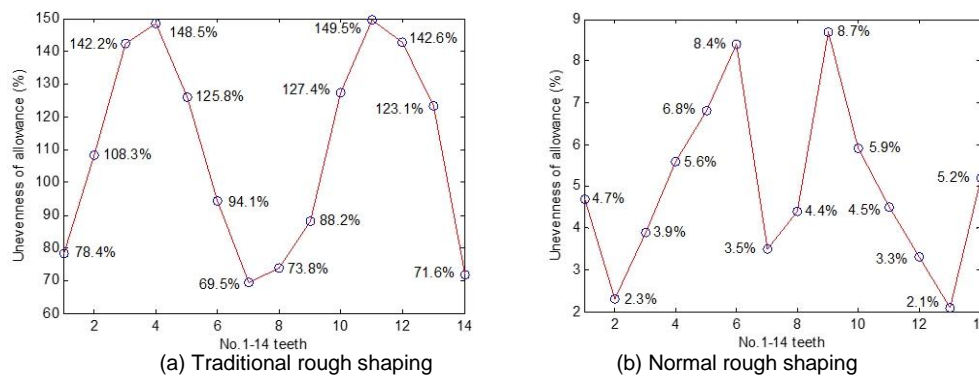


Fig. 12 - Unevenness of allowance in machining experiments

The results show that the machining method with evenly distributed allowance can reduce the average unevenness of the allowance from 110.21% to 4.95% in non-circular gear shaping, and thus the uneven distribution of the allowance can be improved effectively.

Measurement and analysis of the micro-topographies of non-circular gears

The No. 3 teeth of the non-circular gears obtained by the machining experiments are placed on the TRMOS TR-SCAN premium surface analysis instrument, and then 3D topography measurements are conducted. In Fig.13, the cut marks on the tooth surface of the non-circular gear obtained by the traditional shaping is uneven, additional pits and scratches appear, and the roughness is larger. The cut marks on the tooth surface of the non-circular gear obtained by the normal shaping is uniform, has no obvious defect, and the roughness is smaller. The results show that the micro-topography of the non-circular gear can be improved through the machining method with evenly distributed allowance.

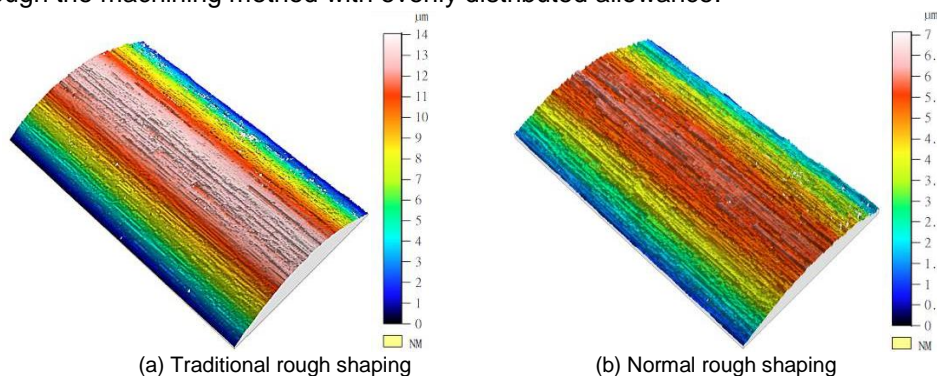
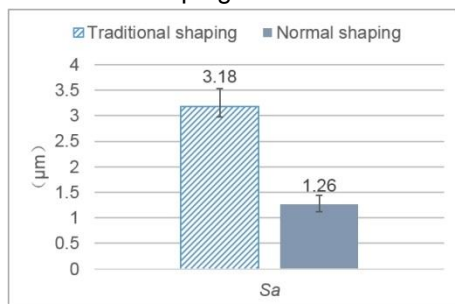
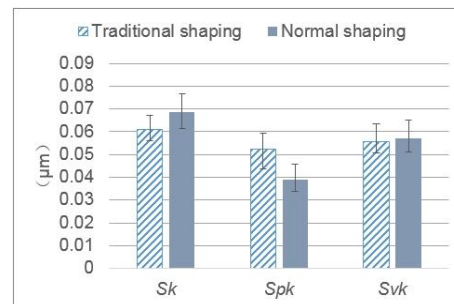


Fig. 13 - Micro-topographies of non-circular gears obtained by machining experiments

The micro-performances of the traditional and normal shaping are compared and analyzed according to ISO25178 and EUR15178N. S_a (arithmetical mean height) is the extension of R_a (arithmetical mean

deviation) to a surface, which is expressed as the average of the absolute value of the difference in the height of each point compared with the arithmetical mean of the surface. S_a is used to evaluate the surface roughness. In Fig. 14, the parameter S_a of the non-circular gear obtained by the normal shaping is reduced from 3.18 μm to 1.26 μm , which is smaller than that of the traditional shaping.

S_k (core roughness depth) is calculated as the difference of heights at the areal material ratio values 0% and 100% on the equivalent line. Specifically, it is a value obtained by subtracting the minimum height from the maximum height of the core surface. S_{pk} (reduced peak height) represents the mean height of peaks above the core roughness, and S_{vk} (reduced valley depth) represents the mean depth of valleys below the core roughness. They are used to evaluate the functional features of surface roughness (Jolivet *et al.*, 2014). In Fig. 15, the parameters S_k and S_{vk} of the non-circular gear obtained by the normal shaping are relatively smaller; meanwhile, the parameter S_{pk} is relatively larger. Therefore, the roughness profile has higher wear resistance and less initial wear quantity. The surface quality of the non-circular gear obtained by the normal shaping is also enhanced.

Fig. 14 - Contrast chart of S_a Fig. 15 - Contrast chart of S_k , S_{pk} , and S_{vk}

The results show that the machining accuracy and surface quality of non-circular gears can be improved through the machining method with evenly distributed allowance. Therefore, the working performance and service life of agricultural machinery products can be optimized.

CONCLUSIONS

The working performance and service life of agricultural machinery are mainly determined by the machining accuracy and surface quality of non-circular gears. This study analyzed the origin of the uneven distribution of allowance of non-circular gears, revealed the influences of the machining methods on the allowance distribution, and established the normal linkage model of non-circular gear shaping. Then, the machining method with evenly distributed allowance was verified by virtual and actual machining experiments, and the relationship between the machining methods and the surface quality of non-circular gears was analyzed by micro-topography measurements. The main conclusions are as follows:

(1) The degree of uneven distribution of the allowance of non-circular gears is proportional to the degree of the radial motion deviating from the normal direction of the gear blank's pitch curve. The normal linkage model of non-circular gear shaping set up in this study can adjust the geometric relationship between the shaper cutter and the gear blank in real time, and then, the even distribution of the allowance in the shaping process is realized.

(2) Theoretically, the average unevenness of the allowance can be reduced from 91.23% to 2.76% through the machining method with evenly distributed allowance. Meanwhile, the average unevenness of the allowance can be reduced from 110.21% to 4.95% in the actual machining. The method can evenly distribute the allowance of non-circular gears.

(3) The non-circular gears obtained by the machining method with evenly distributed allowance have uniform cut marks, no defects, and smooth micro-topography. Meanwhile, the surface roughness is smaller and the micro-performance of the roughness profile is better than that of the traditional shaping. The method can significantly improve the surface quality.

The conclusions in this study can effectively improve the uneven distribution of allowance caused by the change of the curvature of the gear blank's pitch curve and have an important guiding significance for improving the machining accuracy and surface quality of non-circular gears. In future studies, the

machining method with evenly distributed allowance can be applied to finish machining methods with similar machining principles, such as the gear form-grinding based on the shaping linkage model and gear skiving, to further improve the machining accuracy and surface quality of non-circular gears. The conclusions in this study are crucial to improving the working accuracy and service life of agricultural machinery products.

ACKNOWLEDGEMENT

The study was supported by the National Natural Science Foundation of China (Grant No. 51275147).

REFERENCES

- [1] Erkorkmaz K, Katz A, Hosseinkhani Y. et al., (2016), Chip Geometry and Cutting Forces in Gear Shaping, *CIRP Annals - Manufacturing Technology*, London/U.K., Ed. Elsevier, 65-1, pp.133-136;
- [2] He J.L., Li J.G., Wang Z. et al., (2007), Research on Non-circular Gear Grinding Method by Using Gear Generator with Form-Grinding, *Transactions of the Chinese Society of Agricultural Machinery*, Beijing/China, Chinese Society for Agricultural Machinery, Vol.38, Issue 10, pp.145-149;
- [3] Jolivet S., Mezghani S., Mansori M.E. et al., (2014), Numerical Simulation of Tooth Surface Finish Effects on Gear Noise, *ASME 2014 12th Biennial Conference on Engineering Systems Design and Analysis*, New York/U.S.A., Vol.1, pp.V001T04A007;
- [4] Li B., He J., Chen D. et al., (2016), A Linkage Model of Non-circular Gear Shaping and Computer Simulation Processing, *International Conference on Human Centred Computing*, Berlin/Germany, Springer International Publishing Switzerland, Vol. 9567, ISBN:3-319-31853-5, pp.204-214;
- [5] Li D.Z., Xia L., Liu Y.Y. et al., (2014), Research on Non-Circular Gear Hobbing Simulation Based on Piecewise Cubic Spline Fitting, *Key Engineering Materials*, Zurich/Switzerland, Vol.620, pp.357-362;
- [6] Litvin F.L., Gonzalez-Perez I., Yukishima K. et al., (2007), Generation of Planar and Helical Elliptical Gears by Application of Rack-cutter, Hob, and Shaper, *Computer Methods in Applied Mechanics & Engineering*, London/U.K., Ed. Elsevier, Vol.196, Issue 41, pp.4321-4336;
- [7] Liu D.W., Ren T.Z., Jin X., (2015), Geometrical Model and Tooth Analysis of Undulating Face Gear, *Mechanism and Machine Theory*, London/U.K., Ed. Elsevier, Vol.86, pp.140-155;
- [8] Liu Y., (2014), Study of Optimal Strategy and Linkage-model for External Non-circular Helical Gears Shaping, *Proceedings of the Institution of Mechanical Engineers Part C Journal of Mechanical Engineering Science*, London/U.K., Ed. SAGE, Vol.229, Issue 3, pp.493-504;
- [9] Pathak S., Jain N.K., Palani I.A., (2014), On Use of Pulsed-Electrochemical Honing to Improve Micro-Geometry of Bevel Gears, *Materials & Manufacturing Processes*, Vol.29, 11-12, pp.1461-1469;
- [10] Tarapanov A., Anisimov R., Kanatnikov N. et al., (2015), Improving Efficiency of Gear Shaping of Wheels with Internal Non-involute Gears, *IOP Conference Series: Materials Science and Engineering*, London/U.K., IOP Publishing Ltd, Vol.127, ISSN:1757-899X, pp.1-8;
- [11] Tian X.Q., Han J., Xia L., (2015), Precision Control and Compensation of Helical Gear Hobbing Via Electronic Gearbox Cross-Coupling Controller, *International Journal of Precision Engineering & Manufacturing*, Berlin/Germany, Ed. Springer, Vol.16, Issue 4, pp.797-805;
- [12] Wu X.T., Wang H.G., (1997), *Non-circular Gear and Non-constant Speed Ratio*, China P. pp.326-329.
- [13] Xia L., Li D.Z., Han J., (2013), Research on Mathematical Modeling and Kinematic Simulation of Elliptic Family Gears, *Key Engineering Materials*, Vol.579-580, pp.300-304;
- [14] Yu G.H., Yu T.F., Ye B.L. et al., (2015), Design of a Rotary Plug Seeding Pick-up Mechanism, *Journal of Mechanical Engineering*, Beijing/China, China Mechanical Engineering Society, Vol.7, pp.67-76;
- [15] Zhang Y., Zhang D., Wu B., (2015), An Approach for Machining Allowance Optimization of Complex Parts with Integrated Structure, *Journal of Computational Design & Engineering*, London/U.K., Ed. Elsevier, Vol.2, Issue 4, pp.248-252;
- [16] Zheng F., Hua L., Han X. et al., (2016), Linkage Model and Manufacturing Process of Shaping Non-circular Gears, *Mechanism & Machine Theory*, London/U.K., Ed. Elsevier, Vol.96, pp.192-212;
- [17] Zheng F., Hua L., Han X., et al., (2017), Synthesis of Shaping Non-circular Gear using a 3-linkage CNC Shaping Machine, *Journal of Manufacturing Science and Engineering*, Vol.139 (7), pp.1-12;
- [18] Zhou M., Sun L., Du X. et al., (2014), Optimal Design and Experiment of Rice pot Seedling Transplanting Mechanism with Planetary Bezier Gears, *Transactions of the ASABE*, Michigan/U.S.A., American Society of Agricultural and Biological Engineers, Vol.57, Issue 6, pp.1537-1548.

KINEMATICS AND PERFORMANCE INDEX ANALYSIS OF A NOVEL 5-DOF PARALLEL MECHANISM

新型五自由度并联机构运动学及其性能指标分析

Ph.D. Huang Jie, Ph.D. Wang Xuelei¹⁾, Ph.D. Zhao Dongjie²⁾, Ph.D. San Yunlong¹⁾, Prof. Hou Shulin*¹⁾

¹⁾ College of Engineering, China Agricultural University, Beijing/China; ²⁾ School of Mechanical and Automobile Engineering, Liaocheng University, Liaocheng/China

Tel: +8618003199306; E-mail: slhou@cau.edu.cn

Keywords: parallel mechanism, screw theory, Jacobian matrix, global performance fluctuation index

ABSTRACT

A novel 5-Degree-Of-Freedom (DOF) Parallel Mechanism (PM) which can be used in target spraying robot was proposed. The DOF formula of traditional PMs can only calculate the DOF of the mechanism but cannot determine its constraint type. To determine the influence of the PM constraint type and sizes of the moving and fixed platforms on its performance fluctuation index, the study first analyzed the DOF of the novel 5UPS-RPS PM based on screw theory and determined the constraint type of its different sub-chains. Subsequently, inverse kinematics and velocity formulas of the PM were derived, the velocity global performance index was analyzed based on the condition number of Jacobian matrix and the velocity global performance index atlas was drawn. Finally, in view of the deficiency of the velocity global performance index, the global performance fluctuation index formula, which can reflect the fluctuation of the movement performance of the mechanism in the whole workspace, was proposed. The results of the global performance index and global performance fluctuation index atlas of the PM showed that the global performance fluctuation index decreases with the increase of the radii of the moving and fixed platforms and increases with the decrease of their radii. When $r_a=47.7\text{--}50$ cm and $r_b=38.6\text{--}40$ cm, the global performance fluctuation index σ of 5UPS-RPS PM is small. At this time, if $\sigma=0.35322$, then the PM has narrow movement fluctuation in the whole workspace. The results provide an important guide to the size selection of the moving and fixed platforms of the 5UPS-RPS PM and the optimal design of the prototype.

摘要

提出一种可应用于对靶喷雾机器人的五自由度并联机构。传统并联机构自由度公式只能计算出机构的自由度数，而不能确定机构所受的约束类型。为得到并联机构整机所受约束类型以及动平台和定平台尺寸对其性能波动指标的影响，本文基于螺旋理论，首先对新型 5UPS-RPS 并联机构进行了自由度分析，并确定了 5UPS-RPS 并联机构各分支所受约束类型。其次，建立了该并联机构运动学逆解和速度表达式，并利用雅可比矩阵条件数对其进行了速度全域性能指标分析，绘出了速度全域性能指标图谱。最后，针对速度全域性能指标的不足，提出了全域性能波动指标公式，该指标可反映机构在整个工作空间内运动性能波动情况。基于并联机构全域性能指标和全域性能波动指标图谱结果，本研究发现，全域性能波动指标随动平台和定平台半径的增大而减小，随动平台和定平台半径的减小而增大，当 $r_a=47.7\text{--}50\text{cm}$ ， $r_b=38.6\text{--}40\text{cm}$ 时，5UPS-RPS 并联机构的全域性能波动指标值 σ 较小，此时 $\sigma=0.35322$ ，即该并联机构此尺寸时在整个工作空间内运动波动性较小。该研究成果对于 5UPS-RPS 并联机构动平台和定平台尺寸的选取以及样机的优化设计具有重要指导意义。

INTRODUCTION

With the development of agricultural production technology, agriculture automation equipment will play a more and more important role in aspects of alleviating the shortage of agricultural labour, improving labour productivity, reducing production costs, protection of workers' safety and a novel 5-Degree-Of-Freedom (DOF) Parallel Mechanism (PM) which can be used in target spraying robot was proposed. The parallel mechanism is a parallel-actuated mechanism that consists of two or more sub-chains and has at least two DOF. It originates from an entertainment device based on spherical PM proposed by Gwinnett in the 1930s. Compared to serial robot, it has high mechanical stiffness, strong bearing capacity, low weight of the end, small inertia, and no accumulation of position errors. The PM is very popular among people because it complements with serial robot in application (Plitea et al., 2015; Xiangdun et al., 2014; Briot et

al., 2010; Altuzarra et al., 2010). The 5-DOF PM is a very important type among the limited DOF PMs. Compared with 6-DOF PMs, 5-DOF PMs have attracted much attention because of their low cost, simple structures, and easy controllability (Jingtao et al., 2013; Xiulong et al., 2014; Yanbiao et al., 2013). This study proposes a 5UPS-RPS spatial 5-DOF PM with three rotations and two translations. As the proposed PM has simple structure, high bearing capacity, and easy controllability, it can be widely used in the fields of robot manipulator, multidimensional force sensor and human body rehabilitation device.

With the development of high-precision manufacturing and high-velocity machines, better kinematic and dynamic performance designs are increasingly needed. As a scalar, the evaluation index of robot performance is to quantify the performance of the robot. In the robot design stage, the performance index plays a guiding role in the design and evaluation of robot performance. On this basis, researchers have put forward various indexes to evaluate robot performance (Dan et al., 2015; Guiyang et al., 2015; Feibo et al., 2015; Angeles., 2006; Pong et al., 2006; Tian et al., 2014). However, these studies are aimed at a specific PM. The research involves complex computation and heavy workload but fails to reflect the performance fluctuation of the mechanism in the whole working space.

How to evaluate the performance fluctuation of PM in motion is an urgent problem that needs to be solved. Therefore, this study combines the concept of variation coefficient in statistics and utilizes the condition number of Jacobian matrix through simple calculation and strong commonality to analyse the performance fluctuation index of 5UPS-RPS PMs. This study provides a theoretical basis for the optimal design of PM and prevents blindness in size selection.

At present, researchers have conducted numerous works on PM and its performance indexes. Lei Jingtao et al. (Jingtao et al., 2013) designed a 4UPS-UPU PM, solved its inverse kinematics using the vector algebra method, and determined the mapping relationship between the joint variables and end-effector pose. (Xiulong et al., 2014) defined an index that can comprehensively evaluate the dexterity of the PM under different configurations and investigated the influential law of the distribution angles of hinge points on fixed and moving platforms and the radii of the hinge points' circle of both platforms of 4UPS-RPS spatial PM based on the square mean dexterity coefficient. (Yanbiao et al., 2013) proposed a new statistical parameter optimization method for the 5-DOF bonnet polishing machine tool, which provided a basis for the application of the new parallel bonnet polishing machine tool. (Gosselin et al., 1991) optimized the robot design and defined the global performance index of the mechanism. (Liu Songtao et al., 2012) considered the constraint and inertia effect of the two kinds of rotation angles based on kinematic analysis, put forward two kinematic global performance indexes, and applied them in the optimal design of 4-DOF SCARA PM which has three-rotation and one-translation movements. (Hosseini et al., 2015) studied the maximum working space of the Tricept PM, which has two-rotation and one-translation movements and proposed a homogeneous Jacobian matrix that converts the motion velocity of the joint space into that of the operation space to achieve a rapid withdrawal of singular position of the mechanism. (Zhang Dan et al., 2015) proposed a performance decomposition method as basis for the design of complex microrobots. The proposed method could be used in the optimal design of different compliant PMs. (Xin et al., 2015) put forward a new hexapod robot, established its kinematics model, and optimized the design of its geometric parameters using the comprehensive objective function considering the dexterity and payload of the mechanism. Their trajectory tracking experiment verified the correctness of the kinematics model and comprehensive performance indexes. (Wang et al., 2015) carried out scale synthesis on 2-UPR-SPR PM using the motion/force transfer performance index based on screw theory, established the inverse kinematics model of the mechanism, and performed the spiral analysis on it to obtain the local transfer and global performance indexes of the 2-UPR-SPR PM, which were taken as the evaluation criteria of the motion/force transfer performance of the mechanism. (Angeles et al., 2006) made the normalization processing in terms of the length unit in the matrix using the characteristic length, but how to choose the characteristic length of the mechanism has not yet been solved effectively as the selected characteristic length had certain randomness. Another common method was to establish the mapping relation among several points on the joint velocity and the output rigid body to obtain the Jacobian matrix with homogeneous dimension (Pong et al., 2006), but the Jacobian matrix obtained through this method depended on the selected reference points, so the optimal design with the algebraic eigenvalue as the performance index would obtain different optimization results because of the selection of different reference points. (Huang et al., 2014; Haitao et al., 2015) built the mapping matrix, which could characterize the transitive relationship of the force and variational motion in the joint space

and operation space through concepts of dual base and dual space, and they constructed a group of kinematic performance evaluation indexes, which could identify the singular configuration and could be taken as the objective function or constraint condition of size synthesis.

The above research results are mainly based on global performance indexes, but research on the global performance fluctuation of the mechanism is limited. The present study establishes the global performance fluctuation index formula of mechanism by using the condition number of the Jacobian matrix and variation coefficient in statistics and calculates the influence of the different sizes of moving and fixed platforms of the mechanism on its performance fluctuation, which provides a theoretical basis for the optimal design of the mechanism.

The remainder of this paper is organized as follows. Section 3 describes the mechanism of the novel 5-DOF PM and analyses its constraint type by using screw theory. Section 4 presents the kinematic analysis on the mechanism, obtains its Jacobian matrix, constructs the global performance fluctuation index formula by using the condition number of the Jacobian matrix, and obtains the relationship between the moving and fixed platform sizes of the mechanism and the performance fluctuation indexes. Section 5 summarizes the conclusions and provides relevant conclusions.

MATERIALS AND METHODS

DOF Analysis

The 5UPS-RPS PM is composed of a moving platform, a fixed platform, and the sub-chains connecting these two platforms, as shown in Fig. 1(a).

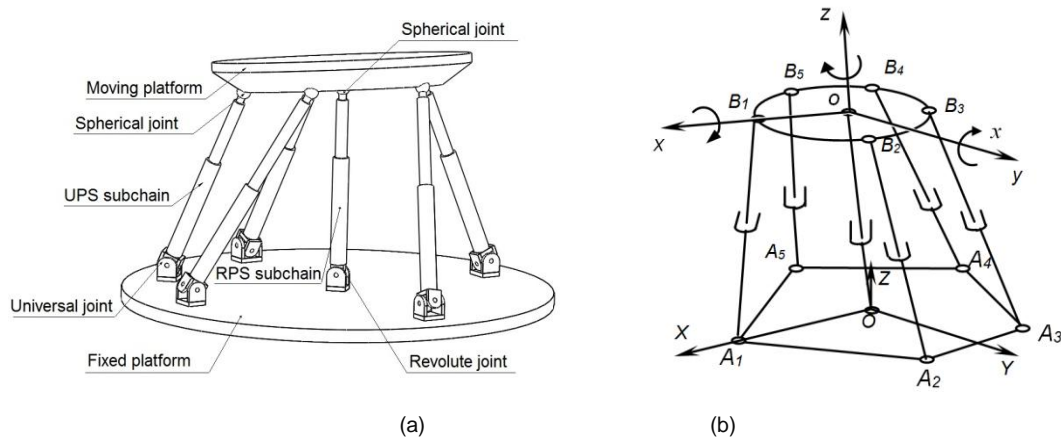


Fig. 1 - 5UPS-RPS PM

The 5UPS-RPS PM has the following characteristics: The fixed platform is connected with the moving platform by 5UPS-type (universal, prismatic, and spherical joints) driving sub-chains and one RPS-type (revolute, prismatic, and spherical joints) constraint sub-chain. It can realize the motion of the mechanism by controlling the lengths of the five driving sub-chains.

Reciprocal Screw of RPS Sub-chain

Screw theory is an important mathematical tool in the study of mechanism, which originated in the 19th century (Du et al., 2015; Wang et al., 2015). According to screw theory, the kinematic pairs of the mechanism can be expressed by $(\$, \$_0)$, where $\$$ refers to the unit vector of the axis of the kinematic pair and $\$ _0 = r \times \$$ (r represents the radius from the origin of the coordinates to the axis of the kinematic pair). The coordinate system O - XYZ and the equivalent screw system are established on the RPS sub-chain, as shown in Fig. 2. The kinematic screw of the RPS sub-chain is expressed as:

$$\begin{cases} \$ _1 = (0 \ 1 \ 0 ; 0 \ 0 \ 0) \\ \$ _2 = (0 \ 0 \ 0 ; \sin\alpha \ 0 \ \cos\alpha) \\ \$ _3 = (\sin\alpha \ 0 \ \cos\alpha ; 0 \ 0 \ 0) \\ \$ _4 = (1 \ 0 \ 0 ; 0 \ l_{op}\cos\alpha \ 0) \\ \$ _5 = (0 \ 1 \ 0 ; -l_{op}\cos\alpha \ 0 \ l_{op}\sin\alpha) \end{cases} \quad (1)$$

Where l_{op} is the length of RPS sub-chain and α is the angle between the RPS sub-chain and Z-axis.

According to the relationship between the motion and reciprocal screws

$$\mathcal{S} \cdot \mathcal{S}^r = 0 \tag{2}$$

The constraint reciprocal screw of the RPS sub-chain is solved as follows:

$$\mathcal{S}_1^r = (0 \ 1 \ 0; -l_{op} \cos\alpha \ 0 \ l_{op} \sin\alpha) \tag{3}$$

Where the reciprocal screw \mathcal{S}_1^r represents a force vector that is parallel to the axis of the revolute pair R and passes the centre of the spherical pair and restricts the movement of the mechanism along the Y-axis.

Reciprocal Screw of UPS Sub-chain

The coordinate system $A_i - X_i Y_i Z_i (i = 1, 2... 5)$ and the equivalent screw system are established on the UPS sub-chain, as shown in Fig. 3. The kinematic screw of the sub-chain is expressed as follows:

$$\begin{cases} \mathcal{S}_1 = (1 \ 0 \ 0; 0 \ 0 \ 0) \\ \mathcal{S}_2 = (0 \ 1 \ 0; 0 \ 0 \ 0) \\ \mathcal{S}_3 = (0 \ 0 \ 0; 0 \ -\sin\beta \ \cos\beta) \\ \mathcal{S}_4 = (0 \ -\sin\beta \ \cos\beta; 0 \ 0 \ 0) \\ \mathcal{S}_5 = (1 \ 0 \ 0; 0 \ l_{A_i B_i} \cos\beta \ l_{A_i B_i} \sin\beta) \\ \mathcal{S}_6 = (0 \ 1 \ 0; -l_{A_i B_i} \cos\beta \ 0 \ 0) \end{cases} \quad (i = 1, 2...5) \tag{4}$$

Where $l_{A_i B_i} (i = 1, 2... 5)$ is the length of UPS sub-chain and β is the angle between UPS sub-chain and Z-axis.

According to the relationship between screws and reciprocal screws, UPS sub-chain has no constraint reciprocal screw. In other words, the mechanism is not constrained by the UPS sub-chain.

According to Equations (1)–(4), the force vector \mathcal{S}_1^r constrains the movement of the mechanism along the direction of the revolute joint R; that is, the mechanism has two translational DOFs and three rotational DOFs.

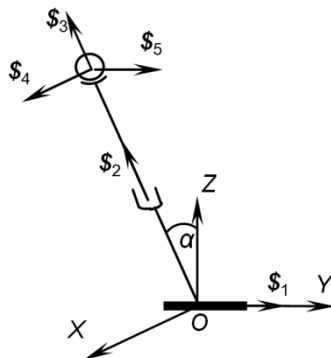


Fig. 2 - Screw system of RPS sub-chain

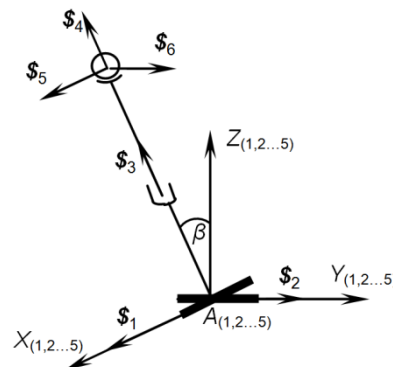


Fig. 3 - Screw system of UPS sub-chain

Inverse Displacement Kinematics Analysis of the PM

The structural diagram of the 5UPS-RPS PM is shown in Fig. 1(b). The fixed coordinate system O-XYZ and the moving coordinate system p-xyz are established on the centres of the fixed and moving platforms, respectively. Among the five universal joints $A_i (i=1,2...5)$ in the fixed platform, the coordinate value of the first universal joint is $(W, 0, 0)$, and the remaining four universal joints are distributed on a circle with a radius of r_a uniformly. The five spherical joints on the moving platform are distributed on a circle which has a radius of r_b uniformly, and the position angle is φ . At the initial time, the coordinate systems O-XYZ and o-xyz are parallel, and the Z-axis is coincident with the z-axis, and the radii of their circumcircles are r_a and r_b , respectively.

The coordinates of A_i ($i=1,2...5$) in the fixed coordinate system O -XYZ and B_i ($i=1,2...5$) in the moving coordinate system p -xyz can be expressed as follows:

$$\begin{cases} A_1 = (A_{1x}, A_{1y}, A_{1z}) = (W, 0, 0) \\ A_2 = (A_{2x}, A_{2y}, A_{2z}) = (\sqrt{2}r_a/2, \sqrt{2}r_a/2, 0) \\ A_3 = (A_{3x}, A_{3y}, A_{3z}) = (-\sqrt{2}r_a/2, \sqrt{2}r_a/2, 0) \\ A_4 = (A_{4x}, A_{4y}, A_{4z}) = (-\sqrt{2}r_a/2, -\sqrt{2}r_a/2, 0) \\ A_5 = (A_{5x}, A_{5y}, A_{5z}) = (\sqrt{2}r_a/2, -\sqrt{2}r_a/2, 0) \end{cases} \quad (5)$$

$$\begin{cases} B_1 = (b_{1x}, b_{1y}, b_{1z}) = (r_b, 0, 0) \\ B_2 = (b_{2x}, b_{2y}, b_{2z}) = (r_b \cos 2, r_b \sin 2, 0) \\ B_3 = (b_{3x}, b_{3y}, b_{3z}) = (r_b \cos 2, r_b \sin 2, 0) \\ B_4 = (b_{4x}, b_{4y}, b_{4z}) = (r_b \cos 2, -r_b \sin 2, 0) \\ B_5 = (b_{5x}, b_{5y}, b_{5z}) = (r_b \cos 2, -r_b \sin 2, 0) \end{cases} \quad (6)$$

After the operation on the moving platform, the coordinates of B_i ($i=1,2,5$) in the fixed coordinate system O -XYZ can be expressed as follows:

$$B_i^O = R(\alpha \beta \gamma) \begin{Bmatrix} b_{ix} \\ b_{iy} \\ b_{iz} \end{Bmatrix} + p ; \quad p = \begin{Bmatrix} X_p \\ Y_p \\ Z_p \end{Bmatrix} \quad (7)$$

Where $p = [X_p \ Y_p \ Z_p]^T$ are the coordinates of point p in the fixed coordinate system and $R(\alpha \beta \gamma)$ is a rotation transformation matrix from the moving coordinate system to the fixed coordinate system and is formed by three Euler rotations of $(\alpha \beta \gamma)$, namely, a rotation of α about the z -axis, followed by a rotation of β about the y_1 -axis, and then a rotation of γ about the x_2 -axis, where y_1 is formed by y rotating about z by α and x_2 is formed by x_1 rotating about y_1 by β . Let λ be one of (α, β, γ) and set $c\lambda = \cos\lambda$ and $s\lambda = \sin\lambda$. Thus, $R(\alpha \beta \gamma)$ is derived as follows:

$$R(\alpha, \beta, \gamma) = \begin{bmatrix} \cos\alpha \cos\beta & \cos\alpha \sin\beta \sin\gamma - \sin\alpha \cos\gamma & \cos\alpha \sin\beta \cos\lambda + \sin\alpha \sin\gamma \\ \sin\alpha \cos\beta & \sin\alpha \sin\beta \sin\gamma + \cos\alpha \cos\gamma & \sin\beta \sin\beta \cos\gamma - \cos\alpha \sin\gamma \\ -\sin\beta & \cos\beta \sin\gamma & \cos\beta \cos\gamma \end{bmatrix} \quad (8)$$

Thus, the formulas for solving the rod length l_i and the unit vector n_i ($i = 1, 2... 5$) of the five driving sub-chains can be expressed as follows:

$$l_i = |B_i^O - A_i| ; \quad n_i = \frac{l_i}{l_i} = \frac{B_i^O - A_i}{l_i} \quad (i = 1, 2... 5) \quad (9)$$

Velocity Analysis of the PM

Let V be the velocity of the moving platform at p and v and ω be the linear and angular velocities of the central point of the moving platform, respectively. They are written as:

$$V = \begin{bmatrix} v \\ \omega \end{bmatrix}_{6 \times 1} ; \quad v = \begin{bmatrix} v_x \\ v_y \\ v_z \end{bmatrix} ; \quad \omega = \begin{bmatrix} \omega_x \\ \omega_y \\ \omega_z \end{bmatrix} \quad (10)$$

By setting r_i as the position vector of the hinge point B_i relative to the central point p of the moving platform, n_i as the unit vector of the active sub-chain i , V_i as the velocity of the hinge point B_i , and v_i ($i = 1, 2... 5$) as the velocity of the active sub-chain i , it can be known from the rigid body dynamics theory that:

$$\mathbf{V}_i = \mathbf{v} + \boldsymbol{\omega} \times \mathbf{r}_i \tag{11}$$

$$v_i = \mathbf{V}_i \cdot \mathbf{n}_i \tag{12}$$

Substituting Equation (11) into (12) will result in the following:

$$v_i = \mathbf{V}_i \cdot \mathbf{n}_i = (\mathbf{v} + \boldsymbol{\omega} \times \mathbf{r}_i) \cdot \mathbf{n}_i = \mathbf{n}_i \cdot \mathbf{v} + (\mathbf{r}_i \times \mathbf{n}_i) \cdot \boldsymbol{\omega} \quad (i=1,2\dots5) \tag{13}$$

$$\Rightarrow \mathbf{V}_H = \begin{bmatrix} v_1 \\ v_2 \\ v_3 \\ v_4 \\ v_5 \end{bmatrix} = \begin{bmatrix} \mathbf{n}_1^T & (\mathbf{r}_1 \times \mathbf{n}_1)^T \\ \mathbf{n}_2^T & (\mathbf{r}_2 \times \mathbf{n}_2)^T \\ \mathbf{n}_3^T & (\mathbf{r}_3 \times \mathbf{n}_3)^T \\ \mathbf{n}_4^T & (\mathbf{r}_4 \times \mathbf{n}_4)^T \\ \mathbf{n}_5^T & (\mathbf{r}_5 \times \mathbf{n}_5)^T \end{bmatrix}_{5 \times 6} \cdot \begin{bmatrix} \mathbf{v} \\ \boldsymbol{\omega} \end{bmatrix}_{6 \times 1} = [\mathbf{G}]_{5 \times 6} \cdot \mathbf{V} \tag{14}$$

Where \mathbf{V}_H is the input velocity of the PM and $[\mathbf{G}]$ is the Jacobian matrix of the velocity of the PM.

RESULTS

Global Performance Index Analysis of the Mechanism

Gosselin has proposed a novel approach to evaluate the average performance of the mechanism in the workspace based on the global performance index (Gosselin C., Angeles J., 1991), which is expressed as follows:

$$\eta_J = \frac{\int_W \frac{1}{K_J} dW}{\int_W dW} \tag{15}$$

Where, η_J is the global performance index of the mechanism, K_J is the condition number of the mechanism, and W is the reachable workspace of the mechanism.

The mathematical meaning of Equation (15) is the average value of the reciprocal of the condition number K_J of the mechanism in the reachable workspace. Its value indicates the average movement performance of the mechanism in the whole workspace. As $1 \leq K_J < \infty$, $0 < \eta_J \leq 1$. The higher the value of η_J , the higher the dexterity and the better the kinematic performance of the mechanism.

Establishing the correct performance evaluation index is the basis for the optimal design of the PM. According to Equation (14), the relationship between the input velocity \mathbf{V}_H and the terminal output velocity \mathbf{V} of the mechanism is as follows:

$$\mathbf{V}_H = [\mathbf{G}]_{5 \times 6} \cdot \mathbf{V} \tag{16}$$

Equation (16) provides the motion equation of the mechanism in the ideal state, but a real robot involves manufacturing, assembly, and position control errors. If the terminal output velocity \mathbf{V} of the mechanism has a certain deviation $\delta \mathbf{V}$ and its input velocity \mathbf{V}_H also has a certain deviation $\delta \mathbf{V}_H$, then the relationship between the input and output velocities can be described as follows:

$$\mathbf{V}_H + \delta \mathbf{V}_H = ([\mathbf{G}] + \delta[\mathbf{G}])(\mathbf{V} + \delta \mathbf{V}) \tag{17}$$

After organization, the following can be obtained:

$$\frac{\|\delta \mathbf{V}_H\|}{\|\mathbf{V}_H\|} \leq \|[\mathbf{G}]\| \cdot \|[\mathbf{G}]^{-1}\| \cdot \left(\frac{\|\delta \mathbf{V}\|}{\|\mathbf{V}\|} + \frac{\|\delta[\mathbf{G}]\|}{\|[\mathbf{G}]\|} \right) \tag{18}$$

Where $[\mathbf{G}]^{-1}$ expresses the generalized inverse matrix of the Jacobian matrix $[\mathbf{G}]$ and $\|[\mathbf{G}]\| \cdot \|[\mathbf{G}]^{-1}\|$ is the condition number of the Jacobian matrix denoted by K_G . As a measure of the kinematic accuracy of the mechanism, K_G indicates the sensitivity of the matrix to the errors. If K_G is high, the slight change of the terminal output velocity will cause significant change in the input velocity. The poor numerical stability will lead to a serious distortion of the transfer relationship between the input and output. At this time, the condition number of the Jacobian matrix K_G is the amplification factor of the input velocity relative to the deviation.

According to Equation (15), the global performance index of the PM can be expressed as follows:

$$\eta_G = \frac{\int_W \frac{1}{K_G} dW}{\int_W dW} \quad (19)$$

Where η_G is the measuring index of the velocity global performance index of the mechanism, $K_G = \|\mathbf{G}\| \cdot \|\mathbf{G}^{-1}\|$, $\|\cdot\|$ is the Frobenius norm of the matrix, and W is the reachable workspace of the mechanism.

The mathematical meaning of Equation (19) is the average value of the reciprocal of the condition number K_G of the mechanism in the reachable workspace. Its value indicates the average movement performance of the mechanism in the whole workspace. As $1 \leq K_G < \infty$, $0 < \eta_G \leq 1$. The higher the value of η_G , the higher the dexterity and the better the kinematic performance of the mechanism.

The purpose of the performance analysis is to find a set of optimal parameters of r_a and r_b , where the maximum values of η_G in the workspace is the optimal target. The sizes of the fixed and moving platforms of the mechanism are changed to study the influence of the size change on the performance of the mechanism. By setting the radius of the fixed platform to be $r_a = 35\text{--}50$ cm with a step length of 5 cm and the radius of the moving platform to be $r_b = 30\text{--}40$ cm with a step length of 2 cm, other sizes remain unchanged. A total of 24 groups of mechanism in different sizes are formed. The global performance index atlas of 24 mechanisms is drawn according to the values of 24 η_G , as shown in Fig. 4. As shown in Fig. 4, the smaller the radius of the moving platform and the larger the radius of the fixed platform radius, the higher the velocity global performance index of the mechanism. In other words, when $r_a = 47.1\text{--}50$ cm and $r_b = 30\text{--}31.9$, η_G is high, the velocity output error is also small. At this time, $\eta_G = 0.006166$, which means that the mechanism has high average dexterity and control precision in the whole workspace at this size.

Global Performance Fluctuation Index Analysis of the Mechanism

The velocity global performance index η_G of the mechanism reflects the average performance of the reciprocal $1/K_G$ of the condition number K_G of the mechanism's Jacobian matrix in the whole workspace, but it cannot reflect the fluctuation amplitude of the movement performance in the workspace. Researchers are not only concerned about the average performance of the mechanism but also hope that the mechanism can maintain a stable movement performance in the whole workspace without wide fluctuations. Therefore, this study proposes a global performance fluctuation index σ formula of the mechanism to evaluate the fluctuation amplitude of the movement performance in the workspace. Set K_{GS} to be the standard deviation of the performance index η_G , that is,

$$K_{GS} = \sqrt{\frac{\int_W \left(\frac{1}{K_G} - \eta_G \right)^2 dW}{\int_W dW}} \quad (20)$$

The global performance fluctuation index σ formula of the mechanism can be expressed as follows:

$$\sigma = \frac{K_{GS}}{\eta_G} = \frac{1}{\eta_G} \sqrt{\frac{\int_W \left(\frac{1}{K_G} - \eta_G \right)^2 dW}{\int_W dW}} \quad (21)$$

The performance fluctuation index σ is the coefficient of variation in statistics. The higher the value of σ , the wider the fluctuation of the performance index η_G of the mechanism in the whole workspace. The smaller the σ , the narrower the fluctuation of the performance index η_G of the mechanism in the whole workspace and the more stable the movement of the mechanism. The size parameters of the mechanism are selected with the same global performance index above. The global performance fluctuation index atlas of the mechanism can be obtained according to Equation (21), as shown in Fig. 5.

As shown in Fig. 5 and according to the meaning of the global performance fluctuation index of the mechanism, we can determine that when $r_a = 47.7\text{--}50$ cm and $r_b = 38.6\text{--}40$ cm, the global performance fluctuation index σ of the mechanism is small. At this time, $\sigma = 0.35322$, which means that the mechanism has small movement fluctuations in the workspace at this size and its movement is stable.

The influence of the important structural parameters (r_a , r_b) on the performance fluctuation index is analyzed individually using the single variable analysis method. The influence curve of (r_a , r_b) on the performance fluctuation index is drawn using MATLAB software, as shown in Fig. 6. Figure 6(a) presents the influence on the performance fluctuation index when only considering the change of r_a . At this time, $r_b = 36$ cm, and the values of other parameters are assigned in accordance with the initial parameters. Figure 6(b) shows the influence on the performance fluctuation index when only considering the change of r_b . At this time, $r_a = 45$ cm, and the values of other parameters are assigned in accordance with the initial parameters. In Fig. 6(a), when the radius of the fixed platform is unchanged, the performance fluctuation index decreases with the increase of the moving platform radius. In Fig. 6(b), when the radius of the moving platform is unchanged, the performance fluctuation index decreases with the increase of the fixed platform radius.

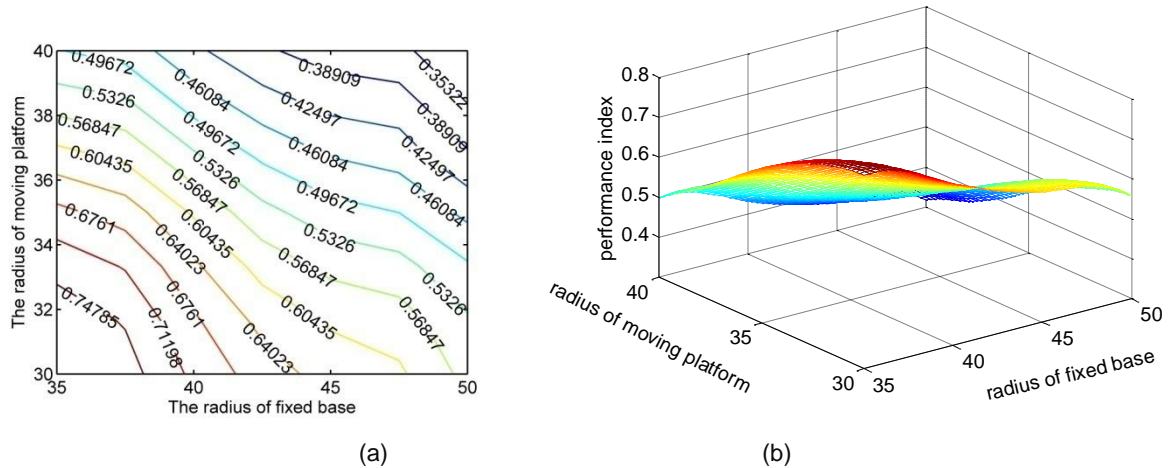


Fig. 4 - Velocity global performance index

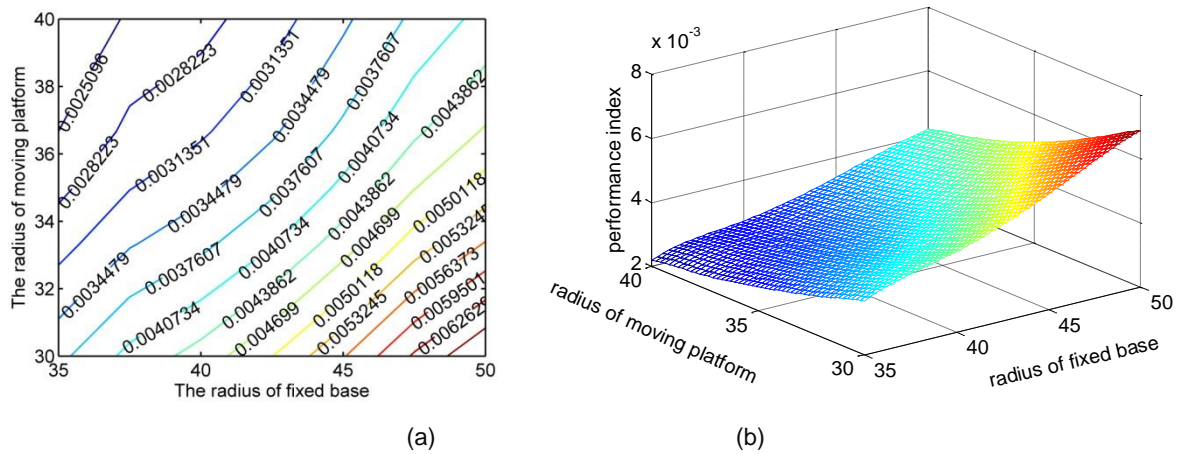


Fig. 5 - Global performance volatility index

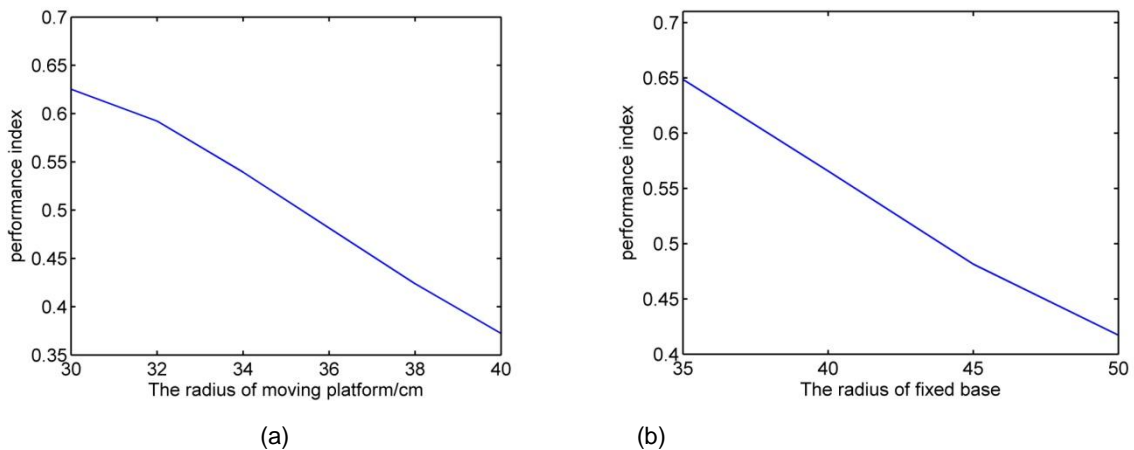


Fig. 6 - Relationship between structural parameters and performance fluctuation index

CONCLUSIONS

Automated spraying operation plays an important role in farmer's health, environment protection, and sustainable agricultural production. Target spraying robot is a key element to automated spraying operation and thus a novel 5-DOF PM which can be used in target spraying robot was proposed. To explore the constraint types of 5UPS-RPS PM and determine the effect of the sizes of fixed and moving platforms on its movement performance, this study used screw theory and the condition number of Jacobian matrix to analyse the influence of different sizes of moving and fixed platforms on the global performance fluctuation index of the PM based on its distribution law in the whole workspace. The following conclusions were drawn:

(1) The UPS driving sub-chains in the 5UPS-RPS PM are not constrained, and the RPS constraint sub-chain is constrained by the force in the direction of the Y-axis, which constrains the whole mechanism by the force in the direction of the Y-axis.

(2) When the radius of the fixed platform increases, the global performance index of the PM increases; on the contrary, when the radius of the moving platform increases, the global performance index of the PM decreases.

(3) The global performance fluctuation index decreases with the increase of the radii of the moving and fixed platforms and increases with the decrease of the radii of both platforms.

This study applies screw theory in analyzing the constraint type of the PM and introduces the variation coefficient in statistics to analyse the performance fluctuation index of the PM, which can guide the size selection of the moving and fixed platforms of 5UPS-RPS PM and the optimal design of the prototype. This study analyses the performance fluctuation index of the PM by using the condition number of the Jacobian matrix without considering the effect of the weight of each component on the performance of the mechanism. Therefore, future research should modify the model with the weights of each component of the mechanism and the condition number of the Jacobian matrix of the PM to make the size selection and optimal design of each component more accurate.

REFERENCES

- [1] Altuzarra O., Loizaga M., Pinto C., et al, (2010), Synthesis of partially decoupled multi-level manipulators with lower mobility. *Mechanism and Machine Theory*, Pergamon-Elsevier Science Ltd, Oxford/England, Vol. 45, Issue 1, pp.106-118;
- [2] Angeles J., (2006), Is there a characteristic length of a rigid-body displacement? *Mechanism and Machine Theory*, Pergamon-Elsevier Science Ltd, Oxford/England, Vol. 41, Issue 8, pp. 884-896;
- [3] Briot S., Bonev I.A., (2010), Pantoperon-4: a new 3T1R decoupled parallel manipulator for pick-and-place applications. *Mechanism and Machine Theory*, Pergamon-Elsevier Science Ltd, Oxford/England, Vol. 45, Issue 5, pp.707-721;
- [4] Dan Zhang, Zhen Gao, (2015), Performance analysis and optimization of a five-degrees-of-freedom compliant hybrid parallel micromanipulator. *Robotics and Computer-Integrated Manufacturing*, Pergamon-Elsevier Science Ltd, Oxford//England, Vol. 34, Issue 1, pp. 20-29;
- [5] Feibo Wang, Qiaohong Chen, Chuanyu Wu et al, (2015), Dimensional Synthesis of a 2-UPR-SPR Parallel Manipulator, *Chinese Journal of Mechanical Engineering*, Editorial Office Chinese Journal Mechanical Engineering, Beijing/China, Vol. 51, Issue 21, pp. 24-32;
- [6] Gosselin C., Angeles J., (1991), A global performance index for the kinematic optimization of robotic manipulators. *Journal of Mechanical Design*, Asme-Amer Soc Mechanical Eng, New York/USA, Vol.113, Issue 3, pp. 220-226;
- [7] Guiyang Xin, Hua Deng, Guoliang Zhong et al, (2015), Hierarchical kinematic modelling and optimal design of a novel hexapod robot with integrated limb mechanism. *International Journal of Advanced Robotic Systems*, Intech Europe, Vol.12, pp.1-14, Rijeka/ Croatia;
- [8] Haitao Liu, Manxin Wang, Tian Huang et al, (2015), A dual space approach for force/motion transmissibility analysis of lower mobility parallel manipulators. *Journal of Mechanisms and Robotics*, ASME, Vol.7, Issue 3, pp.1-7, New York/USA;
- [9] Hui Du, Feng Gao., Yang Pan, (2015), Kinematic analysis and design of a novel 6-degree of freedom parallel robot. *Proceedings of the Institution of Mechanical Engineers Part c-Journal of Mechanical Engineering Science*, Vol.229, Issue 2, pp. 291-303, London/England;

- [10] Hosseini M.A., Daniali H.M., (2015), Cartesian workspace optimization of tricept parallel manipulator with machining application. *Robotica*, vol.33, Issue 9, pp.1948-1957, Cambridge Univ Press, New York/USA;
- [11] Jingtao Lei, Yuanlong Cao, Feng Wang, (2013), Workspace analysis of a 4UPS-UPU parallel mechanism based on the boundary search method. *Machine Design and Research*, Vol. 29, Issue 1 pp. 5-9, Shanghai Jiao Tong University, Shanghai/China;
- [12] Liping Wang, Huayang Xu, Liwen Guan, (2015), Mobility analysis of parallel mechanisms based on screw theory and mechanism topology, *Advances in Mechanical Engineering*, Vol.7, Issue 11, pp.1-13, Sage Publications Ltd, London/England;
- [13] Plitea N., Szilaghyi A., Pisla D., (2015), Kinematic Analysis of a New 5-DOF Modular Parallel Robot for Brachytherapy. *Robotics and Computer-Integrated Manufacturing*, Vol.31, Issue 1, pp.70-80, Pergamon-Elsevier Science Ltd, Oxford/England;
- [14] Pond G., Carretero J., (2006), Formulating Jacobian matrices for the dexterity analysis of parallel manipulators. *Mechanism and Machine Theory*, Vol.41, pp.1505-1519, Pergamon-Elsevier Science Ltd, Oxford/England;
- [15] Songtao Liu, Tian Huang, Jiangping Mei et al, (2012), Optimal design of a 4-DOF SCARA type parallel robot using dynamic performance indices and angular constraints. *Journal of Mechanisms and Robotics*, Vol.4, Issue.3, pp.1-10, Asme-Amer Soc Mechanical Eng, New York/USA;
- [16] Tian Huang, Manxin Wang, Shuofei Yang et al, (2014), Force/Motion transmissibility analysis of six degree of freedom parallel mechanisms. *Journal of Mechanisms and Robotics*, Vol. 6, Issue 3, pp.1-5, ASME, New York/USA;
- [17] Xiangdun Meng, Feng Gao, Shengfu Wu, (2014), Type synthesis of parallel robotic mechanisms: Framework and brief review. *Mechanism and Machine Theory*, Pergamon- Elsevier Science Ltd, Oxford/England, Vol. 78, Issue 4, pp.177-186;
- [18] Xiulong C., Xianyang S., Yu D., (2014), Kinematics Optimum Design of a 5-DOF Spatial Parallel Mechanism. *Transactions of the Chinese Society for Agricultural Machinery*, Vol. 45, Issue 6, pp.303-307, China Agricultural Machinery Association, Beijing/China;
- [19] Yanbiao Li, Dapeng Tan, Donghui Wen et al, (2013), Parameters optimization of a novel 5-DOF gasbag polishing machine tool. *Chinese Journal of Mechanical Engineering*, Vol.26, Issue 4, pp.680–688, Editorial Office Chinese Journal Mechanical Engineering, Beijing/China.

THEORETICAL GROUNDING OF RATIONAL DESIGN FOR STRAW DISPERSER WORKING ELEMENTS OF GRAIN COMBINE HARVESTER

/

ТЕОРЕТИЧЕСКОЕ ОБОСНОВАНИЕ РАЦИОНАЛЬНОЙ КОНСТРУКЦИИ РАБОЧИХ ОРГАНОВ ИЗМЕЛЬЧИТЕЛЯ-РАЗБРАСЫВАТЕЛЯ ЗЕРНОУБОРОЧНОГО КОМБАЙНА

Prof. PhD. Eng.Sc. Rodimtsev S.A.¹⁾, Prof. PhD. Eng.Sc. Kuznetsov Y.A.¹⁾,
Prof. PhD. Eng.Sc. Kolomeichenko A.V.¹⁾, Assoc. Prof. D.Eng.Sc. Goncharenko V.V.¹⁾,
Post Graduate Stud. Yagelsky M.Y.¹⁾, Senior Lecturer Ivanushkina N.M.¹⁾,
Prof. PhD. Phil.Sc. Kalashnikova L.V.²⁾

¹⁾Orel State Agrarian University named after N.V. Parakhin / Russia

²⁾Orel State University named after I.S. Turgenev / Russia

Tel: +79208289219; E-mail: kentury@rambler.ru

Keywords: grain combine harvester, straw disperser; chopper; deflector; guide plate; tailings; uniformity of dispersion

ABSTRACT

The article presents the theoretical description of the interaction process between the straw particle and guide plate concave surface of the deflector of grain combine harvester disperser. The equation of particle present velocity is obtained. It is proved that particle velocity decreases by 8,5% at plate radius reduction from 5 m to 4 m and by 15% when particle angle of attack changes from 25° to 50°. To decrease adverse effect of particle interaction with guide surface we suggest the usage of bladed choppers with slantwise set cast blade.

РЕЗЮМЕ

Выполнено теоретическое описание процесса взаимодействия солоистой частицы с вогнутой поверхностью направляющей пластины дефлектора измельчителя-разбрасывателя зерноуборочного комбайна. Получено уравнение текущей скорости частицы. Установлено, что скорость частицы снижается на 8,5% при уменьшении радиуса пластины с 5 м до 4 м, и на 15%, при уменьшении угла атаки частицы с 25° до 50°. Для снижения вредного влияния взаимодействия частиц с направляющей поверхностью, предложено использование лопастных ножей с косо установленной швырковой лопастью.

INTRODUCTION

One of the most important performance quality indicators of grain combine harvester straw disperser is the dispersion uniformity of tailings' grinded parts (T) along field surface (Skorlyakov V.I., 2015; Skorlyakov V.I. et al, 2013; Yagelsky M.Yu. and Rodimtsev S.A., 2016).

According to agro technical requirements (Yagelsky M.Yu. and Rodimtsev S.A., 2015; Cherkasov G.N. et al, 2013; Maslov G.G. and Trubilin E.I., 2016), non-uniformity of straw dispersion should be no more than 20%. However, field tests data demonstrate sufficient excess of the permitted indicators for some types of grain harvest machinery. Thus, some authors' investigations (Lovchikov A.P. et al, 2016; Sadretdinov D.R., 2016; Yagelsky M.Yu. and Rodimtsev S.A., 2016) proved that for grain combine harvesters of some brands, the variation coefficient of straw dispersion across the mowing width can be up to 75 % and more. Herewith maximum deviation from mean value M_{mean} reaches 137 %, causing the largest mean weight variation of shredded straw on the meter long distances from mean value.

For design solution development, which provides the improvement of shredded straw dispersion across the mowing width, it is necessary to analyse particle interaction of tailings with straw disperser working elements. The investigation targets were grounding the rational design of the tested device choppers.

MATERIALS AND METHODS

To carry out the investigations we used the improved design of straw disperser of grain combine harvester (fig. 1).

In the improved design of straw disperser, choppers are manufactured with blades are set to an angle α to chopper surface. Blades of the pair of choppers are located in a single surface, oriented from the rotor center to its periphery. Choppers pairs located in the center of the rotor have blade surfaces, which are symmetrical each other and oriented to rotor off-center.

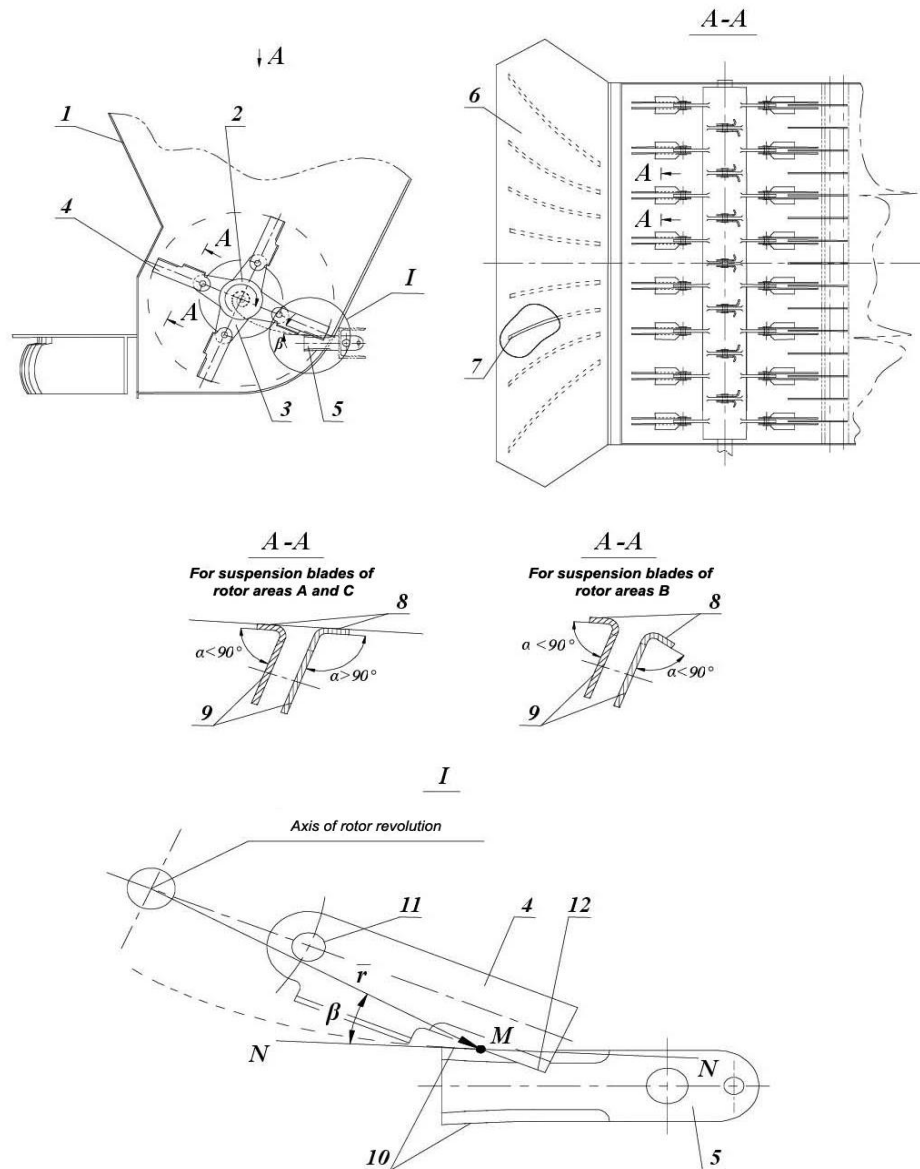


Fig. 1 - Improved design scheme of the straw disperser of grain combine harvester

1 – case; 2 – rotor; 3 – bracket; 4 – chopper; 5 – fixed counter blade of chopper; 6 – straw disperser; 7 – disperser guide plates; 8 – blades of pendular choppers; 9 – blade body; 10 – cutting edge of fixed counter blade; 11 – blade opening; 12 – chopper cutting edge

The increase of the cutting process efficiency and of straw disperser efficiency are achieved due to concave cutting edge 10 of fixed counter blades 5, done in the form of logarithmic spiral, with pole located on rotor revolution axis 2. Angle α of material pinching in cutting pair opening remains constant along the entire length of cutting edge 10 of fixed counter blade 5. This provides equal kinematic cutting mode at the initial and final stages of the process. The extended length of the curved surface of cutting edge 10 of fixed counter blade 5 provides more complete usage of technological potential of the cutting pair.

The qualitative straw dispersion behind combine harvester is achieved by directed airflows, which are formed with blades 8 of pendular choppers 4, their surface vectoring being directed sideway from rotor centre 2. They, together with guide plates 7 of disperser 6, provide uniform dispersion of the chopped mass in full bandwidth.

Usage of logarithmic spiral, with pole located on rotor revolution axis for concave cutting edge of fixed counter blade allows obtaining the next positive result. Because of the known property of logarithmic spiral, angle β between radius-vector \bar{r} , drawn from rotor revolution centre 2 to any point M on cutting edge line 10 of fixed counter blade 5 and tangent N-N to the line of cutting edge 10 at the same point, is the same.

Because of the radial position of longitudinal axis of chopper 4 towards the axis of rotor revolution 2 and its parallel position towards radius-vector \bar{r} , angle α of pinching between cutting edge 12 of chopper 4 and tangent to cutting edge 10 of fixed counter blade 5 at any point, will be the same too.

General view of the set of the experimental working elements for straw disperser of grain combine harvester "John Deere W650" is presented in fig. 2.



Fig. 2 - Set of experimental working elements for straw disperser of grain combine harvester "John Deere W650"

RESULTS

Theoretical analysis of interaction between the stem materials and the working elements of grain combine harvester disperser is carried out with application of known methods of theoretical mechanics, particularly – chapter “Differential equations of particle dynamics”.

Straw coming off the straw rack is captured with rotating vertically straw chopper rotor blades and is taken into the gap between counter cutting elements and then to the equipment bottom.

Being pinched in the opening of the cutting pair “blade - counter blade”, straw stems are chopped fast and having got kinetic energy increment at the account of impulse from the chopper working element linear velocity and impact of directed airflow, they are thrown into deflector opening. Falling on disperser guide plates, grinded particles of tailings change the path of original motion and get scattered throughout the field surface.

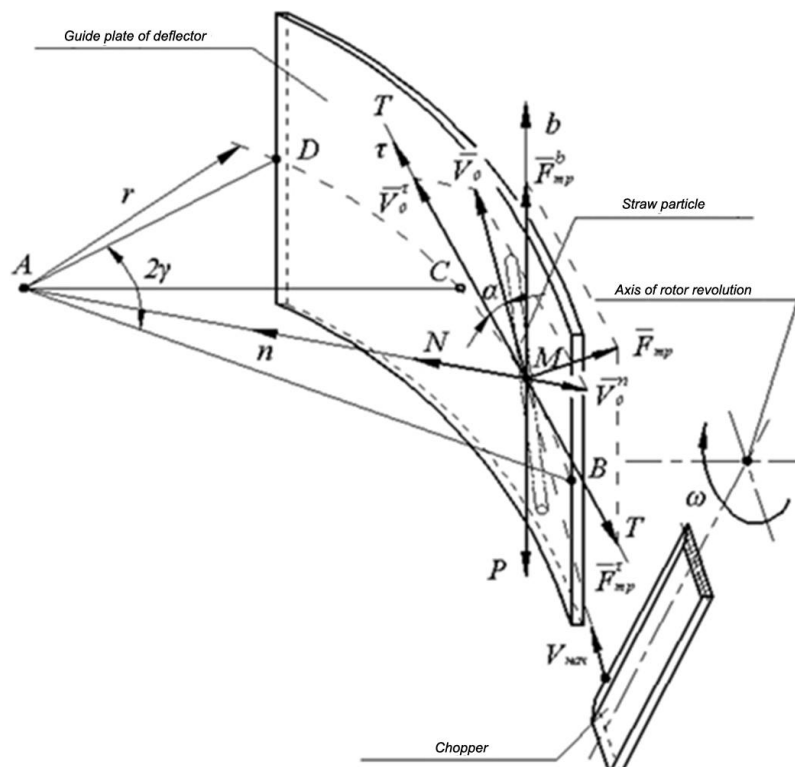


Fig. 3 - Scheme of velocity determination of particle motion along guide plate surface of disperser deflector

It is necessary to point out that, velocity vector $V_{initial}$ of tailings particles, coming from rotating rotor blades is directed perpendicular to its revolution axis. Thus, particle contact with curved surface of deflector's guide plate will be associated with velocity loss caused by the influence of sliding friction force, at particle movement along guiding line. Herewith particle energy losses will be higher the bigger the angle between particle velocity vector $V_{initial}$ and tangent guide plate at the point of initial contact.

Velocity reduction of particles coming off deflector guiding predetermines the reduction of their flying range and dispersion width and thus, increase the distribution non-uniformity.

To estimate in the first approximation the velocity change of particle at its relative movement along the concave surface of the guiding, we should examine the process of their interaction after particle coming off the rotating chopper (fig. 3).

To simplify the problem of studying the particle dynamic characteristics, some assumptions were admitted. Considering the particle as material point, because of its small mass and short duration of impact time, the energy input for particle deformation when reaching the guide plate was not taken into account. Particle velocity $V_{initial}$, at its coming off rotating blade was considered to be equal to the blade linear velocity and the initial velocity of particle V_0 , on its reaching the guide plate:

$$V_{initial} = V_0 \quad (1)$$

Curvature radius of disperser guide plate was admitted constant ($r=\text{const}$) along the plate length. Solving the problem in the simplified position, airflows influence was not considered and it was assumed that maximum value of friction force did not exceed particle gravity force.

Point with mass m , gets on disperser guide plate, which is a part of cylindrical surface of radius r , with initial velocity V_0 . Mutual disposition of vector V_0 and generating T-T guide plate at the contact point are determined by angle α .

In motion of the point along curved path, its velocity changes along the direction. Decomposing vector \bar{V}_0 into two constituents: \bar{V}_0^T – directed along guiding (tangential velocity component \bar{V}_0) and \bar{V}_0^n – directed perpendicular to guiding (normal velocity component \bar{V}_0), we obtain:

$$\bar{V}_0 = \bar{V}_0^T + \bar{V}_0^n \quad (2)$$

Models of velocity components \bar{V}_0 are equal correspondingly:

$$V_0^T = V_0 \cdot \cos\alpha \quad (3)$$

$$V_0^n = V_0 \cdot \sin\alpha \quad (4)$$

In the motion along the curved surface, the material point is affected by the following forces: gravity force \bar{P} , normal reaction of curved surface \bar{N} and friction force \bar{F}_{tp} .

Obviously, gravity action \bar{P} determines point shift vertically. Thus, sum vector \bar{F}_{tp} of friction force will be formed by tangential component \bar{F}_{tp}^T and binormal \bar{F}_{tp}^b , directed upward vertically:

$$\bar{F}_{tp} = \bar{F}_{tp}^T + \bar{F}_{tp}^b \quad (5)$$

Taking into consideration the assumptions made, the point moves along curved plate surface, formed by BCD circle arc, radius r , with central angle equal to 2γ . At curvilinear motion of constrained point, it is easier to solve the problem in projection on an axis of true trihedral.

Differential equation of material point motion in projections on an axis of true trihedral is written as follows:

$$m \frac{dV_T}{dt} = \sum Fk_T ; \quad (6)$$

$$m \frac{V^2}{\rho} = \sum Fk_n ; \quad (7)$$

$$0 = \sum Fk_b \quad (8)$$

where:

V_T – velocity projection on direction of tangent to the path;

\bar{V} – velocity module:

ρ – radius of path curvature at the given point.

F_{k_τ} ; F_{k_n} ; F_{k_b} – projections of force F on the axis of true trihedral (τ – tangential; n – principal normal; b – binormal).

Since the analysis aim is determining the dependence of particle traverse velocity from applied forces impact, the given problem is referred to inverse dynamic problems of material point.

The second axiom or basic law of dynamics, belonging to Newton, establishes the dependence of particle acceleration \bar{a} relatively inertial reference frame on the force affecting it (resultant force) \bar{F} and mass m of point:

$$m\bar{a} = \sum_{k=1}^n \bar{F}_k \quad (9)$$

According to basic law of dynamics and superposition law (9), we obtain:

$$m\bar{a} = \bar{P} + \bar{F}_{\tau p}^b + \bar{F}_{\tau p}^r + \bar{N} \quad (10)$$

Using expressions (6-8), projecting vector equality (10) on axes of natural trihedral, we obtain

$$m \frac{dV}{dt} = -f \cdot N; \quad (11)$$

$$m \frac{V^2}{r} = N; \quad (12)$$

$$0 = +P - F_{\tau p}^b \quad (13)$$

Using (12), we obtain equation (11) in the form:

$$m \frac{dV}{dt} = -f \cdot m \frac{V^2}{r} \quad (14)$$

Reducing left and right parts of equation (14) by m and reducing variables, we obtain:

$$\frac{dV}{V^2} = -\frac{f}{r} dt \quad (15)$$

Integrating left and right parts of equation (15):

$$\int \frac{dV}{V^2} = -\frac{f}{r} \int dt \quad (16)$$

we obtain:

$$-\frac{1}{V} = -\frac{f}{r} t + C \quad (17)$$

Correlation (17) is the first integral of differential equation (14) of material point movement m on axis τ of natural trihedral.

To determine integration constant C , we substitute into equation (17) initial condition of movement (at $t = 0$, $V_0^\tau = V_0 \cdot \cos\alpha$), we obtain:

$$-\frac{1}{V_0 \cdot \cos\alpha} = -\frac{f}{r} \times 0 + C \quad (18)$$

From formula (18), integration constant value C :

$$C = -\frac{1}{V_0 \cdot \cos\alpha} \quad (19)$$

Then, expression (17) will be as follows:

$$-\frac{1}{V} = -\frac{f}{r} t - \frac{1}{V_0 \cdot \cos\alpha} \quad (20)$$

Converting (17), we obtain:

$$\frac{1}{V} = \frac{f \cdot t \cdot V_0 \cdot \cos\alpha + r}{r \cdot V_0 \cdot \cos\alpha} \quad (21)$$

Then, the equation of the current velocity of material point M , at its movement on guide plate of disperser deflector, is as follows:

$$V = \frac{r \cdot V_0 \cdot \cos\alpha}{f \cdot t \cdot V_0 \cdot \cos\alpha + r} \quad (22)$$

From expression (22) it follows that velocity of tailing particle, moving along the deflector plate, decreases with the course of time being on the plate and with the decrease of concave surface radius.

The equation graphical form (22) demonstrates the decrease of particle current velocity by about 13%, at a contact time with the plate of 0.1 sec (fig. 4). Reduction of concave surface radius from 5 m to 4 m results in a decrease of particle movement velocity by 8,5%. Herewith, due to hyperbolic character of function $V(r)$, variation of guide plate curvature radius in its minimum values provides maximum degree of such dependence.

Therefore, it should be pointed out that the intensity of particle velocity decrease at the deflector contact with the plate is conditioned by angle α between velocity vector \bar{V}_0 and the guiding that generates surface T-T. For example, increase of angle of attack α from 0° to 25° (fig. 5), results in reduction of particle movement velocity by 4,2%; at changing α from 25° to 50° , particle movement velocity reduces almost by 15%.

Further increase of the angle between particle velocity vector and the guiding that generates the surface at the contact point causes the faster decrease of particle movement velocity.

The carried out analysis demonstrates negative influence of interaction of tailing particle and the deflector guiding plate on the parameters of its movement.

Those stated above allow to maintain that the reduction of negative influence of guiding plates can be achieved for example by changing the direction of tailing particles flight, after their coming off the chopper.

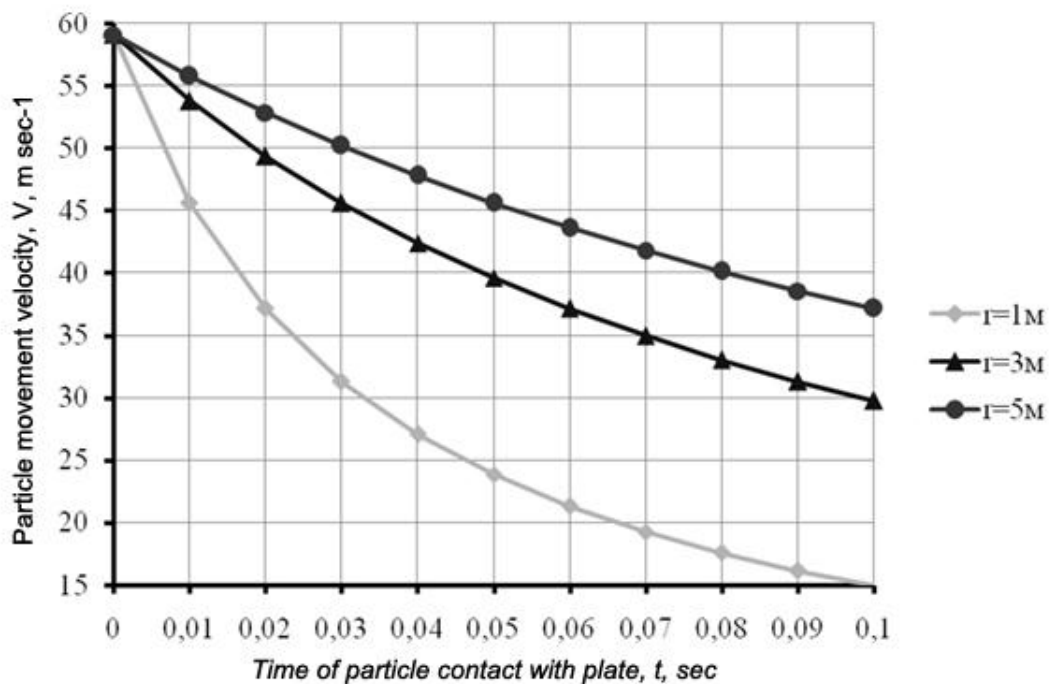


Fig 4 - Influence of radius (r) of deflector guiding curved surface and contact time (t) with straw particle, on its movement velocity (V)

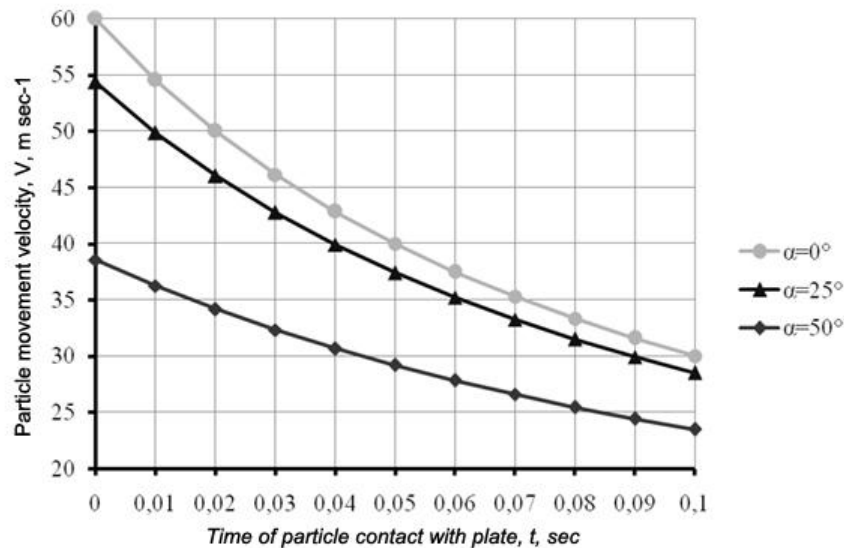


Fig. 5 - Dependence of straw particle movement velocity (V) on the contact time (t) with guide plate surface and attack angle (α), at the moment of the beginning of their interaction

The particle movement path from rotating blade to the periphery of disperse area (fig. 3), reduces the probability of interaction of chopped stems and the guiding, without decrease of quality of straw disperse on the field area. Therefore, the direction of particle flight, under some angle β to apical axis of combine harvester, reduces angle α between velocity vector \bar{V}_0 of the particle and generating T-T deflector guiding, at the contact point. This will also provide the decrease of negative influence of interaction between the guiding and the particle on its movement velocity. Thus, the conditions for increasing uniformity of straw dispersing along the field surface will be created.

Technically, the flight direction change of chopped tailing particles can be achieved by using blades that can combine this task with the main function– straw chopping.

Blades design with blades located perpendicular to choppers plane in its front part is known (Sadretdinov D.R., 2016; Skorlyakov V.I. and Yurina T.A., 2016; Yagelsky M.Yu. and Rodimtsev S.A., 2017). This blade drawback is airflow formed by it, the direction of which as well as the path of chopped particle movement at coming off chopper blades are strictly parallel to combine harvester symmetry axis. This provides low degree of straw distribution uniformity across the width of disperse zone.

The suggested design of straw disperser chopper blades of grain combine harvester provides the following advantages:

- decrease of degree of chopped straw distribution non-uniformity without violation of cutting process kinematics;
- decrease of energy input for chopped straw dispersing at the account of formed powerful airflows with direct effect;
- the proposed technical solution does not cause serious design alterations, but its working elements enhancement is possible in the conditions of any machine work-shop and does not require some extra materials.

CONCLUSIONS

1. The expansibility of chopped straw dispersion width at the account of reducing the particle contact with deflector guide plate is theoretically substantiated. The equation of material point current velocity at its motion along the disperser deflector guide plate is obtained.

2. Based on the experimental data of the field investigations, we plotted diagrams of dependences of chopped particle movement velocity on duration of its contact with the deflector plate for different curve radii of the plate and attack angles at the beginning of the interaction between the particle and the plate.

3. To decrease adverse effect of interaction between straw particle and the surface of disperser deflector guide plate of grain combine harvester, the usage of bladed choppers with slantwise set cast blade is proposed.

REFERENCES

- [1] Lovchikov A.P., Lovchikov V.P., Pozdeev E.A., (2016), Agrotechnical evaluation of straw disposer operation of combine harvesters at grain crops harvesting by direct combining (Агротехническая оценка работы измельчителей-разбрасывателей соломы комбайнов при уборке зерновых культур прямым комбайнированием), *Bulletin of Orenburg State Agrarian University (Известия оренбургского государственного аграрного университета)*, Issue number 2, pp. 55-57, Orenburg / Russia;
- [2] Sadretdinov D.R., (2016), Parameters grounding of straw disposer of grain combine harvester (Обоснование параметров разбрасывателя соломы зерноуборочного комбайна), *Bulletin of Orenburg State Agrarian University (Известия оренбургского государственного аграрного университета)*, Issue number 6, pp. 72-74, Orenburg / Russia;
- [3] Sadretdinov D.R., (2016), Interconnection of straw chopping length and straw disposer construction design (Взаимосвязь длины измельчения соломы и конструкционного исполнения измельчителя-разбрасывателя), *Tractors and agricultural machinery (Тракторы и сельхозмашины)*, Issue number 5, pp. 42-45, Moscow / Russia;
- [4] Skorlyakov V.I., (2015), Evaluation improvement of grain combine harvesters with straw choppers (Совершенствование оценок зерноуборочных комбайнов с измельчителями соломы), *Technique and equipment for village (Техника и оборудование для села)*, Issue number 11, pp. 15-18, Moscow / Russia;
- [5] Skorlyakov V.I., Yurina T.A., (2016), Improvement of performance evaluation of grain combine harvesters (Совершенствование оценок качества работы измельчителей зерноуборочных комбайнов), *Science in the Central Russia (Наука в центральной России)*, Issue number 2, pp. 58-66, Moscow / Russia;
- [6] Skorlyakov V.I., Yurina T.A., Negreba O.N., (2013), Quality of chopping and straw disposing at grain crop harvesting: analysis of requirements and achievements (Качество измельчения и разбрасывания соломы при уборке зерновых культур: анализ требований и достижений), *Agrosnabforum (Агроснабфорум)*, Issue number 2, pp. 23-28, Krasnodar / Russia;
- [7] Yagelsky M.Yu., Rodimtsev S.A., (2017), Types and classification of straw disposer choppers of grain combine harvesters (Типы и классификация ножей измельчителей-разбрасывателей соломы зерноуборочных комбайнов), *Bulletin of Voronezh State Agrarian University (Вестник Воронежского государственного аграрного университета)*, Issue number 1, pp. 114-122, Voronezh / Russia;
- [8] Yagelsky M.Yu., Rodimtsev S.A., (2016), Updating of agrotechnical requirements to combine harvester technologies of grain crops harvesting with chopping and dispersion tailings (Актуализация агротехнических требований к комбайновым технологиям уборки зерновых культур с измельчением и разбрасыванием незерновой части урожая), *Agrotechnics and energy supply (Агротехника и энергообеспечение)*, Issue number 1(10), pp. 28-39, Oryol / Russia;
- [9] Yagelsky M.Yu., Rodimtsev S.A., (2015), Some opportunities for updating agrotechnical requirements to straw choppers of grain combine harvesters (Некоторые предпосылки для актуализации агротехнических требований к соломоизмельчителям зерноуборочных комбайнов), *Agrotechnics and energy supply (Агротехника и энергообеспечение)*, Issue number 3(7), pp. 239-247, Oryol / Russia;
- [10] Cherkasov G.N., Pykhtin I.G., Gostev A.V., Nitchenko L.B., Plotnikov V.A., Ilyina G.P., (2013), Register of technologies of grain crop cultivation for the Central Chernozem Region (Реестр технологий возделывания зерновых культур для Центрального Черноземья), ГНУ ВНИИЗиЗПЭ РАСХН., 249 p., Kursk / Russia;
- [11] Maslov G.G., Trubilin E.I., (2016), Grounding of grain combine harvesters parameters and their efficiency (К обоснованию параметров зерноуборочных комбайнов и их эффективности), *Agricultural machines and technologies (Сельскохозяйственные машины и технологии)*, Issue number 2, pp. 28-31, Moscow / Russia.

TROPICAL WOOD CLASSIFICATION BASED ON LBP-LIKE DESCRIPTOR AND NEAREST NEIGHBOR CLASSIFIER

基于纹理特征及最近邻分类器的木材分类识别

Chao Xiaofei, Cai Cheng, Zhang Zhiyong, Nie Liangbing, Li Shuqin

College of Information Engineering, Northwest A&F University, Yangling, Shaanxi 712100, P.R. China

Email: zhangzhi_9575@163.com

Keywords: tropical wood classification, texture, LBP, nearest neighbour classifier

ABSTRACT

This paper compares the discriminative ability of six LBP-like texture descriptors for tropical wood classification, LBP, uniform LBP, rotation invariant LBP, rotation invariant uniform LBP, covariance of LBP and covariance of LBP difference were considered. Experiments on wood image dataset with 54 wood species was carried out, experimental results show that these six descriptors combined with nearest neighbour classifier achieve recognition rate of 97.50%, 96.64%, 92.84%, 88.55%, 54.40% and 56.53% respectively. LBP is the best and one of the efficient wood texture descriptors among these six LBP-like descriptors. LBP_{8,8} is the best and most stable wood texture feature, the recognition rate of LBP_{8,8} and LBP_{8,2}^{u2} are 97.84% and 97.41% respectively, the time to classify one image by them is 0.28 second and 0.08 second. Compared with existing wood image classification methods, the combination of LBP descriptor with nearest neighbour classifier is very simple, it does not need the feature selection and training process, and it achieves much better time efficiency and a slightly lower recognition rate than the existing algorithms.

摘要

本文对比了LBP、Uniform LBP、旋转不变LBP、旋转不变Uniform LBP、LBP协方差矩阵、LBP差协方差矩阵等6种不同的类LBP纹理描述算子的分类性能。分类对比实验在具有54种木材类别的数据库上进行,实验结果证明六种类LBP算子结合最近邻分类器分别能够得到97.50%、96.64%、92.84%、88.55%、54.40%以及56.53%的分类识别率。其中LBP具有最稳定的木材纹理描述能力,LBP_{8,8}以及LBP_{8,2}^{u2}的识别率分别为97.84%和97.41%,两者识别一副图像所需时间分别为0.28秒及0.08秒。与现存木材分类方法相比,将LBP算子与最近邻分类器结合进行木材分类方法更简单,不需要进行特征选择及训练阶段,且时间效率大大提高而分类识别率只有细微降低

INTRODUCTION

Timbers are usually classified by their appearance and weight based on visual inspection. Whereas, wood colour may change after storing and it is hard to measure the intensity of wood pores precisely. As a unique characteristic of timber, wood textures provide an efficient way for online wood classification. Several different kinds of wood recognition system have been designed in various ways (Khalid et al., 2008; Bremananth et al., 2009; Tang et al., 2009; Khairuddin et al., 2011; Yusof et al., 2013a; Yusof et al., 2013b; Mohan et al., 2014; Taman et al., 2014; Zhang et al., 2014; Ibrahim et al., 2015). GLCM (Gray-Level Co-Occurrence Matrix) has been used to classify wood image (Khalid et al., 2008; Bremananth et al., 2009). Among them, Khalid used GLCM to classify wood dataset with about 20 species; they get the average accuracy of 95% (Khalid et al., 2008). (2D) 2PCA was proposed to classify chordal section wood images and its classification accuracy on datasets of 60 wood classes is 76.67%.

Khairuddin et al. combined BGLAM (Basic grey level aura matrix) with distributions of wood pores under microscopy to classify the tropical wood dataset of 52 different classes; they got accuracy of 94.4% (Khairuddin et al., 2011). Yusof et al. proposed a framework that uses pre-classifier to improve the recognition rate and efficiency (Yusof et al., 2013). Yusof et al. combined the KDA (Kernel discriminant Analysis) and GA (genetic algorithm) to reduce the dimension of the timber database, to improve the recognition rate (98.69%) and the time efficiency (1.2 second to recognize an image of size 768×576) (Yusof et al., 2013). Ibrahim et al. use pre-classifier and nonlinear feature selection to classify tropical wood, their method got lower accuracy of 98.5 but slightly faster recognition speed (1 second to recognize one image) (Ibrahim et al., 2015) compared to the non-linear feature selection method (Yusof et al., 2013).

Time efficiency is the key factor for the wood recognition system to classify the timber online successfully. Compared to GLCM, PCA and Gabor transform, LBP (Local Binary Pattern) is with low computation complexity, resistance to light changes and has the ability to describe details (Nanni et al., 2012). Since texture descriptor is one of the key factors for success texture classification, this paper compares the recognition rate and efficiency of six LBP-like texture descriptors to choose the wood texture descriptor with the promise discriminative ability and good time efficiency. These six LBP-like descriptors are LBP (Local Binary Pattern) (Ojala et al., 1996), uniform LBP (Ojala et al., 2002), rotation invariant LBP (Ojala et al., 2002), rotation invariant uniform LBP (Ojala et al., 2002), covariance of LBP difference (Hong et al., 2014) and covariance of LBP (Hong et al., 2014).

The remaining sections are organized as follows. Section 1 introduces the definition of these six LBP-like descriptors. Section 2 introduces the dataset, the distance measure methods for histograms and covariance matrices and the proposed tropical wood recognition method. Section 3 compares the classification abilities and efficiencies of these six LBP-like descriptors, the confusion matrix of the best LBP-like descriptor is given in this section, it also compares the recognition rate and time efficiency of the optimal LBP-like descriptor with existing methods. Conclusions and possible improvements are discussed in Section 4.

1. LBP-LIKE DESCRIPTORS

1.1 LBP

LBP is a method to extract local grey level information (Ojala et al., 1996). LBP sequence represents the comparison of a pixel to its neighbouring ones in a local area, it compares the feature value (usually grey value) of the middle pixel with its neighbouring pixels, if the feature value of the middle pixel is bigger than those of the neighbouring pixel, then the LBP value of the neighbouring pixel is 0, otherwise the LBP value will be 1. Calculation of LBP is described in equation (1) (Ojala et al., 1996).

$$LBP_{P,R}(x) = \sum_{p=0}^{P-1} S(g_p - g_c) 2^p \quad (1)$$

Where $\{g_p\}_{p \in \{0, P-1\}}$ is the feature value of P neighbouring pixels, with distance R to the central pixel x . g_c is the feature value of central pixel x . $S(x)$ is the step function with $S(x)=1$ when $x \geq 0$ and $S(x)=0$ for otherwise. The bit order and example for calculating LBP (Ojala et al., 1996) is given in figure 1, where P equals 8 and R equals 1.

1.2 Uniform LBP

Most of texture information is represented by a small subset in LBP (Ojala et al., 2002); this subset is called uniform LBP. If the number of bitwise spatial transitions (from 1 to 0 or from 0 to 1) in LBP is not bigger than 2 (including the transition from end to the beginning), then the LBP is a uniform LBP, the other LBP patterns are called the non-uniform patterns. i.e., 01110000 and 10000000 are uniform LBP patterns, but 10000100 and 00100100 are non-uniform patterns. The number of LBP patterns is $P(P-1)+3$, P is the number of neighbouring points. Calculation of uniform LBP is described in equation (2) (Ojala et al., 2002).

$$LBP_{P,R}^{u2} = \begin{cases} \sum_{p=0}^{P-1} S(g_p - g_c) 2^p, & U(LBP_{P,R}) \leq 2 \\ other, & otherwise \end{cases} \quad (2)$$

Where P is the number of neighbouring points, and R is the radius. $S(x) = 1$, if $x \geq 0$, and $S(x) < 0$ for otherwise. $u2$ stands for the number of bitwise transitions (including the transition from end to the beginning) in LBP is not more than 2, $U(LBP_{P,R})$ stands the number of bitwise transitions (including the transition from end to the beginning) in $LBP_{P,R}$ pattern. In Ojala's research, if (P, R) equal $(8, 1)$, the uniform LBP represent at least 90% of the texture information, and if (P, R) equal $(16, 2)$, the uniform LBP represent at least 70% of the texture information. Uniform LBP not only can describe the majority of the texture information, but also for dark spots, smooth region, and the light spots of the edge. It has strong classification ability with higher time efficiency compared to LBP (Ojala et al., 2002).

1.3 Rotation invariant LBP

The classification ability of LBP is irrelative to the binary coding order. A LBP value is a label for its pattern, numerical comparison between two LBPs is meaningless. LBP changes a lot when image rotation happens, while rotation invariant LBP has the same texture classification ability when rotation happens. Rotation invariant LBP treat the different LBPs which rotated from the same LBP as one class. Rotation invariant LBP is denoted as $LBP_{P,R}^{ri}$, its definition is given in equation (3) (Ojala et al., 2002).

$$LBP_{P,R}^{ri} = \min \{ \text{ROR}(LBP_{P,R}, i) \mid i = 0, 1, 2, \dots, P-1 \} \quad (3)$$

Function ROR ($LBP_{P,R}, i$) move LBP binary sequence to the right circularly for i bits, where $i \in [0, P-1]$. Number of $LBP_{P,R}^{ri}$ patterns is 36 when P equals 8. $LBP_{8,1}^{ri}$ is LBPROT (Pietikäinen et al., 2000) when R equals 1.

1.4 Rotation invariant uniform LBP

The occurrence frequencies of each patterns in $LBP_{8,1}^{ri}$ varies a lot and its crude quantization of the angular space at 45° intervals lead to a non-ideal texture recognition rate. $LBP_{P,R}^{riu2}$ provides the vast majority of texture information, which includes the bright spots, flat points, dark spots and different curved edge texture information. Therefore, $LBP_{P,R}^{ri}$ and $LBP_{P,R}^{riu2}$ can be combined to get the rotation invariant uniform LBP. Rotation invariant uniform LBP is denoted as $LBP_{P,R}^{riu2}$, it has $P+1$ different patterns, it is defined as listed in equation (4) (Ojala et al., 2002):

$$LBP_{P,R}^{riu2} = \begin{cases} \sum_{p=0}^{P-1} S(g_p - g_c), & \text{if } U(LBP_{P,R}) \leq 2 \\ P+1, & \text{otherwise} \end{cases} \quad (4)$$

Where $U(LBP_{P,R}) = |S(g_{P-1} - g_c) - S(g_0 - g_c)| + \sum_{p=1}^{P-1} |S(g_p - g_c) - S(g_{p-1} - g_c)|$, and $riu2$ stands for the use of rotation invariant uniform pattern, and U is less or equal to 2, function S is the same as those used in $LBP_{P,R}^{riu2}$. $LBP_{P,R}^{riu2}$ has $P+2$ different values.

1.5 Covariance of LBP

Compared to histogram, covariance matrix of different features of one image is more compact (Hong et al., 2014). Covariance Matrix (CovM) not only combines several different feature channels together, but reflects the covariance of any two of the elementary features as well (Tuzel et al., 2006). LBP is one of the

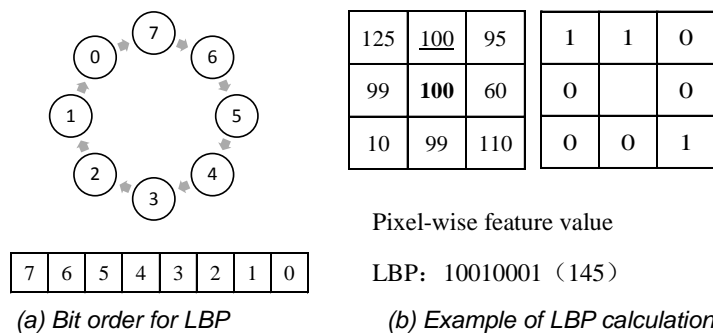


Fig. 1 - LBP descriptor

effective texture descriptors. Covariance matrix of local binary pattern is computed by different LBPs of one image.

Covariance matrix of local binary pattern is denoted as \mathbf{CovM}_{LBP} and can be computed by equation (5) (Tuzel et al., 2006).

$$\mathbf{CovM}_{LBP}(I) = c \sum_{x \in I} (f(x) - \mu)(f(x) - \mu)^T \quad (5)$$

Put N LBPs of one pixel into an N dimensional feature vector $f(x)$, μ is the average vector of the feature vectors in one image area, I is an image area, and $\{f(x)\}_{x \in I}$. The size of \mathbf{CovM}_{LBP} is $N \times N$, c is a normalization factor (Tuzel et al., 2006).

1.6 Covariance of LBP difference

LBPD (Local Binary Pattern Difference) was proposed by Hong et al. (Hong et al., 2014). LBPD of one pixel is the difference between its LBP and LBP mean, LBP mean is the mean vector of LBPs within an image area. LBPD is a real value. LBPD is rotation invariant and insensitive to noises since one bit difference would not contribute much difference to the LBPD. There are three steps to calculate LBPD for one image (area). Firstly, we calculate LBP for one image (area), then calculate the mean vector of this image (area) to get LBP mean vector, the last step is to calculate the difference vector between LBP and LBP mean to get the LBPD for each pixel. A covariance matrix of LBPD with size $N \times N$ of N different LBPDs for one image (area) can be calculated by equation (5) (Hong et al., 2014), covariance matrix of LBPD is denoted as \mathbf{CovM}_{LBPD} , $f(x)$ is an N dimensional feature vector of n LBPDs, μ is the average vector of the feature vectors in one image area, and $\{f(x)\}_{x \in I}$. The size of \mathbf{CovM}_{LBPD} is $N \times N$, c is a normalization factor (Tuzel et al., 2006).

MATERIALS AND METHODS

2.1 Wood database

The dataset used in our experiment contains the timber images of Forest Research Institute Malaysia downloaded from the website <https://info.frim.gov.my/woodid/index.cfm#>. The dataset has images of 54 different tropical timber species, and each species has 9 images, which produce 486 images for the wood database. Resolution of images is about 500x600. Figure 2 provide some examples of the wood images from 8 different wood species in the database. We can see from figure 2 that images of some different wood species share great similarities, this would increase the difficulty of classification.

2.2 Distance measurement

2.2.1 Distance measurement for histograms

Histogram is treated as a vector, therefore, the distance measurement for vectors can be used directly to measure the dissimilarity of histograms (Cha and Srihari, 2002).

Suppose that A and B are histograms. Then the Euclidean distance and Chi-square distance are defined as follows. $H_i(X)$ is the value of the i -th bin of histogram X .

(1) Euclidean distance

Euclidean distance is originated in Euclidean geometry; Euclidean distance is denoted as $D_E(A, B)$, which is defined in equation (6). The bigger the $D_E(A, B)$, the bigger the distance between histograms A and B (Cha and Srihari, 2002).

$$D_E(\mathbf{A}, \mathbf{B}) = \sqrt{\sum_{i=0}^{b-1} (H_i(\mathbf{A}) - H_i(\mathbf{B}))^2} \quad (6)$$

(2) Chi square distance

Based on Euclidean distance, Chi-square distance considers the relative difference of bins in the same position and it pays more attention to the difference of smaller bins (Pele and Werman, 2010). This is more effective for LBP distance description, especially for histogram vectors of uniform LBP, where the non-uniform pattern is usually bigger than uniform patterns, so that Chi-square pays more attention to the uniform patterns which is usually smaller than the non-uniform patterns. Hence, compared to Euclidean distance, Chi-square distance is more suitable for describing the histogram distance. Chi-square distance is denoted as $D_X(A, B)$, The bigger the $D_X(A, B)$, the bigger the distance between histograms A and B . Equation (7) gives the definition of Chi-square distance (Pele and Werman, 2010).

$$D_X(\mathbf{A}, \mathbf{B}) = \sum_{i=0}^{b-1} \frac{(H_i(\mathbf{A}) - H_i(\mathbf{B}))^2}{H_i(\mathbf{A}) + H_i(\mathbf{B})} \quad (7)$$

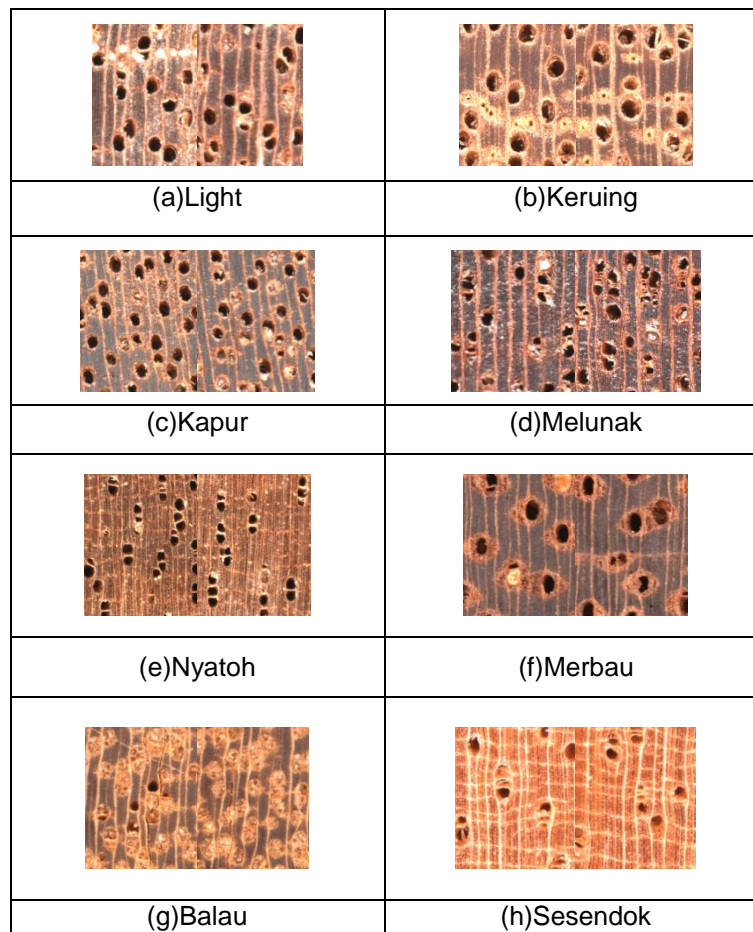


Fig 2 - Wood texture image sample

2.2.2 Distance measurement for covariance matrix

We use one of the Riemannian manifold based metric to calculate the distance of two covariance matrices \mathbf{M}_1 and \mathbf{M}_2 ^[11]. Distance measurement of two covariance matrices is defined in equation (8).

$$d(\mathbf{M}_1, \mathbf{M}_2) = \sqrt{\sum_{i=1}^n \ln^2(\lambda_i(\mathbf{M}_1, \mathbf{M}_2))} \quad (8)$$

Where $\{\lambda_i(\mathbf{M}_1, \mathbf{M}_2)\}_{i=1, \dots, n}$ are the n generalized eigenvalues of two positive definite matrices \mathbf{M}_1 and \mathbf{M}_2 .

Compared to most of the other feature matrices, Covariance Matrix is more compact, it always equals $N \times N$ no matter how big the image size is, where N is the number of elementary features.

2.3 Proposed method

This paper uses $LBP_{P,R}$, $LBP_{P,R}^{ri2}$, $LBP_{P,R}^{ri}$, $LBP_{P,R}^{riu2}$, \mathbf{CovM}_{LBP} , and \mathbf{CovM}_{LBPD} to describe wood image textures, then combines each of these descriptors with Nearest Neighbor (NN) classifier separately. Different (P, R) values for all these six descriptors are compared, where P is the number of neighbours and R is the radius. Because of memory limitation, we set P equal to 8, and R equal to 1, 2, 4, and 8 respectively, so that we get four features for each of these six descriptors, and twenty four features for one image.

Then the average recognition rates of these six descriptors are compared, the best descriptor and its best (P, R) value are selected. The recognition rate for each different feature is the average recognition rate of 10 times classification using random permutation.

(1) Random permutation

In NN classification section, K (we use 3 in our experiment) images are selected randomly as the test images, so that the left images would be the training images (for each class, number of training images is $9-K$).

Then, use NN classifier to recognize the test image, compare the class of nearest neighbor with those of test image, if they are the same, then the classification rate for this test image is 100%, and 0 for otherwise. The classification rate of one random permutation experiment is the average of the classification accuracy of all test images.

Recognition rate can be calculated by the average of the classification rate of 10-times random permutation experiments; this would ensure the representativeness and reliability of the results (Micheals and Boul, 2001).

(2) Procedure for wood recognition:

There are three steps to classify the tropical wood images:

Firstly, turn the RGB image to gray image. The second step is to calculate these twenty four features for each images, using $LBP_{P,R}$, $LBP_{P,R}^{u2}$, $LBP_{P,R}^{ri}$, $LBP_{P,R}^{riu2}$, $CovM_{LBP}$, and $CovM_{LBPD}$ with four different (P,R) values. Finally, classify images by combining different features with NN classifier separately, where distances of $LBP_{P,R}$, $LBP_{P,R}^{u2}$, $LBP_{P,R}^{ri}$, $LBP_{P,R}^{riu2}$ are calculated by equation (7) and distances of $CovM_{LBP}$, and $CovM_{LBPD}$ are calculated by equation (8).

(3) Calculation of recognition rate

Take $R(LBP_{P,R}^X)$ as the recognition rate of $LBP_{P,R}^X$, N is the size of test set, M_t is the number of test images that have been correctly classified in the t-th random permutation experiment, and T is the times of random permutation experiment. Recognition rate of one feature can be calculated by equation (9).

$$R(LBP_{P,R}^X) = \frac{\sum_{t=1}^T M_t}{T * N} * 100\% \tag{9}$$

RESULTS

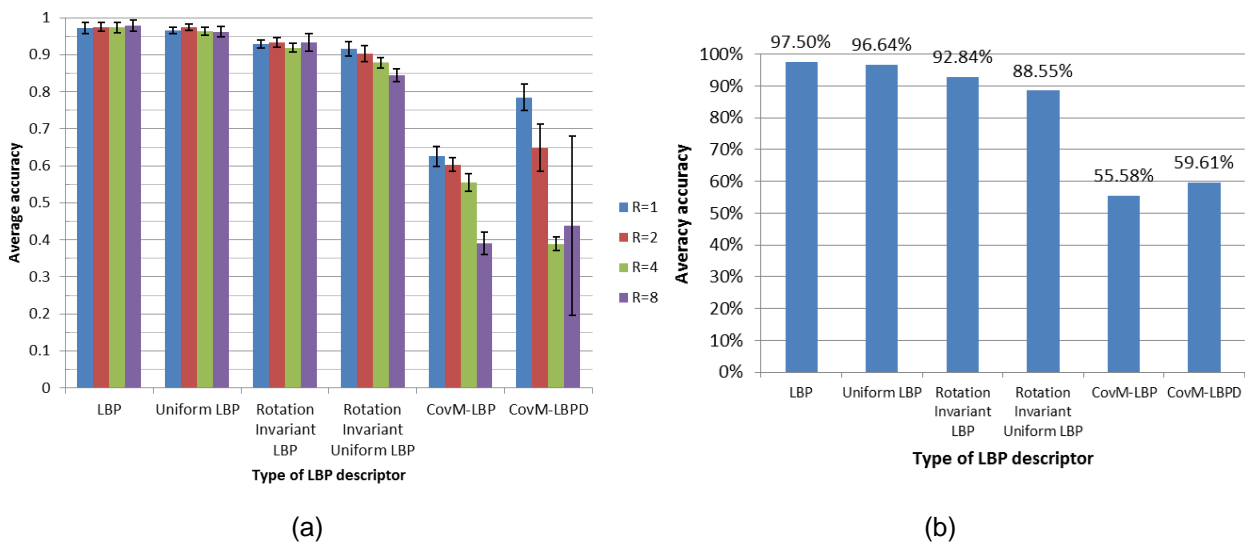


Fig. 3 - Comparison of accuracy of wood classification using different LBP-like descriptors (where P equals 8)

(a) Comparison of classification accuracy and the standard deviation using different LBP-like descriptors with different (P, R) value.

(b) Accuracy of wood classification using different LBP-like descriptors. Wherein, LBP is for $LBP_{P,R}$, uniform LBP is for $LBP_{P,R}^{u2}$, rotation invariant LBP is for $LBP_{P,R}^{ri}$, rotation invariant uniform LBP is for $LBP_{P,R}^{riu2}$, CovM_LBP is for CovMLBP and CovM_LBPD is for CovMLBPD.

Figure 3 compares the classification accuracy and their standard deviation of $LBP_{P,R}$, $LBP_{P,R}^{u2}$, $LBP_{P,R}^{ri}$, $LBP_{P,R}^{riu2}$, $CovM_{LBP}$, and $CovM_{LBPD}$, where P is 8 and R is equal to 1,2,4,8 respectively, so that there are four different bars for each texture descriptors. In figure 3(a), Error bar with standard deviation shows the deviation of recognition rate from their mean, where $LBP_{P,R}^{u2}$ has the smallest standard deviation so that it has the most stable performance, and the $LBP_{P,R}$ is the second steady descriptor, $CovM_{LBPD}$ has the worst stability. Figure 3(b) compares the mean recognition rate of $LBP_{P,R}$, $LBP_{P,R}^{u2}$, $LBP_{P,R}^{ri}$, $LBP_{P,R}^{riu2}$, $CovM_{LBP}$, and

$CovM_{LBD}$, where each descriptor's mean accuracy are calculated by averaging the recognition rate of its four different (P,R) s. It is clearly to see that $LBP_{P,R}$ has the best average classification accuracy of 97.5%, $LBP_{P,R}^{u2}$ is the second best, where its mean recognition rate is 96.64%, recognition rate of different (P,R) values are nearly the same for $LBP_{P,R}$. $LBP_{8,8}$, with a recognition rate of 97.84%, showing the best classification ability, the second best feature is $LBP_{8,2}^{u2}$, with a classification rate of 97.41%.

Figure 4 compares the mean recognition rate of $LBP_{P,R}$, $LBP_{P,R}^{u2}$, $LBP_{P,R}^{ri}$, $LBP_{P,R}^{riu2}$ for different wood species by radar graph (for the clarity of different lines, $CovM_{LBP}$ and $CovM_{LBD}$ with low recognition rates are not included in figure 4). There are 7 concentric circles in the radar graph, where the radius of each circles are the classification rate, and the centre of the circle is relative to the recognition rate of 30%, and the recognition rate of circles from the centre to the outer circle are 40%, 50%, 60%, 70% , 80%, 90%, 100%, respectively. Dots in the outer circle are the wood species names and their class number (i.e., "1 Balau" means the wood class name is Balau, and its class number is 1). Four curves on the radar graph stands for recognition rates of $LBP_{P,R}$, $LBP_{P,R}^{u2}$, $LBP_{P,R}^{ri}$, and $LBP_{P,R}^{riu2}$ respectively. It is clearly to see that these four descriptors have 100% recognition rate for wood species Dammar, Gerutu, Kulim, Kungkur, Nyatoh, Perupok, Pulai, Resak, Tembusu, Terentang, and YellowMeranti, while the recognition rate of these four descriptors are not ideal for wood species Dark, Kapur, Kempas, Keruing, Light, Melunak, Sepetir, and WhiteMeranti.

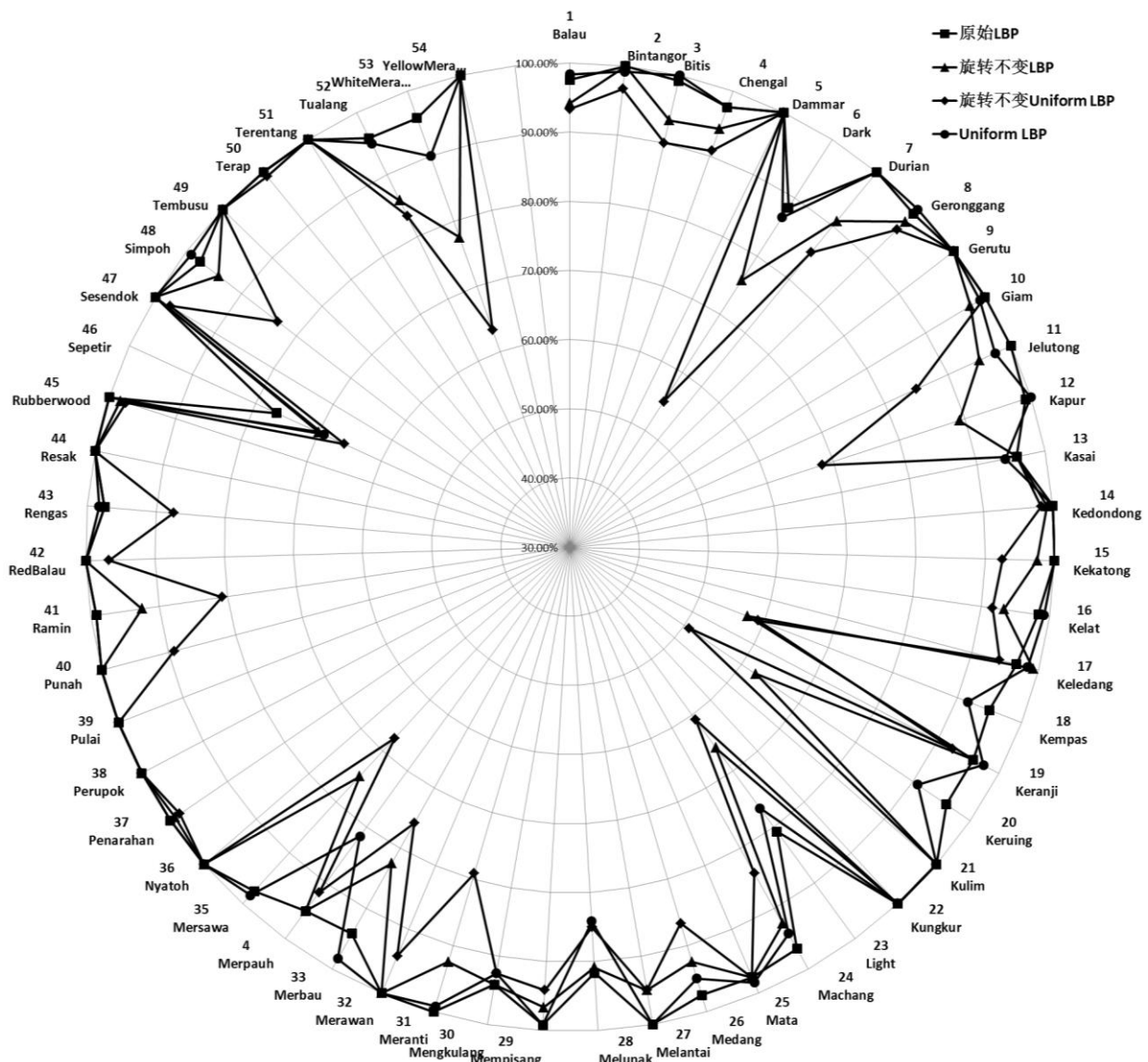


Fig. 4 - Comparison of classification accuracy for four LBP-like descriptors combined with nearest neighbor classifier respectively

Figure 5 is the confusion matrix of $LBP_{8,8}$, numbers from 1 to 54 in figure 5 represent the wood class number in figure 4. Values in figure 4 are between [0%, 100%], white stands for 0%, standard red is the transition colour and black stands for the recognition rate of 100%. The colours of recognition rate in [0%, 33.33%] gradually change from white to standard red, while the colours of recognition rate in (33.33%, 100%) gradually change from standard red to black. The colour bar of figure 5 is shown on its right side. From the colour of diagonal line of figure 5, we can see that $LBP_{8,8}$ has very good classification ability for almost all of the wood classes, only a small portion of the test samples are misclassified to other classes, and most of the misclassified test samples are classified as the wood classes of the same wood family.

Table 1 compares the recognition rate and time efficiency of existing algorithms (Khalid et al., 2008; Khairuddin et al., 2011; Yusof et al., 2013; Ibrahim et al., 2015),. The time efficiency of proposed method ($LBP_{8,8}$ combined with nearest neighbor) is 4.27 times faster than nonlinear feature selection method (Yusof et al., 2013), while its recognition rate is 97.84%, which is only 0.85% lower than those of the nonlinear feature selection method. Recognition rate of $LBP_{8,2}^{u2}$ is 97.41%, which is slightly lower than those of $LBP_{8,8}$, but its time efficiency is 3.6 times of $LBP_{8,8}$.

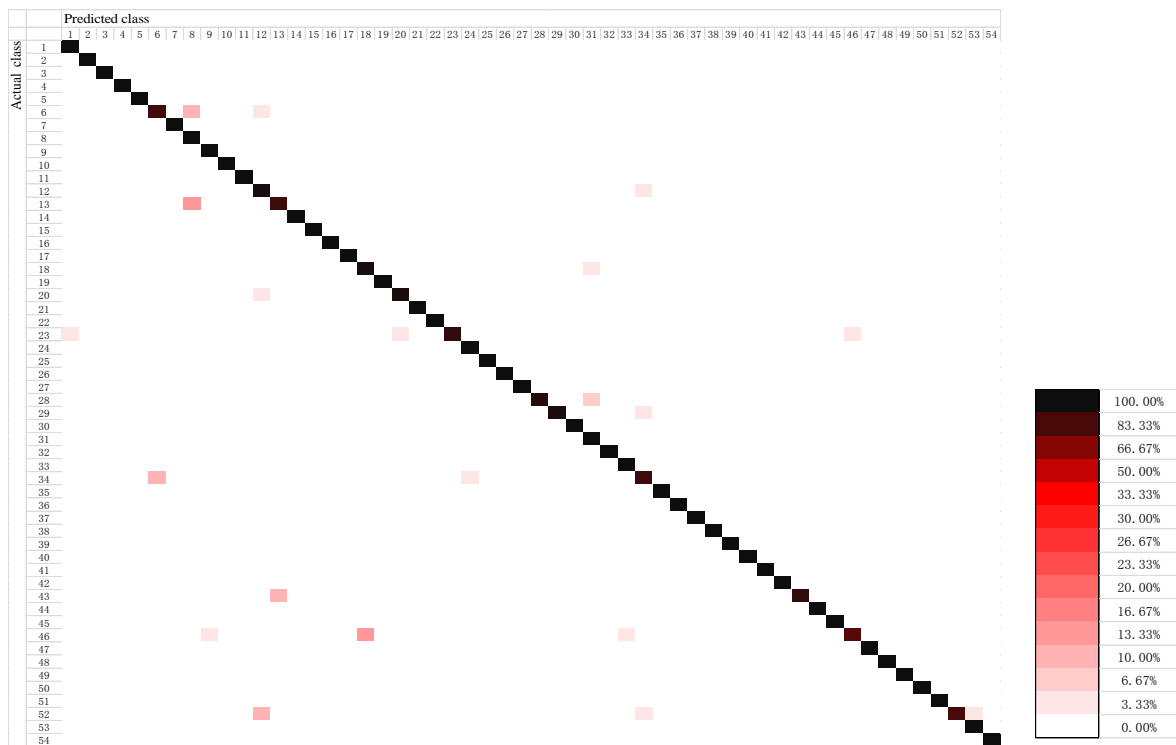


Fig 5 - Global confusion matrix for $LBP_{8,8}$

Table 1

Comparison of existing timber classification methods

Classification methods	Recognition rate	Classification speed (millisecond/image)
GLCM feature extractor (Khalid et al., 2008)	45%	1000
GA feature selection (Khairuddin et al., 2011)	94.4%	1500
Nonlinear feature selection excluding (Yusof et al., 2013)	98.69%	1200
Fuzzy pre-classifier with nonlinear feature selection (Ibrahim et al., 2015)	98.5%	1000 to 1060
$LBP_{8,8}$ with Nearest Neighbor classifier (proposed method)	97.84%	281
$LBP_{8,2}^{u2}$ with Nearest Neighbor classifier (proposed method)	97.41%	77

CONCLUSIONS

Timbers classification by visual inspection has low efficiency and is unreliable. This paper combines six LBP-like texture descriptors with nearest neighbor classifier to classify timber images from 54 wood species, and it compares the wood texture discrimination power of $LBP_{P,R}$, $LBP_{P,R}^{u2}$, $LBP_{P,R}^{ri}$, $LBP_{P,R}^{riu2}$, $CovM_{LBP}$, and $CovM_{LBPD}$. Experimental results show that $LBP_{P,R}$ is the best texture descriptor with a classification accuracy of 97.5% while $LBP_{P,R}^{u2}$ is the second best texture descriptor with a classification accuracy of 96.64%. $LBP_{8,8}$ has the best discrimination power for wood dataset with 54 wood species, its classification accuracy is 97.84%, and the standard deviation of classification accuracy is only 1.52%. Classification rate and its standard deviation of $LBP_{8,8}^{u2}$ is 97.41% and 0.91%. Storage and time consumption of $LBP_{8,8}^{u2}$ are only 32.45% and 26.83% of $LBP_{8,8}$. Thus, uniform LBP is one of the options for wood texture description if higher storage efficiency and time efficiency are needed.

Combination of LBP with wood biological features (*i.e.*, density of wood pores) and other classifiers (*i.e.*, deep learning and SVM, etc.) would be possible methods for future works. Multi-resolution fusion of different texture features would possibly improve the classification rate. For the wood species which are difficult to classify, we need to study their properties to design a more specific targeted recognition system.

ACKNOWLEDGMENTS

This work has been supported by the National Natural Science Foundation of China (No.61202188).

REFERENCES

- [1] Bremananth R., Nithya B. and Saipriya R., (2009), *Wood species recognition using glcm and correlation*. IEEE, pp.615-619;
- [2] Cha S.-H. and S.N. Srihari, (2002), On measuring the distance between histograms. *Pattern Recognition*, 35(6): pp.1355-1370;
- [3] Hong X., Zhao G., Pietikainen M. and Chen X., (2014), Combining lbp difference and feature correlation for texture description. *Image Processing, IEEE Transactions on*, 23(6): pp.2557-2568;
- [4] Ibrahim I., A.S.M. Khairuddin and R. Yusof, (2015), *Incorporation of pre-classifier and nonlinear feature selection for tropical wood species recognition system*. IEEE, pp.1632-1637;
- [5] Khairuddin, U., R. Yusof, M. Khalid and F. Cordova, (2011), Optimized feature selection for improved tropical wood species recognition system. *ICIC Express Letters, Part B: Applications*, 2(2): pp.441-446;
- [6] Khalid M., Lee E.L.Y., Yus R.of and M. Nadaraj, (2008), Design of an intelligent wood species recognition system. *International Journal of Simulation System, Science and Technology*, 9(3): pp.9-19;
- [7] Micheals R.J. and Boulton T.E., (2001), Efficient evaluation of classification and recognition systems. *IEEE*, pp: 50-57;
- [8] Mohan S., Venkatachalapathy K.and Priya S.E., (2014), Wood species identification system. *International Journal Of Engineering And Computer Science*, 3(5): pp.5996-6001;
- [9] Nanni L., Lumini A. and Brahmam S., (2012), Survey on lbp based texture descriptors for image classification. *Expert Systems with Applications*, 39(3): pp.3634-3641;
- [10] Ojala T., Pietikainen M. and Harwood D., (1996), A comparative study of texture measures with classification based on feature distributions. *Pattern Recognition*, 29(1): pp.51-59;
- [11] Ojala T., Pietikainen M. and Maenpaa T., (2002), Multiresolution gray-scale and rotation invariant texture classification with local binary patterns. *IEEE Transactions on Pattern Analysis and Machine Intelligence*, 24(7): pp.971-987;
- [12] Pele O. and Werman M., (2010), The quadratic-chi histogram distance family. In: European conference on computer vision, *Springer*: pp: 749-762;
- [13] Pietikainen M., Ojala T. and Xu Z., (2000), Rotation-invariant texture classification using feature distributions. *Pattern Recognition*, 33(1): pp.43-52;
- [14] Taman I., Rosid N.A.M., Karis M.S., et al, (2014), Classification system for wood recognition using k-nearest neighbor with optimized features from binary gravitational algorithm. *International Institute of engineers*, pp: 1-6;
- [15] Tang Y., Cai C. and Zhao F., (2009), *Wood identification based on pca, 2dpca and (2d)2pca*. IEEE, pp: 784-789;

- [16] Tuzel O., Porikli F. and Meer P., (2006), Region covariance: A fast descriptor for detection and classification. In: Computer vision–eccv 2006, *Springer Berlin Heidelberg*: pp: 589-600;
- [17] Yusof R., Khalid M. and Khairuddin A.S.M., (2013), Application of kernel-genetic algorithm as nonlinear feature selection in tropical wood species recognition system. *Computers and electronics in agriculture*, 93: pp.68-77;
- [18] Yusof R., Khalid M. and Khairuddin A.S.M., (2013), Fuzzy logic-based pre-classifier for tropical wood species recognition system. *Machine vision and applications*, 24(8): pp.1589-1604;
- [19] Zhang Y., Xu C., Li X. and Xue R., (2014), Design of fuzzy classifier for wood board texture based on glcm. *Journal of northeast forestry university*, 42(4): pp.127-130.

COMPARATIVE ANALYSIS OF SOME TIRE DEFORMATION MODELS USED FOR THE PREDICTION OF TRACTION CHARACTERISTICS

/

ANALIZA COMPARATIVĂ A UNOR MODELE DE DEFORMARE A PNEULUI ÎN SCOPUL OBȚINERII CARACTERISTICILOR DE TRACȚIUNE

Prof. Ph.D. Stud. Eng. Roșca R.*¹⁾, Assoc. Prof. Ph.D. Eng. Cârlescu P.¹⁾, Prof. Ph.D. Eng. Țenu I.¹⁾

¹⁾ University of Agricultural Sciences and Veterinary Medicine "Ion Ionescu de la Brad" Iași / Romania;
Tel: 0232-407561; E-mail: rrosca@uaiasi.ro

Keywords: *tire traction, super-ellipse, traction force*

ABSTRACT

In the present paper the deformation of the tire section is under load is taken into account. The tire section is considered to be elliptical; under load the minor axis decreases, while the major axis increases. The equations of the traction model were incorporated in a computer program; the length, width and area of the contact patch, the traction force and traction efficiency are calculated for each value of the wheel slip.

Field tests were performed in order to validate the model; the experimental data were collected during plowing tests. In order to evaluate the precision of the model the predicted data were compared with the test data by the means of a goodness-of-fit analysis.

REZUMAT

Lucrarea prezintă un model pentru interacțiunea pneu-sol, model care se ține cont de deformarea secțiunii pneului. Astfel, se consideră că pneul are în secțiune formă eliptică; sub acțiunea sarcinii verticale secțiunea se deformează, păstrându-și forma eliptică (axa mică se scurtează, iar axa mare se alungește). Ecuațiile pentru modelarea tracțiunii roții cu pneu au fost introduse într-un program de calculator, care determină, pentru fiecare valoare a patinării roții, lungimea și lățimea petei de contact, forța de tracțiune și randamentul de tracțiune.

S-au efectuat teste în câmp pentru validarea modelului, datele fiind colectate la efectuarea arăturii. S-a efectuat o analiză a corelației datelor experimentale cu cele oferite de model pentru a valida modelul dezvoltat.

INTRODUCTION

The tire-soil interaction models can be based on empirical, semi-empirical and analytical methods (Tiwari *et al.*, 2010).

Empirical methods are mainly based on soil properties (cone index, plate sinkage, shear strength) using similitude and dimensional analysis. At the end of the Second World War, this approach evolved as a means of measuring trafficability of soil at the US Army Corps of Engineers, Waterways Experiment Station (Tiwari *et al.*, 2010). The empirical models were developed using traction data recorded from operating vehicles; for some of them, cone index, measured with a standard cone penetrometer, was the only soil property taken into account. Wismer and Luth (1972) developed a widely used model for bias tyres, based on a soil-tyre numeric, which under-predicted the traction force when applied to radial tyres. The Brixius (1987) equations, as a refinement of the Wismer and Luth equations, expressed the gross traction ratio (GTR) as a function of slip and wheel mobility number, using a curve fitting technique in order to evaluate the coefficients for the traction equation (Lee *et al.*, 2016).

The semi-empirical models represent a physical-based approach, which considers the mechanics of the wheel-soil interaction and are suitable for practical applications (Battiato and Diserens, 2017). In the semi-empirical models, the shear deformation of soil is considered; the models are based on soil parameters obtained by the means of a bevameter technique (penetration and shear tests), assuming that the vertical deformation of soil is similar to the deformation under a sinking plate, while the shear deformation of soil under a traction device is similar to the shear action of a torsion device (Tiwari *et al.*, 2010). The parameters involved in the equations are determined experimentally. For agricultural soils, the Janoshi and Hanamoto (1961) equation is one of the most frequently used.

$$\left(\frac{2 \cdot x}{l_c}\right)^k + \left(\frac{2 \cdot y}{l_w}\right)^k = 1, \tag{2}$$

where k is the super ellipse exponent, the minor axis of the super ellipse is assumed to be equal to the tyre width b (Keller, 2005) l_c is the major axis of the super ellipse (length of the contact area) and l_w is the minor axis of the super ellipse (width of the contact area).

The tire-soil pressure was defined using the pressure-sinkage relationship:

$$p = k \cdot z^n \tag{3}$$

where p is the normal pressure [kPa], z is the deformation [m], and k [kPa/m ^{n}] and n are constants.

Based on the tire-soil pressure and assuming that the tire is perfectly elastic (Ghiulai and Vasiliu, 1975) finally leads to:

$$G = \int_0^{2\beta} p \cdot b(\varphi) \cdot r_d \cdot \cos(\beta - \varphi) \cdot d\varphi = q_p \cdot \Delta V_p, \tag{4}$$

where φ is the current angle, defining the position along the contact surface, p is the normal pressure, q_p is the tyre volume stiffness and ΔV_p is the tyre change in volume due to deflection.

In the initial paper (Roşca et al., 2014) the tire change in volume due to deflection ΔV_p was evaluated considering that the tire radius increases from r_0 to r_d as the tire flattens in the contact area, while the tire width was considered constant (fig. 2).

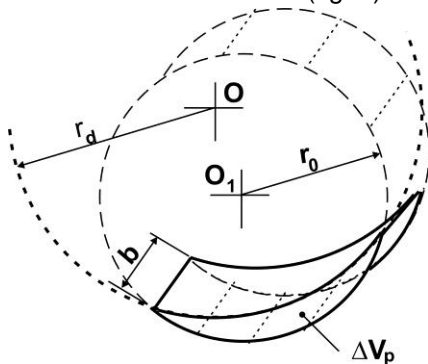


Fig. 2 - Initial tire deformation model

ΔV_p - tyre change in volume due to deflection;
 b - tyre width;
 r_0 - radius of the undeflected tire;
 r_d - radius of the contact patch under vertical load.

Finally, after several transformations of equation (4), the following equation is obtained:

$$k \cdot \int_0^{2\beta} b(\varphi) \cdot r_d^{n+1} \cdot [\cos(\beta - \varphi) - \cos \beta]^n \cdot \cos(\beta - \varphi) \cdot d\varphi + \frac{4}{3} \cdot b \cdot q_p \cdot \beta^3 \cdot r_d^2 = \frac{4}{3} \cdot b \cdot q_p \cdot \alpha^3 \cdot r_0^2. \tag{5}$$

In the present study the deformation of the tire cross-section is considered; the shape of the tire cross-section is approximated by an ellipse (Koutný, 2007), as shown in fig. 3a. Under the effect of vertical load (G , fig. 1), the cross-section is deformed, but the elliptical shape is preserved (fig. 3b): the minor semi-axis decreases and becomes $h - z_p$, while the major axis increases from b (tire width in the unloaded condition) to l_w .

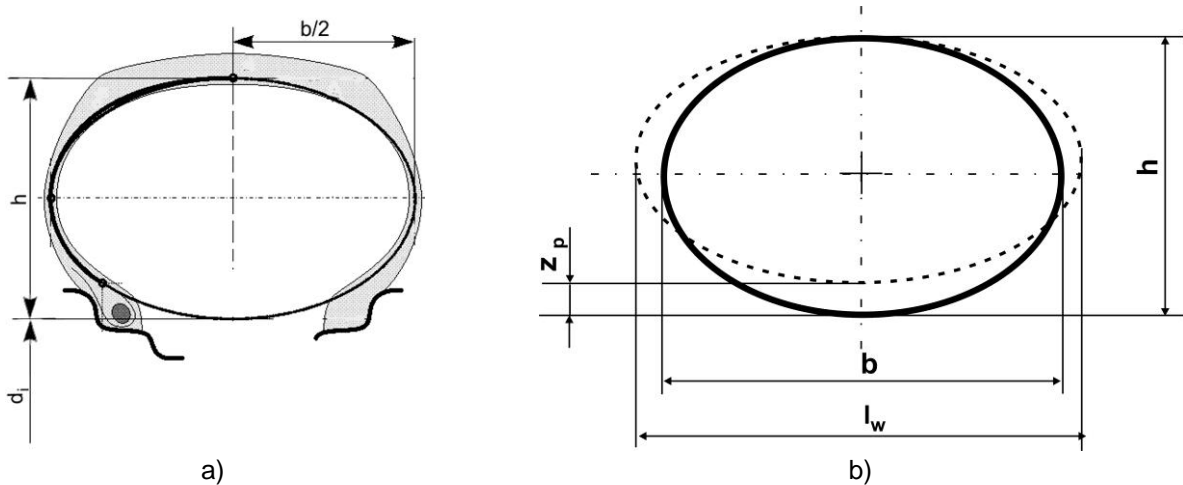


Fig. 3 – Model for tire section deformation

a) tire section prameters; b) tire section deformation under load;

d_i – rim diameter; h – tire section height; b -tire width (undeformed); l_w – tire width (under load); z_p - tire deflection under vertical load

The major axis of the ellipse is calculated assuming that its perimeter remains constant:

$$2\pi \cdot \sqrt{\frac{(b/2)^2 + (h/2)^2}{2}} = 2\pi \cdot \sqrt{\frac{(l_w/2)^2 + [(h-z_p)/2]^2}{2}}, \quad (6)$$

which results in:

$$l_w = \sqrt{b^2 + 2 \cdot h \cdot z_p - z_p^2}. \quad (7)$$

The tire volume change ΔV_p is calculated as the cross-section area multiplied by the length of the contact patch, resulting in:

$$\Delta V_p = 2 \cdot \alpha \cdot r_o \cdot \pi \cdot \frac{b}{2} \cdot \frac{h}{2} - 2 \cdot \beta \cdot r_d \cdot \pi \cdot \frac{l_w}{2} \cdot \frac{h-z_p}{2} = 0,5 \cdot \pi \cdot [\alpha \cdot r_o \cdot b \cdot h - \beta \cdot r_d \cdot l_w \cdot (h-z_p)]. \quad (8)$$

After several transformation 4quation (4) becomes:

$$k \cdot \int_0^{2\beta} b(\varphi) \cdot r_d^{n+1} \cdot [\cos(\beta - \varphi) - \cos \beta]^n \cdot \cos(\beta - \varphi) \cdot d\varphi = q_p \cdot 0,5 \cdot \pi \cdot [\alpha \cdot r_o \cdot b \cdot h - \beta \cdot r_d \cdot l_w \cdot (h-z_p)] \quad (9)$$

The following equations are also obtained from fig. 1:

$$z_c = r_o - z_p - r_o \cdot \cos \alpha, \quad (10)$$

$$z_p = r_o \cdot (1 - \cos \alpha) - r_d \cdot (1 - \cos \beta), \quad (11)$$

where z_p is tyre deflection under vertical load.

A computer program is used in order to solve the systems of equations (1), (5), (10), (11) and (1), (9), (10), (11), respectively. The program displays the following values (fig. 4):

- length of the contact patch, l_c ;
- width of the contact patch, l_w ;
- area of the contact patch;
- calculated value of tire deformation under load, z_p ;
- tire sinkage, z_p ;
- dynamic radius of the wheel, r_d ;
- angle of the contact patch, β ;
- maximum shear stress, τ_{max} ;
- normal pressure, p .

The values of slip, traction force and traction efficiency are saved in a file.

```

Microsoft QuickBASIC
143796 39.69615 37.8305
.5819961 1.70003 .79 2.554772E-02
                                REZULTATE
Lungime pata, lc: .5819961
Latime pata, lw: .3283252
Adincime patrundere, zc: .026358
Inaltime proeminente: .025
Raza dinamica, rd: 1.70003
Deformare pneu, zp: .03 3.045717E-02
Rigiditate volumica pneu: 27000
Presiune proeminente: 370.148
Presiune banda rulare: 7.833548
Beta: 9.860985
Aria: .1739624
Tens. tang. proeminente: 136.189
Tens. tang. banda rulare: 103.6507
Tens. tang. max.: 49.63505
Datele referitoare la forta de tractiune si randament au fost scrise in fisierul
sevar3
Datele ref. la distributia presiunii au fost scrise in fisierul pres_s3
Pres. medie pe supraf. proeminentelor = 218.0986
Pres. medie pe bada rulare = .319587
Press any key to continue

```

Fig. 4 – Output screen of the computer program

In order to evaluate the maximum traction force it is assumed that it is limited only by the soil shear strength; the Mohr-Coulomb equation is used to calculate the soil maximum shear stress:

$$\tau_{max} = c + p \cdot \operatorname{tg} \gamma \quad (12)$$

where c is soil cohesion [kPa], p is the vertical pressure [kPa] and γ is the internal friction angle.

Soil shear tension was calculated using the Janosi and Hanamoto (1961) equation:

$$\tau = \tau_{max} \cdot \left(1 - e^{-\frac{J}{K}} \right) \quad (13)$$

where K is the soil shear deformation modulus and J is the shear displacement.

The maximum traction force was calculated as the product of shear stress and shear area; according to ASAE S296, the net traction force is $F_N = F_t - R_r$, with the wheel rolling resistance R_r being calculated with the relation (Elwaleed et al., 2006):

$$R_r = G \cdot \left(\frac{1}{B_n} + 0.04 + \frac{0.5 \cdot s}{\sqrt{B_n}} \right) [kN]. \quad (14)$$

The wheel numeric B_n is (ASAE D497.7, 1999):

$$B_n = \frac{Cl \cdot b \cdot d}{G} \cdot \left(\frac{1 + 5 \cdot \frac{z_p}{h}}{1 + 3 \cdot \frac{b}{d}} \right), \quad (15)$$

where Cl is the soil cone index [kPa], $d = 2 \cdot r_0$ [m] and h is the tyre section height [m].

The same standard defines the traction efficiency as:

$$\eta_{tr} = (1 - s) \cdot (1 - R_r / F_t). \quad (16)$$

The model was applied to the driving wheel of an U-650 agricultural tractor; the main characteristics of the wheel are presented in table 1.

Table 1

Main characteristics of the driving wheel

Item	Value
Load on the driving tire, G [kN]	11.75
Type of tire	14.00-38
Rim diameter, d_i [m]	0.965
Section height, h [m]	0.307
Exterior diameter of tire, $d_i + 2 \cdot h$ [m]	1.58
Tire width, b [m]	0.370
Tire inflation pressure [kPa]	100

The experimental data were collected during the field tests performed with the U650+P2V plowing unit; the tractor was fitted with a dynamometric frame and an electronic dynamometer, as shown in fig. 5. The plough was mounted on the dynamometric frame and thus the net traction force $F_{t,ef,r}$ was measured directly. During these tests drive wheel slip did not exceed 30% because of the restraints imposed by the plowing process. Different traction forces and drive wheel slips were achieved by changing the operating width and depth of the plough. The traction force for each experimental point was calculated as the average value of nine measurements; the standard error and 95% confidence interval were then evaluated. The experimental results taken into account for the goodness-of-fit analysis are shown in table 2.

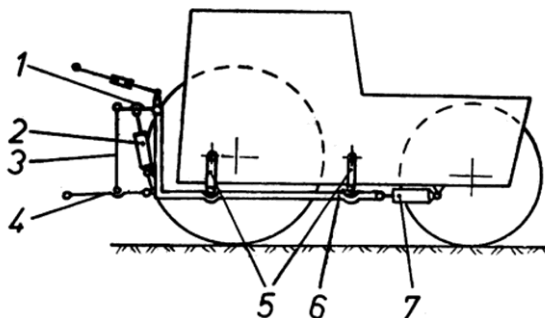


Fig. 5 – Dynamometric frame mount
(Roşca R. et al., 2014)

1,3,4-lifting arms;
2-hydraulic lifting cylinder;
5-frame arms;
6-dynamometric frame;
7-force transducer.

The tests were performed on wheat stubble sandy loam soil, after cereal harvesting; soil characteristics in the test field are presented in table 3.

Table 2

Experimental data for traction force			
Wheel slip [%]	Average traction force [kN]	Standard error	95% data confidence interval
6	1.8033	0.095	0.2179
9	2.3744	0.116	0.2684
14	3.1033	0.082	0.1891
17	3.3067	0.121	0.2797
18	3.6855	0.116	0.2680
20	4.3122	0.175	0.4029
25	4.6777	0.087	0.2003
26	4.7567	0.114	0.2636
29	5.8800	0.141	0.3249

Table 3

Characteristics of the test soil		
Item	Value	
Soil type	Sandy loam soil	
Average bulk density [kg/m ³]	1280	
Average soil water content [%]	9.5	
Soil deformation modulus, K [m]	0.05	
Coefficients for the pressure-sinkage equation	k	55
	n	1.3
Soil cohesion, c [kPa]	25	
Angle of internal friction, γ [°]	32	
Cone penetrometer index, C [kPa]	970	

In order to evaluate the goodness-of-fit between model and experimental data the following criteria were considered (*Schunn and Wallach, 2005*):

- percentage of points within 95% confidence interval of data (Pw95CI) – represents the percentage of model predictions that lie within the 95% confidence interval of each corresponding experimental data point;
- mean absolute deviation (MAD) – represents the mean of the absolute value of the deviation between each model point and the corresponding experimental point:

$$MAD = \frac{\sum_{i=1}^n |m_i - d_i|}{n} \quad (17)$$

where m_i is the model mean for point i , d_i is the experimental data mean for point i and n is the total number of points being compared;

- root mean squared deviation (RMSD):

$$RMSD = \sqrt{\frac{\sum_{i=1}^n (m_i - d_i)^2}{n}} \quad (18)$$

- mean scaled absolute deviation (MSAD):

$$MSAD = \sum_{i=1}^n \frac{|m_i - d_i| \cdot \sqrt{n_i}}{n \cdot s_i} \quad (19)$$

where n_i is the number of values contributing to each experimental data mean d_i ($n_i = 9$) and s_i is the standard deviation for each data mean. A MSAD value of 1.5 means that, on average, the model is 1.5 standard errors off from the experimental data.

- Pearson correlation coefficient r^2 .

RESULTS

For the both tire section deformation models the calculations were performed using the same value for the super ellipse coefficient ($k=3.5$). Table 4 presents some comparative results given by the tire – soil computer simulation; the assumption that the tire cross-section has an elliptical shape and is deformed due to the vertical load of the tire had the following consequences:

- while the length of the contact patch decreased slightly (from 0.533 m to 0.531 m), the width of the contact patch, l_w , increased from 0.3 m to 0.319 m, resulting in a larger area of the contact surface (0.154 m^2);
- the tire radius r_d decreased from 1.4 m to 1.371 m; as the length of the contact patch did not change significantly, the centre angle β increased from 10.916° to 11.19° ;
- the maximum shear stress decreased from 53.3 kPa to 52.01 kPa due to the increase of the contact surface area.

Table 4

Item	Model results	
	Initial tire deformation model (b const.)	Modified tire deformation model (b ellipse)
Length of the contact patch, l_c [m]	0.533	0.531
Width of the contact patch, l_w [m]	0.300	0.319
Tire deflection, z_p [m]	0.02	0.02
Sinkage depth, z_c [m]	0.027	0.027
Area of the contact surface, A_t [m^2]	0.145	0.154
Tire radius, r_d [m]	1.400	1.371
Centre angle of the contact patch, β [$^\circ$]	10.916	11.19
Maximum shear stress, τ_{max} [kPa]	53.3	52.01

Figures 6 and 7 present the predicted and experimental results concerning the traction force and traction efficiency. The charts clearly show that the model predicted higher values of the traction force and traction efficiency when the deformation of the tire cross section was considered, due to the increased value of the contact surface area.

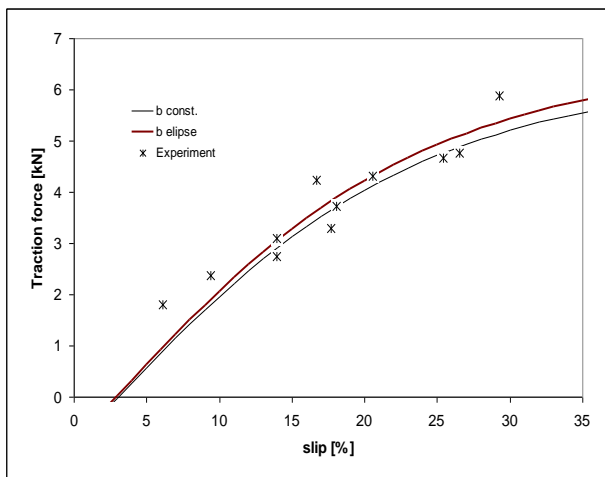


Fig. 6 – Results concerning the traction force

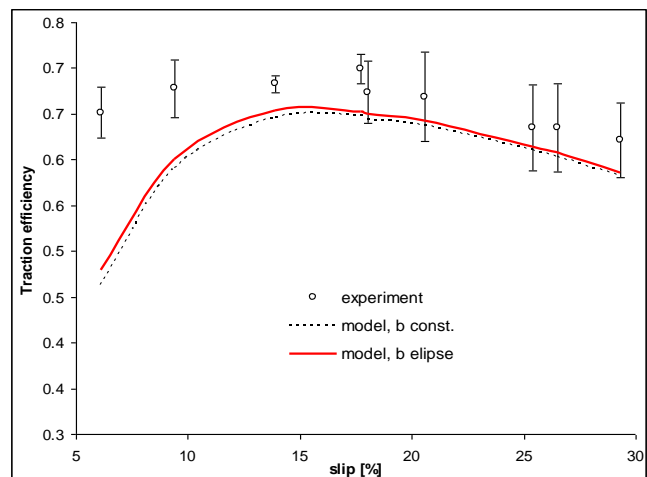


Fig. 7 – Results concerning the traction efficiency

The results of the goodness-of-fit analysis are shown in table 5. Compared to the previous model, the most significant differences were recorded for the traction efficiency: the Pearson correlation coefficient r^2 increased from 0.186 to 0.216, the mean absolute deviation (MAD) decreased from 0.058 to 0.051, root mean squared deviation (RMSD) decreased from 0.0752 to 0.0686 and the mean scaled absolute deviation (MSAD) decreased from 5.225 to 4.557.

Table 5

Goodness-of-fit comparative analysis

Item	Traction force		Traction efficiency	
	Constant cross-section	Deformable cross-section	Constant cross-section	Deformable cross-section
r^2	0.923	0.924	0.186	0.216
PW95CI	66.7	55.6	55.6	55.6
MAD	0.354	0.356	0.058	0.051
RMSD	0.480	0.438	0.0762	0.0686
MSAD	3.122	3.065	5.225	4.577

When referring to the values of the traction force, all the goodness-of-fit parameters recorded better values for the modified traction model, excepting the percentage of points within 95% confidence interval of data (Pw95CI), which has slightly decreased (from 66.7% to 55.6 %).

CONCLUSIONS

A modified semi-empirical model for the prediction of traction performance of a tractor driving wheel is presented in this study. The model assumed that the super ellipse equation describes the shape of the tire-ground contact surface.

The model is a reasonable compromise between the more simple empirical models, for which the range of applicability is limited to the cases having similar conditions to the ones from which the models were derived, and the analytical models, which require in-situ evaluation of a large number of soil properties.

Experimental results from plowing tests were used in order to validate and verify the applicability of the model, by the means of a goodness-of-fit analysis. The analysis showed that the modified traction model provided more accurate results regarding the traction force and traction efficiency than the initial one.

REFERENCES

- [1] Battiato A., Diserens E., (2017), Traction performance simulation on differently textured soils and validation: A basic study to make traction and energy requirement accessible to practice, *Soil&Tillage Research*, Vol. 166, pp. 18-32;
- [2] Brixius W. W., (1987), Traction prediction equations for bias ply tyres, *ASAE Paper 87-1622*, St. Joseph, Michigan/USA;
- [3] Diserens E., Défossez P., Duboisset A., Alaoui A., (2011), Prediction of the contact area of agricultural traction tyres on firm soil, *Biosystems engineering*, Vol. 110, pp. 73-82;
- [4] Elwaleed A.K., Yahya A., Zohadie M., Ahmad D., Kheiralla, A.F., (2006), Effect of inflation pressure on motion resistance of a high-lug agricultural tyre, *Journal of Terramechanics*, Vol. 43, pp. 69-84;
- [5] Ghiulai C., Vasiliu Ch., (1975), *Ground vehicles dynamics (Dinamica autovehiculelor)*, Didactics and Pedagogy Publishing House, Bucharest/Romania;
- [6] Janosi Z., Hanamoto B., (1961), The analytical determination of drawbar pull as a function of slip, for tracked vehicles in deformable soils. *Proceedings of the 1st Intl. Conference Mech. Soil-Vehicle Systems*. Turin/ Italy;
- [7] Koutný F., (2007), *Geometry and mechanics of pneumatic tires*, Zlin, CZE (available at: <http://wanderlodgogurus.com/database/Theory/TireGeometry.pdf>);
- [8] Lee J.W., Kim J.S., Kim K., (2016), Computer simulations to maximise fuel efficiency and work performance of agricultural tractors in rotovating and ploughing operations, *Biosystems Engineering*, Vol. 142, pp. 1-11;
- [9] Keller T., (2005), A model for prediction of the contact area and the distribution of vertical stress below agricultural tyres from readily available tyre parameters, *Biosystems Engineering*, Vol. 92, no.1, pp.85-96;
- [10] Roşca R., Cârlescu P., Ţenu I., (2014), A semi-empirical traction prediction model for an agricultural tyre, based on the super ellipse shape of the contact surface, *Soil&Tillage Research*, Vol. 141, pp.10-18;
- [11] Schunn C.D., Wallach D., (2005), Evaluating goodness-of-fit in comparison of models to data. *Psychologie der Kognition: Reden and Vorträge anlässlich der Emeritierung*, pp. 115-154, W. Tack Ed., University of Saarland Press, Saarbrueken, Germany,
- [12] Tiwari V.K., Pandey K.P., Pranav P.K., (2010), A review on traction prediction equations, *Journal of Terramechanics*, Vol.47, pp.191-199;
- [13] Upadhyaya S. K., Wulfson D., Jubbal G., (1990), Review of traction prediction equations. *ASAE Paper 90 – 1573*, St. Joseph, Michigan;
- [14] Xia K., (2011), Finite element modeling of tire/terrain interaction: Application to predicting soil compaction and tire mobility, *Journal of Terramechanics*, Vol. 48, pp. 113-123;
- [15] *** ASAE D497.7, (1999), *Agricultural Machinery Management Data*. St. Joseph, Michigan, U.S.A.

THEORETICAL JUSTIFICATION OF THE TURN OF A WIDE SPAN TRACTOR (VEHICLE) FOR CONTROLLED TRAFFIC FARMING

/

ТЕОРЕТИЧНЕ ОБҐРУНТУВАННЯ ПОВОРОТУ ШИРОКОКОЛІЙНИХ ТРАКТОРІВ (ТРАНСПОРТНИХ ЗАСОБІВ) ДЛЯ КОЛІЙНОЇ СИСТЕМИ ЗЕМЛЕРОБСТВА

Prof. PhD.Eng. Bulgakov V.¹⁾, Prof. PhD. Eng. Adamchuk V.²⁾, PhD. Eng. Kuvachov V.³⁾, Prof. PhD.Eng. Ivanovs S.⁴⁾

¹⁾National University of Life and Environmental Sciences / Ukraine,

²⁾National Scientific Centre "Institute for Agricultural Engineering and Electrification" / Ukraine,

³⁾Tavria State Agrotechnological University / Ukraine,

⁴⁾Latvia University of Agriculture / Latvia

Tel. +37129403708, e-mail: semjons@apollo.lv

Keywords: wide span tractor, turn, kinematics, dynamic turnability

ABSTRACT

A new scheme of the turn of a wide span tractor (vehicle) is presented for controlled traffic farming on the turning strip. The turn of the tractor, according to the presented scheme, allows moving the tractor to the next working position with better kinematic parameters. In addition to it, the improvement of the turnability characteristics is achieved at such a design embodiment of a wide span tractor when the ratio of its wheelbase to the width of the wheel track is as small as possible. The obtained equations about the movement of the wide span tractor for the offered new scheme of the turn allow estimating the impact of its design, performance, kinematic and power parameters upon the criteria of static and dynamic turnability.

РЕЗЮМЕ

Запропонована нова схема розвороту ширококолієного трактора для колійної системи землеробства на поворотній смузі, за якою переміщення трактора на наступну робочу позицію здійснюється з кращими кінематичними параметрами. При цьому покращення характеристик поворотності досягається при такому конструктивному виконанні ширококолієного трактора, коли відношення його колісної бази до ширини колії є якомога меншим. Отримані рівняння руху для запропонованої нової схеми повороту дозволяють оцінити вплив його конструктивних, експлуатаційних, кінематичних і силових параметрів на критерії статичної та динамічної поворотності.

INTRODUCTION

A peculiarity of using a wide span tractor (vehicle) for controlled traffic farming is the division of the field into the agrotechnical and the engineering area (Antille et al., 2015; Chamen, 2015; Chen et al., 2010; Gasso et al., 2013; Gasso et al., 2014; Kingwell et al., 2011). Turning of the wide span tractor (vehicle) on the turning strip may be accomplished in different ways. Each way of turning has impact on the kinematics of its *curvilinear movement*. Besides, it is desirable that the unproductive losses of energy on the turn and the engineering area should be as low as possible. From the minimization standpoint of unproductive losses, the fields under the engineering area must have a possibility to perform a turn of the wide span tractor in such a way that the actuators of one of its sides remained within the same transport and technological track on which they were positioned but the actuators of the other side transferred their undercarriage to the next operating position (Kuvachov, 2016).

Turnability (a property of the tractor to perform turns with a pre-set curvature of the path) is characterised by kinematic and power parameters. Therefore, correct choice of the latter parameters from a position of the required turnability ensures the movement of the wide span tractor under optimal conditions and minimises the unproductive losses of energy and areas of the field during the turn. For this reason, the scientific investigations aimed at in the study of wide span tractor (vehicle) static and dynamic turnability are highly topical. The turning control of contemporary wide span tractors (Chamen, 1992; Chamen et al., 1994; Chamen, 2000; Chamen, 2015; Onal I., 2012; Pedersen, 2011; Pedersen et al., 2013; Kuvachov, 2015), equipped with wheeled actuators, is adapted for a manual or an automatic mode (Jasiński et al., 2016), and

they are based on a kinematic or a power principle of performing this turn. In kinematic turning there are used schemes for turning steered wheels (front, rear or both simultaneously) in relation to the frame of the machine. There is also known a power (board) method of changing the direction of the movement by turning the machine in a suspended condition (Uleksin, 2011).

In the opinion of the author of the scientific publication, the use of the latter method of turning is efficient under the conditions of limited space on the turning strip, and it allows turning of a machine in the automatic mode without causing damage to the plants in the crossing areas of the traffic track. The theory of the static and the dynamic turnability of a wheeled vehicle has been studied in sufficient detail (Popp, 2010; Rajamani, 2006; Tullberg, 2000; Wong, 2001).

There is a great number of scientific investigations devoted to the turnability issue of agricultural machine and tractor aggregates (Gorin, 2012; Nadykto et. al., 2005; Nadykto et. al., 2012). However, the obtained analytical dependencies cannot practically be applied to the turnability analysis of wide span tractors (vehicles). The reason is the main difference in the design and kinematic scheme of its turn in the coordinate transport system of movement. Still less suitable for further analysis are the results obtained by scientists investigating the turning dynamics of the conventional machine and tractor aggregates.

The aim of the work was theoretical research and justification of the static and dynamic turnability of wide span tractors (vehicles) for controlled traffic farming in order to improve the kinematic and power parameters of the movement.

MATERIALS AND METHODS

We consider in an analytical way two schemes of the turn of a wide span tractor (vehicle) (Fig.1) the kinematic parameters of which – the turning radius, wheels movement angular and linear velocities, the movement path, etc. depend on the design and operating factors (the wheelbase, track width (wheel spacing), maximal turning angles of the steerable wheels, their turning speed, the movement speed, tyre characteristics and so on.

According to the first scheme, which is most widespread among the contemporary brands of wide span tractors (vehicles), the turn is executed by the movement of all the steerable wheels of the tractor around the turning centre positioned in the symmetry centre of its undercarriage (Fig.1 a). According to the second scheme, proposed by us, the turn of the tractor is carried out by turning the undercarriage platform, using the steerable wheels from its one board, around the turning centre positioned in the centre of the space between the wheels from the other board (there the wheels may remain during the turn within the limits of their transport technological track (Fig.1b).

There are at least two ways how to embody our proposed scheme of the turn of a wide span tractor (vehicle) (Fig.1b):

- 1) by kinematic turning of the platform, using the steerable wheels from one board by means of an articulated turning mechanism positioned in the centre of the space between the wheels from the other side;
- 2) by kinematic power turning of the wide span tractor by suspending one of its boards, using lifting mechanisms.

Let us analyse the influence of the basic design parameters of a wide span tractor on the turning kinematic characteristics of the two considered schemes (Fig. 1): the turning radius and the turning angle of the steerable wheels which determine the width of the turning strip. It is clear that the value of the desired width of the turning strip E should be as small as possible but sufficient for the wide span tractor to pass. Depending on the parameters of their undercarriage the optimal width of the turning strip has to be equal to:

$$E = K + b_p, \quad (1)$$

where

K – the wheel track (wheel spacing) width of the wide span tractor;

b_p – the width of the transport technological track.

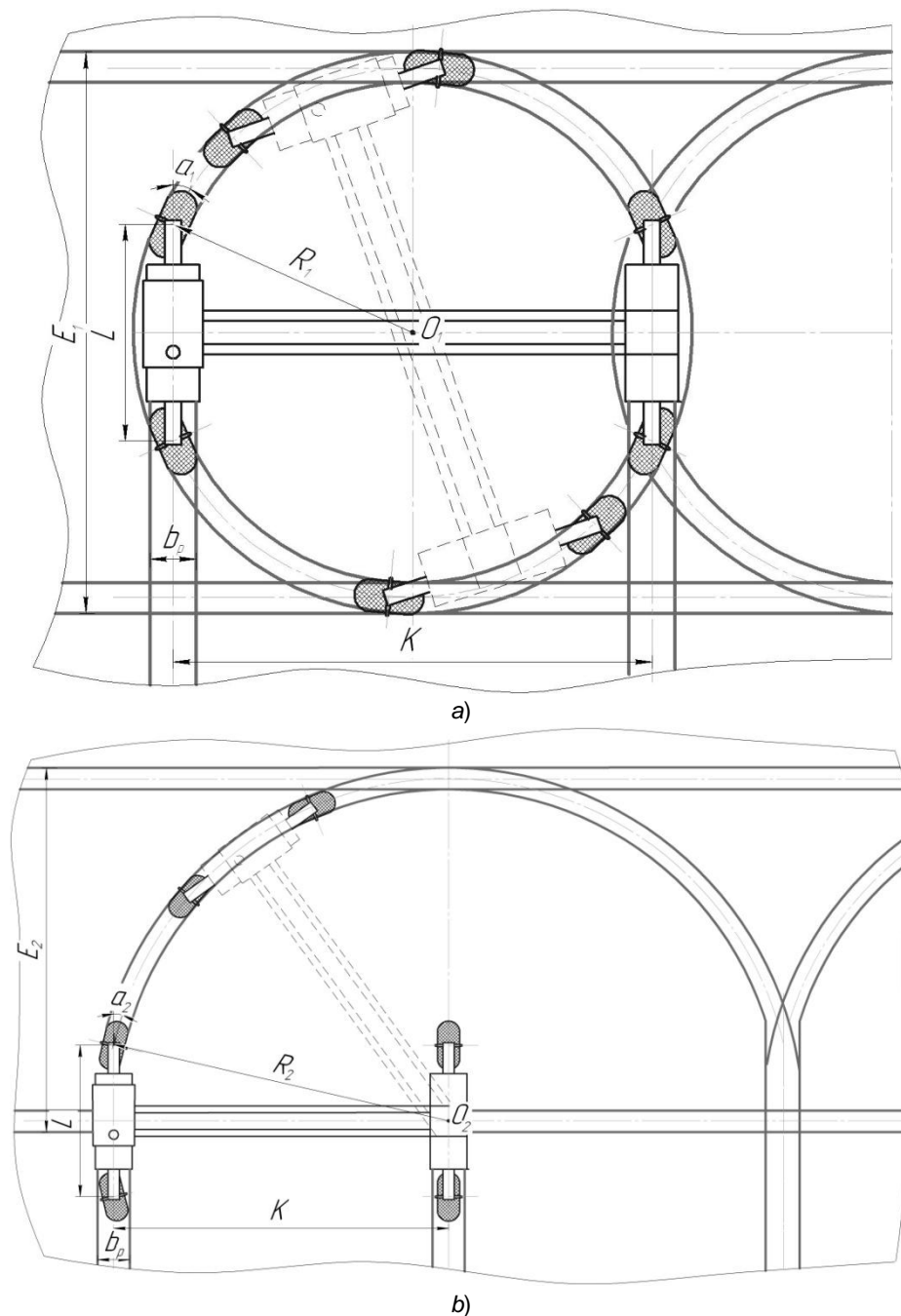


Fig. 1 –Schemes of a wide span tractor (vehicle) turn around the turning centre positioned in its undercarriage symmetry centre (a) and in the centre of the space between one of the boards' wheels (b)

Let us present the basic design parameters of a wide span tractor as a generalised characteristic parameter μ , numerically equal to the relation of its wheelbase L with the width of the wheel track K , which, as a rule, does not exceed 1, that is:

$$\mu = \frac{L}{K} \leq 1 \quad (2)$$

The methods used in the research methodology are: the methods of theoretical mechanics, the tractor theory and operation of agricultural aggregates, using the Mathcad packet. The theoretical investigations, synthesis of wide span tractor (vehicle) design maps and parameters were conducted by simulating the conditions of their performance on the PC.

RESULTS

According to the conventional turn scheme of a wide span tractor (Fig.1 a), the relationship between the kinematic indicators of the turn (the turning angle of the wheels α_1 , the turning radius R_1 and the actual width of the turning strip E_1) and the design parameters, presented as μ , can be expressed by the following dependencies:

$$\begin{aligned} R_1 &= \frac{1}{2}\sqrt{K^2 + L^2} = \frac{1}{2}K\sqrt{1 + \mu^2}, \\ E_1 &= 2R_1 + b_p = \sqrt{K^2 + L^2} + b_p = K\sqrt{1 + \mu^2} + b_p, \\ \alpha_1 &= \arctg\left(\frac{L}{K}\right) = \arctg(\mu) \end{aligned} \quad (3)$$

According to second turn scheme, offered by us, (Fig. 1 b) we find in a similar way that:

$$\begin{aligned} R_2 &= \frac{1}{2}\sqrt{4K^2 + L^2} = \frac{1}{2}K\sqrt{4 + \mu^2}, \\ E_2 &= R_2 + b_p = \frac{1}{2}\sqrt{4K^2 + L^2} + b_p = \frac{1}{2}K\sqrt{4 + \mu^2} + b_p, \\ \alpha_2 &= \arctg\left(\frac{L}{2K}\right) = \arctg\left(\frac{\mu}{2}\right). \end{aligned} \quad (4)$$

By means of the Mathcad packet we estimate the influence of the wide span tractor characteristic parameter μ on the variability degree of the turning strip actual width in relation to the desired one (Fig.2) and the value of the steerable wheels' turning angle (Fig.3) for the two discussed schemes of the turn.

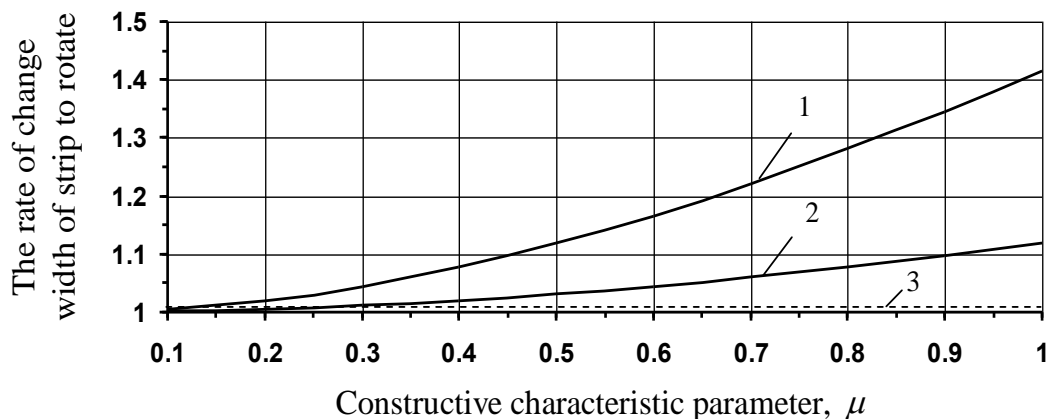


Fig. 2 – Dependence of the variability degree of the turning strip actual width on the constructive characteristic parameter μ for different turn schemes for wide span tractors (vehicles):

1 – scheme in Fig. 1 a; 2 – scheme in Fig. 1 b; 3 – the preferred characteristic

From the analysis of Fig. 2 it results that it is not desirable to increase wide span tractors (vehicles) characteristic parameter μ because it increases the turning strip width. Yet the degree and intensity of such an increase for the discussed turn schemes are different. Thus, increasing μ to 1, the turning strip width for the most widespread first turn scheme (Fig. 1 a) is by 30% bigger than for the other scheme, proposed by us (Fig. 1 b). And, if value μ for the contemporary brands of wide span tractors (vehicles) does not exceed $\mu < 0.5$, then increase in the width of the turning strip according to scheme in Fig.1 b does not exceed 3% of the desired value.

Such a result is on the allowed deviation level from the rectilinear movement of the wide span tractors (vehicles). However, in this case, the organisation of the turn according to the scheme in Fig. 1 a requires an

increase in the turning strip to 12%, which is highly undesirable in terms of optimal land use. Therefore, from this position, the organisation of a wide span tractor (vehicle) turn according to the scheme offered by us Fig. 1 *b* is more appropriate.

Of similar character is the dependence of the steerable wheels turning angle α of the wide span tractor (vehicle) on μ (Fig. 3).

When the turn is executed according to the scheme in Fig. 1 *a*, angle α is twice as great as in the scheme of Fig. 1 *b*. It is not desired to increase the steerable wheels turning angle α , since it requires corresponding complication of the tractor wheels turning mechanism design and higher energy consumption for this process.

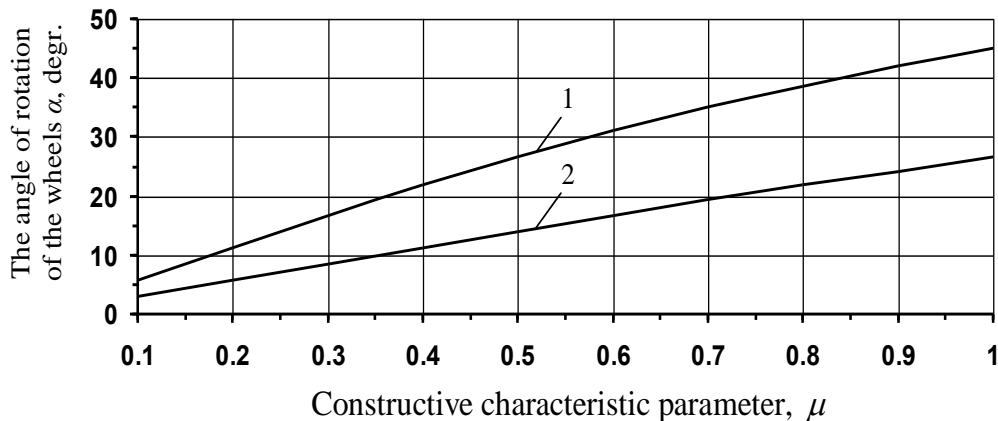


Fig. 3 – Dependence of the steerable wheels turning angle of wide span tractors (vehicles) on the constructive characteristic parameter μ for different turn schemes:

1) – a scheme in Fig. 1 *a*; 2) – a scheme in Fig. 1 *b*

The kinematic parameters discussed by us provide wider but not full information about the *curvilinear movement of the* wide span tractors. Full information about the possibility of a movement with preset kinematic parameters can be obtained by determining the power parameters (the tangential traction forces on the driving wheels, the losses of energy consumed by the tractor to overcome the resistance of the total angular momentum of rotation, etc.) that characterise the static and the dynamic turnability of the wide span tractor.

In order to obtain characteristics of the static turnability, let us consider circular movement of a wide span tractor flat model around the turning centre (point *O*) (Fig. 4) with a constant angular velocity $\omega = \text{const}$, $\dot{\omega} = 0$. The steerable wheels of one board (in the given case – the left one) are turned by angles α_1 and α_2 .

In constructing equations of the movement, we start from the generally accepted concept about a correct turn in accordance with which all the driving wheels of the tractor (in Fig. 4 – the two left-side wheels) are moving without lateral slipping, but crossing of their axes takes place at a point which is the curvature centre of the path travelled. We do not take into account the lateral skid of the wheels since the tractor performs circular movement around its fixed axis, and there is no movement in a perpendicular direction. We consider only those elements of the wide span tractor which execute plane-parallel movements.

Due to the low absolute value, the tangential inertia forces and the inertial moments of resistance to the turn of the wide span tractor and its technological part are ignored. We strictly connect the wide span tractor with the mobile Cartesian coordinate system xSy , the origin of which we place at the centre of its left board masses (point *S*). We draw axis *x* in parallel to the longitudinal axis of the tractor but its positive direction – in the direction of the movement. In the turning mode, a series of corresponding forces act upon the wide span tractor (vehicle).

First of all, these are the driving forces of the front and rear steerable wheels (in our case – the left ones) F_{k1} and F_{k2} , and the resistance forces to the movement F_{f1} and F_{f2} , applied at their centres (points P_1 and P_2), and the inertia force. In order to perform further actions exactly at these points, it is appropriate to divide mass m_b to be applied to its left board into two parts (m_1 and m_2).

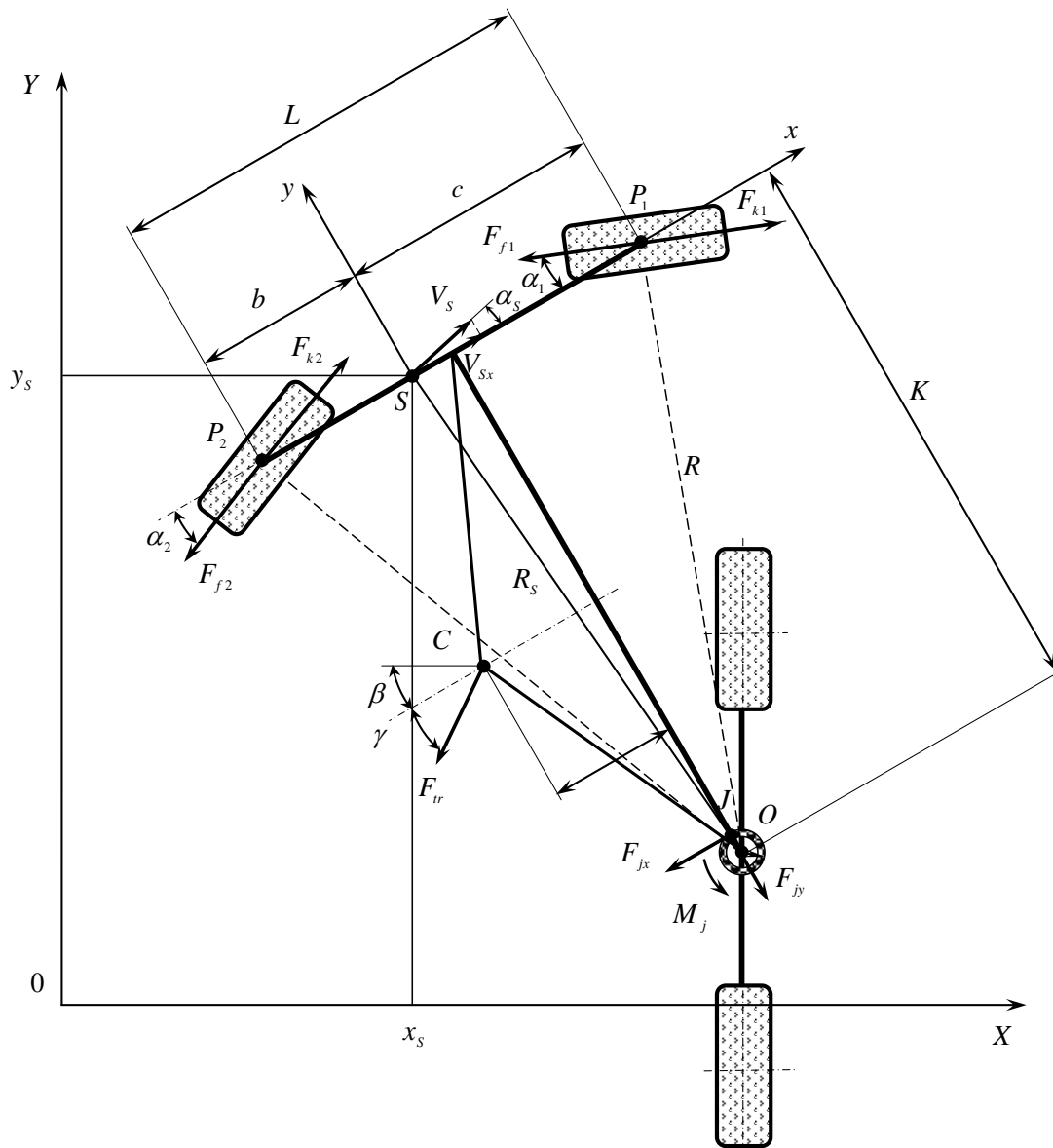


Fig. 4 – An equivalent turn scheme of a wide span tractor (vehicle) with left board steerable wheels

We'll present the impact of the resistance of the tractor technological part operating tools by the main vector F_{tr} , applied at the centre of resistance (point C), the action direction of which on the turn makes angle γ with the tractor longitudinal axis. We present the reactions arising in the articulated turning mechanism of the wide span tractor (vehicle) by forces F_{jx} and F_{jy} , applied at point J , as well as by the resistance moment M_j . The equation of the wide span tractor (vehicle) movement describing the static turnability in relation to the mobile coordinate system xSy is illustrated by the following system of familiar dependencies:

$$\left. \begin{aligned} m_b a_{Sx} &= \sum_{j=1}^n F_{xj}, \\ m_b a_{Sy} &= \sum_{j=1}^n F_{yj}, \\ M_R &= \sum_{i=1}^n M_{Si}, \end{aligned} \right\} \quad (5)$$

where

a_{Sx}, a_{Sy} – acceleration of the centre of masses S in relation to axes x and y of the mobile coordinate system xSy ;

$\sum_{j=1}^n F_{xj}, \sum_{j=1}^n F_{yj}$ – the sum of projections of the j -the forces upon axes x and y of the mobile coordinate system;

M_R – the total moment of resistance to the turn;

$\sum_{i=1}^n M_{Si}$ – the sum of the i -the moments in relation to the masses centre S .

In an expanded form the system (5) will assume the appearance:

$$\left. \begin{aligned} m_b a_{Sx} &= (F_{k1} - F_{f1}) \cos \alpha_1 + (F_{k2} - F_{f2}) \cos \alpha_2 - F_{tr} \cos \gamma - F_{jx} \cos \alpha_S + F_{jy} \sin \alpha_S, \\ m_b a_{Sy} &= -(F_{k1} - F_{f1}) \sin \alpha_1 + (F_{k2} - F_{f2}) \sin \alpha_2 - F_{tr} \sin \gamma - F_{jy} \cos \alpha_S - F_{jx} \sin \alpha_S, \\ M_R &= c (F_{k1} - F_{f1}) \sin \alpha_1 + b (F_{k2} - F_{f2}) \sin \alpha_2 - F_{tr} \sin \gamma \left[\frac{1}{2} L + a \right] + \frac{1}{2} K F_{tr} \cos \gamma - M_j, \end{aligned} \right\} \quad (6)$$

where α_S, a, b and c – the constructive (design) parameters of the wide span tractors the essence of which results from Fig. 4.

For the study of the dynamic turnability of the wide span tractors we use the design diagram in Fig. 4. We consider the tractor movement in a fixed coordinate system XOY connected with the plane of the turning strip. This allows description of the wide span tractor (vehicle) by means of three independent generalised coordinates x_S, y_S, β , where x_S, y_S – the coordinates of the masses centre S while moving in a fixed system of coordinates XOY ; β – the angle between the abscissa axes of the mobile and the fixed coordinate system.

The equations of the plane-parallel movement of wide span tractors, describing its dynamic turnability, in relation to fixed system of coordinates XOY is represented by the following dependencies:

$$\left. \begin{aligned} m_b \ddot{x}_S &= \sum_{j=1}^n F_{Xj}, \\ m_b \ddot{y}_S &= \sum_{j=1}^n F_{Yj}, \\ J_{zS} \ddot{\beta} &= \sum_{i=1}^n M_i. \end{aligned} \right\} \quad (7)$$

where

\ddot{x}_S – acceleration of the masses centre S , directed along axis X of the fixed coordinate system;

\ddot{y}_S – acceleration of the masses centre S , directed along axis Y of the fixed coordinate system;

J_{zS} – the inertia moment in relation to the vertical axis z , passing through point S ;

$\ddot{\beta}$ – angular acceleration of the tractor.

To construct dynamic equations of a wide span tractor movement, we apply the D'Alembert principle. We have:

$$\left. \begin{aligned} m_b \ddot{x}_S &= (F_{k1} - F_{f1}) \cdot \cos(\beta + \alpha_1) + (F_{k2} - F_{f2}) \cdot \cos(\beta - \alpha_2) - F_{tr} \cdot \cos(\beta - \gamma), \\ m_b \ddot{y}_S &= -(F_{k1} - F_{f1}) \cdot \sin(\beta + \alpha_1) + (F_{k2} - F_{f2}) \cdot \sin(\beta - \alpha_2) - F_{tr} \cdot \sin(\beta - \gamma), \\ J_{zS} \ddot{\beta} &= c (F_{k1} - F_{f1}) \cdot \sin \alpha_1 + b (F_{k2} - F_{f2}) \cdot \sin \alpha_2 - F_{tr} \cdot \sin \gamma \left[\frac{1}{2} L + a \right] - M_R. \end{aligned} \right\} \quad (8)$$

The initial conditions ($t = 0$): $x_s = x_0$; $y_s = y_0$; $\beta = 0$; $\dot{x}_s = 0$; $\dot{y}_s = 0$; $\dot{\beta} = 0$.

In Fig. 4 we expose the interrelation of the kinematic radii R_s and R , the forward velocity V_{Sx} and the peripheral velocity V_s of the masses centre S with the wide span tractor (vehicle) constructive (design) parameters:

$$R_s = \sqrt{\left(c - \frac{1}{2}L\right)^2 + K^2} = \sqrt{R^2 - cL + c^2} = \sqrt{K^2 \left(1 + \frac{\mu^2}{4}\right) - c(\mu K + c)}. \quad (9)$$

Consequently, by means of expressions (8) and (9) it is possible to estimate in an analytical way the influence of a wide span tractor (vehicle) design and performance parameters on the criteria of its dynamic turnability, which allows justifying the kinematic and power parameters optimal values of the circular movement during its turning.

CONCLUSIONS

1. The offered new scheme of the turn of a wide span tractor (vehicle) for controlled traffic farming on the turning strip by turning the undercarriage, using the steerable wheels from its one board around the turning centre positioned in the centre of the space between the wheels from the other board, allows shifting of the tractor, simultaneously with the turn, to the next operating position with better kinematic parameters. In addition to it, the improvement of the turnability characteristics is achieved at such a design embodiment of the wide span tractor (vehicle) when the relation of its wheelbase to the width of the wheel track is as small as possible.

2. The obtained equations of the movement of the wide span tractor for the offered new scheme of the turn allow estimation of the impact of its design, performance, kinematic and power parameters upon the criteria of static and dynamic turnability. Correct choice of these parameters values in terms of the required turnability ensures the turn movement of the wide span tractor in an optimal mode and minimises unproductive losses of energy and areas of the field under the engineering area.

REFERENCES

- [1] Antille D. L., Chamen W. C. T., Tullberg, J. N., Lal R., (2015), The potential of controlled traffic farming to mitigate greenhouse gas emissions and enhance carbon remaining in arable land: a critical review. *In Transactions of the ASABE*, vol. 58, no. 3, pp. 707–731;
- [2] Bulgakov V. et al., (2014), *Theoretical mechanics: textbook*, p. 560; Kyiv/Ukraine;
- [3] Chamen W.C.T., (1992), Assessment of a wide span vehicle (gantry), and soil and cereal crop responses to its use in a zero traffic regime. *Soil & Tillage Research* 24(4), pp. 359-380;
- [4] Chamen W.C.T. et al., (1994), Design, operation and performance of a gantry system: experience in arable cropping. *Journal of Agricultural Engineering Research* 59(1), pp. 45-60;
- [5] Chamen W.C.T., (2000), A new methodology for weed control and cereal crop production based on wide span vehicles and precision guidance: *Biotrac 4th EWRS workshop on physical weed control, 20-22 March 2000*, pp. 51-55, Elspeet, The Netherlands;
- [6] Chamen T. (2015), Controlled traffic farming – from worldwide research to adoption in Europe and its future prospects. *Acta Technologica Agriculturae Nitra* 3, pp. 64-73;
- [7] Chen H., Wu W., Liu X., Li H., (2010), Effect of wheel traffic on working resistance of agricultural machinery in field operation. In NongyeJixieXuebao. *Transactions of the Chinese Society of Agricultural Machinery*, vol. 41, no. 2, pp. 52-57;
- [8] Gasso V., Sorensen C.A.G., Oudshoorn F.W., Green O., (2013), Controlled traffic farming: A review of the environmental impacts. *European Journal of Agronomy* 48, pp. 66-73;
- [9] Gasso V., Oudshoorn F.W., Sørensen C.A.G., Pedersen H.H., (2014), An environmental life cycle assessment of controlled traffic farming. *Journal of Cleaner Production* 73, pp. 175-182;
- [10] Gorin G., (2012), Development of a hybrid theory for a steady turn of the machine and tractor aggregate. Kinematics, *Proceedings of the National Academy of Sciences of Belarus*, vol.1. pp. 25-28, Minsk/Belarus;
- [11] Jasiński M., Mączak J., Szulim P., Radkowski S., (2016), Conception of navigation system for autonomous agricultural robot, *Mechanization in agriculture* Vol. 16(202). pp.16-19, Bulgaria;

- [12] Kingwell R., Fuchsbichler A., (2011), The whole-farm benefits of controlled traffic farming: An Australian appraisal. *In Agricultural Systems*, vol. 104, no. 7, pp. 513–521;
- [13] Kuvachov V., (2016), Kinematics of the turn of wide span means of mechanisation of agricultural production for controlled traffic farming., *Bulletin of Sumy National Agrarian University*, Vol. 10/2 (30), pp.46-49, Sumy/Ukraine;
- [14] Kuvachov V., (2014), Specialised vehicle for controlled traffic farming, *Bulletin of Kharkiv National Technical University of Agriculture*, Vol.148. pp. 63-69, Kharkiv/Ukraine;
- [15] Nadykto V., Uleksin V., (2008), Controlled traffic and gantry farming systems, p.270, Melitopol/Ukraine;
- [16] Nadykto V., (2005), On the turnability issue of a machine and tractor aggregate on the basis of a multipurpose power tool, *Proceedings of the Tauride State Agrotechnological University*, Vol. 27, pp. 27-34, Melitopol/Ukraine;
- [17] Nadykto V., Masalabov V., (2012), Investigation of the dynamic turnability of a two-machine machine and tractor aggregate, *Scientific Bulletin of the Tauride State Agrotechnological University*, Vol. 2 (3), pp.15-26, Melitopol/Ukraine;
- [18] Onal I., (2012), Controlled traffic farming and wide span tractors. *Journal of Agricultural Machinery Science* 8(4), pp. 353-364;
- [19] Pedersen H.H., (2011), Harvest capacity model for a wide span onion bunker harvester. Automation and system technology in plant production, *CIGR section V & NJF section VII conference*, pp. 27-36;
- [20] Pedersen H.H., Sørensen C. G., Oudshoorn F.W., McPhee J.E., (2013), User requirements for a wide span tractor for controlled traffic farming. *International Commission of Agricultural and Biological Engineers, Section V. CIOSTA XXXV Conference "From Effective to Intelligent Agriculture and Forestry"*, 3-5 July 2013. pp. 134-136, Billund / Denmark;
- [21] Popp K., (2010), *Ground Vehicle Dynamics*. Springer. p.353;
- [22] Rajamani R., (2006), *Vehicle dynamics and control*. Springer. p.485;
- [23] Tullberg J.N., (2000), Wheel traffic effects on tillage draft. *Journal of Agricultural Engineering Research*, vol. 75. pp. 375-382;
- [24] Uleksin V., (2011), Automation of the vehicle control in gantry farming, *Bulletin of Kharkiv National Technical University of Agriculture*, Vol. 10 (2). pp. 101-110, Kharkiv/Ukraine;
- [25] Wong J.Y., (2001), *Theory of ground vehicles*. John Wiley & Sons, Inc. p.558.

WRITING NORMS

Article Types

Three types of manuscripts may be submitted:

1. **Regular articles:** These should describe new and carefully confirmed findings, and experimental procedures should be given in sufficient detail for others to verify the work. The length of a full paper should be the minimum required to describe and interpret the work clearly (max.10 pages, **even number**);
2. **Short Communications:** A Short Communication is suitable for recording the results of complete small investigations or giving details of new models or hypotheses, innovative methods, techniques or apparatus. The style of main sections has not necessarily to be in accordance with that of full-length papers (max. 6 pages, **even number**);
3. **Reviews:** Submissions of reviews and perspectives covering topics of current interest are welcome and encouraged (max.10 pages, **even number**).

Manuscripts should be written in English (American or British usage is accepted, but not a mixture of these) and submitted **electronically** at the following e-mail addresses: inmatehjournal@gmail.com

Please be sure to include your full affiliation and e-mail address (see Sample manuscript)

The authors are responsible for the accuracy of the whole paper and references.

There are allowed 2 papers by each first author.

The text layout should be in single-column format. To avoid unnecessary errors it is strongly advised to use the “spell-check” and “grammar check” functions of your word processor.

Review Process

All manuscripts are reviewed by 2 members of the Scientifically Review Office. Decisions will be made as rapidly as possible and the journal strives to return reviewers’ comments to authors in approx.3 weeks.

The editorial board will re-review manuscripts that are accepted pending revision.

NOTE:

Submission of a manuscript implies: that the work described has not been published before (excepting as an abstract or as part of a published lecture or thesis) that it is not under consideration for publication elsewhere.

1. REGULAR ARTICLES

- Manuscripts should be concise, in **1.15 line spacing**, and should have 2 cm all over margins. The font should be **Arial 10 pt**. Ensure that each new paragraph is clearly indicated, using **TAB at 1 cm**.
- Title will be **Arial 12 pt**. and explicit figures will be **Arial 9 pt**.
- Text will be written in English.
- Chapters’ titles are written by **Arial 10 pt, Bold, Uppercase** (e.g. **INTRODUCTION, MATERIALS AND METHODS**), between chapters is left a space for 10 pt. At the beginning of each paragraph, TAB of 1 cm.
- The paper body will be written in **Arial 10 pt., Justify alignment**.

TITLE **Arial 12 pt., Uppercase, Bold, Center (in English language)** and **Bold Italic (in native language)**.

Should be a brief phrase describing the contents of the paper. Avoid long titles; a running title of no more than 100 characters is encouraged (without spaces).

AUTHORS **ARIAL 9, Bold, Centre alignment**

Under the paper's title, after a space (enter) 9 pt., write **authors' names** and **affiliations (Arial 8 pt.-Regular)**

When the paper has more than one author, their name will be followed by a mark (Arabic numeral) as superscript if their affiliation is different.

Corresponding author's name (next row), **(Arial 8 pt.)**. Should be added also: phone, fax and e-mail information, for the paper corresponding author (**font: 8 pt., Italic**).

KEYWORDS **(In English)** about 4 to 10 words that will provide indexing references should be listed (**title: Arial 10pt, bold italic, text Arial 10 pt., italic**).

A list of non-standard **Abbreviations** should be added. In general, non-standard abbreviations should be used only when the full term is very long and used often. Each abbreviation should be spelled out and introduced in parentheses the first time it is used in the text. Standard abbreviations (such as ATP and DNA) need not to be defined.

ABSTRACT (*in English and Native language, Arial 10 pt.*), the title *bold*; the text of abstract: *italic*) should be informative and completely self-explanatory, briefly present the topic, state the scope of the experiments, indicate significant data, and point out major findings and conclusions. The Abstract should be max.250 words. Complete sentences, active verbs, and the third person should be used, and the abstract should be written in the past tense. Standard nomenclature should be used and abbreviations should be avoided. No literature should be cited.

INTRODUCTION (*Arial 10 pt.*) should provide a clear statement of the problem, the relevant literature on the subject, and the proposed approach or solution. It should be understandable to colleagues from a broad range of scientific subjects. We should refer to the current stage of researches performed in the field of the paper to be published, by quoting up-to-date specialty studies, preferably published after 2006, excepting certain referential specialty books/studies, especially papers issued in magazines/journals/conferences/ISI quoted symposia or in other international data bases, which are well known and available.

MATERIALS AND METHODS (*Arial 10 pt.*) should be complete enough to allow experiments to be reproduced. However, only truly new procedures should be described in detail; previously published procedures should be cited, and important modifications of published procedures should be mentioned briefly. Methods in general use need not be described in detail.

RESULTS (*Arial 10 pt.*) should be clearly presented. The results should be written in the past tense when describing findings in the authors' experiments. Results should be explained, but largely, without referring to the literature. Discussion, speculation and detailed interpretation of data should not be included in the Results, but should be put into the Conclusions section.

CONCLUSIONS (*Arial 10 pt.*) The main conclusions drawn from results should be presented in a short Conclusions section. Do not include citations in this section.

Formulae, symbols and abbreviations: Formulae will be typeset in Italics (preferable with the Equation Editor of Microsoft Office 2003) and should be written or marked as such in the manuscript, unless they require a different styling. They should be referred to in the text as Equation (4) or e.g. (4). The formulae should be numbered on the right side, between brackets (*Arial 10 pt.*):

$$P = F \cdot v \quad (1)$$

Terms of the equation and the unit measure should be explained, e.g.

P is the power, [W];

F – force, [N];

v – speed, [m/s]

SI units must be used throughout.

Tables should be self-explanatory without reference to the text. The details of the methods used in the experiments should preferably be described in the legend instead of in the text. [The same data should not be presented both in table and graph form or repeated in the text.](#)

Table's title will be typed *Arial 9 pt, Bold, Centered*

In the table, each row will be written Arial 9 pt, single-spaced throughout, including headings and footnotes.

The table should be numbered on the right side, between brackets (*Arial 10 pt.*):

Figure (*Arial 9 pt., Bold, Center*) should be typed in numerical order (Arabic numerals). Graphics should be high resolution (e.g. JPEG). Figure number is followed by what represent the figure or graph e.g.:

Fig.1 – Test stand

Legend: *Arial 8 pt, Italic, Center, e.g.*

1 - plansifter compartments; 2- break rolls; 3 – semolina machines; 4 – reduction rolls; 5 – flour

ACKNOWLEDGMENTS (*Arial 10 pt.*) of people, grants, funds etc should be brief (*if necessarily*).

REFERENCES (*Arial 10 pt.*)

(In alphabetical order, in English and in the original publication language).

Minimum 10 references, last 10 years, minimum 3 references from the last 2 years

It can be used "References" tool from the *Word Editor*.

References should be cited in the text in brackets as in the following examples:

(Babicu P., Scripnic V., 2000)

All references must be provided in English with a specification of original language in round brackets.

Authors are fully responsible for the accuracy of the references.

References should be alphabetically, with complete details, as follows:

Examples:

Books: Names and initials of authors, year (between brackets), title of the book (Italic), volume number, publisher, place, pages number or chapter, ISSN/ISBN:

[1] Vlăduț V., (2009), *Study of threshing process in axial flow apparatus (Studiul procesului de treier la aparatele cu flux axial)*, vol.1, "Terra Nostra" Publishing House, Iași/Romania;

Journal Article: Names and initials of authors, year (between brackets), full title of the paper, full name of the journal (Italic), volume number, publisher, place, page numbers:

[1] Lizhi Wu, Yan Di., (2005), *Demonstrational study on the land consolidation and rehabilitation (LCR) project of saline-alkali soil in arid areas: a case study of Lubotan LCR project in Pucheng County, Shaanxi Province (干旱区盐碱化土地整理工程实证研究-以陕西蒲城县卤泊滩土地整理项目为例)*, *Transactions of the Chinese Society of Agricultural Engineering*, vol.21, no.1, Madison/Wisconsin, pp.179-182;

[2] Leonov I.P., (1973), *Basic machine theory for tobacco stringing. Post-harvest care of tobacco and rustic tobacco (Основы теории машин для закрепления табака на шнуры. Послеуборочная обработка табака и махорки)*, *Collection of scientific articles (сборник научно-исследовательских работ)*, pp.37-45;

Conference or Symposium: Names and initials of authors, year (between brackets), full title of the paper (Regular), full name of the conference/symposium (Italic), volume number, publisher, place, page numbers

[1] Bungescu S., Stahli W., Biriș S., Vlăduț V., Imbrea F., Petroman C., (2009), *Cosmos program used for the strength calculus of the nozzles from the sprayers (Program Cosmos folosit pentru calculul de rezistență la zgomot al aparatelor de distribuție)*, *Proceedings of the 35 International Symposium on Agricultural Engineering "Actual Tasks on Agricultural Engineering"*, Opatija / Croatia, pp.177-184;

Dissertation / Thesis: Names and initials of authors, year (between brackets), full name of the thesis (Italic), specification (PhD Thesis, MSc Thesis), institution, place;

[1] Popa L., (2004), *Research on the influence of structural and functional parameters of the braking system on the braking performance of agricultural trailers (Cercetări privind influența caracteristicilor constructive și funcționale ale sistemelor de frânare asupra performanțelor de frânare ale remorcilor agricole)*, PhD dissertation, Transylvania University of Brașov, Brașov / Romania.

Patents: Names and initials of authors, year (between brackets), patent title (Italic), patent number, country:

[1] Grant P., (1989), *Device for Elementary Analyses*. Patent, No.123456, USA.

Legal regulations and laws, organizations: Abbreviated name, year (between brackets), full name of the referred text, document title/type (Italic), author, place:

[1] *** EC Directive, (2000), *Directive 2000/76/EC of the European Parliament and of the Council of 4 December 2000, on the incineration of waste, Annex V, Official Journal of the European Communities, L332/91, 28.12.2000, Brussels.*

Web references: The full URL should be given in text as a citation, if no other data are known. If the authors, year, and title of the documents are known and the reference is taken from a website, the URL address has to be mentioned after these data:

The title of the book, journal and conference must be written in Italic, the title of the article, chapter of the book, must be written Regular.

Citation in text

Please ensure that every reference cited in the text is also present in the reference list (and vice versa). Do not cite references in the abstract and conclusions. Unpublished results, personal communications as well as URL addresses are not recommended in the references list.

Making personal quotations (one, at most) should not be allowed, unless the paper proposed to be published is a sequel of the cited paper. Articles in preparation or articles submitted for publication, unpublished, personal communications etc. should not be included in the references list.

Citations style

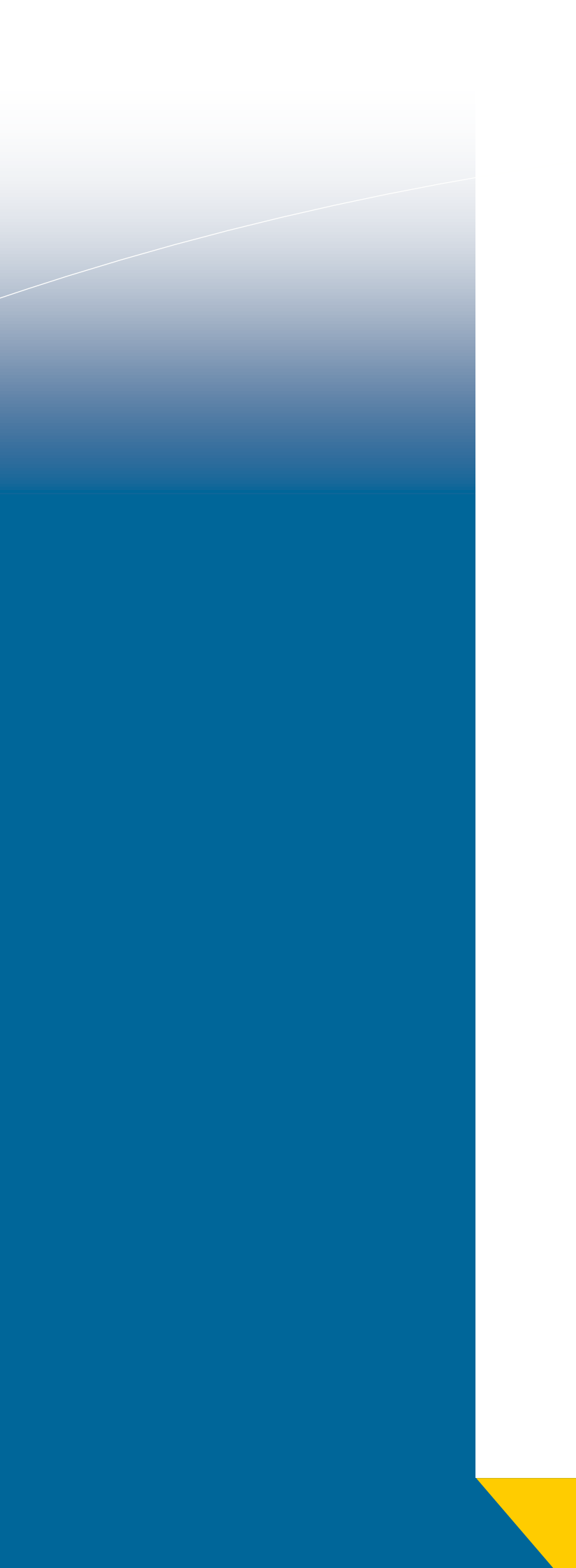
Text: All citations in the text may be made directly (or parenthetically) and should refer to:

- **single author:** the author's name (without initials, unless there is ambiguity) and the year of publication:
“as previously demonstrated (*Brown, 2010*)”.
- **two authors:** both authors' names and the year of publication: (*Adam and Brown, 2008; Smith and Hansel, 2006; Stern and Lars, 2009*)
- **three or more authors:** first author's name followed by "et al." and the year of publication: “As has recently been shown (*Werner et al., 2005; Kramer et al., 2000*) have recently shown”

Citations of groups of references should be listed first alphabetically, then chronologically.

Units, Abbreviations, Acronyms

- Units should be metric, generally SI, and expressed in standard abbreviated form.
- Acronyms may be acceptable, but must be defined at first usage.



Edited by: INMA Bucharest

6 Ion Ionescu de la Brad Blvd., sect. 1, Bucharest, ROMANIA

Tel: +4021.269.32.60; Fax: +4021.269.32.73

<http://www.inmateh.eu>

E-mail: inmatehjournal@gmail.com